THE DEVELOPMENT OF RADIATIVE NEUTRON CAPTURE TECHNIQUES FOR IN-SITU ELEMENTAL ANALYSIS OF THE SEABED

by

Vernon Victor Clement Ranasinghe

June, 1984

A thesis submitted for the degree of Doctor of Philosophy of the University of London and for the Diploma of Membership of the Imperial College.

Department of Geology,
Imperial College,
London S.W.7.

ABSTRACT

Marine exploration for economic minerals has assumed increasing importance during the last two decades. The chance nature of the discovery of many significant mineral deposits in the past emphasizes the need for a systematic approach to seabed exploration. The adaptability of established techniques in continental exploration, such as geophysical and geochemical methods to the marine environment and their application to seabed exploration have inherent limitations. Insitu nuclear techniques have been considered since they are elementally specific and permit a direct analysis of the seabed to be made.

Irradiation of the sea-floor with neutrons results in various types of interactions with the nuclides of the elements present. The most favourable mode of interaction in this application is the radiative neutron capture reaction with its accompanying gamma radiation. These γ-rays have a wide spectral distribution of discrete energies that are characteristic of the elements. The application of this reaction to seabed exploration has been studied using a high resolution γ-ray spectrometer for its development as a nuclear technique in multi-element analysis. Laboratory experiments have been conducted in a simulated marine environment and the feasibility of the method has been shown by determining the parametric relationships involved in the construction of an operational probe and its performance as a towed system on the seabed.

A computer model of a typical probe and its environment has been developed on the basic concepts of the laboratory model. Monte Carlo calculations have been performed using this model for the experimental situations simulated in the laboratory. Comparison of the results obtained from experiment and those from analysis has verified the behaviour of the model under the constraints applied. The model provides a broader insight into the parameters governing seabed interactions and forms the basis for extrapolating the analytical results to predict the behaviour of a variety of seabeds of different elemental composition and physical properties.

ACKNOWLEDGEMENTS

The author gratefully acknowledges the Fellowship awarded by the International Atomic Energy Agency and the sponsorship of the U.K.A.E.A. and The British Geological Survey (Geochemistry Division) under whose auspices this work was performed. In particular, thanks are due to Mr C.G. Clayton of the Applied Nuclear Geophysics Group, A.E.R.E. Harwell for his invaluable help and guidance in all stages of this research. Dr B.W. Thomas is thanked for his stimulating discussions, willing assistance and continued interest in the outcome of the work produced in the thesis. The author is also grateful to Dr D.S. Cronan of the Applied Geochemistry Research Group, Imperial College for his special interest and fruitful discussions relating to the project and assistance in many respects.

The author makes due acknowledgement to his colleagues in the Applied Nuclear Geophysics Group for their help. Reg Strong is particularly thanked for constructing some of the components for the probe assembly and preparing the 'seeding' material for the different seabeds. Mrs J. Richardson's effort in producing a very pleasing typescript is much commended. Finally, the author's indebtedness and especial thanks are due to his wife Pamela for her continued encouragement and support during the course of this research and in the preparation of this thesis.

CONTENTS

LIST OF TABLES

LIST OF FIGURES

CHAPTER 1
INTRODUCTION

1.1 General

Rapidly growing industrialisation the world over is causing an ever-increasing consumption of raw materials and there are at present grounds for disquiet about the ability of some of the land-based ore deposits to meet a continuing exponential increase in demand. The situation is partly reflected by the growing interest in methods of recovering essential metals from low-grade deposits on land and the increased consideration now being given to the exploration and possible exploitation of mineral deposits on the seabed.

A general feature of marine mineral deposits is their occurrence as thin layers of sediment spread over large areas of the ocean floor since they are formed as a result of depositional processes. Resistant detrital minerals such as monazite and ilmenite are derived from the continental land masses and manganese nodules which are currently of interest occur, following chemical accretionary processes on the bed of the deep ocean. Although ore bodies undoubtedly occur in the subsurface rocks beneath the ocean floor, attention is currently focussed on the superficial deposits on the continental shelf areas and the ocean basins since their exploitation falls within the capability of current technology.

Within the last 25 years, studies of manganese nodules of the deep ocean floor have rapidly expanded on account of the realisation of its economic importance as a source of nickel, copper and cobalt. Submarine phosphates have also attracted commercial interest as a potential source of raw material for the manufacture of fertiliser, but perhaps the most important progress has been the recent discovery of metalliferous sulphide deposits associated with volcanically active regions such as the East Pacific Rise, the Bauer Depression and the Galapagos and Gorda Spreading Centres. These have yielded metal contents as

high as 29% zinc, 6% copper, 43% iron and 1.5% silver in chemical assays. Similar metalliferous sediments of the Red Sea Deeps are well known and have attracted the attention of many exploration concerns on account of the high metal content of the Atlantis II Deep which is potentially the richest of any such deposit found so far in this region.

Placers have been mined for several decades on the continental shelf, generally in the near shore areas where the mineral bearing sediments occur in close proximity to similar beach deposits. Notable in this respect are the tin deposits of S.E. Asia and the limited off-shore mining for monazite, ilmenite, rutile, zircon and similar minerals. Such deposits have supplied industry with a steady output of rare-earth minerals for technological applications and exploration efforts are sustained for these minerals in the present time to meet future demands.

1.2 The Need for Marine Exploration

Continued interest in the oceans have been shown by several industrial nations to supplement their needs of essential raw materials. The principal political/economic reasons put forward for embarking on marine exploration and the development of technology associated with such activities are many. Among them are:

(a) the present dependancy of highly industrialised nations for their supplies of raw materials from areas which are politically unstable,

(b) the necessity of ocean mining as the only means of ensuring an adequate supply of strategic minerals to certain countries for their national security,

(c) political and population pressures which will force lesser industrialised nations into ocean exploration,

and (d) competitiveness of seabed mining in relation to corresponding recovery of land-based minerals.

Other important factors for consideration on a national basis are:

(a) the inaccessibility of mining known land deposits located in areas already urbanised by human settlements and which cannot be exploited without creating socio-economic problems,

(b) the recovery of metal pollutants from estuaries and bays which contain a high proportion of industrial wastes for recycling,

(c) the possible solution of environmental problems connected with land mining, by turning to the ocean for alternate sources of these minerals,

and (d) the current development of off-shore technology which would make seabed mining advantageous over land mining.

Several developing nations have already considered marine exploration as a priority in their industrial policy for economic growth. This is currently observed from the many exploration concerns engaged in such activities in various parts of the world and the major mining consortia in existence for the exploitation and development of marine resources (CRUICKSHANK 1981).

1.3 Physiographic regions of the ocean floor and their mineral potential

As a result of the great advances made in marine geology and geophysics in the past several decades, the morphology and environment of the ocean floor are known to a great extent. The nature and mode of occurence of minerals on the seabed are a direct consequence of this environment. A brief description of the regions of the ocean floor in relation to their relative importance from a point of view of mineral potential is considered here.

1.3.1 Physiographic regions

Continents are usually surrounded by a continental shelf which is the shallow submerged platform bordering the continental land mass. It is of variable width (average 75 km.) and slopes gently seaward to the 'shelf break', an increase in slope at an average depth of about 130 m. (FIGURE 1.1). There is a considerable variation in depth of the 'shelf break' from a few tens of metres to several 100 m. but the continental shelf is generally regarded as the region between the mean low water line and those features which terminate at a depth of less than 200 m.

The steeper surface below the 'shelf break' is the continental slope which marks the structural edge of the continent and overlies the change from thick continental crust to thin oceanic crust. It has an average width ranging from 100-200 m. and an average depth ranging from 100 - 200 m. to 1,400 - 3,200 m. The base of the continental slope may terminate in a continental rise comprising the fan of sediments shed off the continents. It may in certain instances end in bordering deep sea trenches or in shallow depressions or it may end abruptly at the deep sea floor.

The Deep Sea region lies beyond the continental slope and rise. Its mean depth is 4 km. and has a rather variable physiography. The dominant geologic feature are the deep ocean basins which show marked relief. At seismically inactive continental margins flat abyssal plains occur and can extend almost to the middle of the ocean basins. Deep-sea trenches or depressions are common in otherwise active regions where oceanic crust is thought to be consumed. Much of the regions seawards of the abyssal plains and trenches is composed of a rolling hill topography broken by isolated seamounts (hills with a relief of over 1 km.) and seamount ranges. Towards the centres of the ocean basins there are usually volcanically active mid-ocean ridges and these are sites of sediment generation.

The continental slope, from the sedimentary point of view, is a site of non-deposition, over which there is a slumping or flow of sediments from the continental shelf destined to come to rest on the continental rise or to be swept by turbidity currents out to the abyssal plain. It may also be a site of slope deposition where only the finer terrigenous material carried across the shelf comes to rest. No mineral deposits of importance have been found so far on the continental slope, though it is thought to have great potential for oil and natural gas.

Studies of the morphology, surface sediment characteristics and evaluation of transport and deposition on the continental shelf have been made by several workers (EMERY 1961, SHEPARD 1963). Attempts have also been made to study the various chemical processes and environmental factors governing the formation of deep sea mineral deposits (CRONAN 1980). From the knowledge gained of the marine environment during the past two decades only the Continental Shelf and the Deep Sea have been recognised and widely accepted as potential regions of mineralisation.

1.3.2 Mineral potential

1.3.2.1 Continental Shelf

The continental shelf is principally floored by detrital sediment derived from the adjacent land masses. Placers and aggregates are the most common surface deposits found but phosphorites, which are a major industrial source of phosphate and other important minerals are known to occur on the continental shelf. Placers include heavy metals such as gold and platinum, resistant detrital minerals such as cassiterite, ilmenite, rutile, zircon, monazite, magnetite, garnet and some gem minerals (EMERY and NOAKES 1968, DUNHAM 1969). Aggregates include sands, gravels and shell material. Since rocks of the continents underlie the continental shelf, subsurface mineral deposits are generally similar in character to those occurring on the adjacent land masses.

1.3.2.2 Deep Sea Region

The Deep Sea floor is thinly covered with sediment and the mineral deposits occurring in this region are the outcome of various geological and chemical processes and are characteristic of the environment in which they are found. Apart from the red clays and oozes which are the dominant sediments of the deep ocean floor, of special significance are the manganese nodules which are found in varying abundances in almost all the deep oceans of the world (CRONAN 1980). These concretionary oxides of Mn and Fe are of significant economic interest and contain enrichments of Ni, Cu and Co to be considered as ore deposits.

The active mid-ocean ridges are often the sites of metalliferous sediment formation. Massive metallic sulphide deposits have been discovered associated with sea-floor spreading centres of these rift zones such as those of the East Pacific Rise (FRANCHETEAU et al 1979). Of these, the sulphides of Cu and Zn are considered to be of potential economic value. Metallic sulphides have also been found in the Deeps situated in the Median Valley of the Red Sea. Some seamounts of the Deep Sea region are also sites of phosphorite deposition.

1.4 Present Methods of Marine Exploration

1.4.1 General Comments

Until relatively recently, all the known mineral deposits on the seabed which are currently being exploited have been either extensions of known continental deposits or the result of an accident al discovery. No systematic approach to marine exploration has been attempted in the past mainly as a result of the paucity of exploration techniques in various scientific disciplines which could be applied directly to the seabed. The standard method is the combination of high resolution subbottom depth profiling and sampling with subsequent shipboard or laboratory

analysis. This procedure has been well developed over the years that it now forms an integral part of any marine survey. Recently, the development of submersibles and visual aids such as underwater cameras and TV systems have added an extra dimension to the measurements. Land exploration methods in other scientific disciplines such as geochemical and geophysical are now being considered but they have restricted use and can only be applied in the search for specific minerals which favour the particular method selected.

1.4.2 General Methods

The use of precision depth recording (PDR) systems and sidescan sonar in mapping seabed topography is widely used in marine surveys. Apart from providing an image of the sea floor, PDR has proved useful in determining the presence of mid-water reflectors, such as between brine and sea-water to locate brine filled basins in the Red Sea (SWALLOW 1969, PUGH 1969). However, this does not have wide applicablility in exploration for metal rich deposits since not all metalliferous deposits are associated with brine (BACKER and SHOELL 1972). It has been suggested (CRONAN 1980) that manganese nodules tend to be concentrated on particular topographic features and the location of a favourable bathymetric environment would indicate a nodule distribution of a specific grade and abundance. Its implication is also demonstrated in the case of the Chatham Rise phosphorite deposits East of New Zealand (CULLEN, KUDRASS and VON RAD 1981). PDR and sidescan sonar have been able to identify regions of high phosphate nodular concentrations from characteristics of the seismic reflection records. The highest concentration of phosphorite is recorded where the bottom reflector consists of overlapping hyperbolae while less or no phosphorite is found in areas with a smooth or irregular rolling topography.

1.4.3 Visual Observations

The early methods of exploration involved direct observation using divers in shallow seas (less than 60-80 m. water depth) and recently by manned submersibles (FRANCHETEAU et al 1979). Underwater photography and TV now provide continuous sequences of features of the sea floor. These have mainly been used to study details of seabed topography and sedimentation including ripple marks in unconsolidated sediment, attitude of sea floor outcrops and distribution of manganese and phosphorite concentrations. Operations of these devices undersea has its limitations. The lack of clarity in the sea, the attenuation of light waves due to transmission in the sea water and the low level of natural illumination at greater depths imposes severe restrictions on their use. Artificial illumination is now used, but in turbid waters direct observation poses a problem which exists even in the deep sea due to the existence of turbidity currents and therefore have a limited range of observation.

1.4.4 Sampling Methods

Sampling provides material that can be readily examined and analysed on the surface and is the most direct method of ascertaining the composition and abundance of the minerals present. Unlike land operations where precise sampling techniques are directed to obtain the type and quantity of sample needed for analysis, retrieving samples from the seabed becomes problematical in a difficult sea environment. Sampling is not always typical of the formation sampled but is largely a function of the design of the sampler and its mode of operation.

1.4.4.1 Sediments and hard formations

Sampling is carried out on the seabed by various techniques depending on the nature and composition of the sea floor. Dredging is done to gather rock fragments or loose nodules from the surface over a distance on the sea

floor while a 'grab' is used to obtain a sample at a precise location. Coring is resorted to recover a sample in the form of a vertical column through the ocean bottom either by gravitational impact or by mechanical vibration. In hard formations drilling techniques are employed to recover samples of rock or consolidated sediments beyond the penetration of conventional coring techniques.

1.4.4.2 Sea water

In areas of metalliferous sediments, specially in regions of high volcanic activity, water sampling is done in geochemical exploration. Samples are generally collected from the seabottom but collection is made at various depths at a precise location in certain instances. Among the many conventional methods available, the free-fall sampling technique is now the most widely used. This method consists of a sampling device which is able to fall through a depth of water unattached to any cable or wire and return to the surface under its own buoyancy.

1.4.5 Geochemical methods

Geochemical techniques as applied to marine mineral exploration uses the concept of dispersion of elements from ore deposits both laterally on the ocean floor or by migration through sea water. By chemical analysis trace elements in sediments, rocks and seawater are determined relative to other elements to discover anomalous chemical patterns. The decrease of concentration of these trace elements in sediments with distance from the source, gives rise to concentration gradients which are used to locate the source of mineralisation.

The development of this concept in locating submarine metalliferous sediments of hydrothermal origin has been illustrated in the case of metalliferous sulphide deposits of the Atlantis II and Nereus Deeps in the Red Sea (BIGNELL

et al 1976). Metal ion migration through sea water has also been observed in the Atlantis II Deep deposits (HOLMES and TOOMS 1972). It is essential however that for the success of this method, the ore forming process should be currently in operation at the time sampling is carried out.

Although geochemical methods have had a measurable success when applied under favourable environmental conditions, the complexity of the processes responsible for sediment transport and entrapment, and the migration of metal ions in sea water limit the application of this technique as a general exploration method.

1.4.6 Geophysical methods

Geophysical methods in continental exploration are well established and have accounted for a large number of successes in locating profitable ore deposits for exploitation. Application of these methods to undersea exploration requires special adaptation on account of the great depths of sea water encountered and in certain of the methods, the physical properties of the sea water precludes their use on the ocean floor. Existing geophysical methods on land have been reviewed by RONA (1972) in relation to continental shelf exploration and by FRANCIS (1977) where the applicability of electrical prospecting methods in the continental shelf has been discussed. Since all geophysical methods rely on the measurement of a physical property of an ore body for its detection, it is essential that the type of mineral sought must be considered in advance, because the method employed must be selected for the specific occurrence anticipated.

1.4.6.1 Seismic methods

The seismic reflection method is primarily used for assessing the thickness of sediments on the ocean floor. High resolution shallow penetration systems are preferred because most deposits of any economic interest are either

on the surface or buried under a shallow overburden. Determination of the thickness of unconsolidated sediment over bedrock is particularly useful in locating placer deposits, which lie buried in ancient river channels on continental shelves which are now submerged. In areas of metalliferous sediments the method permits an estimate of the total thickness of the sediment column.

1.4.6.2 Electrical methods

The application of electrical prospecting methods to mineral exploration of the continental shelf has been reviewed by several workers. (RONA 1972, FRANCIS 1977). Two distinct groups are recognised; one using natural electrical fields flowing in the seabed, self-potential (SP) and telluric and the other utilising applied fields such as Electromagnetic (EM), Induced Polarisation (IP) and Electrical Resistivity (ER). In the EM method no direct physical contact with the seabed is necessary for the measurement of its electrical properties while in the other methods contact with the seafloor is essential. The telluric, EM, IP and SP methods have little or no application in marine mineral exploration on account of the presence of the highly conductive sea water layer. The relative success of the ER method depends on the ability of an electrode configuration to permit a large fraction of the applied current to penetrate the seabed. This is largely a function of the electrode separation in an array. Although the feasibility of the ER method has been demonstrated, the large electrode separations necessary to obtain sufficient penetration into the subsurface layer of the seabed limits its use to very shallow depths of the continental shelf.

1.4.6.3 Gravity method

Marine gravity surveys have been used in the past to study major structural features of continental shelves and margins. Though frequently used in petroleum exploration

to locate sedimentary basins within basement areas, the gravity method is of little importance in locating specific mineral occurrences on the seabed.

1.4.6.4 Magnetic method

Deep towed high resolution magnetometers are able to locate magnetite bearing placers and other magnetic sands. Such surveys using proton-precession magnetometers have been conducted off the coasts of Japan to locate exploitable deposits. The method may have indirect application in the search for metalliferous sulphide deposits by detecting anomalous magnetism (zones exhibiting normal and reversed cycles of magnetisation) associated with active seafloor spreading centres (RONA 1978). Most of the well known mineral deposits such as manganese nodules, phosphorites and other metalliferous sediments exhibit no magnetic properties. Since very few minerals are associated with magnetite, the magnetic method has limitations as a general exploration technique.

1.4.6.5 Nuclear Methods

1.4.6.5a General

During the past decade considerable efforts have been made to establish nuclear measurement techniques alongside the more conventional methods of sampling, seismic profiling etc. A distinct advantage of the method as applied to seabed exploration is the capability of making 'in situ' measurements of concentration of elements thus saving time and cost in sampling, analysis and reduction of data. The method offers the possibility of making static or continuous measurements of the ocean floor and is equally applicable in shallow waters or in deep sea.

Practical considerations concerning radiation penetration and adequate sampling volume mean, that methods employing nuclear techniques are generally based on

spectroscopic analysis of the gamma radiation emitted from nuclides of the seabed material. Measurement of this radiation may be in a passive (natural radioisotope) or active (neutron induced) mode, but in both cases lead to a high degree of elemental specificity, since an individual γ-ray spectrum contains a characteristic signature in terms of intensity and energy distribution of its components.

To obtain an adequate response from the sediments, the γ-ray detector must be in close contact with the seabed and in many respects deployment techniques resemble those used in conventional sampling procedures. However, by providing a continuous record of the seafloor composition when deployed from a towing wire or submersible vehicle, geochemical maps of large areas of the seabed can be constructed which will greatly improve the efficiency of sampling programmes where specific features need to be studied in detail.

1.4.6.5b Natural Gamma Radiation

Natural γ-ray emissions arise from three main sources: uranium, thorium and their daughter products and potassium-40. For practical measurements, γ-ray energies 1.764 MeV (from ^{214}Bi) in the uranium decay chain, 2.614 MeV (from ^{208}Tl) in the thorium decay chain and 1.460 MeV from the β-decay of ^{40}K are preferred since these energies are of sufficiently high intensity and well separated in an energy spectrum. Energy resolution is therefore not critical so that a high efficiency detector such as NaI(Tl) can be used to monitor these radiations.

Ores of uranium and thorium, of which only the latter are likely to occur as placer deposits on the seabed, can be identified by their natural gamma radiation. Deposits associated with a radioactive element can also be differentiated from non-radioactive sands and gravel. Commercial phosphate deposits are commonly enriched in

uranium and could be detected and so are tin-bearing placers associated with radioactive minerals like thorite, thorianite and pyrochlore.

In-situ measurements of natural γ-radiation in phosphorite exploration using a submersible scintillation counter have been reported by SUMMERHAYES et al (1970) and the development of instrumentation including a towed sled for locating off-shore mineral deposits by the detection of γ-rays from seafloor sediments has been described by NOAKES et al. (1974). But perhaps the most highly developed towed system for natural γ-ray spectroscopic analysis is described by MILLER and SYMONS (1973) and MILLER et al (1977). The system continuously monitors the total γ-radiation and the activities corresponding to the energy bands of U, Th and ^{40}K and is able to detect radioactive bearing minerals and discriminate between rock-types and sediments which have characteristic levels of γ-radiation.

For quantitative analysis by measurement of natural γ-radiation, the following disadvantages should be noted:

(a) the mineral of interest is correlated to the U, Th and K content,

(b) the unknown degree of equilibrium between U, Th and their daughter products,

and (c) the sensitivity of the method is undefined since it requires a definite known relationship between the mineral of interest and the associated radionuclide.

1.4.6.5c Induced Gamma Radiation

Seabed determinations of natural γ-radiation are limited in application to those minerals (elements) which

are naturally radioactive and to certain non-radioactive sediments which are associated with them. A wider range of elements can be identified by inducing γ-ray emission in seabed material by neutron-interaction techniques. There are several reactions which can be used, the most important being thermal neutron capture (n,γ), inelastic neutron scattering $(n,n'\gamma)$ and the production of short lived isotopes by either neutron capture or (n,p) reactions.

Due to the presence of seawater overlying the seabed and in the saturated sediments, the neutrons are rapidly thermalised ensuring a high capture rate within the seabed material. Therefore the most favoured reaction for seabed analysis is the (n,γ) capture reaction in which the resultant prompt γ-rays have energies up to about 10 MeV. Such γ-rays have high penetrability and provide an adequate depth of sampling for the method to be applicable in seabed exploration.

The possible use of neutron-capture γ-ray spectrometry in marine exploration was first investigated by SENFTLE et al. (1969) and WIGGINS et al (1969). However, no in situ measurements were carried out. Laboratory studies were made of manganese nodules and gold ore in a simulated marine environment. Experiments were conducted with a 67 μg ^{252}Cf neutron source and a 30 cm^3 Ge(Li) detector. Spectral signatures were obtained for manganese and gold but no sensitivity limits are quoted. A conceptual design of a probe for analysis of the ocean floor was proposed, which consists of a neutron source and detector separately housed in spherical containment and rigidly connected. No reports of its development are available.

Subsequent to these investigations a feasibility study on the neutron capture γ-ray method was undertaken by SENFTLE et al. (1977). The measurements reported were made

from a mobile platform and in sediments consisting mainly of clay and mud a metre thick, in seawater depths ranging from 15-30 metres. The probe containing the ^{252}Cf neutron source was attached to a sealed fibre glass drum which housed the Ge(Li) detector. This had the facility of containing sources of different strengths at selected distances from the detector in port holes drilled into the probe. The detector was contained in the upper section of the assembly and cooled to a temperature close to that of liquid nitrogen (77°K) by solid cryogen in canisters. The entire assembly was surrounded by a fibre glass shell containing fresh water to exclude the effects of chlorine in seawater. Measurements were carried out with the system lowered to the seabottom so that the probe penetrated the sediments with the fibre glass drum resting on the seabed. Control experiments with this geometry established that the measured radiation was principally from sediments close to the detector.

The interference from chlorine in seawater has been highlighted as a limitation of the method and the difficulties experienced in overcoming these effects in the analysis of data are presented. Inspite of the poor counting statistics, energy peaks due to elements such as Ni, Fe, Cu and Ti have been identified but no quantitative analysis has been possible with the data.

Several recommendations were made. A change in configuration of the probe was suggested to improve counting statistics. One consideration was to place the detector in the original location of the neutron source and distribute a number of weaker sources in a suitable array around it for better efficiency of measurement. An alternative method suggested was the use of a source of high energy neutrons (14 MeV) from a neutron generator and pulse sequence the events for greater selectivity.

X-Ray fluorescence (XRF) and neutron activation methods in marine exploration have been considered by WOGMAN (1977). The energy dispersive XRF analyser described uses a 50 mCi ^{109}Cd or ^{57}Co source in conjunction with a 80 mm^2 Ag collimator and a 80 mm^2 Si (Li) diode as a detector. Quantitative measurements at 10 ppm level for about 20 elements have been made in slag pile waste in seawater depths up to 20 m. Depths of operation up to 300 m are claimed with this proto-type instrument.

Equipment based on energy dispersive X-Ray fluorescence techniques is regarded as having limited application on the seabed. The method is generally one of surface identification and the depth of analysis, which extends from a few mm to a cm depends upon the energies of the K and L - X-Rays used (photon energies are in the range 5 - 100 keV). The method is thus restricted to point measurements (static) of a few elements and in favourable circumstances.

A proto-type instrument for in situ static measurements by neutron activation of marine sediments is also reported by the same worker (WOGMAN 1977). The probe employs a 0.2 to 1 mg ^{252}Cf neutron source and a Ge (Li) detector (15% efficiency) cooled by solid cryogen and designed to operate at water depths up to 300 m. The source and detector mounted 4 metres apart, have the facility of operating in tandem, the irradiation time lasting 120 s followed by a 40 s delay and subsequent counting of the gamma photons for periods ranging from 2 to 500 s. Minimum detectable limits for a number of elements have been quoted for a 1 mg ^{252}Cf neutron source and for an irradiation time of 2 mins, delay time 40 s and a counting time of 2 mins. A device for continuous measurements of the seafloor at a towing speed of 1 knot is mentioned as a future development.

Since the irradiation and decay time of a radionuclide are governed by the half-life, the optimum time period for irradiation and counting are variable parameters for each element. These half-lives generally range from several minutes to days, so that in towed systems with speeds of 3 to 4 knots, very high source strengths are implied in obtaining statistically significant countrates in seabed analysis.

The development of an in situ analysis system using neutron capture for manganese nodule exploration has been reported by LANGE and BIEMANN (1975). The instrument incorporates a sampling unit where the nodule material is sucked into an analysis chamber, activated and analysed before transmitting the data to a surface vessel. Since a finite time (10 mins) elapses between successive cycles of sampling, analysis and computation of data the method in effect reduces to sampling at locations determined by the speed of the survey vessel and cycling time of the system.

The application of the (n,γ) capture reaction has been considered by these workers under restricted conditions of field operation. The system designed by LANGE and BIEMANN is a sampling unit for the analysis of a specific type of occurrence (manganese nodules) where the determinations are carried out under optimum conditions for the analysis of the elemental constitutents of the nodular material. The use of this equipment would therefore be best suited to regions on the seafloor where the existence of manganese nodules have been previously established. Continuous measurements are not possible with this type of system and consequently the nodular distribution on the seabed cannot be ascertained by the sampler.

The activation mode of the (n,γ) capture reaction for insitu analysis (WOGMAN 1977), involves large measurement times in a cycle consisting of irradiation, a

delay and a subsequent counting period. For high spatial resolution large source strengths have to be used to compromise with the towing speeds of vessels. For special applications such as in manganese nodule analysis, the important elemental constituent nickel cannot be detected at all by this method and hence is a limitation.

With the probe described by SENFTLE et al, only static measurements are possible under stable seabed conditions. Since one component of the probe assembly (neutron source, γ-ray detector) is embedded in the sediments during a determination continuous profiling of the seabed is not practicable.

1.5 Present Study

In previous investigations by others in this field very little effort has been devoted to understanding and defining the fundamental response of a neutron interaction probe and its relationship to the conditions of the seabed, which in turn affect the calibration, sampling depth and spatial resolution. In this context, probe characteristics relate to the general shape and the nature and layout of internal components (source, detector etc), while the seabed response is determined by the porosity (seawater content), matrix elemental composition and density.

The current work is therefore concerned with the development of the radiative neutron capture (n,γ) reaction as a nuclear technique for in situ elemental analysis of the seabed. The application of this reaction to seabed analysis has been considered in relation to a cylindrical neutron interaction probe capable of being towed continuously on the ocean floor using the 'eel' principle (MILLER et al. 1977). The response of other probe designs can be interpreted in terms of the results obtained with this system, since the present work has been devoted to determining the basic relationships between probe response and the physical characteristics of probe and seabed.

The determinations are based on laboratory experiments using a simple model of a probe in a simulated marine environment. The model consists of a radioisotope neutron source and a high resolution detector for γ-ray spectral analysis. The experimental work is concerned with

(a) the study of parametric relationships between source and detector for various geometry of measurement,

(b) the investigation of the effects of the marine environment by studying reactions from interfering elements present in seawater,

(c) determining the factors governing the calibration of a typical probe system for various seabed types and trace element concentrations,

and (d) investigating the parameters influencing the sensitivity of elements in the seabed and defining their limits of detection by a simple probe for the geometry considered.

A computer model of the probe and its environment has been developed on the concept of the laboratory experimental system for Monte Carlo computational analysis. Calculations have been performed using this model for various seabed conditions including those simulated in the laboratory and to confirm and extend typical probe responses for a range of applications. A comparison of the results of experiment and calculation has been made to establish the behaviour of the computational model under the constraints applied. The model has provided a better understanding of seabed interactions using the (n,γ) method and thus forms a basis for extrapolating the results to predict the behaviour of a variety of seabeds of different physical composition and elemental concentration.

CHAPTER 2

PHYSICAL PRINCIPLES UNDERLYING THE RADIATIVE CAPTURE (n,γ) REACTION AS APPLIED TO SEABED ANALYSIS AND THE SPECTROSCOPIC MEASUREMENT OF GAMMA-RAY YIELDS

2.1 Introduction

In general, neutron interaction techniques involve the use of a neutron source which irradiates the sea-floor with fast (several MeV) neutrons. During 'slowing down' and subsequent diffusion as slow (thermal) neutrons various reactions take place with the nuclides present. Following each reaction, one or more γ-rays may be emitted having energies characteristic of the reaction product. The energies and intensities of these γ-rays are measured with a suitable spectrometer, which presents the data as a spectrum of countrate versus energy. An analysis technique is then used to separate the contribution by the individual γ-rays to the spectrum.

Of the several interactions which occur with neutrons, the radiative capture (n,γ) reaction is of special significance on account of its wide applicability to the detection and analysis of a large number of elements in the seabed. In this chapter, the nuclear processes which involve interactions with seabed elements are presented and the various neutron sources and γ-ray detectors currently available are discussed in some detail in relation to their suitability of application in seabed analysis.

2.2 Penetration of neutrons in the seabed

Three distinct nuclear processes referred to as (1) moderation (2) thermalisation and (3) diffusion, collectively contribute to the penetration of neutrons in the seabed. The interactions which govern these processes, the mechanics involved and the specific energy losses incurred in such interactions are described in several texts (e.g. ISBIN 1963, LIVERHANT 1960). Only a general discussion applicable to the seabed environment is considered here.

The moderation process consists of a series of neutron interactions in which neutrons lose energy by inelastic and elastic collisions. In the process of repeated inelastic collisions, the energy degrades to a value where only elastic collisions are possible. In seawater, neutron moderation is principally attributable to elastic collisions and hydrogen is the main contributor. The process itself is characterised by a parameter referred to as the 'slowing down' length L_s, which is a function of the initial energy of the source neutrons and the scattering properties of the seabed material. A quantity of statistical significance is the root-mean-square distance R_s travelled by a neutron from the source, to where it attains epithermal energies (0.1 - 1.0 eV). This is given by the relationship $R_s^2 = 6L_s^2$ or $R_s = 2.45\ L_s$.

The final process of moderation is termed 'thermalisation' during which the energy of the neutron decreases from an epithermal value to thermal energies (0.025 eV). The energy of the neutrons during this stage of moderation is comparable to their binding energies and to the energy of thermal motion, so that losses of energy by interactions with nuclei are not as efficient as in the moderating process. Consequently, the distance travelled by a single neutron is smaller than the 'slowing down' length L_s. At distances from the source corresponding to 3 or 4 slowing-down lengths, the flux decreases by an order of magnitude so that R_s gives an approximate depth of penetration of the source neutrons in the seabed matrix.

As a result of the processes of moderation and thermalisation, neutrons achieve a thermal energy in equilibrium with the nuclides of the elements present in the seabed and seawater. Consequently, the diffusion of neutrons due to thermal agitation is represented by a 'diffusion length' L_D, which is related to the mean distance travelled by the neutron from the point of conception as a thermal neutron to where it is

absorbed. Thus, the overall effect of diffusion is to increase the volume of seabed sampled. For reactions occurring during the diffusion phase, the penetration is made up of contributions from L_s and L_D, so that the net distance travelled can be described by a migration length M given by

$$M^2 = L_s^2 + L_D^2 .$$

The root-mean-square distance travelled by a neutron during moderation and diffusion is thus equal to 2.45 M.

The 'slowing down' length L_s of neutrons in water saturated sandstone, limestone and dolomite has been calculated by KREFT (1974) for four different neutron sources and various water content. The effect of the initial neutron energy on this parameter is apparent from the results obtained for $^{226}Ra/Be$, $^{238}Pu/Be$, $^{210}Po/Be$ and ^{252}Cf sources. Monte Carlo computations of the 'slowing down' length L_s and 'migration' length M of neutrons from a $^{241}Am/Be$ source (average neutron energy 4.6 MeV) have been carried out for three common seabed constituents: silica - SiO_2, calcium carbonate - $CaCO_3$ and clay - $Al_4Si_4O_{10}(OH)_8$ (SANDERS, L.G.). These are calculated for various porosities of the saturated matrix with pure water and high salinity seawater. The tabulated values are contained in APPENDIX 1 and generally indicate the degree of penetration achievable with neutrons by a nuclear technique considered in seabed analysis.

2.3 Neutron interactions

Neutron interactions are generally a function of the neutron energy and the nuclear properties of the interacting nuclei, and in the seabed the type of interactions that occur depend upon the initial energy of the source neutrons employed. The various interactions induced by a neutron interaction probe and their implication in seabed analysis are discussed here in relation to the nuclear processes already described.

In regions close to a neutron source, the initial energy of the neutrons permit inelastic collisions to take place. Consequently, a neutron of a lower kinetic energy than that of the captured neutron is emitted accompanied mainly by gamma radiation. The interaction is denoted by $(n,n'\gamma)$ and is governed by a threshold energy below which only elastic collisions occur. For elements constituting seawater (Table 2.1) and a majority of those considered in seabed exploration, the threshold energies are high, so that the probability of occurrence of inelastic collisions is low with radioisotope sources considered in a typical neutron interaction probe. This is because energies are relatively low, being 2.3 MeV for ^{252}Cf and 4.6 MeV for (α,n) sources such as $^{241}Am/Be$ or $^{238}Pu/Be$. However, with a sufficiently high energy neutron source (14 MeV) such as a neutron generating tube, inelastic scattering collisions are more likely and the probability of charged particle reactions, e.g. (n,p) are also possible. Such reactions can produce short-lived radioisotopes which may subsequently de-excite by the emission of γ-rays. However, the detection of these γ-rays from continuous measurements of the ocean floor is difficult and cannot be used as a practical method because of the wide range of half-lives involved and the potentially large neutron sources necessary to produce significant countrates.

In seawater, the most easily observed γ-ray from a fast neutron reaction is the 6.1 MeV energy due to $^{16}O(n,n'\gamma)^{16}O$ reaction.

Elastic scattering at energies below the threshold for these reactions further reduces the energy of the neutrons, so that thermal equilibrium is achieved. Elastic collisions mainly provide a mechanism for the degradation of the energy of the source neutrons and are generally of no interest as a reaction for analysis of seabed elements.

The presence of seawater both above the seabed and in the sediments and rocks underlying, contributes to the rapid

thermalisation of the neutrons and thus ensures an optimum neutron capture rate within the seabed. Its adaptability to seabed applications is best illustrated by the following:

(a) the radiative capture (n,γ) reaction occurs at varying rates (depending upon cross section σ_{th}) with almost all nuclides of the elements in the seabed,

(b) seawater provides an ideal environment for the thermalisation of fast neutrons for this reaction, and

(c) the characteristic γ-rays accompanying this reaction are discrete and elementally specific.

2.4 Radiative neutron capture (n,γ) reaction

Radiative neutron capture is illustrated schematically in figure 2.1 for the case of a typical metal in the transitional group of elements of interest in seabed analysis. Capture of a neutron forms the next heaviest isotope in an excited state. The excitation energy may be carried off in a single γ-ray transition to the ground state but in general, transitions occur to many intermediate states (primary transitions) creating secondary transitions which give rise to a cascade of γ-rays of different intensities. The intrinsic sensitivity for detection of an element using this reaction is dependent on the probability of interaction, denoted by its thermal absorption cross-section σ(n,γ) and the energy and intensity of the γ-rays produced.

γ-rays emitted in the decay from the capture state to the ground state of the product nucleus are referred to as prompt γ-rays and have energies up to 10 MeV. These have a high degree of penetration and are applicable to the analysis of bulk material. If the nuclide formed is unstable, then after emission of prompt γ-rays it may offer the possibility of being detected by γ-rays associated with delayed beta-decay. These γ-rays are generally of low energy (< 2 MeV) and have limited use in practice because of the range of half-lives involved.

2.4.1 (n,γ) capture cross-section and energy dependence

The probability with which the (n,γ) capture reaction occurs with an element is represented by a capture cross-section σ (n,γ), which can vary in a complex way with energy E, due to the presence of resonances and threshold reactions. In the region remote from resonances the relationship

$$\sigma(n,\gamma) \simeq \frac{1}{\sqrt{E}} \quad \text{applies}$$

while near resonances, the energy dependence is in accordance with the Breit-Wigner formula (ISBIN 1963). In the region of thermal and resonance energies (0-500 keV) the cross-sections have an irregular pattern for all nuclides. At higher energies (> 1 MeV), the cross-section becomes a relatively, smooth function, the disappearance of structure being due to overlapping of neighbouring resonances. Resonance effects also reduce at higher energies, because of the increased probability of occurrence of inelastic reactions described earlier in the chapter.

2.5 Thermal neutron capture data

The decay schemes and associated γ-ray spectra for all elements from thermal neutron capture have been compiled by GROSHEV et al (1968-69). The γ-ray energies and their corresponding intensities for the natural element as well as individual isotopes are given from experimental determinations. More recent data of the capture cross-sections of elements, the characteristic γ-rays in the energy range 0-10 MeV and their intensities are given by DUFFEY et al (1970). These values have been used to compute some of the parameters of importance to this study.

2.6 Nuclear and physical data of seawater and some common seabed type constituents

The composition of seawater and some common constituent elements of the seabed are presented in relation to the nuclear and physical properties, in order that the various interactions which take place with neutrons could be investigated.

2.6.1 Salinity

The constancy of the relative composition of the major constituents of seawater is well established (GROEN 1967). Empirical relationships have been determined and the important physical parameters can be predicted from measured values of one of the dissolved constituents. 'Salinity' includes the total dissolved salts in grams per kilogram of seawater at the ambient temperature. Table 2.1 gives the ionic constituents of seawater of salinity 34.5‰. Na^+ and Cl^- constitutes 2.95% by weight and hydrogen 10.83%.

Variations occur in the surface salinities of seawater which are largely influenced by local conditions of high evaporation and precipitation. However, in all oceans at great depths salinities generally lie between 34.5‰ and 35.0‰. Notable exceptions are in the Red Sea deep water regions where the salinity is considerably higher, i.e. 38‰ and in the Deeps where brines derived from the evaporites by seawater attain salinities as high as 257‰.

2.6.2 Sensitivity of seawater/seabed type elements to neutron capture (n,γ)

The background radiation observed in a γ-ray spectrum in seabed analysis is mainly from neutron capture by elements in seawater and in the basic rock forming materials. The sensitivities of these constitutents to thermal neutron capture induced by a seabed neutron probe is principally dependent on the thermal neutron capture cross-section σ_a, the intensity I of the γ-rays emitted and

the percentage abundance of the elemental constituents. Table 2.2 presents this data for the most prominent γ-ray energies and a sensitivity index defined by $\frac{I\sigma_a}{A}$ which denotes the importance of the contribution of an element to an observed γ-ray spectrum. The relative sensitivity factor for each of these constituents are defined by the product $\frac{I\sigma_a}{A}$ and its abundance. Two elements Si and Ca from some common seabed types are included for purposes of comparison. For predominantly silica (SiO_2) or calcium rich ($CaCO_3$) seabeds, the relative sensitivity values are high so that significant backgrounds would be expected by these elements in addition to chlorine from seawater.

Chlorine in particular has a wide spectral distribution of γ-rays and is the principal interfering element in seabed analysis. Hydrogen exhibits a single characteristic energy 2.223 MeV with a high relative sensitivity which accounts for a very large percentage of the countrate in a spectrometer system. This line however interferes very little with the higher energy components, which are best suited for mineral analysis.

2.7 Neutron sources for seabed surveys

2.7.1 General

The neutron sources suitable for seabed exploration are of two types:

(1) sealed radioisotope sources
(2) neutron generating tubes.

Radioisotope sources have the distinct advantage of small physical volume and independence of power requirements. Although neutron generating tubes have the disadvantage of being bulkier and less robust and require a power supply for neutron production, they have the

advantage of producing a higher neutron output at high energies and can be operated only when required. Both types of sources therefore exhibit distinct advantages for seabed applications.

2.7.2 Radioisotope sources

Of the several radioisotope neutron sources produced commercially, three sources with relatively high neutron outputs are commonly available: ^{252}Cf, $^{241}Am/Be$ and $^{238}Pu/Be$. The neutron spectra and other characteristics are discussed by LORCH (1973). Radioisotope sources have the disadvantage of being associated with gamma radiation and in both $^{241}Am/Be$ and $^{238}Pu/Be$ the γ-ray yield is higher than in ^{252}Cf. For thermal neutron capture reactions ^{252}Cf is the best choice since it has the highest specific yield 2.3×10^{12} $n.sec^{-1}.gm^{-1}$, (the corresponding yields for $^{241}Am/Be$ and $^{238}Pu/Be$ sources are 7×10^{6} $n.sec^{-1}.gm^{-1}$ and 4.1×10^{7} $n.sec^{-1}.gm^{-1}$ respectively) and the lowest γ-ray emission. The half-life of 2.65 years is short compared to the others but still practicable. The mean neutron energy is 2.3 MeV and is considerably lower than any of the other (α,n) sources (4.7 MeV), so that a higher degree of thermalisation of the neutrons is achieved within shorter distances. The low mean energy also reduces the probability of undesirable high energy reactions with seawater elements as well as constructional materials of a probe assembly.

2.7.3 Neutron generating tubes

Neutron generating tubes make use of either $T(d,n)^{4}He$ or $D(d,n)^{3}He$ reactions for the production of neutrons (MARION and FOWLER 1960). In the former case, nearly monoenergetic 14 MeV neutrons are produced and high yields ($\sim 10^{13}$ $n.sec^{-1}$) are obtained. The neutron yield from the $D(d,n)^{3}He$ reaction is about two orders of magnitude lower, but the low neutron energy, nearly 3 MeV, can be optimised to reduce problems from interfering reactions.

It was mentioned that one advantage of neutron generating tubes is that it can be operated only when required. This facility ensures that operating personnel are adequately protected by switching off the device when not in use thus avoiding the problem of radiological exposure and eliminates the need to include location and recovery equipment within the probe, should the towing cable be severed. This can also be used to practical advantage by operating the neutron tube in a pulsed mode, i.e. time sequencing the gamma signals from the detector in synchronisation with the neutron source to improve signal-to-noise ratio for certain types of applications. Another distinct advantage is that γ-rays are not associated with neutron production, except those resulting from interactions with constructional materials of the generating tube itself.

2.8 Detectors for prompt gamma-ray measurements on the seabed

2.8.1 Introduction

The complexity of spectra from prompt γ-ray emission following thermal neutron capture and the need for precise energy and intensity measurements of several seabed elements favour the use of high resolution detectors. However, for certain applications such as the analysis of a few elements of widely differing energies or the detection of a particular element in seabed exploration, e.g. Mn in manganese nodule detection or when detector resolution is not critical in a survey, a high efficiency detector may be preferred. The choice for seabed analysis is at present from two detector types:

(1) Inorganic Scintillators - NaI(Tl), $Bi_4Ge_3O_{12}$

(2) Germanium Semiconductor detectors - Ge(Li), High-purity Ge

The characteristics of both types of detectors which are of importance to seabed application are:

(1) resolution - ability to distinguish between γ-rays whose energies lie close together;

(2) efficiency - the probability that a γ-ray which enters the crystal will be counted;

(3) radiation damage - degradation of detector performance following exposure to radiation;

(4) operating convenience - ruggedness, associated equipment requirements, configuration.

2.8.2 Scintillation detectors

Thallium activated sodium iodide NaI(Tl) and recently bismuth germanate ($Bi_4Ge_3O_{12}$) or BGO as is commonly abbreviated are characterised by their relatively high efficiency of detection for γ-rays. They have the advantage of availability in large sizes and capability of operation at the ambient temperature. The relatively high average atomic number of both materials ensures a large ratio of photo-electric to compton effect most desirable for seabed analysis. The energy resolution of both detectors is poor compared to germanium semi-conductor types. Nevertheless, this latter disadvantage is off-set by the high efficiency of detection warranted in certain applications using the (n,γ) method.

2.8.2.1 NaI(Tl) detectors

The total intrinsic efficiency of a scintillation detector is a measure of the fraction of γ-rays recorded which enter the crystal corresponding to any energy in the pulse height spectrum. For a 3" x 3" NaI(Tl) detector, in the energy range 2-10 MeV, it is in the region 30-60% depending on the source to crystal distance.

Of more interest in seabed applications is the intrinsic peak efficiency, which is an estimate of the fraction of γ-rays entering the crystal which gives rise to a count in the photo-peak. This is of particular importance, since the peak efficiencies are governed by the size of the crystal and hence on the dimensions of a practical probe. Values of intrinsic efficiency are not well known for all γ-ray energies and crystal sizes, but in the energy range 2-10 MeV for a 3" x 3" crystal this could be approximately 10-2%.

The resolution of a NaI(Tl) detector is commonly given as the full width of the photo-peak at half-maximum (FWHM) divided by the mean photo-peak energy. It is usually reported for the 0.662 MeV γ-ray from ^{137}Cs. Commercially available cylindrical detectors up to 3" x 3" usually have a resolution for ^{137}Cs of 7-10% which falls to 4% in the energy range 1-10 MeV.

2.8.2.2 $Bi_4Ge_3O_{12}$ detectors

Considerable interest has been shown recently in bismuth germanate detectors for γ-ray measurement on account of their special properties resulting from the use of a pure intrinsic scintillator. Material availability in any required size and shape, physical ruggedness, chemical inertness and non-hygroscopic nature make them ideally suited for underwater applications. Although their resolution is not comparable to a similar size NaI(Tl)

detector, higher efficiency and a significant reduction in the compton background observed make them a superior detector for seabed work. A comparison of the full-energy peak efficiency of a (38 mm dia x 38 mm) BGO in the energy range 0.1 - 8 MeV with that of a similar size NaI(Tl) is given by EVANS (1980).

For the 1.33 MeV γ-ray from ^{60}Co, the full-energy peak efficiency of BGO is 4.5 times that of the NaI(Tl) detector and for the 2.754 MeV line of ^{24}Na the efficiency is 5.6 times as high. The higher efficiency of the BGO (7-10%) in the range 0.1 - 8 MeV highlights the advantage of using such a detector where efficiency is the criterion of selection.

Comparatively, the resolving power of the BGO is inferior and is approximately half that of the NaI(Tl) detector for the ^{137}Cs γ-ray and certainly not good enough to resolve the 1.77 and 1.33 MeV photo-peaks of ^{60}Co. The energy resolution of a BGO (FWHM %) for various γ-ray energy has been measured by DRAKE et al (1981). Resolutions vary from 15 - 6% in the energy range 1 - 8 MeV. However, the distinct advantage of BGO detectors is clearly in the superior efficiency and the significant reduction in the compton background for use in seabed analysis.

2.8.3 Germanium semiconductor detectors

Germanium detectors are clearly the preferred choice for the accurate analysis of the complex γ-ray spectra involving several elements on the seabed. The superior energy resolution of these detectors, where many closely spaced γ-ray energies have to be separated shows that both Ge(Li) and high-purity Ge detectors are indispensable for multi-element analysis. A variety of such detectors are available. They are planar or coaxial in design, the basic features being a thick compensated region (GeLi) or a high

purity Ge (HPGe) sandwitched between p- and n-type layers. In practice, a p-type Ge detector is most suitable as it is not damaged by recycling to room temperature and has a low sensitivity to neutron damage (PEHL et al 1979).

Detector efficiency for these devices is customarily specified by comparing the relative counting rate of a Ge(Li) or HPGe detector with a 3" x 3" NaI(Tl) detector, when a ^{60}Co source is located 25 cm from the front face of each detector. Usually, to overcome ambiguities in measurement, a standard calibrated ^{60}Co source for the Ge detector is employed and the calculated value for a 3" x 3" NaI(Tl) detector which is 1.2×10^{-3} counts per disintegration of the source at 25 cm is used. Sensitive volumes of 25 - 50 cc are most common, but detectors are available with a 120 cc sensitive volume. Relative peak efficiencies vary from 5 - 30% for such detectors but for the best resolution detectors, the efficiency is about 10 - 15%.

By convention, the 1.33 MeV γ-ray from ^{60}Co is most commonly used by manufacturers to specify the resolution of Ge detectors. Good germanium detector systems have a typical energy resolution of less than 0.2% compared with 5 -10% for NaI(Tl) detectors. At higher energies, two neutron capture γ-rays from ^{56}Fe are convenient for specification of the resolution, these being 7.646 MeV and 7.632 MeV (separation 14.4 keV). The experimental resolution achieved in a γ-ray spectrometer, incorporating a Ge detector of the types described, is however determined by a combination of several factors, the most important of which is the contribution of the various stages in the pulse amplifying chain and in the analyser unit. Technical advancement in the production of high quality Ge crystals and the design of low-noise amplifiers have made it possible to achieve high spectral resolution for practical applications.

2.8.4 Radiation damage and operating conditions

Neutron activation of sodium and iodine atoms in the NaI(Tl) detector crystal does not present any serious problem. Iodine (^{128}I) decays with a half-life of 25 mins with the emission of γ-rays of energy 0.443 MeV and 0.527 MeV while ^{24}Na (half-life 15.03 hrs.) emits γ-rays of energy 2.754 MeV and 1.369 MeV. These are in the low energy region of a spectrum and no interference is expected with capture γ-rays from seabed elements in the range of interest at higher energies. Similarly, capture γ-rays due to Ge are in the low energy region (CHASMAN et al 1960) and can be avoided by efficient shielding or by locating the detector in a low energy flux region.

The effects of fast neutron damage have serious consequences in Ge detectors. This is manifested in the degradation in the energy resolution after prolonged exposure to a high energy neutron flux and is an important consideration when using such detectors for analysis. Recently, a reverse electrode configuration has been devised to minimise fast neutron damage by a factor of 20 over the conventional p-type material (PEHL et al 1979).

Both BGO, NaI(Tl) and Ge detectors are ideally suited for operation at great depths and are able to withstand the severe vibrations to which a probe is subjected to when towed on the seabed. In the case of Ge(Li) and HPGe detectors, an additional requirement is the cryogenic cooling system, which forms an integral part of the detector. The several methods by which this could be achieved for given geometrical constraints of a probe have been outlined (THOMAS et al 1983). Such systems are able to function satisfactorily under marine conditions, although for continuous measurements a cryogenerator would be more appropriate for prolonged periods of operation.

2.9 Response function of a Ge detector

The response function of a Ge detector to monoenergetic gamma radiation is complex and shows marked variations with energy. For γ-rays in the energy range 100 keV - 1 MeV, the resulting energy spectrum consists of a well resolved full energy peak corresponding to the γ-ray energy and a compton distribution just below it. The interpretation in this case is straightforward since the compton component has a relatively smooth variation with energy. However, it can limit the accuracy of data derived from a complex spectrum if it is necessary to observe weaker full-energy peaks due to other elements in the presence of a compton continuum of a higher energy peak.

With increasing energy and above 1.022 MeV ($2\ m_o c^2$) further peaks occur due to pair production. Annihilation of the positron with an electron in the Ge crystal creates two 0.511 MeV gamma quanta. If both quanta are absorbed the full energy E_γ will be represented as a full-energy peak in the spectrum. If the dimensions of the Ge crystal are small, there is a strong probability that both quanta would be lost in which case a strong peak at $(E_\gamma - 2\ m_o c^2)$ referred to as the 'double-escape' peak occurs. If a single quanta is lost, then a 'single-escape' peak corresponding to $(E_\gamma - m_o c^2)$ will occur mid-way between the full and double-escape peaks. The response function of a Ge detector is best illustrated in the γ-ray spectra obtained in the experimental work, e.g. Figure 5.1 6 for nickel.

The probability of annihiliation quanta escaping from the detector is related to detector volume and shape. As the volume of a detector increases, the content of the full-energy peak increases in relation to the single and double-escape peaks.

Although the cross-section for pair production in Ge increases continuously with increasing γ-ray energy, the double-escape peak efficiency of the detector does not follow the same trend due to the fact that electrons and positrons gain sufficient kinetic energy to escape from the detector. This is characterised by a decrease in efficiency of the detector above 4 or 5 MeV, this energy being largely determined by the volume of the Ge crystal.

2.10 Selection of gamma-ray detectors for applications on the seabed

For multielement analysis, the prime consideration in a detector is a superior energy resolution capable of separating the individual components of the characteristic γ-rays for identification and analysis. Germanium semiconductor detectors Ge(Li) and high-purity germanium (HPGe) fall into this category. The resolution of such a detector is a function of the γ-ray energy and also the detector countrate in the measuring system. There is generally a decrease in resolution at higher energy, due to effects of pair production. The efficiency of detection is also a function of the γ-ray energy and for quantitative measurements detector efficiencies have to be pre-determined for a particular probe system for the range of γ-ray energy of measurement. For low energy, i.e. less than 2 MeV, the full-energy peak is generally used for analysis but above this energy, the double-escape peak is predominant and becomes more useful due to increased pair production.

For the detection of a few elements, whose characteristic γ-rays are widely separated in energy or a particular element such as Mn, a high efficiency detector NaI(Tl) or BGO is more appropriate. Its use will considerably improve the efficiency of a survey by reducing the counting time demanded by other types of detector to obtain significant countrates. Ideally, a high efficiency detector could be employed for reconnaissance surveying for particular mineral (element) occurrences to delineate potential areas of mineralisation followed by static

measurements with a high resolution detector for quantitative determinations. Both types of detector are at present able to fulfil the requirements for incorporation in a probe assembly for marine applications.

Although the normal requirement for a simple probe in seabed work is a single source of neutrons and a suitable detector, there is no restriction in the (n,γ) method as to the number of sources and detectors which could be incorporated in a system. By using an array of neutron sources suitably dispositioned with respect to a single detector or by using a single source of neutrons in combination with a number of high resolution detectors (HPGe), the total detector efficiency could be considerably increased in a probe assembly while maintaining the high resolution of the system. However, the probe geometry has to be re-designed to accommodate such a modification for a towed system.

CHAPTER 3

EXPERIMENTAL TECHNIQUES

3.1 Introduction

The object of the present series of experiments is to obtain neutron capture γ-ray spectra for elements in a simulated seabed and its environment. In particular, emphasis was placed on the analysis of spectral data for energies in the range 0-10 MeV from constituent elements of the seabed and seawater for various parameters of a source-detector assembly. A feature of special importance to this study is the relationship between the instrument calibration and its environment. In this connection, the influence of the physical characteristics of the seabed was determined to interpret the detector response. This Chapter deals with the experimental techniques in the laboratory to simulate the seabed and its associated environment, the general features of the components of the probe system designed for elemental analysis and the various techniques associated with pulse processing, data acquisition and analysis.

3.2 Design of Experimental Tank

3.2.1 General features

The general features of the tank constructed for the experimental work are shown in perspective in figure 3.1 and a sectional view showing details of the arrangement of the components of the system is given in figure 3.2.

The tank measures 1.5 m^3 and is constructed with fibre glass of thickness 3.5 mm and was filled with seawater. It was reinforced with wooden lining 15 mm thick and filled with silica sand (principally SiO_2) up to a depth of 35 cms. A re-entrant tube was positioned in the tank just above the level of the seabed to accept the probe which included a high purity Ge detector with an active volume of 50 cm^3. The components of the probe were assembled in axial geometry within this tube. The outer can of the cryostat housing the detector was introduced through one

end of the tube with the coupling flange of the liquid-nitrogen dewar resting against one side of the tank as shown. The radiation shield and the neutron source were introduced as a composite unit contained in a narrower polythene tube from the opposite end of the re-entrant tube.

A thin polythene tray of depth 15 cms was embedded in the seabed directly under the probe assembly so that known concentrations of elements could be distributed uniformly in it for the various experiments. This arrangment provided an accurate means of measuring the elemental concentrations used in a particular measurement, the quantity of seawater in the saturated matrix and also limited the quantities of material for economic reasons. The tray presented minimal discontinuity between it and the rest of the material in the seabed.

The dimensions of the tank, the depth of the seabed and the height of seawater were determined by previous experiments to simulate 'infinite-geometry' conditions existing on the ocean floor. The materials chosen for the construction of the tank and other features of the system were based on their neutron properties to provide minimum interference with the experimental measurements.

3.2.2 Characteristics of seabed material

The principal material chosen for the seabed was silica sand as it is a common unconsolidated material of simple elemental composition encountered on the ocean floor and it could also be easily simulated in computational models. However, the character of the seabed was changed in subsequent experiments to investigate the response of other host materials found in different environmental conditions.

Analysis of the bulk sand material yielded a high percentage of calcium carbonate, i.e. about 20% $CaCO_3$ in the form of shell fragments. This was removed by drying at a temperature of 200°C for two hours and passing through a sieve of aperture 889 microns. The coarser sand fraction was also removed by the process. The resulting material on analysis contained less than 1% $CaCO_3$ which was acceptable for the experimental work.

3.2.2.1 Density

For computational modelling, a knowledge of the density and porosity of the sand was required. Determinations were therefore made of the solid and bulk density and its grain-size distribution. The solid density of the material (25 samples) was determined by hydrostatic weighing and an average value of 2.67 ± 0.1 gm.cm^{-3} was established. Measurements of the bulk density were made by accurately weighing a fixed volume of the sample (0.5 cubic ft sample volume). 155 samples were selected from the bulk material and the distribution curves are shown in figure 3.3. A mean value of 1.36 ± 0.03 gm.cm^{-3} was obtained.

3.2.2.2 Grain size

100 samples were selected from the same batch of sand for measurements of grain-size, the sample size being 500 g. After preliminary trials the following apertures of sieves were selected; 500, 355, 310, 212, 180, 150 and 106 microns. Sieves were arranged in sequence in a mechanical vibrator for 30 mins. to ensure complete separation and the fractions retained in each sieve were weighed for each sample. Frequency distribution and cumulative curves were constructed for the mean weights of material retained in the corresponding sieves for the samples separated. These are presented in figure 3.3. The frequency distribution curve is skewed about a maximum value of about 212 microns, the centroid of the curve being in the region of the larger apertures.

3.2.3 Salinity and density of seawater in tank

Supplies of seawater for the experiments in the tank were obtained from the sea near Portland, Dorset, where the salinity is generally in the range 35.5 - 36.0‰ during the summer. Stocks were kept in large polythene containers free of contaminants and pumped into the tank when required. Prolonged storage resulted in an increase in salinity due to evaporation but dilution with fresh water restored the salinity to the desired value. Generally, all experiments were conducted with seawater of salinity 35.0‰ at 19.0°C.

Measurements of salinity and temperature were made in situ using a salinity meter, a portable bridge-type instrument supplied by the manufacturer (ELECTRONIC SWITCH GEAR LTD, LONDON) and licensed by the NATIONAL INSTITUTE OF OCEANOGRAPHY, U.K. The meter provided the facility of directly measuring the salinity of the seawater in the tank during an experiment at the ambient temperature. This was possible through a switching device that permitted the measurement of salinity and temperature in succession so that an accurate determination could be made corresponding to the temperature of seawater. Two select ranges were available, 0-32‰ to within 0.5‰ and 32-38‰ with an accuracy of measurement to within 0.05‰ . The average temperature of the seawater for all experimental measurements was 19.0 ± 2.0°C so that the salinity was considered constant for purposes of computation.

The density of seawater was also measured in situ using a hydrometer having a range of measurement 1.000 - 1.050 with an accuracy of 0.001 $g.cm^{-3}$. The seawater had a density of 1.025 $g.cm^{-3}$ at a temperature of 19.0°C. Since the salinity, density and temperature are inter-related, it was possible by measuring all three parameters to obtain an accurate value for the salinity of the seawater. This was essential to compute the atom density of the major elements

constituting the seawater, some of which (H, Cl) contribute strongly to the gamma-ray background in neutron capture measurements.

3.2.4 Seabed materials

Materials used to simulate concentrations of seabed minerals consisted principally of readily available and stable compounds of elements. Costs of some of the desired chemical compounds were prohibitive for the quantities required for the experiments and hence the number of elements were limited.

As a general rule, chemical compounds of a sufficiently high degree of purity and obtainable in granular form were preferred. The important criteria were their degree of insolubility in seawater and stability to chemical decomposition in the marine environment. Oxides of elements were chosen for their simple chemical composition and the negligible cross-section for absorption of thermal neutrons by oxygen. (σ_a = 0.178 ± 0.025 mb.). The effective response of the material was therefore from the constituent element only.

Various trace element abundances of these elements were obtained by mixing these compounds uniformly with dry sand in the required proportions by weight. This was carried out in a rotary mixer for periods of 2 to 6 hours for a batch, depending on the nature and density of the material. To ensure uniform mixing, the grain-size of the compound was selected to be similar to the average size of the sand in the matrix. This also allowed the porosity of the mixture to be computed to a degree of accuracy required for the calculations. Quantities varying from 110-120 lbs. of dry material were required to fill the tray. Samples of material were analysed independently to verify the uniformity of the distribution of elements in the mixture. The important properties of the material used in the experiments are listed in TABLE 3.1.

3.3 Neutron source used in the experiments

The principal source of neutrons employed in the experimental probe was the radioisotope Californim-252. The source supplied by the manufacturers (AMERSHAM INTERNATIONAL) was doubly encapsulated in stainless steel and sealed in a 10 mm long capsule of diameter 7.8 mm and a wall thickness of 0.8 mm. The small physical dimensions of the capsule permitted the source to be mounted inside a brass holder which could be attached to one end of a rod 125 cms long and 10 mm diameter. The rod was constructed of synthetic resin bonded paper, which itself is little influenced by neutrons. This enabled the source to be handled safely from a distance when necessary for an experimental measurement. The source was stored in a lead container and further protected by boron-impregnated resin blocks to minimise the radiation levels when not in use.

3.3.1 Strength of source

The strength of the ^{252}Cf neutron source at the time of acquisition in January 1978 was nominally 5 μg with a manufacturer's calibrated output of 1.3×10^7 neutrons per second. This was rated at 5.65 μg by calibration with a standard 5 μg source for which the neutron emission rate was 1.15×10^7 $n.sec^{-1}$.

A comparison of the neutron output of the source made in April, 1980 with a standard source emitting $2.02 \times 10^6 \pm 1\%$ $n.sec^{-1}$ yielded a value of 6.18×10^6 $n.sec^{-1}$. The determination was carried out using the long counter installed at IBIS in the Nuclear Physics Division, A.E.R.E. Harwell. This agreed closely with the theoretical value obtained using a half-life of 2.65 years for the decay of ^{252}Cf.

3.4 General Probe Design

3.4.1 Source-detector configuration

A sectional view of the source-detector arrangement in the experimental tank is shown in figure 3.2. This simple

configuration is based on the generally accepted concept for continuous seabed measurements using the towed 'eel' principle. The basic components are a ^{252}Cf neutron source, a high resolution germanium detector (HP-Ge coaxial type) and a radiation shield. An enlarged view of the system is shown in figure 3.4. For conditions of axial symmetry, the neutron source was located along the cylindrical axis of the coaxial germanium crystal of the detector.

3.4.2 Radiation shield

The space between source and detector consisted of a composite shield comprising two materials each performing distinct functions of neutron moderation and γ-ray attenuation respectively. For convenience in operation, the assembly was housed in a polythene tube, which could be inserted into the re-entrant tube in the tank.

3.4.2.1 Gamma ray shield

The γ-ray shield in the experimental arrangement consists of a cylindrical block of lead 10 cms long. Lead was chosen among other materials, for its high density 11.34 $g.cms^{-3}$, high atomic number (Z=82) and its relatively high moderating ratio for neutrons. It has also a low absorption cross-section for thermal neutrons (σ_a = 0.170b) such that the sensititivy for detection of the only high energy gamma ray resulting from the (n,γ) reaction produces little interference in the measured spectra. Under conditions of 'good geometry' a thickness of 10 cms attenuates 99.9% of the gamma radiation in the energy range 0.5 - 10 MeV of the source spectrum. From a practical point of view, this thickness was considered sufficient for the shield. The shield also served to scatter fast neutrons from the source out of the direct path of the detector into the seabed. The position of the lead in relation to the neutron source will be discussed in a subsequent section as part of the experimental programme.

3.4.2.2 Neutron shield

The purpose of the neutron shield was to moderate the high energy source neutrons emitted in the direction of the detector and thus reduce the fast neutron flux incident on the detector. Polythene (CH_2) with a density of 0.91 $g.cm^{-3}$ was selected on account of its high hydrogen content, i.e. 5.62×10^{21} nuclei per cm^3. The moderated neutrons were then absorbed in boron-impregnated rubber (FLEX-BORON) commercially available in sheet form, wrapped round the detector can. The thickness of the sheet was 3.2 mm, its density 1.56 $g.cm^{-3}$ and contained 25 percent by weight of 95 percent enriched Boron-10. Its high thermal absorption cross-section (σ_a = 3836b) permitted a large proportion of the thermal neutrons to be absorbed and greatly reduced the probability of (η,γ) reactions with constructional materials of the detector. The hydrogen in the polythene produces a single capture γ-ray of 2.223 MeV, but this lies in the lower energy region of the spectrum.

Liquid moderators containing hydrogen have not been considered on account of the practical problems created in their use as components of a probe on the seabed. Deuterium (D_2O) has a very high moderating ratio 5860 compared with water 62. Nevertheless, its high cost and the fact that its thermal absorption cross-section is greatly affected by light water contamination restricts its use in this application.

3.4.3 Source retaining attachment

A special source-holder was necessary to maintain the neutron source in axial symmetry in the probe. A polythene disc of thickness 4 cms was fitted through its centre with a perspex guide tube of internal diameter 11 mm and length 10 cms. This was inserted into the polythene tube containing the radiation shield until it was in contact with one face of the shield. A tube made of synthetic resin-bonded paper was fitted to the projecting end of the

perspex tube and maintained an axial alignment by means of retaining rings. The neutron source was inserted through this tube and guided along its length to rest against the radiation shield prior to an experiment.

3.5 Spectrometer Arrangement

3.5.1 General

The function of accurately measuring the intensities and energies of γ-rays resulting from interactions with the elements under study was performed by a γ-ray spectrometer. The pulses in the detector were analysed and presented as a spectrum containing discrete energy lines relating to a mixture of individual elements. The components of the spectrometer used in this study consisted of:

(1) a high-purity germanium detector (HP-Ge)

(2) the associated electronics in the pulse amplifying chain

(3) a multichannel analyser, and

(4) a computerised data acquisition and storage system.

3.5.2 Gamma-ray detector

The principal γ-ray detector used in the investigations was a high-purity germanium semi-conductor detector of active volume 50 cc. It was fitted with a side-looking cryostat incorporating a 30 litre liquid-nitrogen dewar, with a typical holding time of 24 days. The germanium crystal 40 mm diameter and 40 mm in length was fabricated with p-type material in a coaxial configuration. The detector window thickness was 1 mm and the distance of the crystal to the front face of the cryostat was less than 5 mm. The entire crystal system was housed in an aluminium can of diameter 6.9 cms, thickness 1.3 mm and length 10 cms. The detector was maintained at liquid-nitrogen temperature (77°K) by a transfer system in which a copper rod (cold finger) permitted a direct

connection between the crystal and the liquid-nitrogen in the dewar. This particular detector employed a 'split vacuum' construction in which the dewar and cryostat vacuums were completely isolated from each other. A distinct advantage of this system was the protection of the germanium crystal from possible contaminants present in the much larger space of the dewar. The vacuum in the cryoscopic system was self-maintained after initial pumping to 10^{-5} torr by cryoadsorption and no external pumping was necessary during its operation. All the detector elements were mounted within the stainless steel cryostat in azimuthal symmetry about the axis of the crystal. The 'cold finger' which maintains contact between the germanium crystal and the cryogen was a solid copper rod of length 10 cms and diameter 19 mm with a split-clamp arrangement at one end for mounting the crystal.

A low-noise charge sensitive pre-amplifier stage incorporating a cooled FET (field effect transistor) was coupled mechanically to the cryostat and the electrical connection was made to the detector through vacuum feedthroughs, together with the high voltage bias for its operation.

The detector was operated with a bias of + 4000 volts at maximum efficiency, over and above the + 2000 volts necessary for full depletion. The leakage current at the operating voltage was less than 100 pA. The relative full energy peak efficiency of the detector compared with a 3" x 3" NaI (Tl) detector was 9.6% and the energy resolution (FWHM) for the ^{60}Co, 1.33 MeV γ-ray energy was quoted as 2.0 keV and FWTM was 3.96 keV at the time of purchase from the manufacturers (PRINCETON GAMMA-TECH).

3.5.3 Power supply and electronics for pulse amplification

A functional block diagram of the detector system and associated electronics, the multichannel analyser and the data acquisition and storage systems is given in figure 3.5.

3.5.3.1 EHT supply for detector

The EHT for the detector was supplied by a mains powered standard bias supply unit through an external variable control and cut-off. The unit delivered a maximum 4000 volt at 2 mA and was applied to the detector through the pre-amplifier, and d-c coupled for better performance.

3.5.3.2 The pre-amplifier

The signal from the detector was fed to a pre-amplifier, which was close coupled to the detector to minimise capacitative loading and its adverse effect on signal-to-noise characteristics. The pre-amplifier, consisting of a low-noise charge sensitive first stage had a fast rise time consistent with the charge collection time in the detector and a long delay time characteristic of charge sensitive amplifiers with capacitative feedback.

3.5.3.3 Main amplifier

The main amplifier provided pulse shaping and linear amplification of the output from the pre-amplifier. The gain factor was adjusted through a combination of coarse and fine controls over the range of operation required for the experiments, without causing saturation of signal pulses. The unit provided an output in the range 0 to + 10 volts. Pulse shaping was carried out by a double

differentiation and integration network to achieve a bipolar shape most suitable for the multichannel analyser.

The amplifier also incorporated a pulse pile-up rejection circuit and an automatic base-line restorer. These two features were specially advantageous at the higher counting rates, typically 3500 cps used in the experimental work. A pulse shaping time of 3 μsec was used for optimum signal characteristics determined by trial over a range of operating conditions necessary for the measurements.

3.5.4 The multichannel analyser

The primary function of the multichannel analyser (MCA) was the conversion of the pulse amplitudes (analog signals) from the main amplifier to equivalent digital numbers. This was performed by an ADC (analog-to-digital converter) and the resulting spectrum was stored in the memory of the computer system. A number of other features were incorporated in the MCA, among them were (a) a zero setting (b) lower level and upper level discriminators (LLD and ULD) and (c) dead-time measurement and correction.

The zero setting was adjustable through the front panel of the MCA and permitted the introduction of a 'zero offset' shift of the origin to suppress very small noise pulses which appear along with the signal or to assign the available channels to the upper part of the spectrum. The LLD provided the facility of excluding unwanted pulses in the lower energy region of the spectrum while the ULD limited the pulses from the higher energy region. This was accomplished in the system by setting the levels in a single channel analyser (SCA) which controlled a linear gate to the MCA. The output from the main amplifier were presented to the linear input from this gate in a parallel arrangement through the SCA and through a fixed time delay circuit as shown. When the input pulse met the amplitude

criteria set by the SCA, the linear gate allowed the pulse to be admitted to the ADC. This facility was used to reduce the countrate and eventual 'dead time' loss in the experiments.

An important feature of the MCA was the provision of an optional facility which eliminated the need for an explicit 'dead time' correction when a train of pulses was fed to the analyser. An input gate was provided to block pulses from reaching the ADC during the time of digitising a previous pulse, the ADC itself generating a logic signal level which held the input gate closed during the time it was occupied. An internal clock provided a train of regular pulses synchronised with an internal crystal oscillator and routed through the same input gate. These were stored in a memory location A and the direct pulses which bypassed the input gate and corresponded to real time in location B. Since the same logic pulse signal from the ADC inhibited both the incoming pulses and the clock pulses simultaneously, the number of clock pulses registered in channel A was a measure of the live time of the analyser. Measurements were made based on a preset fixed live time thus obviating the need for a 'dead' time correction.

3.5.5 Data storage and analysis

The output of the data from the ADC was stored in the memory of the computer controlling the ADC and other peripherals. The system had two 1024 channel blocks allocated for this purpose with a maximum capacity of $2^{20}-1$ for any one memory channel. The following peripherals were available on the computer.

(a) a video display unit for visual monitoring of the data and other functions

(b) a teletype for digital output of the contents of each channel and for controlling the functions of the computer

(c) paper-tape output for subsequent processing on the main computer to obtain graphical print-outs of spectra

and (d) facility for storage of data on magnetic disc.

The video display unit had on it permanent scale lines and two rows of 32 alphanumeric characters for labelling of data. A cursor in the centre of the display was used to extract information from any channel in the spectrum, in terms of its channel position and current contents. The contents of the memory were displayed on the video as a bar histogram representing the number of counts in each channel versus the channel number. This was in effect a graphical representation of the differential pulse height spectrum accumulated in an experimental run. The display could be selected either to be on a linear scale or on a log-scale to show detail over a wide range of the channel content.

All the programmes necessary for data acquisition, processing and the ancilliary functions were held on magnetic disc and loaded using the switches on the console. Once loaded, a programme could be made self-starting before use.

A keyboard was provided with a multiple option for performing all the tasks necessary for data acquisition, analysis, storage and other related functions. Data acquisition was automatically terminated based upon preset values of live time, real time, elapsed time or counts in a particular channel. The computer was programmed to re-cycle a sequence of events and record the acquired data automatically on disc.

CHAPTER 4

APPLICATION OF COMPUTATIONAL METHODS TO SPECIFIC PROBLEMS RELATED TO SEABED NEUTRON INTERACTION ANALYSES

4.1 General

The development of the (n,γ) capture reaction as a nuclear technique for seabed analysis has been undertaken primarily as an experimental study and forms the basis of this thesis. However, a limited amount of computational work was considered essential:

(1) to verify some results of the experimental work

and (2) to understand certain aspects in the application of the method, for which experimental simulation proved difficult.

Monte Carlo calculations were therefore carried out to study the various aspects of the performance of the neutron interaction probe under different operating conditions, as an aid to determining the design parameters of the probe and evaluating the response to various types and condition of seabed. Parameters which have been evaluated include the intrinsic sensitivity of the method, the effective depth of seabed material that can be sampled and perturbations on the space, energy distribution of the neutron flux arising from variations in the matrix elemental concentration and in the physical state of the seabed itself. The detector sensitivity for various minor elements in a given seabed type and fixed seawater content will depend to a large extent on the strength and distribution of the thermal neutron flux in the seabed. Hence, the evaluation of this parameter has been considered in this chapter as a pre-requisite in discussing the results of the experiments.

The fundamental concepts of the Monte Carlo method and the characteristics of the computer code used in the calculations (McNID II) together with the basic input data for the computer programme are contained in APPENDIX 2.

4.2 Computer model of the experimental system

The experimental system in the tank was made to conform to the geometry requirements of McNID II by means of suitable radial and axial surfaces in a cylindrical coordinate system. Figure 4.1 shows a vertical section in the form of a grid. The neutron source is located at the origin with the vertical line through the origin being the central axis. The detector in the probe assembly is on a radial axis through the source and an axial surface demarcates the regions representing the seabed and seawater.

Each mesh area on the grid surface when rotated in its position about the central axis generates an annulus, so that in this model the seabed and seawater are adequately represented by this geometry. In the case of the shield components, the annuli corresponding to these in the computer model are not representative of the components in the experimental probe and a finite volume of seawater in the experimental tank is now replaced by shielding material. This is not considered serious for purposes of calculation since the neutron shield material (polythene) is comparable in its moderating properties to seawater and the gamma shield tends to affect only the direct neutrons travelling from the source to the detector. Since the important γ-ray contribution to the detector response is from the seabed itself, these effects were considered small in influencing the neutron flux computed with this model.

4.3 Geometry of computer model

Ten radial and 14 axial surfaces specified the annular regions. The radial surfaces were defined with respect to the central vertical axis of the coordinate system. These were spaced uniformly 5 cm apart in the region 0-50 cm (FIGURE 4.1).

This value was fixed by adjustment in the course of a few trials. Calculations with a narrower spacing in a given computer time accounted for a fewer number of neutron scores in the smaller annular regions with poor statistical reliability on the results.

The spacing of the axial planes was primarily intended to define the regions of the seabed and seawater and the lateral dimensions of the probe components as shown. A spacing of 10 cm was chosen in the region 0-30 cms in the seabed and 70-100 cms in seawater. This was decreased to 5 cm in the region 30-50 cms and 60-70 cms. Between 50 cm and 60 cm two axial planes at 51 cm and 59 cm were chosen to take into account the wall thickness of the probe.

4.4 Features of the computed flux

The neutron flux computed by the McNID II programme is an average value for each of the annular regions shown in Figure 4.1. This is assumed as the value of the flux at the mean radius corresponding to the inner and outer radial boundaries of an annulus. The spatial distribution of the flux for a particular energy group in the system was obtained by plotting the values obtained by calculation with respect to the mean radius of the annulus. The errors associated with these values denote the statistical fluctuations in the number of neutrons accounted for in each annulus.

4.5 Computation of gamma-ray countrates

The γ-ray countrate corresponding to a particular nuclear reaction with an element in the seabed was computed by the following procedure:

(1) the average neutron flux was obtained for each of the annuli of the system specified by its geometry and nuclear parameters

(2) the neutron flux was converted into a γ-ray emission rate for each annulus corresponding to a particular reaction, i.e. (n,γ) using the reaction parameters, volume of the annulus and the abundance of the nuclide under consideration

(3) the contribution of the gamma flux from an annulus was computed at the detector

and (4) the computed gamma flux was then converted into a countrate at the detector for uncollided γ-rays, with known values for the detector characteristics such as efficiency, cross-sectional area etc.

The method of calculation is presented by considering a typical annular region corresponding to a grid area as shown in Figure 4.2. An elemental volume of this region bounded by two diametral planes subtending an angle $d\theta$ is considered in the computation. The average reaction rate with a nuclide of an element is dependent on the product of the magnitude of the thermal flux density, the macroscopic cross-section Σ_a for the (n,γ) reaction and the volume of the elemental region considered. The gamma emission rate was thus computed with a knowledge of the intensity of the particular γ-ray emitted in the reaction. The gamma flux due to this volume at the detector location depends on its distance, the solid angle subtended by this volume at the detector and the attenuation of the gamma photons in reaching the detector. The attenuation of the photons for the particular γ-ray energy was computed for the material of the seabed matrix from the nuclear parameters. The total gamma flux was obtained by integrating the flux contribution by this elemental volume over an angle 2π.

A subsidiary computer programme (THOMAS 1982) was used to calculate the gamma flux contribution from each of the annuli at the detector, using the data for the thermal neutron flux generated by the McNID II programme. The parameters incorporated in this second programme included, the macroscopic

thermal absorption cross-section Σ_a of the seabed element, the intensity of the γ-ray from the reaction, an attenuation factor for the γ-ray energy in the seabed matrix and the radial and axial coordinates of the annuli. Since the total attenuation is a function of the detector - annulus distance, this was recalculated by the programme for each increment $d\theta$ around the annulus. The computed gamma flux for each annular region was placed in an array corresponding to its location denoted by I,J in figure 4.1. The gamma flux from a region was obtained by merely summing up the individual values in the array corresponding to this region.

The number of counts in the detector in an experimental situation was obtained by the same programme by supplying the detector area and efficiency for the particular γ-ray energy as input.

4.6 Calculations of the spatial distribution of neutron flux in the seabed and seawater

4.6.1 Introduction

The response of a neutron interaction probe is critically dependent on the thermal neutron flux distribution in the seabed, which is in turn a balance between the thermalising effects of seawater and the degree of absorption by elements in the seabed. Calculations were therefore made to determine the neutron flux distribution in the seabed and its environment. A general feature of the McNID II calculations undertaken for this purpose is that the behaviour of neutrons during slowing down from source energies was considered by dividing the neutrons into several energy groups. For purposes of this study, only two groups have been considered - a thermal energy group (0 - 0.1 eV) and a fast energy group (1 - 10 MeV).

4.6.2 Neutron flux distribution for a point source in an infinite seawater medium

Neutron fluxes were calculated for the simple case of an isotopic ^{252}Cf neutron source in an infinite seawater medium of salinity 35% . Similar calculations were made for pure water. The spatial neutron flux distributions for an assumed source strength of 1 μg ^{252}Cf are shown in figure 4.3.

Several features of these curves are of importance. The thermal flux (0 - 0.1 eV) is greatest near the source and falls off rapidly with distance. At 30 cm, it is down by three orders of magnitude, the values for seawater being relatively lower than for pure water. This difference is attributed to the higher absorption rate of neutrons by chlorine in seawater.

In the case of the fast neutron flux (1 - 10 MeV), the variations observed for seawater and pure water are similar. At the source, the fast flux is naturally higher than the corresponding thermal flux, since ^{252}Cf produces a fission neutron spectrum with a weak low energy component. At finite distances from the source thermal neutron production increases at the expense of the fast neutron flux.

4.6.3 Neutron flux distribution in the simulated seabed for two different types of neutron sources in the neutron interaction probe

Thermal and fast neutron fluxes were computed for a silica type seabed containing 20% seawater by weight using

(1) a 1 μg ^{252}Cf fission-type source of average neutron energy 2.3 MeV

and (2) a 14 MeV monenergetic source such as a neutron generating tube.

The neutron emission rates were assumed to be the same, in order that a comparison could be made of the effects of the different initial energy of the source neutrons on the flux distribution in the seabed and seawater.

The thermal and fast neutron flux obtained in the two cases are presented in figures 4.4, 4.5 and 4.6. The flux is shown as a function of the distance L in two selected layers, each 5 cm thick. A layer immediately underlying the probe and an overlying seawater layer were selected, although calculations were made for several layers embodying a large thickness of seabed and seawater in the system.

The thermal neutron flux in the seabed and seawater layers (Figure 4.4) for ^{252}Cf show similar variations close to the source, though its magnitude in the seabed is slightly higher than in seawater. Beyond 10 cm a divergence of the flux is observed and at a distance of 50 cm the thermal flux in the seabed is about twice that in seawater. The fast neutron fluxes follow similar trends with distance in the two layers.

For comparison, the calculated flux (thermal and fast) for the 14 MeV monoenergetic source is plotted along with those obtained for ^{252}Cf (FIGURES 4.5 and 4.6). Near the source, the ^{252}Cf yields a thermal flux in the seabed layer which is about 3 times the corresponding flux for a 14 MeV source (curves 1 and 3). This is explained by the difference in the average initial neutron energy of the two sources, the low energy neutrons of ^{252}Cf producing a higher thermal flux within a relatively short distance from the source. A cross-over of the two thermal flux curves (1

and 3) is observed around 20 cm and the greater penetrability of the 14 MeV neutrons is apparent beyond this distance. In the seawater layer (FIGURE 4.6), this cross-over occurs at a shorter distance of 12 cm due to the higher moderation in seawater and the thermal flux follows the same trend as in the seabed layer.

The fast neutron flux in both the seabed and seawater are higher in magnitude for the 14 MeV source than observed with ^{252}Cf. In both the seabed and seawater layers, the distribution of the fast and thermal neutron flux shows that greater penetrability of the source neutrons can be achieved with a higher energy neutron source.

The benefits of increased penetration of 14 MeV neutrons must however be judged against any increase in radiation damage etc. resulting from increase in the fast flux at the detector position.

4.6.4 Neutron flux distribution in the seabed and its dependence on seawater content

The thermal neutron flux distribution in a silica-type seabed was calculated for three different levels of seawater content, since experimental efforts to simulate and measure the response in the laboratory proved ineffective. Seawater contents of 20%, 40% and 60% by weight were used to account for a wide variation in seabed saturation. Although values over 40% are unrealistically high in natural situations, nevertheless calculations were made to ascertain the effect of seawater content on the thermal flux distribution. The calculated flux for a seabed layer immediately underlying the probe considered in the experimental tank is given as a function of distance from the neutron source (FIGURE 4.7).

As expected the thermal flux is greatest near the source for the seabed containing 60% seawater, the lowest

flux being produced by a seawater content of 20%. The curves mutually cross-over at about 12 cms beyond which the curve for 60% seawater content exhibits the lowest thermal flux values. The thermal flux for the 40% seawater content gives intermediate values. Thermal fluxes computed for several deeper layers showed similar variations with distance. These curves show that at the cross-over point, the thermal flux in the seabed is independent of the seawater content. For distances beyond this point, the seabed with the highest seawater content produces the lowest thermal flux, the variation being more pronounced with distance.

4.6.5 Neutron flux distribution in seabeds containing elements with high neutron absorption cross-sections

The effect on the neutron flux distribution for various concentrations of particular trace elements was studied by the same model and source-detector geometry. Two elements copper (σ_a = 3.85 barns) and manganese (σ_a = 13.3 barns) were selected and different concentrations of each element were assumed to be uniformly distributed below the surface of a silica-type seabed containing a fixed seawater content of 20% by weight. The calculated spatial distributions of the thermal and fast neutron flux for 5% and 20% copper are shown in figures 4.8 and 4.9 respectively.

For both concentrations, the thermal flux in the seawater layer is higher than that in the seabed close to the source, but this condition is reversed at a distance greater than 15-20 cm. Comparing the layers with different Cu concentration, it is generally observed that in the seabed, the thermal flux with 20% Cu is lower than with 5% Cu for all distances from the source. This is due to the relatively higher absorption of thermal neutrons with

increase in concentration of copper. In seawater the thermal flux is practically the same for both percentages of copper, indicating little interaction across the seabed/seawater interface.

In the case of Mn, the thermal absorption cross-section is about 3.5 times that of Cu so that the problem of self-absorption of thermal neutrons is more significant. The flux distributions in this case are shown in figure 4.10. With 5% Mn, the thermal neutron flux distribution in the seabed and seawater is similar to that observed in the case of Cu with a cross-over at about 20 cm (curves 1 and 2). With 20% Mn, the thermal flux is however much lower in all cases reflecting the higher absorption rate of thermal neutrons within the seabed matrix.

4.6.6 General conclusions

Analysis of the neutron flux distributions for the different situations calculated, show that

(1) In seawater and in the seabed, the moderation of fast neutrons is accomplished within a relatively short distance from the source and the thermal neutron flux which provides the useful signal is greatest at the source.

(2) Changes in the nature of the seabed do not affect the neutron fluxes in the overlying seawater, so that the contribution to the background by this medium is a constant.

(3) Seabeds with different seawater content exhibit a common thermal flux at 12-15 cm and considering simple geometry in a probe, the optimum source-detector separation is in the range 20 - 30 cm.

and (4) Increase in the trace element concentration of an element will depress the thermal neutron flux and hence the signal. This will present calibration problems for a few elements.

4.7 Calculation of gamma-ray countrates at the detector

4.7.1 Calculation of the effective interrogation depth of the seabed by a neutron interaction probe

The effective depth of interrogation by a probe depends upon the depth of penetration of neutrons in the seabed and the subsequent attenuation of γ-rays in returning to the detector. Calculations were made to estimate these effects based on the probe design used in the experimental work for a source-to-detector distance of 35 cm. The results obtained are shown in figures 4.11 and 4.12. These refer to a 5% concentration of Cu distributed uniformly below the surface of the seabed containing 20% seawater by weight. Figure 4.11 shows the contours of the percentage contribution to the detector countrate from unit volume in terms of the maximum value close to the surface. Figure 4.12 displays the same data as percentage integral counts as a function of depth below the seabed. These results show that the effective thickness of seabed being sampled extends to about 10 - 15 cm. This depth is a function of the properties of the seabed, and hence on the seabed type, trace element concentration and seawater content. The source-detector distance for the type of probe system considered in these calculations would exert some influence on the depth sampled since their relative position determines the region of the seabed from which the contribution to the detector countrate is a maximum.

4.7.2 Calculations of the detector countrate and its variation with trace element concentration.

Computer calculations were made to study the relationship between countrate and elemental concentration for an artificial seabed of sand containing varying

concentrations of copper and manganese nodule material. In each case, the concentrations were uniform to a depth several times the effective depth sampled by a probe with source-detector separation 30 cm. The results are shown in figure 4.13. In the case of copper, the seawater content was assumed constant at 20%. For calculations relating to Mn nodules, the seawater content was varied from 20% to 40% to simulate different concentrations of nodule material in the seabed.

The range of concentrations for both elements considered in the calculations are unrealistically large (normal concentrations of manganese vary from 15% - 30% Mn and copper less than a few percent) but these calculations show the non-linearity in the relationship expected between countrates and elemental concentration of elements with significantly large absorption cross-section.

4.7.3 Calculations of the perturbation on the thermal neutron flux in the seabed due to shield components

Calculations of the thermal neutron flux in the seabed were made to investigate the effect of the lead shield, which has high neutron scattering properties. Figure 4.14 shows the data obtained both with and without the lead shield, replacing it in the latter case by polythene moderator. The enhanced thermal flux in the seabed due to the presence of the lead is observed in the distribution curves, which are shown as a function of distance from the neutron source.

The total uncollided gamma flux per source neutron at the detector was calculated for various positions of the lead shield with respect to the neutron source in the probe assembly. This variation is shown in figure 4.15 for a fixed source-detector separation of 35 cm. These results are discussed in a subsequent chapter in relation to the experimental work carried out.

CHAPTER 5

EXPERIMENTAL MEASUREMENTS IN THE SIMULATED SEABED

5.1 Introduction

It was mentioned in the introductory section in Chapter 4 that the development of the (n,γ) capture reaction as a technique for seabed analysis was undertaken by both experimental measurements and computer calculations in a simulated seabed. Importance has however been attached to experimental measurements, so that the results obtained for the complex situations studied in the simulated seabed environment could be directly applied to practical problems encountered in seabed analysis. The experimental data therefore form the basis on which the empirical relationships between the various parameters of the system have been established. These have been used to study the factors influencing the behaviour of the laboratory simulated seabed system and determine the limits of applicability of the computer calculations.

The main feature of the experimental work is the measurement of the energies and intensities of the characteristic γ-rays emitted by elements in the seabed in order to establish their identities and sensitivities of their detection. Since the measurements involved the response of the probe to gamma radiation, experimental work was considered important to investigate the factors which influence this response.

This Chapter describes the experimental work undertaken

(a) to demonstrate the feasibility of the neutron capture reaction as a technique for elemental analysis of the seabed

(b) to investigate the different parameters involved and their relationships in the development of the technique to seabed exploration

(c) to establish empirical relationships governing the physical events in the system in order that the method could be applied to any given seabed and environmental conditions

(d) to determine the lower limits of detectability of elements for a practical towed device on the seabed

and (e) to determine values of the parameters involved in constructing a seabed probe for optimum performance as a spectrometric device.

5.2 Establishment of 'infinite-geometry' conditions in the laboratory simulated seabed

5.2.1 General

The two principal media involved in seabed analysis are the seabed material and the overlying seawater. The boundaries of these are infinite in extent compared with the dimensions of a simple source-detector arrangement considered in seabed analysis. This would mean, that large volumes of material must be considered in laboratory experiments to simulate conditions existing on the seabed in order to obtain comparable results.

When large masses of material are involved, both neutron and gamma radiation are subject to many stages of interaction and on the seabed both unscattered and scattered radiation are able to reach a detector system. In a laboratory model where the material constituting the media have finite dimensions, there is a high probability of scattered radiation leaving the system and therefore a smaller fraction of the radiation present reaches the detector. Radiation from extraneous sources also contributes to the system and is able to invalidate the results of experimental measurements. Thus, the extent to which the physical conditions existing on the seabed are simulated in the laboratory is important from the point of

view of the reliability of data obtained from the laboratory model. Preliminary experiments were therefore conducted to determine the minimum dimensions of the experimental tank, depth of seabed material and height of seawater which would ideally simulate the seabed and its environment in terms of neutron and gamma transport.

5.2.2 Experimental tank

A test tank with dimensions 1.5 m^3 was constructed for the experiments and set up on a wooden platform in the centre of the laboratory so that constructional features of the room had little influence on the measurements. The tank was lined with polythene and partly filled with silica sand. This was saturated with seawater of salinity 34.5‰ measured at the ambient temperature of 19°C. A linear arrangement of a ^{252}Cf (2.5 μg) neutron source, a radiation shield and a high purity Ge detector of active volume 50 cm^3 were configured in axial symmetry on the sandbed. It was reasonable to expect under these conditions that the detector was sensitive only to changes in the quantities of seawater and seabed material in the tank.

5.2.3 Criterion for measurements

The criterion adopted in the experiments was that, for distances beyond the minimum dimensions required to establish 'infinite-geometry' conditions in the tank, the scattered gamma radiation reaching the detector would remain unchanged, if a further quantity of material with the same composition and density were introduced. Thus, the γ-ray response from the elements in the system was monitored for this purpose by determining the counts registered by the detector within a preset time. Net counts corresponding to the principal γ-ray energies of silicon, chlorine and hydrogen were used.

5.2.4 Depth of seabed

For a fixed depth of sand and source-to-detector distance, γ-ray spectra were obtained for the elements in the tank. Four different source-to-detector distances were used and a series of determinations were made by progressively increasing the depth of sand. The minimum depth of sand above which constant counts for silicon, chlorine and hydrogen were obtained was determined.

5.2.5 Height of seawater

A further set of experiments was conducted to determine the minimum height of seawater in the seabed. This was carried out in the tank described in Chapter 3 with the re-entrant tube resting on silica sand of depth 35 cms. The depth of sand was pre-determined as explained in the previous section and a depth of 35 cms. was selected to satisfy the criterion for conditions of 'infinite-geometry' as well as convenience in operating the detector and ancilliary equipment at this height in the tank. The neutron source, radiation shield and detector arrangment were the same as in the previous experiments.

Gamma-ray spectra were obtained in this case, for a fixed source-to-detector distance over a wide range of seawater heights. The minimum height above which the various counts in the seawater and seabed elements remain unchanged was determined.

5.2.6 Experimental results

Figures 5.1 and 5.2 show the results of the experiments to determine the minimum seabed depth for four source-detector separations. In these experiments a lead disc of thickness 3.8 cms served as a γ-ray shield and was positioned midway between source and detector. The rest of the radiation shield was of polythene. Several positions of the lead shield with reference to the neutron source were tried for a fixed source-to-detector distance and yielded results compatible with the configuration used.

The curves show the net counts in the full energy and double escape peaks of Si (3.539 MeV and 4.934 MeV), Cl (6.620 MeV and 7.790 MeV) and H (2.223 MeV) as a function of the depth of seabed. These indicate a saturation in the countrates beyond a depth of about 20 cms.

For determinations of the minimum height of seawater in the tank, a lead disc of thickness 7.2 cms was used as a γ-ray shield with various lengths of polythene as moderator. The same source-to-detector configuration was employed as in the earlier experiments. The results obtained for a selected source-to-detector distance of 29.7 cms from several experimental runs carried out are represented in figure 5.3. The net gamma counts in the energy peaks corresponding to silicon decrease at first and reach a constant value with increase of seawater in the tank. This initial decrease is principally due to the compaction of the sand with the addition of seawater thus altering the distance of the level of sand from the source-detector arrangement. For elements in seawater, i.e. chlorine and hydrogen, the counts increase from values corresponding to those of the saturated seabed to a constant response as shown. It is observed that beyond a seawater height of around 15-20 cms. no variation in the counts for silicon, chlorine and hydrogen occurs.

5.2.7 Geometry conditions represented in the experimental tank

The minimum dimensions determined by the foregoing experiments for the depth of sand and height of seawater would normally represent 'infinite-geometry' conditions in a laboratory model tank. However, due to restrictions imposed by the constructional features of the detector and its associated electronics, (see FIGURE 3.2) its attitude in the tank in relation to the boundaries of the materials conforms only to conditions of 'semi-infinite' geometry due to the absence of material in one dimension at the

detector. For low energies where the gamma quanta are subject to the greatest angular changes in scattering, the probability of quanta returning to the detector is greatest. For this reason any correction to account for the finiteness of the medium at the detector would be negligible for materials which strongly attenuate the low energy quanta. For the material in the tank and the range of gamma energies of interest in this work, this effect was considered negligible. No corrections were therefore made to the experimental data and the conditions simulated in the tank were accepted as adequately representing 'infinite-geometry' as in a marine environment.

5.3 Factors influencing the sensitivity of detection of elements in the seabed

5.3.1 Introduction

The sensitivity for detection of elements by a measuring system on the seabed is dependent on a number of factors, the most critical of these being the signal-to-background ratio. The useful signal is determined by the nuclear parameters of an element $\frac{I\sigma_a}{A}$, the strength of neutron source used, the efficiency and geometrical factors, but in the final analysis the magnitude of the background ultimately determines the minimum signal detectable.

In the seabed, background radiation forms an integral part of a gamma spectrum and is an important criterion in the detection and estimation of abundances of elemental constituents. The most significant contribution to the general background is from the seawater due to hydrogen and chlorine, which have high relative sensitivities of detection.

An additional component of detector background arises from the secondary gamma radiations produced by interactions between the source neutrons and the shielding and constructional materials of the probe. Most important of these are the capture γ-rays produced when a neutron is moderated and absorbed within the detector shield or probe casing. The γ-rays associated with the neutron source itself may in certain instances contribute significantly to a region of the spectrum of interest. Hence, an investigation of the origins of background radiation, its levels and its specific contribution to the observed spectra is important from the point of view of optimising the source-detector geometry in the probe to ensure a very high signal-to-background ratio.

5.3.2 Sources of background radiation

For purposes of this study, background radiation has been defined as any radiation detected by the probe which does not originate from the element or elements analysed. In this context two components are recognised.

(1) background from radiation associated with the probe system in a measurement. This includes gamma-radiation from the neutron source, shielding material and constructional materials of the probe.

and (2) a component associated with the environment in which the measurements are made. This constitutes the background from elements in seawater and seabed-type material which forms the matrix for the trace elements.

5.3.2.1 Contribution from neutron source

In this Section, an attempt has been made to compare the effects of γ-ray background due to two neutron sources, ^{252}Cf and $^{241}Am/Be$, which could both be appropriate in the

current application. These two neutron sources contrast significantly in terms of the different nuclear processes involved in neutron production, the difference in the mean energy of the neutrons and the detailed shape of the γ-ray spectrum associated with each. The neutron and gamma spectra of these two sources are shown in figure 5.4.

A. Californium-252

(1) Gamma spectrum

Radioisotope neutron sources have the general disadvantage of being associated with γ-rays and in ^{252}Cf, the gamma activity is derived from the processes of spontaneous fission, α- decay and from the equilibrium fission products. The significant contribution is from the fission prompt γ-rays and the gammas from the fission products (STODDARD 1965). The gamma contribution is about 5.7 per neutron emitted over the range 0.6 - 5.0 MeV so that an average energy of 1.0 MeV is assumed for the source gamma-rays.

(2) Neutron spectrum

The neutron radiation originates principally from spontaneous fission. A secondary source of neutrons is that due to (α,n) reactions following interactions of α-particles with light elements particularly oxygen. This contribution which is below 5 MeV constitutes a negligible proportion, 2.6×10^5 compared with the total emission rate 2.4×10^{12} per gram of the nuclide. The mean neutron energy for the source is 2.3 MeV and the spectrum shows a smooth variation free of fine structure extending over an energy range 0.6 - 13 MeV.

B. Americium/Beryllium

(1) Gamma spectrum

In ^{241}Am/Be, γ-rays are produced by the decay of the α- emitter and de-excitation of nuclei formed by induced reactions. An abundance of high energy γ-rays are produced at an energy of 4.43 MeV. Since the output of Be(α,η) sources is typically 60 neutrons per 10^6 α- particles, the intensity of the de-excited γ-rays will normally be low in comparison with the α- emitter γ-rays. Thus the γ-ray emission per neutron is about 0.7 at 4.43 MeV from the (α,n) reaction compared with 6×10^3 from the α- decay of ^{241}Am predominantly at 600 keV.

(2) Neutron spectrum

Peaks are observed at several energies the most dominant being at 3.3 MeV, 4.3 MeV, 5 MeV, 6.8 MeV and 7.7 MeV. A high energy component occurs at about 9.5 MeV though of very low intensity. A mean neutron energy of 400 keV is assumed for the low energy component and an average value of 4.6 MeV is typical for the high energy component of the source spectrum.

5.3.2.2 Comparison of neutron and gamma source spectra of ^{252}Cf and ^{241}Am/Be

A comparison of the neutron and gamma source spectra shows a distinct difference in the average neutron and gamma energies associated with these sources. ^{252}Cf has a low average neutron and gamma energy, 2.3 MeV and 1.0 MeV respectively, and a smooth variation in the high energy region representing typically a fission spectrum. ^{241}Am/Be has correspondingly higher average values, 4.3 MeV, and several high energy components in its gamma spectrum. For an unshielded source, these energies would yield higher backgrounds due to the increased probability of threshold reactions with light elements.

5.3.2.3 Experimental comparison of source backgrounds in observed γ-spectra in the simulated seabed

The gamma spectra obtained are for a silica seabed containing 4.3% Mn using ^{252}Cf and $^{241}Am/Be$ sources. The same source-detector geometry was adopted in both sets of experiments and a lead shield 10 cms. thick was used as an attenuator of the source γ-rays. The strength of the two sources in terms of neutron output was 4.28×10^6 n.sec^{-1} for ^{252}Cf and 2.5×10^6 n.sec^{-1} for $^{241}Am/Be$. Under the conditions of the experiment it was not possible to isolate the background radiations due to the individual sources from the general background observed. Instead, a comparison of the effects due to the different source characteristics has been considered.

Figures 5.5 and 5.6 show the differential γ-ray energy spectra obtained with the two sources for a seabed containing 4.3% manganese. The general background arises mainly from Compton scattering events in the detector, gamma emissions by elements in the seabed and seawater and from unresolved low intensity γ-rays. The contribution of the source γ-rays is considered as a constant background radiation to this general background level.

To ascertain whether the source gamma photons contribute significantly to the general background it is necessary to identify characteristic lines such as those observed in the source spectrum. In the case of ^{252}Cf, no characteristic lines are found in its source spectrum and the direct effect of source radiation to the general spectrum cannot be readily observed. With $^{241}Am/Be$ an energy line corresponding to 4.43 MeV should be identifiable. This however is not apparent in figure 5.6 and it is reasonable to assume that the effect of source gamma radiation is small under the shielding conditions of the experiment.

Comparison of the spectra reveals certain features in the spectrum obtained with the $^{241}Am/Be$ neutron source which are absent in that obtained with ^{252}Cf. These are the inelastic scattering events due to the interaction of fast neutrons with oxygen in the seabed and seawater. The double-escape peak due to this reaction $^{16}O(n,n'\gamma)$ is clearly resolved. Other possible reactions with polythene (^{12}C) and the seabed material (^{28}Si) are hardly visible in the appropriate energy region. A general conclusion is that these reactions do not interfere with the general background and $^{241}Am/Be$ sources can be used in a probe for seabed analysis.

Although individual characteristics of the source spectra are not identifiable, a comparison of the backgrounds has been made by taking ratios of countrates. It is assumed, that if there is no significant contribution from the source γ-rays to the general background level in the spectra, then the ratio of the counts in corresponding energy peaks as well as their backgrounds would be similar and equal to the ratio of the strengths of the two sources. A departure of these ratios from this value would imply a significant contribution from the individual source backgrounds to the general background in the spectrum.

Table 5.1 gives the ratios computed from the spectra obtained with the two neutron sources. The ratio of the net peak counts for hydrogen, chlorine and manganese are seen to be constant within the statistical errors of measurement and agree quite well with the ratios of the corresponding background counts. These values are also consistent with the ratio of the total countrates 1.67 ± 0.02 observed for four different source-to-detector distances. These however are found to be lower than the ratio of their source strengths which is 1.71 ± 0.001. This discrepancy may be due to the difference in the spatial thermal neutron flux distribution in the seabed

arising out of the higher initial neutron energies of ^{241}Am/Be.

The results of experiments show that the source γ-ray backgrounds resulting from a high energy neutron source such as ^{241}Am/Be have little effect on the general background of a seabed spectrum and are not significant in the method developed for seabed analysis. A greater penetration of neutrons may be obtained using ^{241}Am/Be but with limitations imposed on the size of source and source-to-detector distance in a practical system, this would not be a particular advantage.

5.3.3 The effect of using different gamma shielding material on the detector response

5.3.3.1 General

In seabed analysis, the need for alternative shielding material in a probe may arise if the element sought is in a class of materials commonly used for shielding purposes. Typical materials such as lead, platinum, tungsten and tin normally used in shielding γ-rays in spectrometric applications may themselves be candidates in a seabed exploration programme. In such instances, an alternative material has to be found for a radiation shield. In order to assess the characteristics of two common materials which may be considered in a seabed probe and their effect on the general background, the performance of lead and tin has been compared experimentally.

5.3.3.2 Physical and nuclear properties

Lead and tin have good properties as shielding material for gamma-rays, i.e. a high density and high atomic number. As a γ-ray shield they are particularly effective against low energy gamma photons because of the high photo-electric absorption and also against high energy gamma photons because of the high pair-production cross-

section. Apart from these basic requirements, they have comparatively low thermal absorption cross-sections for incorporation in a probe for seabed analysis. Table 5.2 lists the important physical properties and nuclear data for some elements considered in γ-ray shields.

5.3.3.3 Gamma-ray attenuation

Gamma-ray attenuation is an important criterion of the effectiveness of a material in shielding. Figure 5.7 represents the variation of the mass attenuation coefficients (μ/ρ) for these elements in the energy range 1-10 MeV. The general form of the curves is a high attenuation coefficient at low energies falling steeply with increasing γ-ray energy to a characteristic minimum and progressively increasing to a more or less constant high value in the higher energy region. The minima occur at 3 MeV for lead and at about 4.5 MeV for tin.

The attenuation of gamma photons in a shield for various energies was computed for comparison, as the fractional incident photons removed by the shield in passing through a thickness of 10 cms of the material. A comparison of these values gives a ratio of 1.016 (lead to tin) for 1 MeV gamma photons and 1.076 for photons of mean energy 4.5 MeV. The values and ratios computed for other energies imply that lead is marginally more efficient than tin in its attenuation of gamma photons at all energies and by comparison is a better attenuator at high energies. For equal thicknesses of lead and tin, the performance of these materials as shielding against source radiation is more or less similar for a ^{252}Cf neutron source. Lead, however is more effective for use with a $^{241}Am/Be$ source since the energy for tin for which the attenuation coefficient is a minimum is also the average γ-ray energy of this source.

5.3.3.4 Gamma-radiation from (n,γ) capture reaction

5.3.3.4a General comments

An important discriminating factor in a comparative study is the investigation of the production of undesirable gamma radiation from thermal neutron capture in lead and tin which contributes to the general background in an observed spectrum. This eventually governs the choice of the alternative shield material depending on the nature and distribution of the radiation produced by the shield in the energy range of interest in a spectrum. A point worth noting is that a material which produces a single identifiable energy line by thermal neutron capture is a better choice than one which gives a series of poorly resolved energy lines over a wide energy range of a spectrum. For this reason the capture γ-rays of lead and tin are discussed.

(A) Lead

For the natural element, the prominent gamma rays due to neutron capture in lead are 7.368 MeV from ^{208}Pb with an intensity of 94.77% and 6.736 MeV from ^{207}Pb having a low intensity of 5.08%. The spectral distribution is given in Nuclear Data Tables. (GROCHEV, BARTHOLEMEW et al 1969).

(B) Tin

Since the natural element has no fewer than 10 isotopes, the capture γ-rays have a very wide distribution of energies over the range 0.2 MeV - 9.0 MeV and of very low intensity. The distribution is given in Nuclear Data Tables (GROCHEV, BARTHOLEMEW et al 1968).

The highest intensity γ-rays are centred around 2.65 MeV with a significant contribution from a large number of γ-rays of low intensity below 5 MeV. No characteristic lines of high intensity are observed but a general contribution to the background may be expected on account of the wide spectral distribution.

5.3.3.5 Experimental determinations

5.3.3.5a General

The experiments conducted were for a simulated silica seabed containing 24% zinc and 6% sulphur using lead or tin shields of identical dimensions (cylinders of diameter 7.5 cms and length 10.0 cms). The measured γ-ray spectra are shown in Figures 5.8 and 5.9 and were obtained with a 2.5 μg ^{252}Cf neutron source and a counting time of 120 mins for a source-detector distance of 30 cm. Five other source-detector separations were used and the results from these were considered in the analysis.

5.3.3.5b Objective of the experiments

The general background radiation levels were studied in the two cases in an attempt to identify the contributions from

(1) gamma radiation associated with the ^{252}Cf source and

and (2) gamma radiation from neutron interactions with shield material from the (η,γ) reaction

For this purpose, ratios of the peak counts and background counts were computed for the corresponding γ-ray energies in both spectra. These ratios should be fairly constant if there is no significant contribution to the general level of background radiation. The tabulated results are given in Table 5.3.

5.3.3.5c Discussion of the results

A general comparison of the spectra reveals an increase in the level of background in the case of tin, below 4 MeV. The ratios of the background counts in the spectra also reflect this increase and is most noticeable for the background ratios obtained for the regions 3.0 -

3.3 MeV and 2.5 - 2.6 MeV. This is consistent with the background ratios obtained in the case of hydrogen 2.223 MeV.

The prominent γ-rays of lead (7.368 MeV/6.736 MeV) were not identified. In the case of tin, no spectral lines were visible. This is due to the very low intensities and the inability of the detector to resolve some of the lines from the general background.

The increase in the general background observed in the spectrum obtained with the tin shield could be attributed to several effects. Perturbations in the neutron flux distribution could occur due to the slightly different neutron scattering properties of tin and lead. If such a change were significant, then the ratios of the counts in the photo-peaks for the seabed and seawater elements will be the same as the background ratios in the entire energy range of the spectra, since both spectra were obtained under the same conditions of geometry. The constancy of the ratios in the energy region 4 - 8 MeV show that such an effect is small and unobservable.

Therefore, the change in the background below 4 MeV could be the net result of two effects. The lower attenuation of the source γ-rays in tin could provide a noticeable increase in the observed spectrum, since the relative intensity of the fission gammas is significant in the energy range below 4 MeV. The second effect is the contribution from the capture γ-rays of tin which are most effective in the region below 4 MeV. These could enhance the general background but are of very low intensity and unlikely to be resolved into individual peaks. Under the conditions of the experiment, it was thus not possible to isolate the contributions from each of these effects from the general background and the higher background observed for tin is due to the sum of these two effects. The ratio

of the total countrates obtained for other source-to-detector distances show values consistent with changes in the background observed for these distances. These are given in Table 5.4.

5.3.3.5d Observations on the experimental results

The choice of gamma shielding material for a probe should be considered on the following characteristics:

(1) the transmission of source γ-rays in the material. This decides the thickness of shielding and hence the limitations imposed on the source-to-detector distance in a probe.

(2) the probability of neutron interactions with the material. High intensity γ-rays could interfere with characteristic energy lines of elements sought on the seabed and a significant contribution to the background radiation could lower the sensitivity of detection.

and (3) the effective increase in the total countrate of the system due to significant background contribution by a material. A high countrate would be a limiting factor in maintaining good detector resolution.

5.3.4 Effects of background radiation from the marine environment on the limits of detection of seabed elements

5.3.4.1 Introduction

In the analysis of seabed sediments, the main background in a gamma spectrum is due to constituent elements of seawater and the seabed type elements which form the matrix composition. It arises principally from

neutron capture and inelastic scattering reactions in the matrix elements, especially from chlorine in seawater. These peaks are superimposed on a continuous background mainly from Compton scattering in the detector. The background radiation in the energy range 5 - 10 MeV is particularly important since most of the characteristic energies of elements of interest in seabed exploration lie in this energy region. The sensitivity for detection of elements is dependent on this general background and is therefore important from the point of view of ascertaining the scope and limitations of the nuclear technique.

5.3.4.2 Experimental data

Gamma-ray spectra were obtained for concentrations of several elements distributed uniformly in a silica seabed in the experimental tank. The mean measured seawater content in the sand matrix was 24 ± 3% by weight. A 2.5 μg Californium-252 neutron source was used in the probe for a counting time of 120 min in each case and for several source-to-detector distances, using a high purity Ge detector of 50 cc. active volume. Spectra in pure seawater and in a pure silica seabed were also obtained under the same experimental conditions for purposes of comparison.

5.3.4.3 Analyses of gamma-ray spectra

The spectrum for seawater (FIGURE 5.10) is typical of background countrates for an off-bottom measurement on a seabed survey. The gamma spectrum consists of a series of well resolved energy peaks due to chlorine and hydrogen (not shown in the figure), superimposed on the general Compton background. The entire spectral distribution covers the principal energies of chlorine and their multiple peaks due to pair production in the detector. A complete list of these energies and their corresponding intensities are given by DUFFY and EL-KADY (1970).

A comparison of the seawater spectrum with that obtained for a pure silica seabed (FIGURE 5.11) shows that in the energy region greater than 5 MeV, the backgrounds are similar. Below 5 MeV, the general background level increases progressively and at 3 MeV an increase of about 20% of the background at 5 MeV is observed. This is due to the gamma lines of silicon from the seabed and the Compton distribution for these energies which form the additional component of the background. Above 5 MeV the background due to chlorine again dominates the spectrum and the effect of the low intensity lines due to silicon is hardly noticeable in the general levels observed. Hence, in the absence of any trace elements, figure 5.11 would represent a typical γ-ray spectrum for a towed device on a silica type seabed.

The relevant data for some of the seabed elements for which gamma spectra were obtained are listed in Table 5.5. The concentrations of the elements are small, i.e. less than 5% except in the case of zinc (24%) so that the silica content in the seabed matrix would not be materially different in all the experiments. The background levels above 5 MeV would therefore be expected to be more or less the same in these spectra. The individual spectra for these elements are given in Figures 5.12 to 5.18 for a source-to-detector distance of 30 cms and for the same data acquisition time.

Individual spectra were compared with that of figure 5.11 which represents the same seabed type matrix for all the elements. The general background in all these spectra is the same within the limits of error of the measurements. This is particularly apparent in the energy range 5 - 10 MeV. The Compton scattering contributions from individual elements to the spectra are small, so that in effect, the presence of the elements in relatively small concentrations has not altered the general levels of background from the

seabed. The differences in the countrates observed in some spectra are due to the slightly different gain settings on the spectrometer used in the accumulation of these spectra and normalisation with respect to the background level in the silica seabed spectrum shows the similarity in these levels. The ratios of the net counts in some selected chlorine energy lines in the higher energy regions were taken with respect to hydrogen (2.223 MeV). These yielded similar values showing the constancy of the seawater contribution to all the spectra. The ratios are given in Table 5.6.

5.3.4.4 Background spectra of some common seabed type elements

The γ-ray spectra for two common seabed type elements were obtained under the same experimental conditions. These are for calcium carbonate and clay. A third spectrum for a mixed seabed consisting of equal percentages by weight of silica (SiO_2) and $CaCO_3$ was also obtained. These are shown in figures 5.19 - 5.21.

In the case of calcium carbonate (40% Ca) the general background in the region greater than 5 MeV is the same as for a pure silica (46% Si) seabed as shown in Figure 5.11. The spectrum for calcium carbonate however shows characteristic gamma lines at 6.420 MeV for Ca and its associated, single and double-escape peaks. Below 5 MeV, the general Compton background level is lower than for silicon. The level for the mixed seabed of calcium carbonate and silica is identical to that obtained for pure silica.

For the seabed consisting entirely of clay, energy lines from alluminium 7.724 MeV and silicon 3.539 MeV and 4.934 MeV are clearly resolved in the spectrum in addition to the general background contribution from chlorine in the seawater. These levels are consistent with those obtained for silica and calcium carbonate type seabeds and for the seawater content in the material used for the experiments.

5.3.4.5 Conclusions

The background radiation levels measured experimentally are for a probe with cylindrical geometry since this is the most likely form for a simple towed device on the seabed. The influence of seawater is high for such geometry and the background is constant and dominated by chlorine and to a lesser degree by the seabed matrix elements. The presence of small concentrations of trace elements i.e. less than 5% in the case of elements with high thermal neutron absorption cross-section, does not significantly alter the background. This general level of background is an integral part of all spectral determinations made on the seabed. Any attempt to increase the sensitivity for detection of an element requires the reduction of this background. This could be achieved if the topography of the seabed and the form of the towing vehicle, e.g. submersible, permits the use of a probe design of non-cylindrical geometry that would substantially reduce the effect of chlorine in the seawater.

5.4 The Gamma ray sensitivity of seabed elements as a function of source-to-detector distance

5.4.1 General

For a given geometry of measurement, the countrate in the detector for a particular γ-ray energy is a function of the neutron source strength, source-to-detector distance and the gamma attenuation characteristics of the media in the system. The attenuation itself is complex involving several factors, the most important of which is the composition of the seabed matrix. Correlation of the attenuation coefficient in terms of known parameters is difficult due to the complexity of the several processes involved in the transport of gamma photons to the detector. Therefore for a given type of seabed and strength of neutron source, the nature of the variation of the detector countrate with source-to-detector distance has been

investigated experimentally. The results are considered important from the point of view of:

(1) establishing the strength of neutron source in a seabed application that would give statistically significant countrates for a selected source-to-detector distance in a probe

and (2) ascertaining the nature of the gamma attenuation in the system so that a comparison of the individual contributions from seawater and seabed elements to the total countrate in the detector could be made.

5.4.2 Experimental Determinations

Capture γ-ray spectra were obtained for different elements distributed uniformly in a silica sand matrix using a 2.5 μg ^{252}Cf neutron source and a 50 cc. high purity Ge detector as in the earlier experiments. The measurements were conducted under the same geometry conditions, for a range of source-to-detector distances, which is of practical interest in applications to the seabed and within the constraints imposed by the technique. The principal γ-rays corresponding to the elements were used as indices of sensitivity for their detection. Countrates of hydrogen and chlorine from the seawater and the principal element of the seabed type, e.g. silica, calcium were also computed.

Since the number of measurements conducted for this purpose was considerable, data relating only to some selected elements are represented in the figures. However, the results derived are from an analyses of the data from all the measurements carried out, for this purpose.

5.4.3 Data Analyses

Data obtained from the gamma-spectra were fed into the Computer (HARWELL, IBM 3018K) as input for a regression analysis using a multivariable regression programme written in FORTRAN and based on the minimising programme LSFIT. This programme fitted experimental data to different types of equations, (linear, polynomial, exponential etc). After an initial trial with the data for hydrogen the best fit obtained was an exponential function and this was adopted for the rest of the data.

The countrate ϕ, for any γ-ray as a function of source strength S, and source-to-detector distance L can be described by an expression of the form

$$\phi\ (S,L) = \phi_o \exp\ (-\alpha L) \qquad (A)$$

where ϕ_o and α can be determined by regression analysis of the experimental data. ϕ_o can generally be evaluated in terms of a neutron source of known strength and α is related to the attenuation characteristics of the media involved in the transmission of the gamma quanta.

In the above expression α has the dimensions cm^{-1} and thus represents a constant related to the linear attenuation coefficient for a γ-ray of a particular energy in the material media of the system. Since measurements were carried out with the source-detector arrangement located at the seawater-seabed interface, both the saturated seabed and the overlying seawater are involved in the propagation of the γ-rays.

The production of γ-rays is principally determined by the thermal neutron flux distribution within the system and the spatial distribution of the γ-rays governs the media in which they travel to reach the detector. The complexity of

the system is best understood by referring to the seabed under study. For a point source such as ^{252}Cf and for the source-detector geometry considered in the experiments, both the thermal and fast neutron flux distributions are spatially different in the seawater and in the seabed as shown by Monte Carlo calculations (FIGURE 4.4). This is a direct consequence of the difference in the material composition of the two media and the nuclear properties of the constituent elements. The resulting gamma flux distributions for seawater and seabed elements would therefore be spatially different for the various capture γ-rays produced. Hence, for a given geometry of source and detector configured on the seabed, the spatial capture γ-ray distribution for the seawater elements in the upper half space would be virtually the same for all seabed situations and is governed only by the seawater constituents. The gamma flux distribution in the seabed would however vary according to the trace element, its concentration and its thermal neutron absorption cross-section. Monte Carlo calculations have shown that the highest thermal neutron flux in the seabed is generated near the source, but the region of maximum contribution to the detector countrate by the resulting γ-rays is a compromise between the neutron transport in the seabed and the attenuation of these gamma rays in reaching the detector. This is illustrated in figure 4.11 in the case of a silica seabed containing 5% copper for which the γ-ray countrates were computed for a selected source-to-detector separation of 35 cms. The maximum γ-ray countrate is from a region in the seabed approximately half-way between source and detector. This region would vary, since both the thermal and gamma flux distributions are spatially dependent, and would be a function of the distance of the detector from the source. Thus the value of α obtained by experiment would not ideally represent a simple attenuation of gamma photons from a single source in the seabed. This is also seen from figure 4.11 where the total contribution

to the detector countrate is from the effective volume distribution within the seabed material, the importance of these contributions diminishing as a function of depth. Nevertheless, the constancy of the values obtained for α in almost all seabeds containing concentrations of trace elements suggest that α could be interpreted as an effective attenuation function for the seabed system considered as a whole.

5.4.4 Discussion of the results

Figures 5.22 and 5.23 show the results obtained for the 2.223 MeV characteristic gamma-ray of hydrogen and some of the important chlorine γ-ray energies from two seabed types, e.g. silica and calcium carbonate. The data presented in each case are semi-logarithmic plots of countrate (counts in 120 mins.) as ordinate and source-to-detector distance L as abscissa. Results from similar experiments for seawater and for a silica sandbed containing pure water are also included.

5.4.4.1 Values of 'α' for seawater elements

A. Hydrogen

Table 5.7 gives the values of α obtained for the 2.223 MeV gamma-ray which is the predominant energy in any seabed spectrum for seabeds containing various trace elements. The values of α obtained are fairly constant for the seabeds with different elements and an average value of -0.0870 ± 0.001 compares well with that for pure seawater which is only slightly different.

The contribution to the countrate in the detector arises mainly from the γ-rays in the seawater overlying the sediments and from the saturated seabed. A contribution from the hydrogen in the polythene material incorporated in the radiation shield also enhances the countrate. Since the thickness of the polythene was progressively increased for different source-detector distances the value of α

obtained will not necessarily correspond to the linear attenuation coefficient μ of a 2.223 MeV γ-ray in a seawater medium. For a γ-ray of this energy in seawater, assuming a parallel beam of photons and neglecting the contribution to the countrate due to multiple scattering the corresponding value for μ is -0.0472. This is a factor of about 1.8 lower than that obtained by measurement.

The countrates represented in figure 5.22 as a function of source-to-detector distance show an exponential decrease with distance for the situations given. The near parallelism of the graphs show the constancy of the value of α in all these cases, within the errors quoted for the countrates (<0.6 percent).

(B) Chlorine

For chlorine, similar exponential relationships were observed as for hydrogen. The data are shown in figure 5.23. The values of α obtained from regression analysis are higher than those computed under ideal conditions in seawater. Table 5.8 gives these values for the principal chlorine energies and the corresponding computed values μ.

5.4.4.2 Values of 'α' for seabed elements

The variation in the countrate with source-to-detector distance L is shown in figure 5.24. Five different elements representing a wide range of gamma energies were selected from the experiments to study the characteristics of the seabed media. Silicon and calcium are common seabed type elements while the rest are minor elements uniformly distributed as concentrations within the silica seabed.

These elements also show an exponential decrease in the countrates for the characteristic energies with increasing source-to-detector separations. Slight variations in the values of α are observed. Table 5.9

gives the measured values obtained for α for the energies listed and the corresponding computed values of the linear attenuation coefficients μ for the various seabeds in which the elements were seeded, assuming the attenuation to take place only in the seabed matrix.

The values of α obtained in each case by experiment are found to be slightly lower than the corresponding calculated values.

5.4.5 Conclusions

For seawater constituents and for the elements in the seabed the variation of the countrate observed is exponential with source-to-detector distance. The attenuation itself is complex and for this reason the measured coefficient α is associated with the attenuation in the entire system rather than in a particular medium. The values obtained for 'α' have been presented as a function of γ-ray energy in Figure 5.25.

For seabed elements α is lower than the corresponding linear attenuation coefficient μ computed by assuming the attenuation to take place in the seabed material only and for conditions of narrow-beam geometry. In the case of the seawater elements the reverse is observed for chlorine and hydrogen. This may be attributed to the difference in the spatial distribution of the thermal neutron flux in the seabed and seawater media which governs the gamma flux. Since the flux in the seawater falls at a faster rate than in the seabed with distance, this may be reflected in the apparent increase in α observed for the elements of seawater.

5.5 Factors affecting the calibration of a neutron-interaction probe

5.5.1 Introduction

An important aspect of the experimental work pertaining to the nuclear technique is the design of an operational probe for seabed analysis. The calibration of such a probe depends primarily on the thermal neutron flux distribution in the seabed and its relative contributions between the thermalising effects of seawater and the absorption due to elements of relatively high capture cross-section. The effects arising from these conditions have been investigated in order to determine the limitations of this technique to practical applications in the seabed and to interpret the data obtained from a probe system.

5.5.2 The effective depth of seabed sampled

5.5.2.1 General

The effective depth of seabed sampled by a probe is an important parameter of the method and depends on

(1) the depth of penetration of the source neutrons

and (2) the subsequent attenuation of the capture γ-rays in reaching the detector.

Monte Carlo calculations presented earlier in Chapter 4 (Section 4.3) relating to some selected elements show that the thermal neutron flux in the seabed matrix governs the depth of penetration of the source neutrons. The attenuation of the capture γ-rays produced by these neutrons generally determine the detector response and controls the effective depth sampled.

5.5.2.2 Depth of penetration

The important feature of the flux distributions discussed in section 4.3 is the near exponential fall off

in magnitude of the flux with distance from the source. In all these instances, a well thermalised spectrum is achieved within a relatively short distance. With increase in the trace element concentration in the seabed the thermal flux decreases so that fewer reactions take place at the same depth. Also with the same seabed characteristics, a higher thermal flux distribution is achieved by neutrons of high initial energy at a greater depth. This is clearly observed in the seabed for which thermal flux distributions were computed using a ^{252}Cf point source and 14 MeV monoenergetic source of neutrons.

The results from Monte Carlo calculations show that the depth of penetration of neutrons is governed by the initial energy of the neutrons and also on the macroscopic total absorption cross-section of the seabed matrix. This implies that for the same spectral energy distribution of the source neutrons different degrees of penetration can be achieved in seabeds of different nuclear properties. On the other hand, for seabeds of similar composition a greater degree of penetration is obtained with a source of high initial energy.

5.5.2.3 Gamma-ray attenuation

The gamma-ray flux at the detector due to an element in the seabed at a depth r from the detector is given by,

$$\Gamma = \int_v \phi(r).\Sigma_n.f.\Omega.\exp - \sum(\Sigma_i.di).dv$$

where $\phi(r)$ is the thermal neutron flux at $\underline{r}$, Σ_n is the macroscopic cross-section for (n,γ) reaction, f is number of γ-rays emitted per interaction, Ω is the solid angle subtended by the detector at $\underline{r}$, di is the path length in the ith material in the seabed matrix for the γ-rays travelling within Ω, Σ_i is the total macroscopic cross-section in the ith material and dv is the volume element considered at $\underline{r}$.

Of special significance is the exponential factor which effectively governs the gamma flux at the detector. It represents the total attenuation due to the seabed material and is a function of the γ-ray energy. Hence, the countrate in the detector due to a source of gamma photons from a seabed element would greatly depend on the particular energy of the γ-ray and the distance travelled in the seabed before reaching the detector. This distance would vary according to the trace element concentration of high Σ_i that would significantly contribute to the attenuation, and the seawater content of the seabed matrix.

5.5.2.4 Effective depth sampled

The effective depth of seabed sampled by the source neutrons is thus a combination of the processes of neutron transport in the seabed and the subsequent γ-ray attenuation. This is a variable parameter, which is a function of the energy of the source neutrons, and the nuclear and gamma attenuation characteristics of the seabed. Monte Carlo calculations supported by experimental measurements show that for common seabed materials encountered in marine surveys and for small trace element concentrations, the effective depth of seabed sampled using a ^{252}Cf source is fairly constant 10-15 cms. for a probe design similar to that used in the experimental work.

5.5.2.5 Results of experimental work

The results of calculations made in Chapter 4 were verified experimentally in the case of copper and nickel 'seeded' separately in various thicknesses of the simulated seabed below the probe. The data obtained with a 2.5 μg ^{252}Cf neutron source are presented in Figures 5.26 and 5.27. Figure 5.26 shows the countrates obtained in the copper 7.915 MeV full-energy peak for two percentages, 2.5% and 5.0% copper uniformly distributed in the various layers for a source-detector separation of 30 cm. Similar results

are displayed in Figure 5.27 for a silica seabed containing 3% nickel. In this case, the detector countrate in the 8.999 MeV full-energy peak of nickel is shown for three different source-detector separations as a function of depth of the 'seeded' layer. The saturation effect with increasing depth can be clearly observed suggesting an effective sampling depth of about 10-15 cm which is in agreement with the results obtained from Monte Carlo calculations.

The depth of sampling has also been investigated experimentally for a calcium carbonate seabed. The countrates obtained for the 6.420 MeV gamma-ray (full and double-escape peaks) of calcium, as a function of the depth of the calcium carbonate layer for three different source-to-detector distances are shown in Figures 5.28 and 5.29. The integral counts show a saturation from about 10-15 cms. which agree well with the rest of the data.

From the experimental results obtained for copper, an early saturation in the 7.915 MeV full-energy peak countrate is indicated for 2.5% copper in the simulated seabed relative to the higher percentage of 5%. This seems to suggest that for a fixed source-detector separation, the effective depth of sampling may be smaller for low abundances of elements. The source-detector separation is also found to exert some influence on the effective depth of seabed sampled. For the seabeds containing 3% nickel and calcium carbonate, saturation in the respective γ-ray peak countrates are observed at shallower depths for large source-detector separations. Hence, greater depths of sampling may be obtained in a seabed with small source-detector separations in a neutron interaction probe.

Both these effects however are small considering the low percentage abundances of elements which are normally found on the seabed and the limitations imposed on the

source-detector distance in a probe assembly. Nevertheless, these results show the limits of the depth of interrogation using this technique for the particular geometry of measurement considered in seabed analysis.

5.5.3 The effect of the perturbations on the spatial distribution of the thermal neutron flux due to variations in the matrix elemental concentration

5.5.3.1 Introduction

Large variations in the abundance of elements with significantly high neutron absorption cross-sections will affect the linearity of the countrate with elemental concentration. This is important since the effective sampling depth is small compared with typical source-to-detector distances (30 cm in the present experimental system). The effect would create problems in calibration and interpretation of data from a seabed containing high concentrations of these elements.

Monte Carlo calculations of these effects were made for an artificial seabed of sand (SiO_2) containing varying concentrations of copper and manganese nodule material. These are presented in section 4.7.2 of Chapter 4.

5.5.3.2 Discussion of the computed results

The relevant data are presented in Figure 4.13. For copper (σ_a = 3.9 barns) the detector countrate increases with percentage concentration though not linearly. For concentrations less than about 5% the relationship is near linear and above this value the non-linearity is more pronounced. At 40%, the countrate has increased only by a factor of 2.5 of its value at 10%. Beyond 40% there is a decreasing trend in countrate for a further increase in concentration of copper.

In the case of manganese, the variation in countrate is steeper than it is for copper, a large change in countrate occurring for concentrations up to about 10%.

Beyond 10%, the curve assumes a gentler slope and a well defined maximum is seen to occur at about 20%. For concentrations greater than 20%, the countrate decreases and for 40% it is virtually the same as for a concentration of 10%. This implies that ambiguities might arise in practice when exploring for such elements which may lead to uncertainties in the measured concentrations.

5.5.3.3 Experimental work carried out

To verify the results of computation experimentally for the same probe geometry modelled in the Monte Carlo calculations, the variation in peak countrate (full-energy) for the principal γ-ray energies of copper and manganese for three different concentrations was determined. The results are shown in Figures 5.30 and 5.31 for a 15 cm layer in each case, which is about the effective depth sampled by the probe. The calculated response curves taken from Figure 4.13 are shown superimposed on the experimental data for comparison. In figures 5.30 and 5.31, the peak countrates for copper and manganese have been calculated in absolute terms based on measured values of the efficiency of the spectrometer used.

Although the range of concentrations covered in the experiments is small, nevertheless the experimental curves follow closely the trends predicted by Monte Carlo computations. In the curves obtained for copper and manganese, the non-linearity in the countrates for the various percentage concentrations is clearly observed. Both the shape and magnitude of the effects are in close agreement with those of the calculations. In the case of manganese the maximum countrate for the 7.244 MeV gamma ray can be predicted to occur close to a concentration of about 20%. This is deduced from the trend of this curve beyond a concentration of 15% Mn.

5.5.3.4 The implications of seabed analysis for elements with a high thermal neutron absorption cross-section

The reaction rate in most materials in the seabed would be the same, if the shape of the spatial distribution of the thermal neutron flux were to remain constant. Since the thermal absorption cross-sections vary inversely as the neutron velocity ($\frac{1}{v}$ dependence) the product of neutron flux (increasingly proportional to v) and the cross-section would remain unchanged. In the seabed, neutrons entering the thermal group would diffuse in a manner which depends on the scattering and absorption cross-sections. Elements having a high absorption cross-section such as manganese (σ_a = 13.3 barns) compared with copper (σ_a = 3.9 barns) can significantly alter the spatial thermal flux distribution and create a depression in the flux. This effect would be more pronounced near the source region where the maximum thermal flux is produced.

In a probe with relatively large source-to-detector distances, i.e. 30 cm or more in a practical system, a large change in the flux would manifest itself in a significant lowering of the detector countrate. In prospecting for an element such as manganese, this could be interpreted as a genuine decrease in the percentage of manganese in the seabed or a diminution of the flux, due to a substantially large increase in the manganese concentration. Ideally, if the thermal neutron flux in the seabed could be monitored continuously, the countrate can be directly related to the percentage abundance of the element. In the absence of this facility, the ambiguity can be resolved to obtain meaningful values for the manganese concentrations.

A method suggested is the simultaneous monitoring of the background in a region of the spectrum where no contribution from the element (manganese in this case)

under analysis is observed. Any change in the thermal flux due to the presence of large concentrations of the element would be reflected by a corresponding decrease in the background countrate. This decrease in terms of a countrate can be obtained in relation to the normal seabed background observed over a relatively inert material, e.g. silica type seabed. A positive correction could then be made to the observed countrate for this element by a value proportional to this decrease in the background countrate. In practice, selected regions of the spectrum can be monitored and changes in the backgrounds correlated, to detect an anomalous situation. The method is applicable if other seabed conditions remain the same, and do not influence the background countrate at the same time when surveying a manganese-rich zone for example.

5.6 The use of empirically determined spectral ratios in the evaluation of countrates from elements whose energy peaks are coincident with those of chlorine

5.6.1 Introduction

The γ-ray response from a seabed is a continuous spectral distribution of energies due to neutron capture and inelastic scattering events in the detector. The complexity of the spectrum has already been discussed in the earlier sections. The dominant energy peaks are from chlorine superimposed on a background due to Compton scattering. As an example, a typical pulse-height spectrum is shown in Figure 5.14. The data is from a seabed containing 2.9% iron and 2.5% titanium obtained with a 2.5 μg ^{252}Cf neutron source in a counting time of 120 mins. Due to the multiplicity of the peaks from pair-production in the higher energy region (3 - 10 MeV) there is a wide energy region in the spectrum, where characteristic energy lines due to an element have a high probability of coinciding with chlorine peaks. Thus, in certain instances, the detection of an element in the spectrum has to rely upon a single energy line, the other energy lines

overlapping with lines from chlorine. At high energies, the countrate in the full-energy peak is small compared to that of the single and double-escape peaks of an element, and consequently there are large errors of measurement. The situation is shown in Figure 5.14 where the double-escape peak of iron is coincident with a chlorine peak and the full-energy peak of titanium also coincides with a chlorine double-escape peak. To resolve this situation, an empirical method was developed using spectral ratios of countrates in the prominent energy peaks of chlorine, to isolate the contribution by an element, when one or more of its energy peaks overlap with a spectral energy peak of chlorine. The method is particularly applicable to a spectrum when the energy peaks have relatively high countrate components (single and double-escape) and the estimation can then be carried out with reasonable statistical accuracy.

5.6.2 Outline of the method

The production of the first and double-escape peaks from an incident gamma photon is primarily governed by the detector characteristics and the geometry of the source-detector configuration. It is virtually independent of the seabed properties. The parallelism of the graphs obtained by plotting the net counts in the full, single and double-escape peaks for elements, as a function of source-to-detector distance on a semi-logarithmic plot, suggested a constant relationship between the countrates for any two selected parameters. Since pair-production is the dominant process in the detector at high energies, the ratio of the counts in the full-energy peak to the corresponding double-escape peak would give a higher ratio of statistical confidence.

Ratios of the net counts in the full-energy peak to the double-escape peak for some important chlorine energy lines were determined from the spectra obtained for various

seabed types and different source-to-detector distances. These ratios have been established as constant values for the particular geometry of measurement and seabed environments. A change in these ratios would thus imply a contribution in countrate from an energy line of an element, coincident with one of the spectral lines constituting the ratio. With a predetermined value for this ratio the contribution in countrate due to the element can be evaluated. This can also be used to calculate its abundance and to correlate the countrates obtained in other associated peaks for a positive identification of the element.

5.6.3 Experimental results

Figures 5.32 to 5.35 show the data obtained by plotting the countrates in the full and double-escape peaks obtained from a series of measurements carried out in which more than 100 spectra were recorded. The values are for various seabeds and different source-to-detector distances. Six principal energy lines were chosen including that of hydrogen (2.223 MeV) and silicon (3.539 MeV). Apart from chlorine 7.790 MeV and 7.414 MeV energies which give a pure spectral ratio, the total countrates in chlorine 6.620 (d) + chlorine 6.111 (s) and chlorine 6.111 (f) + chlorine 6.620 (s) were used as single spectral lines due to overlapping. Data from the measurements were fed to a computer (HARWELL - IBM 3018 K) for a multivariable regression analysis using the minimising programme LSFIT. After a trial run with the data for hydrogen, a linear regression line was chosen as the best fit to the countrates. This was adopted for the rest of the data.

5.6.4 Application of the method to some selected elements

The method was applied to the data obtained for two elements, 3% iron and 5% copper distributed in a silica seabed in each case. The determinations made were to estimate the contributions by each of the elements to the total countrate observed in the respective chlorine peaks.

5.6.4.1 Iron (3% Fe)

The two principal γ-ray energies of iron 7.632 MeV and 7.646 MeV could only be partially resolved by the detector system (ΔE_γ = 14 keV) and therefore these are treated as a single energy spectral line. In the spectrum for iron the double-escape peak energy is coincident with the chlorine 6.620 MeV (f) energy peak. The full-energy and the single-escape energy peaks are uncontaminated. The regression line for the data given in Figure 5.34 is expressed by the relation,

$$Y = 15.0 + (0.223 \pm 0.004)\ X$$

where Y = countrate for the Cl 6.620 MeV (f)

X = countrate for Cl 6.620 MeV (d) + Cl 6.111 MeV (s)

The values of the countrates obtained by experiment for the Cl 6.620 MeV (d) + Cl 6.111 MeV (s) were substituted in the above equation and the corresponding countrates for the Cl 6.620 MeV (f) were obtained for the different source-to-detector distances L. The contributions by the iron double-escape peak energy (Fe 7.632 (d) + Fe 7.646 (d)) were determined by the difference between these values and those obtained by experiment for the Cl 6.620 MeV (f) + Fe (7.632 + 7.646) (d). The results and the relative magnitudes of the errors are given in Table 5.10. The errors in the residual counts obtained for the iron double-escape peak vary from about 7% for small source-to-detector distances (20 cm) to about 15% for 55 cm. The results are shown in Figure 5.36(a) together with the experimental values obtained for the full-energy peak of iron. These values show that the counts in the Fe (d) comprises about 26% of the total counts in this composite chlorine peak.

5.6.4.2 Copper (5% Cu)

Similar analyses were carried out for two energy lines of copper - Cu 7.915 MeV (s) which is coincident with

the chlorine 7.414 MeV (f) and Cu 7.637 MeV (d) which overlaps the chlorine 6.620 MeV (f) energy line.

(A) The regression line for the analysis of Cu 7.915 MeV was obtained by the data of Figure 5.35 and is expressed by

$$Y = 22.0 + (2.404 \pm 0.0056)\ X$$

where Y = counts in the Cl 7.414 MeV (f)

X = counts in the Cl 7.414 MeV (d)

The relevant data are given in Table 5.11.
The errors associated with the estimation of the counts due to copper, range from 10% for a source-to-detector separation L of 25 cm to 14% for L = 45 cm. The net counts from the copper 7.915 MeV (s) to the total counts observed in the contaminated energy peak is about 26%.

(B) For the copper 7.637 MeV (d), the same regression equation for the determination of the counts for iron was used since the overlap is with the same 6.620 MeV (f) of chlorine. The results of the computation are presented in Table 5.12.

The errors in the estimation of the counts are in the range 15-16% for the source-to-detector separations considered. The values obtained from the regression equation together with the experimental data obtained for the Cu 7.637 (f) from the same γ-ray spectra are given in Figure 5.36(b) as a function of the source-to-detector distance. The errors in the experimental values for these countrates vary from 16-20%. The contribution of the copper counts to the total counts in the contaminated peak is about 20%.

5.6.5 Conclusions and usefulness of the method in seabed analysis

The method developed can be used for the analysis of spectral data where a high contribution in countrate is expected from an element whose characteristic γ-ray energy is coincident with a background chlorine peak. In the three cases for which counts were evaluated from the spectral ratios, the contribution from the various elements were greater than 20% of the total countrate observed for the composite peak.

The consistency of these ratios for chlorine as well as hydrogen and silica for a particular probe geometry, implies that variations in these ratios can be used for the detection of elements by monitoring these in a seabed survey to estimate its abundance. Several characteristic γ-ray energies of elements are found to be either coincident with chlorine background lines or poorly resolved by the spectrometric device so that they occur as a composite peak. In these instances, the method described is the only means of identifying these elements as well as assessing their abundance in the seabed by relating variations in these empirical ratios to elemental concentrations.

5.7 Determination of the sensitivity for detection of elements in the seabed

5.7.1 Introduction

The sensitivity for detection of an element is a relative measure of the effectiveness with which a spectrometric device is able to ascertain its occurrence in the seabed. In the present work, the minimum abundance of an element which produces a statistically significant countrate in a probe system is defined as its sensitivity for detection in the environmental conditions in which it is measured.

The sensitivity for detection of an element on the seabed is primarily a function of the nuclear properties of the element, its environment and the characteristics of the neutron interaction probe used in analysis. For a given seabed type (sand, clay, mud etc) and for a constant seawater content of the seabed matrix, this factor will mainly depend on the neutron capture cross-section and the branching ratio of the γ-rays of interest. In particular, for an assumed thermal neutron flux distribution ϕ_{th} ($n/cm^2 .sec$) in the seabed, the number of gamma photons N_γ, of a given energy emitted per second by a single element is given by

$$N_\gamma = N_o \cdot \omega \left(\frac{I\sigma_a}{A}\right) \phi_{th} \quad \text{photons/grm} \qquad (1)$$

where N_o = Avogadro's number (6.028×10^{23})

ω = weight of the element per gram of the seabed material

σ_a = thermal neutron absorption cross-section of the element in barns

A = atomic mass

and I = intensity of the γ-ray (usually expressed as the number of gamma photons emitted per 100 neutrons absorbed).

The factor $\left(\frac{I\sigma_a}{A}\right)$ as given in equation (1) is an intrinsic property of an element and contains only the nuclear properties and is independent of seabed conditions and detector characteristics. In elemental analysis, the quantity measured is the countrate due to gamma photons produced in the effective volume of the seabed which ultimately reach the detector. The sensitivity is therefore subject to several external factors which are related to seabed composition, background radiation and

also to the probe characteristics, such as source strength, detector efficiency, geometry of measurement and counting time. Determinations were therefore made in-situ of the sensitivity for detection of some of the elements of interest by the probe system developed. The results have been used to compute the sensitivities of other important elements in a similar seabed environment.

5.7.2 Method of Determination

The number of counts C observed for a particular γ-ray energy E_γ, in a given time t with a neutron source of known strength can be expressed in terms of equation (1) by

$$C = k.\omega \left(\frac{I\sigma_a}{A}\right)E_\gamma.\xi(E_\gamma).t \qquad (2)$$

where ξ = efficiency of the detector for a γ-ray of energy E_γ

k = constant (depends on N_o, ϕ_{th} which is proportional to source-strength and an attenuation factor relating to the transmission of γ-rays in the seabed).

The number of counts C in a time interval t is the quantity measured by the detector and is obtained from the total counts in the γ-ray energy peak less the background in the γ-ray spectrum. The net counts in a peak is therefore dependent on the background radiation levels associated with the measurement. In order to obtain statistically significant counts in a γ-ray energy peak, the minimum counts corresponding to the lower limit of detection should be at least two standard deviations (2σ) above background. This includes a confidence limit of 95% in the countrate and is a reasonable guide as to its detectability. To determine this minimum limit of detection, the net counts in the γ-ray energy peak for a known abundance of an element is determined by experiment together with the

statistical error σ associated with its measured background. From a knowledge of the variation of the percentage abundance of the element with countrate such as that obtained for copper and manganese (Figures 5.30 and 5.31), an error of 2σ in the background countrate can be expressed in terms of a percentage weight of the element. This would correspond to the lowest limit of detection for the element as specified by the source strength, counting time and the probe geometry.

Experimental measurements can be made for a range of elements under the same conditions of geometry and the sensitivity values determined in terms of a percentage abundance. These could then be used to compute the sensitivities of other elements for a neutron source of any given strength and counting time.

5.7.3 Experimental measurements

γ-ray yields for some selected elements were obtained from laboratory measurements for seabeds prepared by uniformly distributing known percentages of the elements in a predominantly silica seabed matrix. Determinations were made with a 2.5 μg ^{252}Cf source and a 50 cc. high purity Ge detector for a source-detector geometry as configured in a towed spectrometric device. γ-ray spectra were obtained for these elements for a typical source-to-detector distance of 30 cm and a counting time of 120 mins in each case.

Table 5.13 shows these elements and their important characteristics. The principal γ-ray energies of the various elements and the elemental concentrations in the simulated seabed are also included for purposes of computation. The factor $(\frac{I\sigma_a}{A})$ for the γ-ray energies of the elements were obtained from the tables of DUFFEY and EL-KADY (1970).

In the calculations for the sensitivity for detection of the various elements the background radiation levels were obtained from the individual spectra of the elements in the region of their characteristic energies. The net counts in the γ-ray energy peaks given are those corresponding to their percentage abundance in the simulated seabed. It is observed from the countrate versus percentage abundance curves obtained experimentally for two elements, copper and manganese (Figures 5.30 and 5.31) that the initial region of these curves is nearly linear. The sensitivities were therefore deduced on this linear relationship, since the total count corresponding to 2σ of the background level is very much lower than the net counts in the γ-ray energy peak obtained for the percentage abundance of the element in the seabed. The values obtained for the sensitivities are given in Table 5.13. These represent the sensitivity values measured experimentally and extrapolated to operational conditions of a 100 μg ^{252}Cf neutron source and a counting time of 15 mins.

5.7.4 Calculation of the sensitivities for detection of other elements based on the experimental measurements

5.7.4.1 General outline of the method

From equation (2) it is possible to calculate the sensitivities for detection of any element from determinations made with a known abundance of an element (or elements) in the simulated seabed. The constant 'K' is first determined for a known concentration of a particular element in the simulated seabed. For this purpose, the number of counts C in a selected γ-ray energy peak of the element is measured experimentally with a neutron source of known strength in a specified counting time. The factor $\left(\frac{1\sigma}{A}\right)$ for the particular element and γ-ray energy is evaluated from known parameters and the efficiency ξ of the detector is obtained from an experimentally determined curve of detector efficiency versus γ-ray energy. With known factors of $\left(\frac{I\sigma}{A}\right)$ and ξ for a selected γ-ray energy of

any other element (or elements) and using the already determined value of K, the number of counts obtained for unit abundance of the element using the same source and counting time can be evaluated from equation (2).

Referring to background levels in the observed γ-ray spectra discussed earlier and the degree of constancy observed in these backgrounds for most elements in the seabed, the number of counts representing two standard deviations of the background for the selected γ-ray energy was determined. This was obtained as follows: From the known value of the resolution of the detector used, the number of channels in the γ-ray spectrometer which represents the total counts in the γ-ray energy peak was determined. The total background would therefore be the value of the general background radiation level for a single channel multiplied by the number of channels demanded by the resolution of the detector to represent this energy peak. The statistical deviation 2σ was then derived from these counts. Using this value and the counts obtained for unit abundance of the element from equation (2) the sensitivity of the element in terms of minimum abundance was determined. This method of computation was extended to other elements by the same procedure.

In practice, the value of K was determined experimentally from the data for several elements with known abundances distributed in a silica seabed matrix. The number of channels in the spectrometer system representing a significant percentage of the countrate corresponding to a particular γ-ray energy was determined in relation to the resolution of the spectrometer system for the range of energies considered in the spectrum.

5.7.4.2 Determination of 'K' by experiment

Equation (2) can be re-written in a convenient form for purposes of calculation as

$$C = K\lambda \qquad (3)$$

where $\lambda = (\frac{I\sigma_a}{A})E_\gamma . \xi(E_\gamma).\omega$

and C = number of net counts obtained by the 2.5 μg ^{252}Cf neutron source in a counting time of 120 mins.

For the elements listed in Table 5.13 the net counts C were determined for the principal energies from the γ-ray spectra obtained for these elements. The factor $(\frac{I\sigma_a}{A})$ was computed for the γ-ray energies selected for each of the elements and ξ was obtained from an experimentally determined curve shown in Figure 5.38. (The determination of the efficiency of the detector system as a function of γ-ray energy is given in the following section). By plotting C against λ for the elements chosen, an average value of K was obtained. This is shown in Figure 5.37 where the linear relationship between the countrates for the various elements and their nuclear properties and detector characteristics is clearly established. A value 328.6 ± 0.03 was obtained by a regression analysis of the experiment data and is for a probe system incorporating a 2.5 μg ^{252}Cf source and a counting time of 120 mins. For an operational system considered on the seabed using this technique, i.e. a source-strength of 100 μg ^{252}Cf and a shorter counting period of 15 mins, the value of K was extrapolated to meet this requirement.

5.7.4.3 Computation of sensitivities

The factor $(\frac{I\sigma_a}{A}).\xi$ was evaluated for all the elements of interest by choosing a convenient γ-ray energy which does not interfere with any of the chlorine spectral lines. This was multiplied by the new value of K to obtain

the net counts per unit percentage abundance of the element. The backgrounds were determined from an analysis of the measured spectra for the elements from which the value of K was calculated. A value of 2σ was then computed for each element corresponding to its characteristic γ-ray energy, on the background obtained for 4 to 5 channels in the γ-ray spectrum. This adequately represented the background contribution under an energy peak for the characteristic γ-ray energy. The sensitivities were evaluated for all the elements using these factors and the values are presented in Table 5.14.

The lower limits of detection for the elements measured experimentally and extrapolated to operational conditions on the seabed using a 100 µg ^{252}Cf neutron source and a 15 min counting time (Table 5.13), agree well with the calculated data presented in Table 5.14. Experimental values obtained for several seabed-type elements such as silica, calcium and alluminium agreed closely with those calculated.

5.7.4.4 Determination of the efficiency of the high- purity Ge detector as a function of gamma-ray energy

The effect of the variation of the efficiency of the detector with γ-ray energy and the consequent decrease in the countrates observed with increase in energy, has to be taken into account in determining the sensitivity for detection of an element. Since the γ-ray energy of the elements are in a region where the efficiency of the detector is most sensitive to variations in energy, it was necessary to determine this variation as a function of γ-ray energy, for the detector used in the experiments.

The method adopted was similar to that described by KANE and MARISCOTTI (1967). The initial step was to obtain the relative efficiency curve for the full-energy peak

using a set of radioactive sources. It was necessary that the spectra of γ-rays emitted by each source contained at least two prominent lines of known relative intensity and preferably widely spaced in energy. Under these conditions, ratios of the full-energy peak efficiency at different energies can be calculated from a measurement of the different source spectra obtained with the detector. Spectra were obtained under the same conditions of measurement and the net peak counts were determined for each of the energies. The values for the net counts were determined with a statistical accuracy of less than 1%. The relative efficiencies were normalised to unity for the ^{22}Na 1.275 MeV γ-ray. The full-energy peak efficiency curve obtained is shown in Figure 5.38 together with the γ-ray sources used in the determinations.

The determination of the relative efficiency curve for the double-escape peak requires a γ-ray source with energies well above the normal limit set by radioactive isotopes. In the present work, these determinations were made using the γ-ray energies of the elements in the seabed material itself and the net counts in the full and double-escape peak energies were computed from the experimental data. With a knowledge of the intensities of these γ-rays and combining with the double-escape peak efficiency of the highest available radioactive source (^{208}Tl) the relative double-escape peak efficiency curve was determined. This is incorporated in Figure 5.38. Energies of silicon 3.539 MeV and 4.934 MeV were used at the lower energy region to tie up with the full-energy peak efficiency curve and some of the energies of the elements in the seabed provided the data beyond 5 MeV. Where necessary both curves have been extrapolated to cover the energy range up to 10 MeV.

The curves obtained for the full and double-escape peak efficiencies are unnormalised and used as such in equation (2) for the determination of k. The curves may be

transformed into absolute efficiency curves if necessary with a knowledge of the γ-ray emission rate for any one source used in the determinations. In this application, the need for this did not arise since k was evaluated in terms of relative efficiencies for the γ-rays under consideration.

5.7.5 Discussion of the results

As stated earlier, the sensitivities for the detection of the elements computed are for the particular geometry of the probe system used in the experiments and therefore dependent on the probe characteristics. In general, the sensitivity for detection can be improved by lowering the background radiation and increasing the detector characteristics (source strength and counting time) to achieve a higher degree of detection. The background from the seabed-type element and from seawater is more or less a constant contribution for all measurements. This forms an integral part of all spectra and is the major contributing factor to the general background. For a cylindrical design of probe, such as that developed for the experimental work, the influence of chlorine from seawater is very high and dominates the background of all spectra. A different geometry for a probe could be adopted so that the system is less sensitive to this background.

It is however, within the scope of the method to minimise γ-ray contributions from constructional materials of the probe by using alternative materials that do not produce significant background contributions in the region 5 - 10 MeV. Constructional materials such as steel will significantly raise the level of the background and the total countrate of the system, thereby lowering the sensitivity of detection.

The values quoted for the sensitivities for detection are generally a guide to the potential of the method in

seabed analysis. The background levels selected from the spectra in the computation of those values have been chosen to be intentionally higher than the observed levels for the same conditions of experiment. Therefore the values presented in the table are generally an overestimation of the minimum abundances representing the sensitivities.

5.8 The response of an infinitely thick layer of sediments underlying a relatively inert seabed material

5.8.1 Introduction

In continental shelf regions, where placer deposits are likely to be found environmental factors governing the transport and deposition of the sediments generally favour the occurrence of more than one type of sediment at a location. Although exceptions to this could be found certain heavy minerals such as ilmenite, rutile, monazite, zircon etc. are found in close association with one another. Some of these deposits may be overlain by a relatively thin sediment cover of no importance in seabed exploration. A placer such as ilmenite which is sensitive to this method of detection may be covered with an overburden of zircon, which has a relatively lower limit of detection. This situation is important from the point of view of the response of the infinitely thick buried layer to a detector system.

5.8.2 Experiments conducted

For convenience in simulating this situation, the effect of a sandbed (SiO_2) buried under varying thicknesses of calcium carbonate was studied experimentally. For this purpose, different thicknesses of pure calcium carbonate were distributed over a bed of sand and γ-ray spectra were obtained for the elements in the system using the probe developed for the laboratory measurements. The sensitivity of the buried thickness of sand was measured using the 3.539 MeV γ-ray of silicon and a convenient countrate for the measurements was obtained with a 30 cm source-to

detector separation. The net counts in the full-energy peak were recorded by progressively increasing the thickness of the calcium carbonate layer until no response from the silicon was observed. The countrates obtained as a function of the depth to the top of the sandbed are presented in Figure 5.39.

5.8.3 Discussion of the results

The countrates plotted in the figure are the integral values from the silicon in the buried layer of sand which extends to infinity at depth. With no overlying calcium carbonate, the maximum countrate for silicon is obtained, and a zero countrate is observed when the γ-rays produced by thermal neutron capture in the sand (SiO_2) are attenuated in passing through the calcium carbonate overburden to such an extent that no counts of statistical significance are registered in the detector. The thickness of calcium carbonate for this condition is slightly less than 12 cm as seen in the figure. The response from the silica layer is principally governed by the neutron transport in the overlying calcium carbonate layer and the consequent thermal neutron flux distribution in the silicon layer. The countrates observed in the detector are thus controlled by the attenuation properties of the overburden for the characteristic γ-ray of silicon.

5.9 The effect of seawater content on the γ-ray countrate of elements in a seabed

5.9.1 Introduction

It was discussed earlier that background radiation forms an integral part of a seabed spectrum and effectively controls the sensitivity for detection of elements. The major contribution is from chlorine in seawater overlying the sediments and to a lesser extent from the seawater saturating the seabed. Analyses of the γ-ray spectra from seabeds containing various concentrations of elements have been made in Section 5.2.4.3 and the similarity of these

backgrounds has been established. This is attributed to a certain extent to the constant seawater content of the seabeds for which these spectra were obtained. The presence of hydrogen (neutron moderation) and chlorine (high capture cross-section) in seawater means that any variation in the seawater content of the sediment would result in a change in the thermal neutron flux distribution in the seabed. Large variations of seawater content can therefore affect the countrate of elements in the seabed and the sensitivity for their detection. Experiments were therefore undertaken to examine this effect.

In dealing with unconsolidated sediments such as placer deposits, the concept of seawater content is more appropriate in describing the matrix composition rather than the term 'porosity' which is commonly used to describe the percentage voids in a geological formation. This is usually of consequence, since sediments in a marine environment are always saturated and the number of interacting nuclei is more significant to the method under study than porosity. Also in certain types of sediment such as clay changes in compositional volume occurs with absorption of seawater. Hence, in the present work the percentage weight of seawater per unit mass of the seabed matrix is referred to as the seawater content.

5.9.2 Thermal neutron flux distribution in a silica-type seabed layer

Monte Carlo calculations carried out to ascertain the nature of the thermal flux distribution in a common seabed type material such as silica for three different seawater contents, 20%, 40% and 60% were discussed in Section 4.64 (Chapter 4). The computations carried out were for the probe geometry represented in the experiments with a 1 μg ^{252}Cf neutron source and the thermal flux immediately in the seabed layer underlying the seawater is shown as a function of distance from the neutron source in Figure 4.7.

It is observed that the thermal flux is highest near the source for the seabed containing 60% seawater, the seabed with 20% seawater producing the lowest flux. Around 12 cm the curves have a mutual cross-over point beyond which they decrease progressively with distance. The countrate at any point in the seabed will depend on the neutron flux as well as the number of interacting nuclei per unit mass of the seabed matrix. Since the number of nuclei is a constant parameter for a particular seabed with a constant seawater content, the countrates will be spatially dependent. The effects of this will be discussed in relation to the experimental work carried out.

5.9.3 Experimental determinations

5.9.3.1 General

It was expected that various grain sizes of a common material such as silica sand would provide a suitable range of seawater contents for the experiments. Five grain sizes were selected, four from the same source of bulk material of silica sand. The largest grain size was obtained from shingle-type beach material (pea-size) predominantly silica, but containing a small percentage of iron, (< 1%) as a constituent element.

TABLE 5.15 lists the important characteristics of the material of the seabeds. The seawater content expressed as a percentage was determined by experiment on a large number of samples.

5.9.3.2 Seawater content of the seabeds

The data given in TABLE 5.15 show that for the range of grain sizes selected, the seawater contents lie within a very close range and experimentally no perceptible effect on the countrates would be expected from the seabeds. Theoretical considerations show that for spherical grains of material (non-absorbing) in hexagonal packing the

porosity (or seawater content) is independent of grain size. For an ideal situation it has a value of 47.6% which in terms of silica of density 2.67 $g.cm^{-3}$ and seawater (density 1.025 $g.cm^{-3}$) corresponds to a saturation of 25.9% by weight of seawater. It can be deduced from this analysis, that in unconsolidated sediments such as placers and assuming no absorption of seawater takes place by the constituent elements, the deposition of the material under the ambient conditions results in a more or less constant value for the seawater content. This is influenced only to a very small degree by the shape of the grains.

The seawater contents and the corresponding porosities of the seabeds are represented in figure 5.40. For comparison, similar data for some of the seabeds in which various elements were distributed in the earlier experiments are also included. The three values for which the fluxes were computed are also shown in the figure.

It is observed that the seawater saturation in the seabeds generally lie within a very close range, between 20% and 25% which corresponds to porosities of 40% - 47% within the errors associated with these determinations. These values are lower than the maximum theoretical value of 26% for sediments of this type. The thermal neutron flux distributions from the silica type seabed with no other constituent element present would therefore approximate closely to the computed curve for the 20% seawater content. The fluxes from this curve can thus be used to study the effect of the variation in the countrates with seawater saturation. For the seabeds for which gamma-ray spectra were obtained for analysis, the seawater content had an average value of about 21%.

5.9.3.3 Analysis of the gamma-ray spectra of the various seabeds containing different seawater contents

For comparison of data, the net countrates in the γ-ray energy peaks obtained with a 2.5 μg ^{252}Cf neutron source for a source-detector separation of 30 cm were obtained for the principal energies of hydrogen and chlorine. These values are presented in TABLE 5.16.

The countrates reflect the more or less constant seawater content of the seabeds for which the γ-ray spectra were obtained. Very little variation is observed within the errors of measurement. The seabed with shingle, though slightly higher in seawater content does not show any significant difference in the countrates. The exceptionally high countrate obtained in the case of chlorine 6.620 MeV is due to a coincident composite γ-ray energy peak of iron (Fe 7.632 MeV and Fe 7.648 MeV) which was found to be a constituent element of shingle. Therefore the thermal flux distribution in all these seabeds would not be expected to be different to that shown in Figure 4.7 for the seabed with 20% seawater content, except that the fluxes would be lower by a factor of 2.5 due to the lower source strength (1 μg) used in computing this flux.

To compare the effect on the countrates with variation in seawater content, reference is made to the thermal flux distribution curves in Figure 4.7. Relating the 20% seawater content thermal neutron flux curve to the experimental seabeds, the expected variation in countrates due to 40% and 60% seawater content can be estimated. At a distance of 30 cm in the seabed the thermal flux is lower by factors of 0.63 and 0.39 for the seabeds containing 40% and 60% seawater respectively compared to the 20% seawater content seabed. The number of interacting nuclei per gram in these seabeds are higher by factors of 2 and 3

respectively. Hence the net increase in countrate would be proportional to the factors 1.26 and 1.17. It is worth noting that although the thermal neutron flux in a seabed is a function of distance from the neutron source, the number of nuclei responsible for the production of γ-rays is spatially independent for a seabed with a constant seawater content. For this reason the rate of fall of thermal flux may not be compensated by the increase in the number of interacting nuclei for seabeds containing a high percentage of seawater. Therefore at distances far from the source a lower contribution to the detector countrate may be obtained in a seabed with a very high seawater saturation, as shown by the lower factor of 1.17 in the case of the 60% seawater content curve.

For a detector placed 30 cm from the neutron source, the maximum contribution from the seabed to the detector countrate would be from a region approximately half-way between source and detector as shown in Figure 4.11 for the same probe geometry. On this basis, the maximum contribution to the γ-ray countrate would be from a region 12-15 cm from the neutron source. However, in this region the thermal neutron flux is seen to be independent of the seawater content in the seabeds. Thus the countrates observed for the 40% and 60% seawater content seabeds would be higher than those observed for the seabed with a 20% seawater content by factors of 2 and 3 respectively for chlorine and hydrogen.

In practice, seawater contents of over 26% for non absorbing material are not observed so that for placer type deposits if an average value of 20% is accepted in seabed analysis the countrates observed for hydrogen and chlorine with a 2.5 μg ^{252}Cf source and a source-to-detector distance of 30 cm would be similar to those tabulated in TABLE 5.16.

5.9.3.4 Comments

For unconsolidated sediments it has been shown that the seawater content is fairly constant for different grain sizes and is about 20% for a seabed containing average grain size material. While this is generally the case for material with non absorbing properties, values of over 26% have been observed for certain other materials. This is particularly true for substances which absorb seawater resulting in a change in compositional volume. For samples of clay, laboratory determinations yielded an average seawater content of 41 ± 2% which is considerably higher than that for silica-type material. An increase in dry volume of 10% was observed in this case. This effect was also observed with pure calcium carbonate. The value determined was 25 ± 2% with a resulting increase in volume of 11%.

It is also pertinent to consider seabed material with hydrogen and oxygen as constituents. In most clays the OH in its chemical composition can be reflected as an apparent increase in countrate and intepreted as a change in seawater content. In nodular material such as manganese, the seawater content is variable with an average of 13%, the maximum being 24% and minimum 8%. These values indicate how the hydrogen and chlorine countrates could vary in a seabed survey and their possible effect on the background of an observed γ-ray spectrum.

5.10 Investigation of the perturbations in the neutron flux distribution due to probe components

5.10.1 General

The radiation shield in the experimental probe system employing a neutron source and a γ-ray detector for seabed analysis has been dealt with briefly in Chapter 3. It was stated that the two material components of the shield (polythene and lead) possess distinct nuclear properties, which perform the desired functions of neutron moderation

and gamma attenuation respectively. An inevitable outcome of this functional dependence of the shield materials on its nuclear properties, is a perturbation of the neutron flux distribution in the seabed that would otherwise be expected from an unshielded source. In seabed exploration, where the flexibility of the geometry of source and detector exists in designing a probe, this is an important factor. It is reasonable to assume that in the arrangement considered in the laboratory experiments, the degree to which the perturbation occurs, depends on

(1) the nuclear properties of the selected shield components

and (2) the disposition of these components in relation to the neutron source or detector.

The direct determination of the neutron flux distribution in the seabed has not been attempted by experiment, but where necessary computer simulation studies have been undertaken for this purpose. However, the γ-ray response of the detector provides an indirect method of ascertaining the perturbation in the neutron flux distribution due to components in a radiation shield. The importance of studying this effect arises from the fact that for a given choice of shield components and a particular source-to-detector distance, the γ-ray countrate from elements in the seabed may be enhanced for a particular disposition of the components in the radiation shield.

Experiments were therefore conducted to determine an optimum arrangement of the shield components, within the limitations allowed by their functions, to obtain the highest response for a particular source-detector separation.

5.10.2 Shield components and their related nuclear properties

5.10.2.1 Neutron shield

The presence of hydrogen in the neutron shield (polythene - CH_2) is characterised by a marked effect on neutron moderation because of the specific features of the interaction of neutrons with hydrogen nuclei. In particular, the interaction cross-section of hydrogen for neutrons has a high value which increases with decreasing neutron energy (GARBER, D.I. and KINSEY, R.R., 1976*). As a result of each interaction, the probability of a neutron losing half of its energy is high and this loss of energy increases with increasing angle of scatter. Therefore any interaction of neutrons with hydrogen nuclei in the polythene causing either a decrease in the initial energy or scattering at a large angle from its initial direction will greatly reduce their probability of directly reaching the detector. Such scattered neutrons will inevitably contribute to the neutron flux in the vicinity of the shield.

5.10.2.2 Gamma-ray shield

The choice of lead or other materials for a gamma-ray shield has already been discussed in relation to their nuclear properties. Lead, in particular has a high moderating ratio on account of its high scattering cross-section and its relatively smaller absorption cross-section. The angular distribution of these scattered neutrons is isotropic in the laboratory system as for all heavy nuclei. This would imply that a large proportion of the incident neutrons would be scattered away from the direct path of the detector and contribute to the neutron flux in the seabed. Since the thickness of lead used in the probe is one-third of the source-to-detector distance,

* 'Neutron Cross-Sections', BNL-325, Vol. 2 (Curves).

its position relative to the neutron source is critical in influencing the neutron flux distribution in the seabed.

5.10.3 Experiments conducted

The experimental layout of the source-detector configuration was similar to that shown in Figure 3.4 (Chapter 3). A lead disc 10 cms thick was chosen for the gamma-ray shield and the intervening space between source and detector was filled by polythene. Gamma-ray spectra were obtained for a fixed source-to-detector distance for a particular seabed for various positions of the lead shield relative to the neutron source. Three source-detector separations were used and different elements were 'seeded' as uniform mixtures with silica sand for the seabed material. The net γ-ray counts in the peaks corresponding to the principal energies of elements in the seabed and seawater were calculated from the spectra. The relevant data of the experimental situations investigated are given in Table 5.17.

The countrates obtained for the various elements in the seabed and seawater were plotted as a function of the distance of the lead shield from the ^{252}Cf neutron source. These are given in Figures 5.41 and 5.42. A qualitative discussion of the results obtained has been attempted.

5.10.4 Discussion of Results

A characteristic of all the graphs presented is that the maximum countrate for all elements in the seabed and seawater is obtained when the γ-ray shield is adjacent to the neutron source. This is observed for all source-to-detector distances. The countrates for the elements decrease with increasing distance of the γ-ray shield from the neutron source and falls steeply when the position of the shield approaches the detector and a minimum countrate is observed when the shield is adjacent to the detector.

The sharp drop in countrate occurs when the source end of the shield is roughly half-way between source and detector, for all source-to-detector distances. This is observed for a source-detector separation of 35 cms for which the unscattered γ-ray flux at the detector has been computed by Monte Carlo calculations as a function of the position of the lead shield from the neutron source. Figure 4.15 shows these results. The steep gradient occurs at about 17 cms for this source-detector separation, which generally agrees with the experimental results observed for this separation.

The decrease in countrate as well as the sharp drop observed when the lead shield is midway between source and detector is explained by considering the effects of neutron moderation in the polythene, and the attenuation of the γ-rays in reaching the detector. When the lead shield is adjacent to the source the source neutrons are scattered by the shield into the surroundings thereby producing the highest thermal flux for the position of the lead. The moderation and thermalisation of the source neutron principally takes place in the seabed. When the shield is further away from the source, the source neutrons are first moderated by the polythene before reaching the lead shield. Thus the energy of the source neutrons is degraded first before any scattering occurs. Therefore less high energy neutrons penetrate the seabed and the percentage of neutrons in the seabed is considerably reduced which is reflected by a lower γ-ray yield.

At distances further away from the source, fewer fast neutrons are available for scattering, to augment the direct source neutrons entering the seabed, and the γ-rays produced in the seabed and seawater are also attenuated by the proximity of the lead shield to the detector. These two combined effects account for the steep fall in countrate observed and at positions approaching the detector the attenuating properties of the lead predominate

to give the lowest countrate when the shield is virtually adjacent to the detector face. The position of the lead shield therefore should be adjacent to the neutron source to obtain optimum countrate for the geometry represented by the probe in the experimental system.

The influence of the lead shield is shown in Figure 4.14 for the case of a silica seabed with a 20% seawater content. The thermal flux distributions with the 10 cms lead shield adjacent to the neutron source and the shield replaced by an equivalent thickness of polythene were computed for the seabed layer as a function of radial distance from the source. The higher thermal flux distribution with the lead shield is apparent in the curves obtained, thus resulting in a higher countrate than if it were replaced by a moderating material such as polythene.

CHAPTER 6

APPLICATION OF THE RESULTS OF EXPERIMENTAL WORK TO THE DEVELOPMENT OF AN OPERATIONAL PROBE AND ITS EXPECTED PEFORMANCE IN SEABEDS CONTAINING ELEMENTS OF CURRENT ECONOMIC INTEREST

6.1 Introduction

Experimental studies undertaken in this thesis have shown the feasibility of the radiative capture (n,γ) reaction as a practical means of making in situ elemental analysis of the seabed. The technique has been developed by designing a neutron interaction probe capable of being operated as a towed device on the seabed. The particular design adopted for the probe in this study was prompted by two important considerations:

(1) it is the simplest working model of a probe assembly that could be employed both in experimental work and computational analysis

and (2) axial symmetry in a probe is a desirable feature in a practical towed system as shown in the case of the natural γ-ray seabed spectrometer.

An operational probe for seabed analysis involves several essential features in its design. An important consideration is a suitable pressure vessel to house the basic components of the probe assembly and having a sufficiently large wall-thickness to operate at the appropriate depth. The constructional material as well as its thickness would undoubtedly affect adversely the response of the probe, the former in contributing to the background of an observed γ-ray spectrum and the latter in attenuating considerably the γ-rays from neutron capture by elements in the seabed. The internal configuration of a typical probe designed on the results of experiment as a towed device is given by THOMAS et al (1983). Although the general principle of operation is the same, the constructional features between the

laboratory probe with which this study was conducted and the operational system designed for seabed analysis are different. Hence, in applying the results of experiment to evaluate the performance of an operational probe, the effects on the probe response arising from these differences have to be taken into consideration.

6.2 Types of probe systems applicable to seabed analysis

6.2.1 General

A neutron interaction probe consists in principle of a neutron source and a γ-ray detector suitably configured for the detection and analysis of seabed sediments. The various sources and γ-ray detectors suitable for undersea operations have already been dealt with in Chapter 2. Sources and detectors can be considered as independent units of operation in a probe assembly, so that a variety of probe systems could be developed for seabed analysis. However, the response of each probe system will depend on the particular geometry employed.

Two types of systems are of particular interest in seabed work:

(1) 'towed' systems by which continuous measurements of the seabed are possible

and (2) systems, which are capable of making only static determinations.

However, in the case of 'towed' systems static determinations are generally possible with the towing vessel stationary.

In towed systems, components of the probe assembly are housed in a suitable containment vessel which is either enclosed in a flexible hose ('eel') for smooth operation on the seafloor or mounted rigidly on a sled. In both cases,

the source/detector arrangement is usually positioned above the seafloor during towing operations. These systems are deployed by long cables, usually 2 to 3 times the seawater depths depending on the towing configuration.

Probe assemblies developed for making solely static measurements need not necessarily conform to the rigid requirements as for towed systems. Flexibility of design and geometry are acceptable so that good signal-to-background ratios could be achieved in the measurements. Instruments developed for such determinations are generally lowered on to the seabed by cables from mobile platforms or from a suitable vessel.

Submersibles are now widely used for undersea operations so that both systems could be directly operated from such a vehicle (manned) or remotely controlled from a surface vessel (unmanned). Measurements could be made from a submersible in any type of seabed terrain and both surface probes as well as systems developed for penetrating the seafloor can be operated without much difficulty. Moreover, from a manned submersible sampling could be carried out simultaneously and with a sample analysis unit installed in the vehicle direct correlation of countrate and elemental concentrations could be established in a survey, apart from visual identification of the sediments.

6.2.2 Advantages and limitations of the types of probe systems

Towed systems can be used for rapid reconnaissance surveys where large areas of the seabed have to be explored in a short period of time. The distinct advantage of the system is the continuous monitoring of the seabed thus providing a complete record of the elemental constituents and their abundances. The spatial resolution is however governed by the counting time and speed of the towing vessel. The effective depth of seabed sampled is generally

10 - 15 cm with a fission type neutron source but greater with other types such as a 14 MeV source from a neutron generator. The disadvantage is the high background due to chlorine for a cylindrical type of probe, since a large volume of seawater envelopes the system while being towed.

With static analysis systems, the greatest advantage is the ability to optimise the counting time and other parameters to meet the required sensitivity of measurement at a particular location. By using a penetrating probe system, the background could be considerably reduced providing a higher signal-to-noise ratio for a determination. The disadvantage is the limited data obtained so that extrapolation of the results has to be carried out between stations for purposes of ascertaining the continuity and boundary limits of the sediment type. Thus, the spatial resolution of the measurements is dependent on the station spacing which is generally governed by the density of determinations in a surveyed area. The depth of sampling is variable and with penetrating probes great thickness of sediment could be analysed and where necessary the variation of elemental concentration with depth could be ascertained.

In a virtually unknown seabed region, towed systems are most appropriate in delineating areas of mineralisation followed by static determinations at specific locations for correlation and calibration of data.

6.2.3 Environmental factors governing the operation of probe systems

Environmental conditions on the seabed influence to a great extent the operation of a probe system. Three factors are of importance in this respect:

(1) Depth of seawater

(2) Topographic conditions

and (3) Temperature conditions

6.2.3.1 Depth of seawater

In Continental Shelf exploration seawater depths are generally around 200 m, while in deep sea regions depths of 6500 m and over could be encountered in surveys for manganese nodules. The operational capability of towed systems based on the 'eel' type has been demonstrated in the case of the natural γ-ray seabed spectrometer on the continental shelf and used successfully in depths up to 1000 m in relatively smooth seabed conditions. Probes mounted on sleds can be towed in continental shelf regions although this system is relatively susceptible to rolling and pitching in rough seabed terrain. Details of a sled being developed for manganese nodule analysis have already been mentioned earlier (LANGE and BIEMANN 1975). This particular sled is designed for towing at depths of over 6500 m of seawater within tolerable limits of pitch and roll. Towed systems could therefore be operated satisfactorily at great seawater depths.

Instruments devised purely for making static determinations could be operated at any seawater depth from surface vessels as well as from submersibles. The use of undersea vehicles provides more reliable information as to the precise location of a probe during a measurement since the uncertainties associated with probe location by using long cables are great.

6.2.3.2 Terrain conditions

In continental shelves consisting of wide, relatively shallow areas towing conditions are ideal and both 'eel' type systems and sleds could be conveniently operated. But in narrow, steep topographically varying areas such as sometimes found in the deep sea regions

difficulties would arise due to snagging of cables on obstacles. Sleds are more difficult to manoeuvre and continuous contact with the seabed sediments may not be possible during towing operations. In smooth terrain this could easily be achieved while in highly variable topography the tendency is for probe systems to overide rock outcrops so that continuous data cannot be obtained. Static measurements may be possible and the use of manned submersibles should be considered under these conditions.

6.2.3.3 Temperature conditions

Stable and low temperature conditions are essential for optimum performance of electronic components and other ancilliary equipment of a probe assembly. Fluctuations of temperature are generally accompanied by instability in the gain of amplifying systems. With germanium semiconductor detectors cryogenic cooling is essential for their operation which in a seabed environment exhibiting high temperatures, may be difficult to maintain.

In volcanically active regions low and stable temperature conditions are not generally found. In mid-ocean ridges subsurface seafloor temperatures are around 500°C and in the Red Sea regions where polymetallic sulphide deposits occur, temperatures as high as 100-150°C are common. In the Atlantis II Deep, the temperature of hot brines varies generally between 25-100°C. Therefore to maintain optimum operating conditions cooling of the instrument package is essential along with the requirements of detector cooling. This entails additional components such as cryogenerators, gain stabilisation equipment etc. to be incorporated in a probe assembly if reliable data are to be obtained with a probe system operating in a high temperature environment.

6.2.4 Geometrical alternatives of probe systems which could be used in seabed analysis and their influence on the detector response

6.2.4.1 Towed systems

For making continuous measurements on the ocean floor a probe should have the characteristics of being able to be towed easily on or in direct contact with the sediments. The simplest is thus a cylindrically shaped probe device in which case both neutron source and γ-ray detector conform to cylindrical symmetry. Normally both source and detector are configured on the central axis of the cylindrical containment so that during towing the attitude of the source and detector with respect to the seabed remains unchanged inspite of the tendency of the probe to spin about the towing cable. This symmetry is thus considered to be most practical for making in situ measurements by a towed system. The same geometry is favoured for instruments mounted on a sled.

However, in a cylindrical design a large volume of seawater surrounds the probe, since only a limited surface is in contact with the seabed at all times. In loose sediments, this condition may be somewhat less severe if the probe gouges into the seabed. The influence of chlorine is therefore high for this type of probe geometry. The situation could be somewhat improved by having both source and detector arranged asymmetrically within the probe to lie close to the seabed although it would be difficult to maintain the desired position while being towed. This could be achieved by mounting the probe rigidly on a sled, but the advantage may be off-set by the fact that the probe itself may have to be mounted at a considerable height above the runners of the sled.

Projections in a cylindrical probe to house both source and detector in separate compartments could be considered so that both components are embedded in the

sediments during towing. But the same difficulty arises as in the case of asymmetrical mounting in maintaining the correct attitude of the source and detector on the seabed and if fixed on a sled the safety of the probe in regions of rough terrain is not assured.

In towed systems any geometry other than that considered here would not be an advantage to obtain a higher detector response. Improvements to the signal may be achieved by enveloping the probe within a thick shielded jacket to prevent seawater surrounding the probe. This would also allow neutrons to be absorbed at the same time preventing them from reaching the seawater thus reducing the chlorine background. However the size of the probe system would be considerably increased and this would impose restrictions on the towing capabilities of the probe.

The signal could also be enhanced by locating the neutron source in common shielding material in the centre of a cylindrical probe with twin detectors either NaI(Tl) or Germanium positioned on either side and equidistant from the common source. The signal output from both detectors could be combined to give an integrated countrate and for this purpose two matching detectors could be used. With Ge detectors, the efficiency of the system could thus be considerably improved while maintaining the good resolution of the system.

6.2.4.2 Systems for static measurements

Equipment for making solely static determinations have no restriction with regard to probe size provided they conform to operating requirements on the seabed, e.g. pressure, temperature etc. For this reason, the geometry of source and detector could be varied and used effectively to obtain a higher detector response than for a towed system operating under similar seabed conditions. A

flexibility of this type of system is that the neutron source or γ-ray detector or both could be embedded in the seabed thus increasing the desired signal and eliminating the interference from chlorine in the overlying seawater. Since sources and detectors operate as independent units in the application of this method, a combination of several sources and detectors could be considered to obtain a higher response from seabed elements. This could be achieved by employing an array of detectors in conjunction with a single neutron source to increase the overall detector efficiency and is a distinct advantage if high-resolution Ge detectors are considered. With independent source and detector units, positions could be interchanged to obtain average countrates and the distance between source and detector can be varied to optimise the signal from particular seabed elements. A higher signal could be achieved by embedding both source and detector as independent units in the sediments with the intervening medium being the material sampled or a cylindrical probe system could be employed in a vertical attitude to obtain similar results. In both cases, the interference from the overlying seawater is eliminated. A neutron generating tube (14 MeV) is more appropriate with an independent unit since great depths of penetration could be achieved and no shielding material is required, this being provided by the sediments sampled. Higher source strengths could be used coupled with large size detectors for better countrate statistics.

6.2.5 Factors governing the development of a probe for seabed analysis

Several factors govern the development of a neutron interaction probe to obtain an optimum response from seabed elements. Of special importance are:

(a) strength of neutron source
(b) detector size
and (c) source-detector distance

Other factors which particularly influence the measurements are:

(d) probe constructional materials

(e) the influence of detector countrate on the resolution of the system

and (f) losses in signal transmission

6.2.5.1 Factors limiting neutron source-strength

In principle a large neutron source strength ensures a high γ-ray countrate in a detector and a consequent increase in sensitivity for the detection of seabed elements. However, the strength of source is also governed by three other important factors:

(1) safety to operating personnel in keeping with proper health physics requirements

(2) fast neutron damage to Ge semiconductor type detectors

and (3) the need to fix an optimum total countrate at the operating source-detector separation to ensure a good resolution of the spectrometer system.

6.2.5.1a Safety to operating personnel

On account of their small physical size radioisotope sources are easily accommodated in a probe of normal dimensions (diameter 127 mm, length 1 m in the natural γ-ray probe). A 100 μg ^{252}Cf source capsule (emission rate ~ 10^8 n.sec^{-1}) has physical dimensions of dia. 7.8 mm and length of 10 mm and an equivalent $^{241}Am/Be$ source capsule has dimensions dia. 3 cm and height 6 cm. Therefore very high source strengths can be used without undue increase in the probe dimensions. The neutron dose rates in air at 1 m from a 100 μg ^{252}Cf source and an equivalent strength of 100 Ci $^{241}Am/be$ source is 100 mrem/hr. The gamma dose rates are 10 mr/hr for ^{252}Cf

source and 100 mr/hr in the case of the ^{241}Am/Be source under the same conditions of measurement. Higher strengths could be employed for these sources if these dose rates could be kept within permissible limits with adequate shielding when the source is in storage on the deck of a ship and while transferring in and out of the probe. Source strengths of 1 mg ^{252}Cf have been suggested by other users (LANGE and BIEMANN 1975) for an analysis probe with proper safeguards.

6.2.5.1b Fast neutron damage

The fast neutron flux at the detector is an important criterion which limits the choice of source strength when used with semiconductor Ge(Li) or high-purity Ge detectors since eventual deterioration in resolution is inevitable. Although the detector lifetime is specified by the user, economic considerations generally require that a compromise should be made between indiscriminate replacement of a detector and the continuity of a survey. The effect of fast neutron flux for various source-detector separations has been considered by SENFTLE et al (1979) for the case of bore-hole measurements using a ^{252}Cf source. These results could be applied to seabed conditions, where these fluxes would be considerably lower due to the high moderation in a seabed. Hence, the strength of neutron source could be selected depending on the desired lifetime of the detector for other fixed parameters of the probe.

6.2.5.1c Optimum total countrate

In order to operate a detector system satisfactorily without impairing its resolution, the total detector countrate has to be within certain limits depending upon the spectrometer electronics. This is dependent on the particular features of the pulse amplifying system used in the acquisition and analysis of the pulses arriving at the detector. If very large source strengths are to be employed to increase the sensitivity of

measurement, then higher quality electronic processing of signals is required to maintain resolution.

6.2.5.2 Detector size

The size of detectors presently available conforms to the dimensions of normal probes. However, there is a limitation if several detectors are to be employed in a towed system, while in other systems difficulties may arise in using several detectors to probe the seabed. The response of a probe assembly would therefore be dependent on the capability of the type of system to accommodate more than one detector since an overall increase in efficiency is desirable. Detector crystals in the case of scintillator types are now fabricated to suit the particular probe designed and to preserve the other essential characteristics.

6.2.5.3 Source-to-detector distance

The source-detector distance is an important parameter which could be varied to optimise the response from seabed elements. For a linear arrangement of source and detector as in a cylindrical type of probe, the γ-ray countrate from seabed elements has been shown to decrease exponentially with distance and is a function of the γ-ray energy considered. The signal-to-background ratio on the other hand is found to increase with distance, so that there is a distinct advantage in operating a probe with large source-detector separations. The range of source-detector distances in practice is governed by several other factors. The lower limit is dependent on two important considerations; firstly, on the thickness of the radiation shield and secondly on the fast neutron flux incident on the detector for Ge semiconductor type of detectors. The thickness of the γ-ray shield which is necessary to reduce the background countrate from source γ-rays should attenuate at least 90% of the source gamma radiation. Considering lead as a suitable material for a γ-ray shield the minimum thickness required to attenuate 90% of the

source γ-rays from a fission-type source is about 10 cm. The corresponding thicknesses for platinum, tungsten and tin are 5 cm, 6cm and 18 cm respectively. In an operational system, the source-detector distance should be at least several times the thickness of the γ- shield since the proximity of the detector to the shield would attenuate the γ-rays from seabed elements. The fast neutron flux on the detector is of course governed by the strength of the neutron source, and the source-detector separation selected purely on this consideration depends upon the expected working life of a detector. In the case of germanium semiconductor detectors this is an important factor.

Theoretically, there is no restriction to the upper limit for a source-detector separation but practical considerations depending on convenience in handling and towing generally demand that probes should be 1-2 metres in length. These dimensions usually include the requirements of housing other essential components so that the actual source-detector distance is less than this value. For source-detector separations used in the experimental work, i.e. 25-55 cm it was observed that with a given neutron source strength, the signal-to-background increases continuously within this range. Experimental determinations also reveal that the highest γ-ray countrate is obtained for a given source-detector separation with the γ-ray shield adjacent to the source. On these considerations source-detector distances of 30-40 cm are good practical values for a cylindrical design of probe using a 2.5 μg ^{252}Cf neutron source used in conjunction with a Ge semiconductor detector and a γ-ray shield of at least 10 cm of a suitable material such as lead.

For systems designed solely for making static measurements, there is no restriction to the upper limit for source-detector separations in a probe assembly. Large distances can be employed to obtain a high detector signal in relation to the background although the source strength may be a limiting factor since this would have to be increased considerably to maintain a high sensitivity for detection.

6.2.5.4 Probe construction materials

Materials for the construction of a neutron interaction probe should possess certain fundamental properties:

(1) capability of being fabricated with a required wall-thickness to withstand high pressure conditions at great depths without yielding, i.e. typically 7000 m of seawater including a safety factor for operation

(2) easily machinable to required specifications

and (3) stability to seawater corrosion.

The common engineering materials which satisfy these requirements are stainless steels, aluminium alloys and recently carbon fibre. For given dimensions of a cylindrical type of probe, i.e. outer diameter and length, different wall-thicknesses have to be used to enable the various materials to operate satisfactorily at the same depth. For a probe length of 30" and diameter 4.75", a wall-thickness of 0.135" is required for a stainless steel body (chrome/nickel alloy) to operate on the continental shelf, i.e. < 200 m seawater depth. For an aluminium-magnesium alloy the corresponding thickness is 0.178". For a stainless steel probe to operate at seawater depths around 6500 m, the wall-thickness would have to be increased to at least 2 cm and considerably greater with an aluminium-magnesium alloy.

Stainless steels used for underwater constructional purposes contain a fair percentage of chromium (16-18%) and nickel (10-14%) with either 2-3% of molybdenum or less than 1% titanium to increase corrosion resistance. A further 1-2% of manganese is also added for stability. Aluminium alloys contain about 5% magnesium and have all the other characteristics suitable for marine applications. For purposes of comparison naval brass contains 60% copper, 39.25% zinc and 0.75% tin. While all these materials could be used in the construction of a natural γ-ray seabed probe, where only the attenuation of the γ-rays by the thickness of the probe need be considered, difficulties may arise when using a neutron interaction probe due to the production of undesirable capture γ-rays by elements in the construction materials. Cr, Ni, Ti and Mn have low detection limits (<0.3%) using the (n,γ) capture technique. (TABLE 5.14). For Al and Mg these limits are very much higher. It is clear that stainless steel would produce a significant background in a seabed γ-ray spectrum thus limiting the sensitivity for detection of other elements. Aluminium produces only a single prominent capture γ-ray of energy 7.724 MeV and may be considered for a probe. Brass contains a very high proportion of Cu and Zn and is therefore unsuitable for a probe incorporating a neutron source. On the other hand carbon fibre could be considered on account of its good mechanical and engineering properties and its relative insensitivity to thermal neutron capture.

The attenuation of γ-rays in a probe material from seabed elements is another important aspect to be seriously considered. For a stainless steel probe with a thickness of 0.135" the attenuation of γ-rays in the energy range 6-8 MeV is about 8%. For an aluminium alloy considered here with an increased thickness of 0.178" the corresponding attenuation is only 3%. This is acceptable for probe thicknesses considered on the Continental Shelf. In the

Deep Sea for a stainless steel probe and for a wall thickness of 2.5 cm the γ-ray attenuation in the energy range 6-8 MeV is about 45%. The corresponding attenuation for an alluminium alloy probe of the same thickness is only 15%. These figures show the necessity of selecting appropriate construction materials for a probe to obtain the highest sensitivity for detection of seabed elements.

6.2.5.5 Countrate and detector resolution

In the (n,γ) capture mode, the useful data occur in a narrow peak in the complex spectrum obtained in seabed analysis. The peaks are superimposed on a continuous background thus representing only a small fraction of the total counts recorded. In the experimental work the detector countrate was kept below 5000 cps for a minimum source-detector separation of 20 cm in order to ensure that the resolution of the detector system was maintained at a satisfactory level without being impaired. With this countrate a counting time of 120 mins was required to obtain statistically significant counts in the γ-ray energy peaks of elements in the seabed. Although adequate statistical accuracy can be achieved by employing long counting periods, the data acceptance of the electronics is a limiting factor to achieving a high statistical accuracy in a short time. This is therefore the limiting factor in obtaining high spatial resolution in delineating gradients of mineral concentrations on the seabed. For example in a seabed containing 2.5% copper about 200 counts would be required in the 7.915 MeV γ-ray peak to achieve an acceptable statistical accuracy. With conventional electronics capable of operating up to 10 kHz a counting time of 120 mins is required, which is clearly not acceptable when towing at 3-4 knots. However, electronics capable of operating up to 100 kHz are now available so that this could be used to obtain a high spatial resolution and accept high detector countrates without impairing the resolution of the system.

6.2.5.6 Signal losses in transmission

In probe systems designed for towing from surface vessels, it is often desirable to provide electrical power and signal transmission to the ship using a single coaxial cable. For operations at relatively shallow depths such as in the continental shelf regions, the effect of signal attenuation and interference from the power supply could be tolerated within acceptable limits. At seawater depths where great lengths of cable are used signal losses and interference become serious and impair the quality of the data. To maintain good resolution and to enable the equipment to operate at high counting rates a pulse height analyser should be included in the probe. At great depths, i.e. 6500 m the signal pulses could be digitised and transmitted to the towing vehicle for this purpose.

In operations carried out with a submersible, data could be acquired from the seabed using short lengths of cable in a more standard form thus circumventing the adverse factors encountered in signal transmission.

6.2.6 Criteria for detection of probe contact with the seabed

For elemental analysis, an important requirement is to maintain the probe in continuous contact with the seabed during its operation. In the case of the natural γ-ray spectrometer, it is possible to monitor this situation from the level of radioactivity observed, since there is a large and rapid drop in the γ-ray countrate from the seabed when the probe is off-bottom. With a neutron interaction probe the capture γ-rays in the overlying seawater are responsible for the major part of the signal so that the same criterion cannot be used. However, from the experimental work carried out a measurable change in the background radiation has been observed in the lower energy regions, i.e. < 3 MeV when the probe is in contact with the seabed. In the case of a silica-type seabed this change

is found to be about 25% so that this could be used as a criterion when towing a neutron interaction probe. Additional criteria are the characteristic γ-ray lines from the seabed type elements such as Si, Ca, Al etc observed when the probe is in contact with the seabed, but these are in general too weak for continuous control purposes.

6.3 The expected performance of an operational probe in seabeds containing some selected elements of economic importance

6.3.1 General

As outlined in the introductory chapter, the two physiographic regions of the ocean floor of importance in seabed exploration are the Continental Shelf and the Deep Sea. The mineralisation of these regions, the mode of occurrence of the deposits and their economic significance to the mineral industry have been discussed by MERO (1965) and recently in detail by CRONAN (1980). In assessing the performance of a probe in the analysis of these deposits two important factors need to be considered. They are:

(1) the physical conditions of the seabed

and (2) the associated sediments in which these deposits occur.

On account of the variability of these factors, four different types of mineral deposits have been selected to demonstrate the scope of the technique and to illustrate the wide range of problems encountered in its application to seabed analysis. For this purpose the minimum abundances of elements which could be detected by an operational towed system using a 100 μg ^{252}Cf neutron source and a counting time of 15 mins as given in TABLE 5.14 are used. These values are based on the response of a cylindrical type of probe having a source-detector separation of 30 cm. As discussed in the earlier section, various types of probe systems involving different geometry

of measurement could be employed, so that these minimum detectable limits could be considerably improved to exploit the full potential of the analysis technique. Since the method is elementally specific, its application is limited only to the detection and determination of the elemental constituents of a deposit. However, under favourable circumstances the mineral itself can be identified from these constituents if there is no ambiguity in interpretating the results. The different types of deposits selected for this study are:

(a) placer deposits which occur on the Continental Shelf

(b) nodular barite and phosphorite concretions found in the deep continental shelf regions

(c) polymetallic sulphide deposits associated with regions of submarine volcanic activity

and (d) manganese nodules of current economic interest which occur in the Deep Sea.

6.3.2 Placer type deposits

The placer deposits considered in this study are the fine grained very heavy minerals, gold and platinum found in bays and estuaries off Alaska, the important alluvial tin deposits predominantly of S.E. Asia and the light-heavy minerals such as monazite, ilmenite, rutile, magnetite etc. found off the Coasts of India, Sri Lanka, Australia and to a limited extent off Florida.

6.3.2.1 Seabed conditions

The continental shelf regions in which these placers occur represent two types of seabed environment:

(a) wide, relatively shallow and uniform plains usually found adjacent to stable lowland coasts

and (b) narrow, steep topographically variable areas commonly associated with rugged coast lines.

Although the distribution of sediments in these environments is somewhat irregular, a generalisation is that in open shelf areas sand is the most common seabed type constituent, while in protected bays and inland seas mud and clays are predominant.

The specific minerals likely to occur at any single location constitute a limited range depending on the seabed environment. A characteristic of interest to this study is the particulate nature of all the mineral concentrations, which generally occur on the surface of the seafloor, although buried deposits are not uncommon as in the case of tin. Hence, the thickness of sediments of near surface placers is well within the range of seabed sampled by a towed system, which extends from 10 - 15 cm. Experimental measurements have also established the near constancy of seawater content of these unconsolidated sediments (20-30%). This implies that in the analysis of placers, the background in a γ-ray spectrum obtained by a neutron interaction probe would be practically constant as shown by measurements in the case of similar elements 'seeded' in the simulated seabed.

6.3.2.2 Seabed analysis

A feature of the type of elements found in placers is the low to moderate thermal absorption cross-section for neutrons. Therefore, for the abundances expected in the analysis of these sediments, no significant perturbations in the thermal neutron flux distributions are expected in seabeds containing these elements. Gold is a possible exception σ_a = 98.8b but the concentrations found are low so that for most elements, a near linearity can be expected in the variation of countrate with abundance.

6.3.2.2a Gold and Platinum

The lowest limit of detection by a surface probe for gold and platinum using a 100 μg ^{252}Cf neutron source and a counting time of 15 min is 0.3% and 4.0% respectively, assuming the associated sediment type to be silica. Under these conditions the detection is not difficult provided the concentrations are well above the minimum detection limits quoted. However, in the seabed environment in which both these elements are found, muds are the dominant seabed type material, so that a higher background could be expected than with silica. The minimum detectable limits would therefore be considerably higher than those given by amounts proportional to the increased seawater content in mud (by about 10%). Static systems with neutron source and γ-ray detector embedded in these sediments could overcome this difficulty but with a towed device a higher source strength coupled with a large counting time could achieve the same result.

Gold has several characteristic γ-rays of which the 6.252 MeV, 6.319 MeV and 6.457 MeV energy lines are well resolved to be observed in a spectrum. Their intensities are comparatively low so that its detection is somewhat limited on account of the very low abundance of gold normally found associated with seabed sediments. On the other hand, platinum has only one energy line 5.255 MeV of comparable intensity to gold but its sensitivity of detection is lower by an order of magnitude (4.0%). Static determinations with a penetrating probe system are therefore the only possible means of overcoming the practical difficulty of estimating the very low concentrations of these elements in the seabed.

6.3.2.2b Tin deposits

The thermal absorption cross-section of tin (Sn) is relatively low (0.63 barns) and no characteristic γ-rays above 3 MeV are known to have high sensitivities for detection by this method. This situation is represented in Table 5.14 by assigning a lowest limit of 100% Sn for its detection. However, tin produces a series of low energy capture γ-rays below 3 MeV, which could contribute significantly to an observed γ-ray spectrum from a sea-bed containing tin bearing sediments. Such a spectrum would be similar to that shown in Figure 5.9 which has been obtained experimentally by using a tin γ-ray shield in the probe.

The increase in the background radiation levels in the low-energy region i.e. < 3 MeV can be monitored by using a high efficiency γ-ray detector such as NaI (Tl) or a BGO. For quantitative analysis a prior calibration of the probe system with known concentrations of tin is essential.

6.3.2.2c Ilmenite and other associated deposits

Ilmenite ($FeTiO_3$) is one of the important placer minerals in industry. It is found in the shallow regions of the continental shelf, 40 - 60 m and usually occurs in association with several other placers, notably magnetite (Fe_3O_4), rutile (TiO_2), zircon ($ZrSiO_4$) and monazite (phosphate of Yr, La, Ce containing variable amounts of ThO_2). Of these, monazite is naturally radioactive and is easily detected by a natural γ-ray seabed spectrometer due to its high thorium content. Zirconium is relatively insensitive to detection, the lowest limit of detection being 20% Zr which corresponds to 40% zircon. Such percentages of zircon are rarely found to be concentrated in placers and hence its detection by this method is not possible except in association with other easily detectable minerals.

The elements iron and titanium are the principal constituents of ilmenite ($FeTiO_3$), magnetite (Fe_3O_4) and rutile (TiO_2). The detection of Fe using the γ-ray energy lines 7.632 MeV and 7.646 MeV is relatively easy, the lowest limit of detection being 0.3%Fe which would correspond to 0.4% Fe_3O_4 if magnetite is the only mineral present. In the γ-ray spectra obtained with 3% Fe in the simulated seabed (Figure 5.12), the full-energy peaks of iron occur as a composite peak due to the poor resolution of the spectrometric system at the time of measurement. These two energy lines can be resolved by a good resolution detector in a practical seabed survey so that quantitative estimates of Fe (or magnetite) could be made. The analysis technique could therefore be used to detect Fe on the seabed if magnetite is the only mineral present. Magnetic methods however provide the best exploration technique for magnetite but in combination with measurements carried out with a neutron interaction probe, the presence of ilmenite and rutile could be established in a placer containing all three minerals.

Rutile, as a mineral could be similarly detected in the seabed by the 6.760 MeV (54% intensity) and 6.418 MeV (36.5% intensity) lines of titanium. The lowest limit of detection using the higher intensity energy is 0.1% Ti (0.17% rutile). The double-escape peak of the 7.790 MeV γ-ray energy of chlorine occurs very close to the principal energy of 6.760 MeV of Ti. This difference in energy 10 keV could be resolved with a good resolution detector or the double-escape peak (5.740 MeV) which is not contaminated can be used since it provides a higher countrate. The lower intensity line of 6.418 MeV could also be used to obtain a second measurement since the presence of both energy lines confirm the presence of Ti in the seabed. For quantitative analysis, the method suggested in Chapter 5 could be employed where the titanium counts in the full-energy peak could be extracted from the contaminated chlorine peak. The γ-ray spectrum for 3% Ti in a silica seabed using rutile as the 'seeding' material is shown in Figure 5.13. Several photo-peaks of Ti can be seen and well differentiated from the more intense chlorine peaks from seawater and with improved resolution of the detector system, better peak differentiation and statistical confidence could be achieved.

The presence of magnetite and rutile as individual minerals in a placer deposit could be established if these are the only Fe and Ti bearing minerals present in the sediments. If ilmenite is also present then the detection of Fe and Ti by the analysis technique could not provide a unique interpretation of the results. The detection of ilmenite on the other hand is relatively easy as in the case of magnetite and rutile since the elemental constituents are the same, i.e. Fe and Ti. The γ-ray spectrum obtained for a seabed containing 2.9% Fe and 2.5% Ti in a silica sand matrix is shown in Figure 5.14. The percentages used are identical to the proportion in which these elements occur in ilmenite, which

in this case corresponds to 7.9% of the mineral. Since the lowest limit of detection of Fe is 0.3% and Ti is 0.1% the minimum abundance of ilmenite detected on this basis is about 0.3%. Analysis of beach deposits rich in placer type minerals reveal high percentages of ilmenite (75-80%), rutile (6-10%) and magnetite (2-3%). The percentages in off-shore deposits may be somewhat lower but nevertheless high enough to be analysed by this technique. Similarly, in the magnetite deposits off the coasts of Japan, the percentages of Fe and Ti are 56% and 12% respectively. These values indicate the facility with which the (n,γ) analysis technique can be employed to obtain reliable data in prospecting for these deposits.

It would not be possible from a γ-ray spectrum in which both Fe and Ti peaks are observed to confirm the presence of ilmenite by taking ratios of the countrates observed in the Fe and Ti energies. This is because of the possible contribution to the Fe and Ti energy peaks if magnetite and rutile occur together in the same deposit. However, if ilmenite is the only mineral present, then the ratio of the counts in the energy peaks of Fe and Ti would be a constant (approx. 1.17) this being the proportion of these elements in ilmenite. Hence this ratio could be used as an index to determine the occurrence of this mineral. By combining this analysis technique with other geophysical methods such as seabed magnetometer measurements and limited sampling, these ambiguities can be resolved when prospecting for placers containing several minerals having common elemental constituents.

Two other placer minerals of interest in seabed exploration are cinnabar (HgS) and chromite ($FeCr_2O_4$) both having low minimum limits of detection by this technique. The minimum limit for chromium (Cr) is 0.2% and for mercury (Hg) is 0.03%, which are sensitive enough to be detected provided they occur in sufficient abundance on the seabed.

Mercury has several prominent γ-ray energies of which the 5.967 MeV is of high intensity to provide a good sensitivity for its detection. The presence of a peak due to S (5.420 MeV) along with Hg should give a positive identification for this mineral. Since the minimum detectable limit (0.03%) for Hg is equivalent to 0.35% of HgS, concentrations of more than 0.1% cinnabar could be easily detected.

Chromium also has several prominent γ-ray energies, the 8.884 MeV and 7.939 MeV are well resolved in a seabed spectrum containing this element (Figure 5.15). These energies are in the upper region of the spectrum and consequently are associated with a very low background from seawater and a total absence of interference from chlorine. The spectra shown is for a concentration of 3.8% Cr in a silica sand matrix obtained under the same conditions of experiment as in the case of Ti and Fe.

6.3.3 Nodular barite and phosphorite concretions found in the deep continental shelf regions

6.3.3.1 Barite

Barite ($BaSO_4$) as nodular concretions has been reported from several locations in the deep sea regions of the Continental Shelf. The occurrences off Sri Lanka are in seawater depths of about 1250 m while those off Indonesia and California are in shallower waters 304 m and 650 m deep respectively. Nodules from these locations generally average 75-77% $BaSO_4$ which corresponds to 45% elemental barium. This is much higher than the lowest limit of detection of 6% Ba by a surface probe. With a penetrating system the sensitivity of detection could be increased by a factor of 4 which lowers this limit to about 1.5% Ba. Data from the Deep Sea Drilling Project show that nodular barite tends to increase in abundance with depth (DEAN and SCHREIBER 1977) so that there is a distinct advantage in operating probe systems capable of penetrating the sediments.

The associated sediments are usually glauconite sands in which SiO_2 predominate (50%) with lesser amounts of Fe_2O_3 (25%). The characteristic barium γ-ray energy is the 4.096 MeV line which is the most intense of all the other barium γ-ray energy lines. An interfering γ-ray energy is the double-escape peak of silica (Si 4.087 MeV). This is however, very low in intensity and could be resolved with a detector having a resolution better than 10 keV. No interference would be expected with other elemental constituents from the associated sediments.

6.3.3.2 Phosphorite deposits

The phosphorite deposits of economic interest found on the continental shelf are in seawater depths of less than 1000 m and generally occur as nodular concretions. Oceanic seamounts, islands and atolls are other important environments for phosphorite formation.

The major elemental composition of phosphorites from various submarine localities is given in CRONAN (1980a). The average P_2O_5 values vary from 20-30% giving a maximum value of about 14% elemental phosphorous. Calcium oxide forms the major constituent of the nodules and averages 70% Ca. Similar deposits off the coasts of S.W. Africa consist of phosphatized muds and compacted sediments in addition to fine grained nodules. The sediments record the highest phosphorous content, i.e. 14% P while the fine grained nodules average about 12% P. Deposits off Peru and Chile contain 5-12% P and averages about 24% Ca with a higher SiO_2 content than nodules from the other regions.

The Chatham Rise deposit off the coast of New Zealand illustrates the nature and distribution of a phosphorite nodule field (CULLEN et al. 1981). The deposit consists of loose nodular gravels and occurs along the crest of the Chatham Rise showing a patchy distribution ranging from 10-300 m in length. The nodule formation is

sometimes 70 cm thick with individual grains a few mm to about 15 cm across underlain with limestone. The average P_2O_5 content is 21.5% (9.4% elemental phosphorous) and the sediment itself contains about 80 kg of phosphorite per m^2. The uranium content in individual nodules is found to vary from 0.004% to .044%.

Exploration for phosphorite could be carried out with a towed natural γ-ray seabed spectrometer using the 1.764 MeV γ-ray of the decay of uranium (from ^{214}Bi) commonly found in association with these deposits. The method is an indirect one and depends primarily on the occurrence of uranium in the deposit. For quantitative analysis a definite relationship between the uranium and phosphorous content of the deposit should be known. The method has been applied to phosphorite prospecting using a submersible scintillation counter (SUMMERHAYES et al. 1970) where determinations were made at previously sampled locations. Concentrations as low as 0.3% P_2O_5 have been correlated with the countrates observed. The overall patchiness of this type of nodular deposit suggests continuous profiling systems for meaningful interpretation of the results, and the assessment of the grade of a deposit requires the determination of the elemental concentrations in the nodular material.

The analysis of phosphorite on the seabed is best undertaken by a neutron interaction probe using a neutron generating tube as the source. The advantage here is that the source could be used in a pulsed mode, so that by time sequencing the events in the analysis technique it may be possible to observe both the natural γ-rays from the associated uranium as well as the neutron capture γ-rays from P, Ca and other constituents during a single traverse of the seabed. A germanium high resolution detector could meet the requirements both for natural γ-ray measurement and the capture γ-rays from P although a high efficiency scintillation detector should be applicable.

The most intense capture γ-ray emitted by phosphorous is the 3.900 MeV energy and together with the detection of the calcium 6.420 MeV γ-ray in a seabed spectrum generally confirms the occurrence of phosphorites. The minimum detection limits of phosphorous by a typical probe designed for surface measurements is about 7% and below the concentrations found in phosphorites and phosphatic sediments. The depth of sampling extends to about 10-15 cm but for deeper assessment of sediments a penetrating probe system could be employed. The sensitivity of detection would in this case be increased and optimum counting times can be used for reliable countrates.

No interference from any of the γ-rays from Ca and Si is expected with the γ-ray of phosphorous. However, the 3.900 MeV line from P lies close to the double-escape peak of the Si 4.934 MeV and may require the use of a germanium high resolution detector. The detection of calcium in the presence of silicon is best illustrated in the γ-ray spectra obtained for those elements in the simulated seabed (Figures 5.19 and 5.21). These were obtained for pure $CaCO_3$ and for a mixture of $CaCO_3$ and SiO_2 in equal proportions by weight. The γ-ray energies of each of these elements are well resolved and easily identified in the concentrations they occur in these seabeds. Using the double-escape peak of Ca 6.420 MeV about 20,000 counts would be obtained for a pure $CaCO_3$ seabed (40% Ca) and about 12,500 counts for the silica mixed seabed (20% Ca). This would correspond to about 650 counts for 1% Ca using the same probe characteristics for which the lowest limits of detection were determined. Hence for the abundances occurring in phosphorites, significant countrates could be obtained for calcium with a seabed neutron probe. Since the principal constituents consist mainly of phosophorous and calcium, the countrates obtained for those two elements could be used to assess the grade of a nodular field.

6.3.4 Polymetallic sulphide deposits

6.3.4.1 General comments

The metallic minerals considered here are the outcome of several submarine volcanic processes, and consequently, high temperature conditions are associated with the environment in which they occur. The effect of temperature on the operation of a neutron information probe for analysis of such deposits has already been discussed earlier. Nevertheless, probes can be designed to overcome these effects and satisfy the operational requirements.

The best described sediments are found in the Red Sea and several others are known to occur along the world mid-ocean Ridge system and in island arcs. Of these, the mid-Atlantic Ridge, the East Pacific Rise and the Galapagos region are of interest since they represent different seabed conditions. Polymetallic deposits have been classified into three distinct types (CRONAN 1980). They consist of:

(1) sulphides of copper, zinc and iron
(2) oxides of iron and manganese
(3) silicates of iron.

These are found to occur at a number of locations on the ocean floor. Of the three types, the sulphides of copper and zinc are considered at the present time to be of economic importance.

6.3.4.2 The Red Sea deposits

6.3.4.2a Nature of sediments and seabed conditions

The deposits of the Red Sea region occur in several Deeps averaging a seawater depth of 2000 m and represent a diversity of sediment components both laterally and in depth over relatively small distances. The elemental constituents are principally those of the

minerals in the three groups mentioned. The data available from the Atlantis II Deep, illustrate the general characteristics of the sediments of this region and the environment in which analysis has to be undertaken.

The mineral bearing sediments in the Atlantis II Deep covers an area of 60 km^2 with an average thickness of 10 m, the maximum depth to basement is about 15 m. The brines, which have a chlorine content of 156 g/litre at a temperature of 62°C occupy the bottom 200 m of the 2000 m deep water column. The physical nature of the sediments indicate the existence of cohesive muds in the seabed and shows a gradual consolidation with depth. TABLE 6.1 presents data of the stratigraphy, mineral distribution and chemical variation with depth of the deposit, which is typically representative of those found in this environment. The sediments are stratified showing two sulphide zones of mineralisation which occur within 10 m of the surface. The percentage of solid material is less than 20% up to 10 m and is about half this value within 5 m of the seabed.

6.3.4.2b Seabed analysis

Analysis of the Red Sea deposits could be made using a towed system. Within a depth of 5 m of the sediments the solid material content of 8% would imply that the probe may be embedded in the sediments during towing. A close grid interval in surveying is essential to obtain a representative analysis of the sediment distribution due to the variability of this type of deposit within short traverses of the seabed.

The chlorinity of the brine in this location is 152‰ compared with a value of 19.3‰ for normal seawater of salinity 35‰. This is an increase by a factor of 7.8, so that a general increase in the chlorine background by this factor would be expected in a γ-ray spectrum of the

sediments. The limits of detection by a towed system for Zn, Cu, Fe and Ag are given in TABLE 5.14 and are Zn (2%), Cu (0.3%), Fe (0.3%) and Ag (2.0%). The modified detection limits due to this increase in background mean that Fe is the only element sensitive to detection by such a probe system and Ag is not detectable since the concentrations are in the ppm range. However, in other regions of the Red Sea, concentrations of zinc as high as 30% Zn has been observed which could be easily detected. If the effect of brine is reduced by having the probe embedded in the sediments a decrease in background by a factor of 4 could be achieved for a seabed containing 30% brine. This will increase the sensitivity for Zn and Cu which, with some optimisation of probe design would permit an in-situ determination of these elements. A higher value for the neutron source strength coupled with a larger source-detector distance would considerably improve the signal-to-background ratio to give the sensitivity required in the analysis of these elements. For static determinations using a penetrating probe system, an appropriate geometry and longer counting times could be adopted to obtain significant countrates above background. This system could also be used to advantage to assess the variability of the sediment distribution with depth.

6.3.4.3 The East Pacific Rise and other related deposits

6.3.4.3a General

A characteristic of the sediments of the mid-Ocean Ridge is the similarity in the origin of the deposits, which occur as fine-grained poorly consolidated material often mixed with varying amounts of calcium carbonate. These sediments generally contain several base and precious metals including Co, Pb, Mo, Ni and Ag in the ppm range while Zn and Cu are found in high percentages. The higest grade deposits are reported to occur in the East Pacific area so that the locations considered for this

analysis are the East Pacific Rise (21°N), the Galapagos region (00° 36'N and 86° 06'W) and some related deposits in the vicinity.

6.3.4.3b Sediment distribution and its environment

The deposits in the East Pacific Rise (EPR) at 21°N occur in seawater depths of around 2600 m, as mounds 10 m high and 3-4 m wide aligned parallel to the crest of the Ridge. These are enriched in Zn and Cu. Flat encrustations composed of the same material as the mounds with native S also occur in the same environment. Samples containing a few tenths of a percent Ag have been recovered from this region. The sulphides are generally porous and native sulphur occurs as encrustations both on the prominences and on the ocean floor. The seabed temperature near the active vents through which sulphide-bearing solutions discharge is about 350°C.

The best surveyed area of the deep sea floor in the Galapagos region is the mounds field, as it is known and has a thin uniform sediment cover consisting of rapidly accumulating siliceous/carbonate oozes presently 25-30 cm thick. The mounds occur paralleling the spreading axis with individual mounds 15-20 m high and 50 m wide at their base. These are encrusted with manganese some of which attain thicknesses of over 6 cm. The Mn crusts contain as much as 45% Mn and less than 1% Fe. The temperature conditions in this region are relatively stable and low.

Sulphide rich sediments also occur in the Galapagos Rift which is about 20 km north of the mounds field. The sulphides contain up to 27% Cu and 31% Fe and are low in zinc (1.5%). Silver is present in concentrations of 0.005% and Mn is found widely dispersed

in sediments around these deposits. The temperatures near the vents are 10-11°C and rapidly falls off on mixing with seawater.

In the Galapagos Region, no high salinities are observed and the seawater depths are around 2700 m. The chemical analyses of samples dredged from this region are given by CRONAN (1980).

6.3.4.3c Analysis of sediments

A common feature of the environment in which metallic deposits occur is a dissected seafloor topography, both in the East Pacific and Galapagos regions. The distribution of the mounds alongside the ridge with conelets interspersed among them generally makes towing unfavourable on this type of terrain. Since the important elements Zn, Cu and Ag are confined to these mounds, analysis is best undertaken by a submersible. Static measurements with a penetrating neutron probe could make ideal determinations in individual mounds. The depths of seawater are within the range of operation of any of the probe systems.

In the East Pacific Rise, the columnar mounds contain as much as 27% Zn, 6% Cu and 1-1.5% Ag with significant amounts of native S. The values for Zn and Cu are above the lowest limits of detection by a towed system, these being 2.0% Zn and 0.3% Cu. The value for Ag is 2.0% which is marginal but well within the capability of detection by a probe with an increased sensitivity. A typical γ-ray spectrum of a silica type seabed containing zinc sulphide is given in Figure 5.8. This is for a concentration of 24% zinc and 6% sulphur. The 7.863 MeV γ-ray of zinc is clearly resolved with no interference from

chlorine in the seawater. The energy peaks due to sulphur are also visible but the effect of background at lower energies is seen in this spectrum. A similar γ-ray spectrum for Cu is given in Figure 5.17 in which the copper peaks at 7.915 MeV and 7.637 MeV are clearly seen. Comparison of these two spectra shows that with Zn and Cu occuring in the same sediments there would be no interference in the energy peaks of these elements, although the most prominent γ-ray energy of Ag (5.700 MeV) and S (5.420 MeV) is located in the lower energy region of the spectrum. With a probe system optimised to the analysis of these elements, the detection of Ag would be relatively easy and with static measurements significant counts in the various energy peaks could be obtained for longer counting periods.

In deposits of the Galapagos Region and in its vicinity, the percentages of Cu and Fe are very high so that quantitative estimates could be made easily. The percentages of Zn are rather low, about 1.5% in the Galapagos Region which is marginal since its lowest limit of detection is 2.0%. Though some of the peaks of Cu and Fe lie close together in a spectrum where both elements occur, at least one energy line is observed to be situated in a region where it could be monitored and a high degree of accuracy can be attained since their abundances are unusually high in this region, i.e. 27% Cu and 31% Fe. Of special note is the high concentration of Mn found as encrustations (average 45% Mn). The effect of such abundances on the response of a detector system has been already discussed in Chapter 5. Although the detection of Mn at these concentrations is relatively straightforward, quantitative analysis is more complicated due to non linearities in the calibration of a probe for manganese.

6.3.5 Manganese Nodules

6.3.5.1 Introduction

The current interest in manganese nodules as a potential source of nickel and copper was mentioned briefly in the introductory chapter. The economy of mining such nodules lies in the significant amounts of a variety of minor and trace elements found to be associated with the nodules. Of these Ni, Cu and Co reach individual concentrations of about 1.5% though not in the same nodule. The major constituent elements Mn and Fe are found in varying proportions, so that whilst the absolute concentrations of these two elements are not of prime importance the ratio Mn/Fe is nevertheless a useful parameter, since studies have shown that nodules with Mn/Fe ratios between about 1.75 - 5.0 are generally those which are most enriched in Ni and Cu.

The quasi-surface distribution of manganese nodules is a reasonable match to the range of depths sampled by a towed neutron interaction probe. The important elemental constituents of these nodules have relatively low minimum limits of detection by the method of analysis, i.e. 0.3% Mn, 0.3% Fe, 0.3% Cu and 0.1% Ni so that reliable estimates of individual concentrations of these elements could be made. The ratio Mn/Fe can be monitored directly by this method during a seabed traverse to assess the economic potential of a deposit. The particular factors which influence these measurements are the seabed environment and the nature and elemental constituents of the associated sediments. Data in this respect have been obtained mainly from MERO (1965), CRONAN (1980) and more recent information from CRONAN (personal communication).

6.3.5.2 Seabed environments

Manganese nodules are known to occur under different environmental conditions in relatively shallow waters, in deep sea regions and under limited conditions in inland

lakes. The diversity of the deposits and the variability of their distribution on an ocean wide basis has been described by MOORBY (1978) in relation to his studies on the Indian Ocean nodules. On account of these factors, a variety of seabed conditions could be associated with manganese nodules so that the performance of a neutron interaction probe in the analysis of such nodules is best evaluated in relation to known deposits on the seabed.

6.3.5.2a Near shore and lacustrine deposits

In shallow, near shore marine deposits, such as those of the Baltic Sea, small spheroidal concretions and crust-like accretions of Mn and Fe are fairly common. Spheroidal concretions are most abundant at the sediment-seawater interface and partly covered by a thin mobile layer of sediment. Very occas ionally are these found buried to a depth of more than 10 cm.

Nodular material from lacustrine deposits of Canada, U.S.A. and Russia, exhibit similar characteristics as near shore deposits. The nodules invariably occur as surface concentrations and rarely are found buried below a few cm in the sediments.

A common feature from the point of view of manganese nodule analysis are the shallow water depths, which are generally below 1000 m and the near surface concentration of these deposits in both environments. In the case of marine deposits the seabed matrix in which the nodules occur include sands, muds and gravels, while the lake beds generally contain a mixture of gravels, coarse grained sand and hard glacial clays. The seabed or lake bottom in each case provide stable towing conditions for a surface probe and the depth of concentration of the nodular material which is less than 10 cm ensures maximum sampling of the nodules. The absence of chlorine in a lacustrine environment is a distinct advantage in the application of neutron interrogation methods to lake bed exploration.

6.3.5.2b Deep Sea deposits

Manganese nodules in the Deep Sea occur in several topographical features of the ocean floor which include seamounts, elevated marginal plateux, mid-ocean ridges, deep water continental borderlands and the deep ocean floor itself.

In seamounts, the nodules are confined to prominences which are complex topographically. The seawater depths at which they occur are variable but generally around 1000 m.

Data from plateau areas are available only from a few locations. Well known are the deposits of Blake Plateau off the coasts of Florida, U.S.A. These are extensive, very rich in nodule concentration and cover an area of about 200,000 km^2. Seawater depths vary between 200-1000 m.

In mid-ocean ridges the common occurrences are on volcanic rock outcrops. These are found generally on the flanks of both active and inactive systems. The topographic conditions typical of this environment are illustrated in the TAG area of the Mid-Atlantic Ridge (CRONAN 1980). The nodular material is confined to the slopes of the ridge on volcanic rocks in bathymetric depths around 2000 m - 5000 m.

Water depths in deep water continental borderland areas are around 3000 m - 4000 m and the characteristics of the nodules are very similar to those from shallow marine environments discussed earlier. These yield the highest concentration of Mn and by far the lowest Fe content though poor in trace elements.

The manganese nodules on the deep ocean floor are recognised as the most abundant of the deposits and occur in seawater depths between 4000 m - 6000 m. Concentrations of nodules, in the North Pacific are found to be mostly in a broad band of gently rolling abyssal hills. In the Indian Ocean, nodules in the deep sea are found in elevated areas as well as in basins. The nodules in the basins are normally confined to the slopes of the edges of these features.

6.3.5.3 Composition of Manganese nodules

6.3.5.3a Near shore and lacustrine deposits

The nodules from shallow marine deposits are different to those from other environments in several respects, important factors being the highly variable Mn/Fe ratio and the low content of trace elements (less than 0.01%). The Mn/Fe ratio has a wide variability, about 45 to less than 0.1 but on the average Fe is more abundant than Mn in these deposits.

Similar values for trace element content are observed in lacustrine deposits as a general rule, but individual lakes are found to contain relatively high Ni, Cu and Co though the concentrations are in the ppm range.

6.3.5.3b Deep Sea nodules

The compositon of known manganese deposits from various environments in the deep sea gives a general indication of the percentage elemental concentrations of trace metals to be expected when surveying in a particular seabed environment. This is of interest to the (n,γ) analysis technique since their detection by a seabed probe implies certain minimum limits of concentration of these elements in the nodules. Therefore the average abundances of Mn, Fe, Ni, Cu and Co and the ratios Mn/Fe for the different seabed environments are presented in TABLE 6.2.

Manganese nodules in the deep sea are found to be enriched in Ni, Cu and Zn among other metals but low in Co. Concentrations of the trace elements usually increase with increasing depth in many of the locations. Mn is highest in the basins and lowest of all in the mid-ocean ridges. In the Pacific region the variation of the minor elements is not principally dependent on the major constituents Mn and Fe, although within the abyssal environment covariance between some major and trace elements is observed. Ni and Co are invariably found in the Eastern Pacific nodules which are rich in Mn, while Co and Fe covary. Generally, in this environment high Ni (1.5%), Co (0.3%) and Cu (1.3%) are found with a Mn/Fe ratio in excess of 1. The combined percentages of Ni, Cu and Co are roughly in excess of 3%.

In the Indian ocean similar relationships of the trace element content to the major constituents Mn and Fe are observed and nodules rich in Ni and Cu are found with a high Mn content. In deep water areas, manganese is highest (20% Mn) while in other regions the iron content is found to exceed 40%. High Ni (1.5%) in basins is common but in elevated areas concentrations are low.

From the data presented in TABLE 6.2, the greatest compositional differences in the manganese nodules are found in deposits from four environments; continental borderlands, seamounts, active ridges and the abyssal seafloor. Continental borderlands are rich in Mn and low in trace elements. Seamounts have high Co content. Active ridges have a low Mn/Fe ratio due to the high Fe content and lower than average Mn but abyssal nodules have the highest Ni and Cu and concentrations which are found to increase with seawater depth.

6.3.5.4 Associated sediments

Sediments associated with manganese nodules are of importance to the analysis technique since their nature and composition contribute to the general background of an observed γ-ray spectrum which influences to a great degree the response of a seabed probe. The density of nodule concentration on the seafloor would no doubt reduce this background considerably but this factor is variable so that the response from the associated sediments forms a component of the background. On the other hand, the sediment type by its reflection of seabed conditions usually serves as a guide to the average composition of a nodule field although the chemical composition of the sediment itself has no bearing on the elemental constituents.

The seabed sediments associated with manganese nodules are marine clays, siliceous and calcareous oozes and terrigeneous sediments. Other sediments found in restricted environments consist of coral sands and coral debris. In the Pacific as well as in the Indian Ocean, the most abundant of nodules are found in red clays, although the highest ore grade nodules have been found in siliceous oozes. Hence, these two types can be considered as being the dominant sediments to be encountered in the Deep Sea. Terrigeneous sediments are common in near shore deposits while muds and clays are characteristic of lake bottoms.

Red clay is mainly (85%) hydrated aluminium silicate and consist of about 6% of other minerals. About 4% constitutes siliceous and other organisms. The solid particle content between is 5% and 10% in which the total elemental contribution from Fe, Mn and Cu from the manganese grains is about 1 - 2%. The average value of Al_2O_3 is 15% which corresponds to about 7% elemental aluminium.

The principal constituent in siliceous oozes is SiO_2 which varies from 50% to 70% depending on the contributing organism. This corresponds to 24% - 32% silicon. Fe is less than 0.7% and Al between 4 and 6% from the other minerals present. Calcium in the $CaCO_3$ frequently found in these sediments varies between 6 and 7 percent.

In calcareous oozes, the $CaCO_3$ is between 65 and 70 percent though in certain sediments higher values are observed. These correspond to 26% - 32% Ca and silicon in the SiO_2 content averages 5%. The Al and Fe contents are about 2.5% and 1% respectively. Coral sands and coral itself consist of more than 90% $CaCO_3$ (36% Ca).

Calcium, silicon and al uminium, apart from being the principal constituents of the various associated sediments are also minor constituents of manganese nodules. Calcium averages less than 2%, Si less than 7% and Al is about 4%.

Depending on the type of sediment associated with the nodules the background contribution would depend on the abundance and sensitivity to detection of the elemental constituents of the sediments. The silicon contribution is the highest from siliceous oozes (24 -32%), to a smaller extent from calcareous oozes (5%) and less than 2% from clays. The Al contribution is the highest (7 - 10%) from red clays. It is about 4 - 6% from siliceous oozes, and less than 3% from calcareous oozes. Fe is found in smaller percentages 3 - 4% in clays, less than 2% in calcareous oozes and less than 3% in clays. The Mn content of the red clays is about 1 - 2% in which Cu is in very minor quantities. The salinity of seawater in all the nodule occurring regions is around 34 - 35‰ and the seawater content of the sediment depends upon its type.

6.3.5.5 Analysis of Manganese nodules

'Towed' seabed spectrometer systems and static surface probes are generally favoured in manganese nodule analysis, since the surface concentration of the nodules provides maximum sampling by this technique and a higher signal-to-background ratio than a penetrating probe on account of the background contribution from the deeper sediments. These can be successfully operated in the deep sea in relatively smooth seabed conditions, but in rugged and highly variable topography, submersibles are suitable alternative vehicles from which any of the probe systems could be deployed.

The sensitivity of detection of the principal compositional elements of manganese nodules and of the associated sediment types are given in TABLE 6.3. These correspond to minimum abundances, that could be detected by a suitable probe (towed device) with a 100 μg ^{252}Cf neutron source and a high resolution γ-ray detector, in a counting time of 15 min. TABLES 6.4 and 6.5 presents average compositions of manganese nodules from different regions of the Indian and Pacific oceans in various sediments. The Mn/Fe ratios as well as the nodule grades have been computed to show the possible correlation between these two parameters. TABLE 6.6 gives the maximum, minimum and average contents of elements in the nodules from both these oceans from an analysis of a large number of samples. These data serve as a guide to the likely abundances of the principal elements present in Mn nodules and are of importance to the performance of a probe considered in the analysis.

The characteristic γ-rays listed in table 6.3 can be used to identify the elemental constituents in manganese nodules from a seabed spectrum. As examples, typical γ-ray spectra obtained in a simulated seabed for Mn, Fe, Ni and Cu are given in figures 5.5, 5.12, 5.16 and 5.17 respectively. These are for different concentrations of

the elements in a silica type seabed obtained under the same conditions. The energy peaks are seen to be well resolved and identifiable from the more intense peaks due to chlorine from seawater, so that for quantitative estimates of the concentrations present, the net counts in any convenient energy peak can be used. These will be proportional to the abundances but for absolute determinations of the elemental concentrations, a calibration of the probe system in terms of detector countrate and abundance has to be undertaken for each of the elements.

A general seabed γ-ray spectrum obtained for manganese nodules would be a composite pulse-height energy distribution curve incorporating all the peak energies of the various elemental constitutents. The characteristic peaks due to Mn, Ni, Co and Si, Al and Ca (from associated sediments) would be well separated from the chlorine lines, while some of the peaks of Fe and Cu are either contaminated with chlorine lines or overlap each other. With a high resolution detector system ($\Delta E < 5$ keV) these could be resolved, but the full-energy peaks of Cu and Fe can be otherwise used to detect these elements. For quantitative work the method developed in this study and discussed in Chapter 5 can be applied to calculate the countrates in the contaminated peaks. At high γ-ray energies, the countrates in the full-energy peaks are smaller than that of the corresponding first or double-escape peaks but in the case of Fe and Cu, due to the low minimum detection limits (0.3%) substantial counts can be accumulated in the full-energy peaks to obtain statistically significant results using a short counting time.

In a seabed survey the analysis is best carried out by monitoring the counts in the individual energy peaks corresponding to the elements. The abundances of Mn and Fe

in the nodules from various seabed environments given in TABLES 6.4 - 6.6 show that the average values for Mn and Fe are 16.63% and 13.11% respectively. Assuming the analysis is carried out by a probe for which the minimum detection limits for Mn and Fe are 0.3% for each element, about 1000 counts would be obtained in the full-energy peak corresponding to the combined Fe 7.646 MeV and Fe 7.632 MeV lines per unit abundance of Fe. This corresponds to about 12,000 counts for 13.11% Fe. The corresponding counts for 16.63% Mn in the full-energy peak of Mn 7.244 MeV would be 7,250. Higher counts would be obtained for Mn in the double-escape peaks of both the Mn 7.244 MeV and Mn 7.058 MeV energies.

The ratio of Mn/Fe can be monitored directly during a survey using these countrates to determine the quality of a manganese nodule field since high ratios of Mn/Fe are associated with high trace element concentration. This is shown from the correlation of these ratios with the grade of a nodule as observed in TABLES 6.4 and 6.5. Simultaneously, the net counts in the individual peaks of Ni, Cu and Co could be integrated, after the necessary corrections have been made for detector efficiency, to directly monitor the potential grade of a nodule distribution on a single traverse of the seafloor.

The data for the trace elements Ni, Cu and Co given in TABLES 6.4 - 6.6 show that the concentrations of these elements in a nodule are only a few percent. The lowest limits of detection under the same conditions of measurement as Mn and Fe are 0.1% Ni, 0.3% Cu and 0.2% Co. Thus the mean values quoted are marginal compared to the minimum limits of detection of these elements. From the experimental work carried out in the simulated seabed with various percentages of Cu, a net count of about 400 would be obtained in the 7.915 MeV full-energy peak for 1% copper. This corresponds to a count of 650 for the maximum concentration of Cu observed in nodules. Similarly, in the

8.999 MeV double-escape peak of Ni, a count of 3500 would be obtained for a maximum abundance of 1.68% Ni and about 290 counts for the minimum of 0.136% Ni. For an average value of 0.545% Ni this is about 1200 counts. Counts for Co in the 6.877 MeV or 6.706 MeV would be considerably higher than for Ni, since the efficiency of detection is greater at lower energies. Hence corrections made for the efficiency of the detector would undoubtedly increase these countrates correspondingly for better statistical accuracy. Determinations can be made by optimising the parameters of a probe assembly thereby increasing the sensitivity of detection by at least an order of magnitude. By employing high source-strengths coupled with large source-to-detector separations, a higher signal-to-background ratio would aid their detection.

The non linearity of countrate with high elemental concentration has already been discussed in relation to elements with unusually large thermal absorption cross-section such as manganese. With high concentrations of Mn found in nodules (max. about 40%), ambiguities could arise in quantitative analysis. Corrections can be made and the methods suggested in this regard should overcome the difficulties in interpretation of the results. Cobalt has a very high σ_{th}, 38b compared to 13.3b for Mn but the abundance of Co in nodules is very low the maximum being only 2.57% Co that perturbations in the neutron flux in the seabed are unlikely with these concentrations. A percentage of 2.57% Co is equivalent in its thermal neutron absorption to about 7% Mn which is on the linear part of the countrate versus abundance curve.

Two other factors are to be considered in manganese nodule analysis with a neutron-interaction probe; the effect of seawater content in a nodule and the response of the associated sediments. The maximum seawater content of nodules is found to be 30% by weight, so that this is above

the value for a normal seabed such as that simulated in the laboratory. Considering the effect of this increase, the chlorine countrate would be higher by a factor of about 1.5 for a source-detector separation of 30 cm as discussed in Chapter 5. This would reduce the sensitivity for detection of elements in a nodule, but its effect could be overcome by a probe geometry designed to increase the overall detection sensitivity.

High grade nodules are generally found to occur in siliceous oozes, which compositionally consists of more than 60% SiO_2 in the matrix. The minimum detection limits of the elements in a nodule as given in TABLE 6.3 would not be affected since these values have been measured for the simulated seabed under similar environmental conditions. The γ-ray energies of silicon are in the lower energy region of the spectrum so that no interference with the detection of other elemental constituents in a nodule is expected.

Similarly the presence of carbonate ooze as an associated sediment with nodules would not influence the detection and analysis to a significant extent. The additional energy peaks due to Ca (6.420 MeV) would be superimposed on the general background of a γ-ray spectrum but the background itself would not alter appreciably to decrease the sensitivity for detection of other elements in a nodule. This is clearly observed in the spectra obtained for Si, Ca and a mixture of SiO_2 and $CaCO_3$ in equal proportions by weight (Chapter 5). In the case of pelagic clays, a distinct energy line due to Al can be identified in the spectrum, but again no effect is observed in the background although a high percentage of seawater is found in clays.

CHAPTER 7

SUMMARY AND CONCLUSIONS

The present studies of the development of the neutron radiative capture reaction as a technique for in-situ elemental analysis of the seabed indicate its feasibility in marine exploration and assaying the economic potential of mineral deposits. The technique can be incorporated into analytical equipment which can be towed continuously on the seabed or deployed as a static device to penetrate the sediments. The environmental conditions affecting their operation such as seawater depth, seabed topography and high temperatures could be overcome in the design and mode of deployment on the seafloor and is not a limitation of this technique. Experimental measurements carried out in a simulated seabed have defined the essential parameters which determine the response of a typical neutron interaction probe and its relationship to the physical conditions of the seabed.

The technique can be applied directly to the analysis of the known mineral deposits on the Continental Shelf and the Deep Sea. Most important in this respect are the elements Ti, Fe, Cr, Au and Hg associated with placer deposits, Mn, Fe, Ni, Cu and Co in manganese nodules, Zn in metallic sulphide deposits among other constituents, P in phosphorites and Ba in barite. All these elements have very low minimum limits of detection with this technique in the concentrations that naturally occur in these deposits. A notable exception among the economic placer deposits is tin, where a direct analysis is not possible on account of its low interaction rate with neutrons. However, an indirect method of determining tin can be adopted using this technique provided the ore mineral occurs in high concentrations.

The effective depth sampled by a continuously towed device in seabeds containing small concentrations of trace elements and a seawater content normally associated with unconsolidated sediments extends from about 10 to 15 cm. This is an acceptable range considering the quasi-surface distribution of many types of mineral deposits which are generally restricted to within about 50 cm in a marine environment.

For high concentrations of trace elements with significantly large absorption cross-sections, the non-linear relationship between countrate and elemental concentration becomes significant in determining instrument calibration as has been observed for copper and manganese. Ambiguities which will arise in the interpretation of data when assaying deposits such as manganese nodules can be resolved by observing the neutron flux changes in the seabed through the effects on the γ-ray yields from normal rock-forming elements in the sediments.

It has become evident in the analysis of γ-ray spectra measured for various trace elements distributed in a silica seabed of unconsolidated material that the seawater content and the general background levels are practically constant. The dominant contributions to the background are from hydrogen and chlorine in seawater, the latter being the major interfering element in limiting detection sensitivity. Chance overlap of trace element γ-ray energy peaks with those of chlorine does not present a problem due to the multiplicity of spectral energy lines. Methods for analysis of elements contaminated by chlorine have been outlined in the present study.

The influence of chlorine on the background radiation levels is high for a cylindrical probe of the type considered in this study. Its effect can be substantially reduced by an alternative choice of probe design with non-cylindrical symmetry such that the minimum limits of detection could be further reduced to improve accuracy and/or spatial resolution.

For quantitative analysis using this technique, a laboratory instrument calibration of countrate and elemental abundance is desirable due to variation of environmental conditions in which in-situ analysis is undertaken on the seabed. Cross calibration with accurate sample analyses will also be necessary in practice together with other established geophysical and geochemical methods currently used in marine exploration.

REFERENCES

BACKER, H and SCHOELL, M. (1972)
'New Deeps with Brines and Metalliferous Sediments in the Red Sea'
Nature, 240 (1972) 153-158

BARTHOLEMEW, G.A. et al (1967)
'Nuclear Data Tables'
3A, Nos 4-6 (1967).

BENDAL, D.E. (1966)
'McNID - A Monte Carlo Programme for Calculating the Penetration of Neutrons in Systems with Cylindrical Symmetry'
AEEW-R 308, Unpublished.

BIGNELL, R.D., CRONAN, D.S. and TOOMS, J.S. (1976)
'Metal Dispersion in the Red Sea as an Aid to Geochemical Exploration'
Trans. Instn. Min. Metall. B 85 (1976) 274-278.

CHASMAN, C., JONES, K.W. and RISTINEN, R.A. (1965)
'Fast Neutron Bombardment of a Lithium-Drifted Germanium Gamma-Ray Detector'
Nucl. Instr. Meth. 37 (1965) 1-8.

CRONAN, D.S. (1977)
'Marine Manganese Deposits'
Edit. G.P. Glasby, Elsevier, Amsterdam, (1977) 11-44.

CRONAN, D.S. (1980)
'Underwater Minerals'
Academic Press, London, 1980.

CRUINKSHANK, M.J. (1981)
'The Status of Deep Sea Mining'
Ocean Industry (1981) 93-94.

CULLEN, D., KUDRASS, H.R. and VON RAD, U. (1981)
'Preliminary Results of the 1981 Sonde Investigation of the Chatham Rise Phosphorite Deposits of New Zealand'
Rept. N. Zealand Oceanographic Inst. (1981) DSIR. N. Zealand.

DRAKE, D.M., NILSSON, L.R. and FAWCETT, J. (1981)
'Bismuth Germanate Scintillators for High-energy Gamma Radiation'
Nucl. Instr. Meth. 188 (1981) 313-317.

DUFFEY, D., EL-KADY, A. and SENFTLE, F.E. (1970)
'Analytical Sensitivities and Energies of Thermal-Neutron-Capture Gamma Rays'
Nucl. Instr. and Meth. 80 (1970) 149-171.

DUNHAM, K.C. (1969)
'Practical Geology and the Natural Environment of Man'
Quart. Journ. Geol. Soc. Lond. 124 (1969) 101-129.

EMERY, K.O. (1961)
'Submerged marine terraces and their sediments'
Ann. Geomorph. N.S. Suppl. Vol. 3 (1961) 2-29.

EMERY, K.O. and NOAKES, L.C. (1968)
'Economic Placer Deposits of the Continental Shelf'
Tech. Bull. ECAFE, Vol. 1 (1968) 95-111.

EVANS, A.E. (1980)
'Gamma Ray Response of a 38 mm Bismuth Germanate Scintallator'
IEEE. Trans. Nucl. Sc. NS 27(1) (1980) 172-175.

FRANCHETEAU, J. et al (1979)
'Massive Deep-Sea Sulphide Ore Deposits discovered on the East Pacific Rise'
Nature, 277 (1979) 523-528.

FRANCIS, T.J.G. (1977)
'Electrical Prospecting on the Continental Shelf'
Inst. Geol. Sc. Report No: 77/4 (1977) 1-41.

GROEN, P. (1967)
'The Waters of the Sea'
D. Van Nostrand Publ. Co. Princeton N.J.

GROSHEV, L.V. et al (1968-1969)
'Nuclear Data Tables'
5A, Nos 1-4 (1968-1969)

HOLMES, R and TOOMS, J.S. (1972)
'Dispersion From a Submarine Exhalative Orebody'
Proceedings of the 4th International Geochemical Exploration Symposium Inst. Min. Metall. (1972) 193-201.

ISBIN, H.S. (1963)
'Introductory Nuclear Reactor Theory'
Reinhold Publishing Corporation, Chapman & Hall, Ltd., London

KANE, W.R. and MARISCOTTI, M.A. (1967)
'An Empirical Method of determining the Relative Efficiency of a Ge(Li) Gamma-Ray detector'
Nucl. Instr. Meth. 56 (1967) 189-196.

KREFT, A. (1974)
'Calculation of the Neutron Slowing Down Length in Rocks and Soils'
Nukleonika, 19 (1974) 145-156.

LANGE, J.P. and BIEMANN, W.G. (1975)
'Development of Components for an in-situ analysis for the Exploration of Manganese Nodules'
7th. Annual Offshore Tech. Conf. 2 (1975) 585-592.

LIVERHANT, S.E. (1960)
'Elementary Introduction to Nuclear Reactor Physics'
John Wiley & Sons, Inc. London.

LORCH, E.A. (1973)
'Neutron Spectra of $^{241}Am/B$, $^{241}Am/Be$, $^{241}Am/F$, $^{242}Cm/Be$, $^{238}Pu/^{13}C$ and ^{252}Cf neutron sources'
Int. J. Appl. Radiat. Isot. 24 (1973) 585-591.

MARION, J.B. and FOWLER, J.L. (1960)
'Fast Neutron Physics, Part 1'
Interscience Publishers Ltd. London.

MERO, J.L. (1964)
'The Mineral Resources of the Sea'
Elsevier Publishing Co. Amsterdam.

MILLER, J.M., ROBERTS, P.D., SYMONS, G.D. and MERRIL, N.H. (1977)
'A Towed Seabed Gamma-Ray Spectrometer for Continental Shelf Surveys'
Int. Symp. Nuc. Tech. IAEA, Vienna (1977) 465-498.

MILLER, J.M. and SYMONS, G.D. (1973)
'Radiometric traverse of the seabed off the Yorkshire Coast'
Nature, 242 (1973) 184.

MOORBY, S.A. (1978)
'The geochemistry and mineralogy of some ferromanganese oxides and associated deposits from the Indian and Atlantic Oceans'
Ph.D. Thesis, University of London (Unpublished).

NOAKES, J.E., HARDING, J.L. and SPAULDING, J.D. (1974)
'Locating off-shore Mineral Deposits by Natural Radioactive Measurements'
J. Marine. Tech. Soc. 8 (1974) 36-39.

PEHL, R.H., MADDEN, N.W., ELLIOT, J.H., RAUDORF, T.W., TRUMMEL, R.C. and DARKEN, L.S. Jr (1979)
'Radiation Damage Resistance of Reverse Electrode Germanium - Coaxial Detectors'
IEEE, Trans. Nuc. Sc. NS-26, N1 (1979) 321-323.

PUGH, D.T. (1969)
'Hot Brines and Recent Heavy Metal Deposits of the Red Sea'
Springer - Verlag, N. York (1969) 3-9.

RONA, P.A. (1972)
'Exploration Methods for the Continental Shelf: Geology, Geophysics, Geochemistry'
NOAA Tech. Rpt. ERL 238-AOML 8, U.S. Dept. of Commerce. (1972).

RONA, P.A. (1978)
'Criteria for Recognition of Hydrothermal Mineral Deposits in Oceanic Crust'
Econ. Geol. 73 (1978) 135-170.

SANDERS, L.G. (Private communication)
AERE Harwell, Applied Nuclear Geophysics Group.

SENFTLE, F.E., DUFFEY, D. and WIGGINS, P.F. (1969)
'Mineral Exploration of the Ocean Floor by in-situ Neutron Absorption using a Californium-252 Source'
J. Marine Tech. Soc. Vol.3 No. 5 (1969) 9-16.

SENFTLE, F.E., TANNER, A.B., PHILBIN, P.W., NOAKES, J.E., SPAULDING, J.D. and HARDING, J.L. (1977)
'In-situ Capture Gamma-Ray Analyses for seabed exploration. A feasibility study'
Proc. Symp. Nuc. Tech. and Min. Resources, IAEA, Vienna (1977) 75-91.

SHEPARD, F.P. (1963)
'Submarine Geology'
Harper and Row Publ. N. York. 1963.

STODDARD, D.H. (1965)
'Radiation Properties of Californium-252'
UNAEC Report DP-986, E.I. Du Pont de Nemours & Co
Savannah River Laboratories, Aiken, S.C. USA.

STOLTZ, H. and STANDING, K.F. (1977)
'Underwater Prospecting for Radioactive Minerals'
47th Annual Meeting of Soc. Expl. Geophy. Calgary, Canada.

SUMMERHAYES, C.P., HAZELHOFF-ROELFZEMA, B.H., TOOMS, J.S. and SMITH, D.B. (1970).
'Phosphorite Prospecting using a Submersible Scintillation Counter'
Econ. Geol. 65 (1970) 718-723.

SWALLOW, J.C. (1969)
'Hot Brines and Recent Heavy Metal Deposits in the Red Sea'
Springer - Verlag, N. York (1969) 3-9.

THE RADIOCHEMICAL CENTRE (1976)
'Neutron Sources: Americium-241/Beryllium and Californium-252'
Tech. Bull. 76/7 (1976).

THOMAS, B.W. (Private communication)
AERE Harwell, Applied Nuclear Geophysics Group.

THOMAS, B.W., CLAYTON, C.G., RANASINGHE, V.V.C. and BLAIR, I.M. (1983)
'Mineral Exploration of the Seabed by Towed Seabed Spectrometers'
Int. J. Appl. Radiat. Isot. 34 No. 1 (1983) 437-449.

WIGGINS, P.E. and HICKEY, D.G. (1969)
'Prospecting the Ocean Floor with Neutrons'
Naval Eng. Journ. (1969) 79-84.

WOGMAN, N.A. (1977)
'In-situ X-Ray Fluorescence and Californium-252 neutron Activation Analysis for Marine and Terrestrial Mineral Exploration'
Proc. Symp. Nucl. Tech. and Min. Resources, IAEA, Vienna (1977) 447-462.

APPENDIX 1

Monte Carlo computations of neutron characteristic lengths 'L$_s$ and 'M' in some selected seabed media

1. Neutron Source

^{241}Am/Be (mean neutron energy 4.6 MeV)

2. Values of physical parameters used in the computations

a. Density

Seawater	1.180 gm.cm^{-3}
Purewater	1.000 gm.cm^{-3}

Silica - SiO_2	2.65 gm.cm^{-3}
Calcium Carbonate - $CaCO_3$	2.71 gm.cm^{-3}
Clay - $Al_4Si_4O_{10}(OH)_8$	2.42 gm.cm^{-3}

b. Salinity

Seawater	250‰

Normal salinities of seawater are in the region 34 - 35‰. The value used in the computation is for brine found in the Red Sea Deeps and represents extreme salinity conditions found on the seabed.

3. Values of 'slowing down' length L_s and 'migration' length M

TABLE 1. Silica - seawater (saturated)

porosity (%)	migration length, M (cm)	slowing-down length, L_s (cm)
0	35.080 ± 0.218	30.418 ± 0.218
2.5	27.276 ± 0.182	23.636 ± 0.188
5	22.754 ± 0.166	20.246 ± 0.178
10	18.684 ± 0.152	17.088 ± 0.173
20	14.576 ± 0.136	13.772 ± 0.161
30	12.676 ± 0.125	12.495 ± 0.158
40	11.346 ± 0.150	11.284 ± 0.162
60	9.829 ± 0.122	9.766 ± 0.176
80	8.929 ± 0.128	8.699 ± 0.145
100	7.908 ± 0.103	7.777 ± 0.130

TABLE 2. Calcium carbonate - seawater (saturated)

porosity (%)	migration length, M (cm)	slowing-down length, L_s (cm)
0	29.202 ± 0.206	25.964 ± 0.193
2.5	23.781 ± 0.175	21.523 ± 0.172
5	21.319 ± 0.170	19.493 ± 0.194
10	17.603 ± 0.160	16.431 ± 0.170
20	14.443 ± 0.146	13.362 ± 0.153
30	12.276 ± 0.123	11.840 ± 0.139
40	11.050 ± 0.119	10.718 ± 0.133
60	9.686 ± 0.115	9.477 ± 0.145
80	8.757 ± 0.130	8.569 ± 0.133
100	7.908 ± 0.103	7.777 ± 0.130

TABLE 3. Silica - purewater (saturated)

porosity (%)	migration length, M (cm)	slowing-down length, L_s (cm)
0	35.080 ± 0.218	30.418 ± 0.218
2.57	27.866 ± 0.164	23.035 ± 0.203
5.14	24.062 ± 0.143	19.824 ± 0.170
10.26	19.654 ± 0.116	16.163 ± 0.178
20.46	15.581 ± 0.106	12.985 ± 0.141
30.61	13.178 ± 0.089	11.362 ± 0.135
40.69	11.691 ± 0.088	10.546 ± 0.139
60.69	9.820 ± 0.092	9.109 ± 0.140
80.46	8.890 ± 0.113	8.364 ± 0.152
100	8.138 ± 0.092	7.656 ± 0.130

TABLE 4. Calcium carbonate - purewater (saturated)

porosity (%)	migration length, M (cm)	slowing-down length, L_s (cm)
0	29.202 ± 0.206	25.964 ± 0.193
2.57	24.360 ± 0.165	20.936 ± 0.171
5.14	21.413 ± 0.143	18.496 ± 0.168
10.27	17.943 ± 0.126	15.550 ± 0.171
20.48	14.861 ± 0.109	13.078 ± 0.164
30.63	13.095 ± 0.119	11.411 ± 0.148
40.72	11.521 ± 0.093	10.349 ± 0.126
60.72	9.708 ± 0.083	9.096 ± 0.128
80.48	8.902 ± 0.102	8.343 ± 0.153
100	8.138 ± 0.092	7.656 ± 0.130

TABLE 5. Clay - purewater (saturated)

porosity (%)	migration length, M (cm)	slowing-down length, L_s (cm)
0	11.612 ± 0.088	10.377 ± 0.134
2.5	11.642 ± 0.097	10.309 ± 0.125
5	11.209 ± 0.088	10.148 ± 0.124
10	10.984 ± 0.090	9.909 ± 0.120
20	10.386 ± 0.082	9.550 ± 0.129
30	9.935 ± 0.082	9.146 ± 0.129
40	9.500 ± 0.085	8.745 ± 0.130
60	8.737 ± 0.086	8.068 ± 0.129
80	8.401 ± 0.104	7.931 ± 0.150
100	8.138 ± 0.092	7.656 ± 0.130

TABLE 6. Silica - clay - purewater

volume fractions			migration length, M (cm)	slowing-down length, L_s (cm)
silica	clay	water		
0.3	0.5	0.2	11.73 ± 0.10	10.50 ± 0.13
0.6	0.2	0.2	13.72 ± 0.10	11.70 ± 0.14
0.7	0.1	0.2	14.79 ± 0.10	12.57 ± 0.14

APPENDIX 2

A. Monte Carlo computer method

1. Fundamental concepts

The transport of neutrons in the seabed and its environment can be simulated within a digital computer by a numerical procedure based on statistical considerations. The method relies on finding estimates of physical quantities by a repetitive process described by a set of deterministic laws related to the problem and by probabilities governing the occurrence of the physical events. The applicability of the method arises from the fact, that the macroscopic cross-section Σ for the physical events could be interpreted as the probability of interaction per unit distance travelled by the neutron within the seabed.

The sequence of events (a set of neutron histories) is generated by conceptual tracking of individual neutrons through successive events. When sufficient histories have been recorded, they are compiled into statistical averages and the population studied. Fluctuations in the results are expected as in other statistical processes, but a large number of histories is followed to obtain the desired accuracy.

2. Basic parameters

The procedure adopted in Monte Carlo calculations is related to certain basic parameters. One such parameter is the geometry by which an experimental system can be represented. The geometry identifies the location of each type of material in the system and also provides the boundaries over which the average fluxes are computed. The macroscopic cross-section Σ describes the nuclear characteristics of each region.

The neutrons are tracked through the regions on the basis of random selection of reaction parameters. This is carried out by the generation of random numbers which specify an event in an unambiguous manner in accordance with the probability laws governing nuclear interactions. By this means, it is ensured that the probability of occurrence of a given interaction is identical to the probability that the corresponding random number will be selected. The result of the event is thus inferred from the behaviour of the random number.

The method has inherent uncertainties which arise due to the limitations in the finite number of neutrons examined. These errors are random and variance reduction methods have been incorporated into computer programs for reducing the uncertainty associated with a limited amount of numerical calculation.

B. General characteristics of McNID II Programme

McNID II Monte Carlo Programme

McNID II is a Monte Carlo Programme which solves neutron penetration problems in systems represented in cylindrical polar geometry without angular dependence. The general description of the programme written in FORTRAN IV and its use are contained in an unpublished text by the author BENDAL (1966). The geometry has proved satisfactory in representing the experimental system as shown by the close correlation of the computed and experimental data. The detail with which the system is modelled is however limited by the requirements of computing time and storage space and hence the incentive to keep the geometry as simple as possible in the present application. The parameters of importance to the problems studied are presented.

Geometry

The system is divided by a family of coaxial cylindrical surfaces intersected by a set of planes perpendicular to the axis of the cylindrical coordinate system. The annular regions so formed enables the material composition of the seabed and its

environment to be defined and also provides regions over which the average neutron flux could be computed. The boundaries at either end can be made finite, in which case the neutrons are reflected, while the outer radial boundary allows them to escape.

Neutron source

The source is contained in an annular region and could be sampled either from an isotopic distribution (^{252}Cf) or have a constant value (14 MeV monoenergetic source). The source energy in the case of ^{252}Cf could be chosen from a distribution specified in histogram form.

Tracking and scoring flux

For purposes of estimating the average flux in an energy region of interest, the energy range could be divided into intervals referred to as 'bins'. The flux in each energy bin and in each 'scoring' region could be computed by accumulating the track length of all neutrons passing through that region with the appropriate energies. An estimate is made of the standard deviation of each result.

Variance reduction

Two methods are used to improve the efficiency of the Computer Programme, the first is a combination of splitting and Russian roulette and the other is a form of importance sampling. The object of the first is to concentrate 'particles' towards the regions of greatest interest, which effect is counterbalanced by assigning a weight to them when scoring. In the second, the purpose is to increase the proportion of those source neutrons most likely to contribute to the score. Again, the weighting factors are adjusted so that the magnitude of the results remain unaltered.

Nuclear events

The section of the programme which determines the nature of the physical event (i.e. scattering, absorption etc.), the time sequence and its outcome is contained in a programme held in the

IBM 3081 K Computer installed at A.E.R.E, Harwell. This uses the UKAEA NUCLEAR DATA LIBRARY as its source of input but processes it into a form acceptable for McNID II calculations.

The cross-sections for the various nuclear events are represented by constant values over a large number of energy intervals and the energy distribution and the angle of scatter are specified by numbers of equiprobable intervals. Additional routines are available so that the thermal energy group data supplied could be incorporated in the programme.

C. Data for McNID II Programme

Source Data

The Californium-252 source was confined in a cylindrical volume of dimensions 0.5 cm in the radial and axial directions. As the flux output from the programme was for a source strength of 1 neutron per second, a factor of 0.23400E 07 was included to account for the strength of the Cf-252 used in the experiments.

For the purpose of the computations, the source was considered to be uniformly distributed within the volume specified and therefore no importance sampling was carried out for the source.

The energy of the source was supplied to the programme in histogram form with 12 energy intervals in the range 0.015 MeV to 14 MeV, the same importance being attached to each energy interval.

ENERGY	INTENSITY	IMPORTANCE
0.15000E-01		
0.11000E 00	0.27400E 02	0.10000E 01
0.41000E 00	0.15600E 03	"
0.91000E 00	0.33600E 03	"
0.20200E 01	0.69800E 03	"
0.30100E 01	0.43600E 03	"
0.36800E 01	0.20000E 03	"
0.44900E 01	0.16800E 03	"
0.54900E 01	0.12600E 03	"
0.67000E 01	0.81900E 02	"
0.10000E 02	0.64200E 02	"
0.14000E 02	0.82800E 01	"

Energy Intervals

Five energy intervals were considered for the computation of the average flux. These are given below.

0	———	0.10000E-06	MeV
0.10000E-06	———	0.10000E-05	MeV
0.10000E-05	———	0.10000E-02	MeV
0.10000E-02	———	0.10000E 01	MeV
0.10000E 01	———	0.10000E 02	MeV

The cut-off energy was set at zero MeV for the problem and the programme ceases to track a particle when its energy falls below this value.

Importance Values

The importance of the annular regions for the application of the variance reduction methods was designated by integers from 1 upwards. This is a relative measure of the expected score at a measured point due to a neutron in the region and indicates whether the importance of one region is greater than, equal to or less than another region considered.

Trial runs were first carried out by assigning the same importance values to all regions. The neutron flux so obtained for each region was analysed in relation to its location and values were duly assigned for the system so that these increased radially from the source to the detector and then decreased over the rest of the region. In the axial direction, the values decreased from the source outwards in the seabed and seawater though on a lesser scale.

Nuclear Data

The total number of materials in the system and the number of nuclides constituting each material were specified. For each nuclide, the reference number which is the ordinal number of the nuclide in the NUCLEAR DATA TAPE, the properties of the nuclide in terms of the number of nuclei present, the total cross-section and the absorption cross-section of the materials were fed to the computer.

Limits were placed on the number of neutron histories, i.e. number of neutrons started from the source, the number of collisions and the running time of the programme based on obtaining statistically significant values for the fluxes and on the limitations imposed on utilising computer time and cost.

Computer Data Output

The average neutron fluxes for each energy interval were obtained for all annuli designated by the region parameters for the whole system. The standard deviations given represent purely statistical errors and do not include errors arising from a simplification of the geometry or to uncertainties in the nuclear data supplied.

For each region, the particle density and the collision density obtained by adding up particle collisions weighted by the mean free path of the neutron were obtained as additional output data.

TABLE 2.1

Principal constituents of seawater

(Salinity 34.5‰) *

Ionic constituent		Gram/kg of seawater	Proportion to the sum
Chloride	Cl^-	18.980	55.044
Sulphate	SO_4^{--}	2.649	7.632
Bicarbonate	HCO_3^-	0.140	0.406
Bromide	Br^-	0.065	0.189
Fluoride	F^-	0.001	0.003
Boric Acid	H_3BO_3	0.026	0.075
Sodium	Na^+	10.556	30.613
Magnesium	Mg^{++}	1.272	3.689
Calcium	Ca^{++}	0.400	1.160
Potassium	K^+	0.380	1.102
Strontium	Sr^{++}	0.013	0.038
		34.482	100.000
Water (with traces of other substances		965.518	
		1000.000	

* Data from GROEN (1967)

TABLE 2.2

Sensitivities of seawater and some seabed type constituents for (n,γ) reaction

Element (Natural isotopic abundance)	Abundance (% weight)	σ_a (barns)	Prominent Prompt γ-rays (MeV)	Sensitivity * $I\sigma_{a/A}$
Hydrogen	10.825	0.332	2.223	32.94
Chlorine	1.898	33.2	8.579	2.16
			7.790	6.22
			7.414	7.99
			6.620	9.38
			6.111	14.80
			5.715	4.33
			4.980	3.58
			3.062	3.50
Sodium	1.056	0.534	6.395	0.59
			3.982	0.50
			3.879	0.15
			3.588	0.41
			3.098	0.22
Magnesium	0.127	0.063	3.916	0.10
Sulphur	0.088	0.512	5.420	0.67
			4.870	
			3.221	0.31
ONLY THE MOST INTENSE GAMMA-RAY IS QUOTED				
Calcium	0.040	0.430	6.420	0.30
Potassium	0.038	2.10	5.380	0.39
Bromine	0.006	6.70	7.576	0.09
Carbon	0.003	0.0034	4.934	0.02
Strontium	0.0013	1.21	6.237	0.07
Boron	0.0005	0.50	4.470	3.70
SEABED TYPE ELEMENTS				
Calcium	20.0	0.430	6.420	0.30
Silicon	46.0	0.160	4.934	0.40
			3.539	0.45

* A = Atomic mass, I = γ-photons/100 neutrons absorbed

TABLE 3.1

Properties of the Seabed Materials

Chemical composition	Molecular weight	Density ($g.cm^{-3}$)	Nature and minimum purity	Solubility in water ($g/100\ cm^3$)
SiO_2	60.07	2.67	granular, 97%	insoluble
$CaCO_3$	100.09	2.71	powder, 98%	0.0014
TiO_2	79.90	4.26	granular, 98%	insoluble
Cr	51.996	7.20	powder, 99%	insoluble
MnO_2	86.93	5.03	granular 85%	insoluble
Fe_3O_4	231.54	5.18	granular 98%	insoluble
Ni	58.71	8.90	powder, 99%	insoluble
CuO	79.54	6.48	granular, 98%	insoluble
ZnS	97.43	4.10	powder, 99%	0.00065
ZnO	81.37	5.61	powder, 99%	0.00016
ZrO_2	123.32	5.89	powder, 99%	insoluble

TABLE 5.1

Measured ratios of peak counts and background counts of hydrogen, chlorine and manganese in the simulated seabed using ^{252}Cf and $^{241}Am/Be$ neutron sources

Element	Energy (MeV)	Ratio of peak counts	Ratio of backgrounds
Hydrogen	2.223 (f)	1.70 ± 0.02	1.66 ± 0.01
	(d)	1.69 ± 0.02	1.66 ± 0.01
Chlorine	7.790 (f)	1.70 ± 0.11	1.66 ± 0.19
	(d)	1.67 ± 0.08	1.69 ± 0.10
Chlorine	7.414 (f)	1.66 ± 0.05	1.69 ± 0.07
	(d)	1.67 ± 0.07	1.68 ± 0.05
Chlorine	6.620 (f)	1.69 ± 0.05	1.66 ∓ 0.07
Chlorine	6.111 (d)	1.71 ± 0.03	1.70 ± 0.02
Manganese	7.244 (f)	1.67 ± 0.09	1.71 ± 0.11
	(d)	1.67 ± 0.08	1.70 ± 0.09
Manganese	7.058 (d)	1.69 ± 0.07	1.67 ± 0.09

f = full energy peak

d = double-escape peak

TABLE 5.2

Important physical properties and nuclear data for some materials considered in γ-ray shields

Element	Tin (Sn)	Tungsten (W)	Platinum (Pt)	Lead (Pb)
Atomic No.	50	74	78	82
Atomic Wt.	118.69	183.85	195.09	207.2
Density ($grm.cm^{-3}$)	7.29	19.35	21.45	11.34
$\Sigma_s (cm^{-1})$	0.1481	0.3145	0.6622	0.3683
$\Sigma_{th} (cm^{-1})$	0.0233	1.195	0.6622	0.00569
Energy for min. γ-attenuation (MeV)	4.5	3.5	3.25	3.0
γ-attenuation of 10 cms. thickness of material				
1.0 MeV	0.9837	0.9984	0.9996	0.9998
4.5 MeV	0.9209	0.9995	0.9998	0.9909
14.0 MeV	0.9532	0.9999	0.9999	0.9984

TABLE 5.3

Ratios of Counts, for various Energy Peaks and Background Levels

Element	Energy (MeV)	Ratio of Counts Tin/Lead (Photo-peak)	Background Levels
Hydrogen	2.223 MeV (f)	1.01 ± 0.008	1.163 ± 0.042
Chlorine	6.620 MeV (f)	0.98 ± 0.160	0.98 ± 0.120
Chlorine	6.111 (d)	1.01 ± 0.08	0.99 ± 0.10
Chlorine	7.414 (f) (d)	0.99 ± 0.11 1.01 ± 0.09	1.01 ± 0.09 0.99 ± 0.10
Chlorine	7.790 (f) (d)	0.96 ± 0.12 0.99 ± 0.12	0.99 ± 0.09 0.97 ± 0.07
Selected energy regions	2.5 - 2.6 3.0 - 3.3 4.1 - 4.2 6.2 - 6.3 6.6 - 6.7		1.16 ± 0.04 1.14 ± 0.02 1.09 ± 0.03 1.01 ± 0.05 0.98 ± 0.05

TABLE 5.4

Ratio of total Countrate for Various Source-to-Detector Distances 'L' - Tin/Lead

L (cms)	Ratio of Countrate (Tin/Lead)
25	1.148 ± 0.02
30	1.125 ± 0.03
35	1.167 ± 0.04
40	1.188 ± 0.05
45	1.191 ± 0.06
50	1.201 ± 0.08

TABLE 5.5

Percentage abundance and materials used in 'seeding' and seawater content of seabed matrix

Element	Percentage abundance	Seawater content *(% Wt.)	Material used in 'seeding'
Titanium	3.0	23	TiO_2
Iron	3.0	24	Fe_3O_4
Nickel	3.0	23	Ni (metal)
Zinc	24.0	24	ZnO, ZnS
Copper	5.0	23	CuO
Chromium	3.8	22	Cr (metal)
Manganese	4.3	22	MnO_2

* Error ± 2 percent.

TABLE 5.6

Ratios of net counts in some selected chlorine energy peaks to that of Hydrogen

Element in seabed	Cl 6.620 (f)	Cl 6.111 (f) + Cl 6.620 (s)	Cl 7.414 (f)	Cl 7.790 (f)
Titanium (3%)	0.017	0.046	0.011	0.008
Magnanese (4.3%) (2.0%)	0.016 0.017	0.046 0.047	0.010 0.011	0.007 0.007
Copper (5.0%) (2.5%)	- - - -	0.052 0.053 0.054 0.055	- - - -	0.007 0.008 0.008 0.008
Chromium (3.8%)	0.16	0.054	0.012	0.007
Zinc (24.0%)	0.18	0.052	0.011	0.008
Iron (2.9%) and Titanium (2.5%)	-	0.052	0.011	0.008
Nickel (3%)	0.017	0.053	0.012	0.007

TABLE 5.7

Measured attenuation of the 2.223 MeV capture γ-ray of Hydrogen in various seabed environments

Seabed constitution (% elemental composition)	α (cm^{-1})	Seawater content (% by weight)
3.0 Ti	-0.0863 ± 0.0010	23
3.8 Cr	-0.0861 ± 0.0005	22
3.0 Fe	-0.0861 ± 0.0004	24
3.0 Ni	-0.0889 ± 0.0005	23
*4.3 Mn	-0.0888 ± 0.0003	22
2.5 Cu	-0.0879 ± 0.0004	22
2.5%Ti + 2.9%Fe	-0.0854 ± 0.0008	25
24.0%Zn + 6%S	-0.0884 ± 0.0003	24
Silica seabed with pure water	-0.0872 ± 0.0006	20
Pure seawater	-0.0883 ± 0.0004	100

* Value determined using a 1 Ci ^{241}Am/Be source.

Errors on seawater content ± 2%

TABLE 5.8

Measured and calculated attenuation of the principal γ-ray energies of chlorine from seawater

Chlorine Energy (MeV)	α (cm^{-1}) experimental	μ (cm^{-1}) computed
6.111	0.066 ± 0.001	0.0272
6.620	0.062 ± 0.002	0.0262
7.414	0.060 ± 0.001	0.0248
7.790	0.058 ± 0.003	0.0243

TABLE 5.9

Measured and calculated attenuation of the principal γ-ray energy of some seabed elements

Element	Principal energy (MeV)	Seawater Content * (% by weight)	α (cm^{-1}) experiment	μ (cm^{-1}) computed
Silica (Si)	3.539	20	-0.0648 ± 0.001	0.0777
Calcium (Ca)	6.420	25	-0.0539 ± 0.002	0.060
Titanium (Ti)	6.760	23	-0.0551 ± 0.006	0.0599
Manganese (Mn)	7.244	22	-0.0519 ± 0.002	0.0593
Nickel (Ni)	8.999	23	-0.0455 ± 0.008	0.0535

* Error ± 2 percent

TABLE 5.10

Contribution by the 7.632 MeV and 7.646 MeV capture γ-rays of iron to the countrate in the 6.620 MeV γ-ray peak of chlorine

L (cms)	Counts (Expt) Cl 6.111(s) + Cl 6.620(d)	Counts (Equation) Cl 6.620(f)	Expt. Counts Cl 6.620(f) + Fe(d)	Residual Counts Fe(d)
20	33,021 ± 392	7367 ± 158	10,021 ± 101	2654 ± 187
25	29,004 ± 289	5360 ± 129	7,352 ± 86	1992 ± 155
30	17,590 ± 227	3932 ± 97	5,307 ± 73	1375 ± 121
35	12,917 ± 194	2892 ± 66	3,902 ± 63	1010 ± 91
40	9,400 ± 144	2108 ± 55	2,806 ± 53	698 ± 76
45	6,888 ± 137	1549 ± 45	2,111 ± 46	562 ± 64
50	4,955 ± 106	1119 ± 34	1,529 ± 39	408 ± 52
55	3,727 ± 101	846 ± 29	1,133 ± 34	287 ± 44

TABLE 5.11

Contribution by the 7.915 MeV capture γ-rays of copper to the countrate in the 7.414 MeV γ-ray peak of chlorine

L (cms)	Cl 7.414 (d) (Expt.)	Cl 7.414 (f) (Equation)	Cl 7.414 (f)+ Cl 7.915 (s) (Expt.)	Cu 7.915 (s) Residual
25	9480 ± 161	3828 ± 83	5202 ± 120	1372 ± 145
30	6784 ± 138	2739 ± 67	3697 ± 82	958 ± 105
35	4887 ± 127	1973 ± 58	2651 ± 50	678 ± 76
40	3506 ± 62	1416 ± 31	1903 ± 47	487 ± 56
45	2598 ± 55	1049 ± 26	1352 ± 32	303 ± 41

* f = full energy, s = single-escape, d = double-escape peaks

TABLE 5.12

Contribution by the 7.637 MeV capture γ-rays of copper to the countrate in the 6.620 MeV γ-ray peak of chlorine

L (cms)	Cl 6.620 (f) + Cl 6.111 (s) (Expt.) Counts	Cl 6.620 (f) (Equation)	Cl 6.620 (f)+ Cu 7.637 (d) (Expt.)	Cu 7.637 (d) Residual
25	21,841 ± 419	4862 ± 138	6092 ± 120	1232 ± 182
30	16,346 ± 320	3639 ± 104	4519 ± 92	881 ± 138
35	12,004 ± 230	2672 ± 76	3295 ± 71	623 ± 104
40	8,802 ± 165	1960 ± 55	2406 ± 47	446 ± 72
45	6,500 ± 126	1447 ± 41	1764 ± 35	317 ± 53

TABLE 5.13

Nuclear characteristics and measured sensitivities for detection of some elements in the simulated seabed

Element	Atomic Mass (A)	Thermal cross-section σ_a (Barns)	Principal γ-ray energy (MeV)	Intensity I	$I\sigma_a/A$	Abundance Seabed (%)	Relative Eff. of Detec. (ξ)	$(I\sigma_a/A).w.\xi$ (λ)	Net counts in 120 mins (C)	Sensitivity measured (%)
Nickel	58.71	4.6	8.999 (d)	41.65	3.2	3.0	0.410	3.94	1261 ± 71	0.10
Copper	63.54	3.9	7.915 (f)	28.4	1.72	5.0	0.154	1.32	418 ± 39	0.25
						2.5	0.154	0.66	228 ± 39	0.25
Zinc	65.37	1.1	7.863 (f)	11.7	0.197	24.0	0.156	0.737	203 ± 33	2.24
			(d)				0.400	1.891	592 ± 88	1.90
Chromium	51.99	3.1	8.884 (f)	24.14	1.44	3.8	0.138	0.755	248 ± 24	0.17
			(d)				0.410	2.243	731 ± 63	0.17
Titanium	47.9	6.1	6.760 (d)	54.07	6.87	3.0	0.380	7.83	2579 ± 150	0.10
						2.5		6.53	2196 ± 158	0.11
Manganese	54.94	13.3	7.058 (f)	11.35	2.75	2.0	0.178	0.98	319 ± 27	0.31
			(f)			4.3	0.178	2.10	614 ± 70	0.29
			(d)			4.3	0.390	4.61	1402 ± 122	0.23

(f) = full-energy peak
(d) = double-escape peak

TABLE 5.14

Calculated sensitivities of detection of some important elements

Element	Atomic Mass A	Thermal neutron absorption cross-section σ (barns)	Intensity I(%) (photons/100 neutrons)	Sensitivity Iσ/A	Lowest limit of detection in SiO_2 matrix (counting time 15 min source 100 μg ^{252}Cf) wt%
Nickel	58.71	4.6	42	3.2	0.1
Copper	63.54	3.9	28	1.7	0.3
Zinc	65.37	1.1	12	0.2	2.0
Molybdenum	95.94	2.7	3.5	0.1	8.0
Silver	107.87	63	1	0.6	2.0
Tin	118.69	0.63	<1	<0.005	~100
Gold	196.97	100	5	2.5	0.3
Mercury	200.59	372	16	29	0.03
Lead	207.19	0.17	95	0.08	2.0
Chromium	51.99	3.1	24	1.4	0.2
Cobalt	58.93	38	8	5.0	0.2
Selenium	78.96	12.3	4	0.6	2.0
Niobium	92.91	1.1	1	0.012	40
Antimony	121.75	5.5	1	0.05	20
Barium	137.34	1.2	16	0.15	6.0
Tantalum	180.95	19	<1	≤0.1	5.0
Tungsten	183.85	19.1	4	0.46	2.0
Platinum	195.09	9.6	4	0.20	4.0
Vanadium	50.94	5.0	19	1.8	1.0
Manganese	54.94	13.3	12	2.8	0.3
Iron	55.85	2.62	25	1.2	0.3
Zirconium	91.22	0.19	16	0.03	20
Magnesium	24.312	0.06	40	0.1	8
Titanium	47.90	6.1	54	6.9	0.1
Cadmium	112.40	3620	2.3	75	0.01
Silicon	28.08	0.16	80	0.45	2.0
Calcium	40.08	0.43	28	0.30	3.0
Aluminium	26.98	0.23	20	0.18	2.5
Phosphorous	30.97	0.18	18	0.11	7.0
Sulphur	32.06	0.52	42	0.68	2.0

The sensitivity values based on (Iσ/A) indicate the relative range of values under ideal conditions and are restricted only by the values of basic nuclear data. In practice, the sensitivity depends also on background radiations levels, source-strength, counting time and on other operational parameters. In a towed system, counting time is related to towing speed and the last column indicates the minimum abundances of elements which could be detected by a typical system.

Table 5.15

Physical characteristics of silica material and seawater content of the seabed matrix

Mesh No BSS	Aperture Grain-size (mm.)	Dry Density of sand ($g.cm^{-3}$)	Porosity (% volume) Exptl.	Sea-water content (% wt.)
85 - 60	0.18 - 0.25	2.64	40.2	20.7
60 - 44	0.25 - 0.355	2.61	39.4	20.2
18 - 8	0.853 - 2.0	2.62	39.3	20.2
8 - 5	2.0 - 3.35	2.68	41.8	21.6
Pea-Shingle	5.0 - 9.0	2.62	43.8	23.4

Table 5.16

Countrates in γ-ray energy peaks of hydrogen and chlorine for seabeds with different seawater content

Seawater Content (% Wt.)	Matrix Density ($g.cm^{-3}$)	Net counts in peak in 120 mins counting time						
		Hydrogen 2.233 MeV (f)	Chlorine 6.111 MeV (d)	Chlorine 7.790 MeV (f)	Chlorine 7.790 MeV (d)	Chlorine 7.414 MeV (f)	Chlorine 7.414 (MeV) (d)	Chlorine 6.620 MeV (f)
20.7	1.99	209,558 ± 579	10,125 ± 173	1762 ± 63	4409 ± 134	2307 ± 72	5159 ± 134	3393 ± 125
20.2	1.98	208,988 ± 573	10,051 ± 173	1535 ± 58	4234 ± 134	2546 ± 83	5703 ± 138	3379 ± 119
20.2	1.99	207,037 ± 575	10,268 ± 190	1610 ± 59	4153 ± 119	2340 ± 76	5302 ± 142	3376 ± 131
21.6	1.99	210,903 ± 596	10,365 ± 198	1617 ± 55	4430 ± 110	2333 ± 76	5190 ± 130	3442 ± 119
23.4	1.92	206,243 ± 591	11,141 ± 236	1553 ± 53	4367 ± 125	2370 ± 125	5393 ± 129	4667 ± 125 *

* Peak contaminated with Fe 7.648 MeV (d) + Fe 7.632 (d)

Errors on seawater contents ± 2%.

TABLE 5.17

Abundance and principle γ-ray energies of elements in the simulated seabed

Source-detector distance (cms)	Element 'seeded' and abundance (%)	Principal Gamma-Ray Energy	
		Elements 'seeded' (MeV)	Seabed and Seawater (MeV)
30 cms	2.5% Ti + 2.9% Fe	Ti 6.418 (f) Ti 6.760 (d)	Si 3.539 (f) H 2.223 (d)
35 cms	3% Ni	Ni 8.999 (f) Ni 8.999 (d)	Cl 7.790 (f)
40 cms	3% Zr	Sensitivity low for detection	Cl 6.111 (d) Cl 6.620 (f) Cl 7.414 (d)

f = full energy

d = double-escape

TABLE 6.1

Stratigraphy, mineral content and chemical variation with depth in Atlantis II Deep

Depth (m)	Mineral Content	Solid matter %	Zn	Cu	Ag	Fe
			% in solid matter		ppm	%
0 - 3	Amorphous + iron silicates	7	2	0.4	50	30
3 - 5	Sulphides + iron silicates	8	3.5	0.7	70	20
5 - 8.5	Limonites + hematite + manganite + iron silicates	15	0.3	0.1	20	45
8.5 - 10	Sulphides + silicates	20	3.5	0.9	80	20
10 - 15	Limonite + marl + pyrite	40	?	?	?	35

* DATA from MILL (1983).

TABLE 6.2

Average abundances of the important elemental constitutents in Manganese nodules and encrustations from different environments (Percentage wt.).

Element	Sea-mount	Plateau	Active ridges	Other Ridges	Contin-ental border-lands	Marginal sea-mounts	Abyssal nodules
Mn	14.62	17.17	15.51	19.74	38.69	15.65	16.78
Fe	15.81	11.81	19.15	20.08	1.34	19.32	17.27
Ni	0.351	0.641	0.306	0.336	0.121	0.296	0.540
Co	1.150	0.347	0.400	0.570	0.011	0.419	0.256
Cu	0.058	0.087	0.081	0.052	0.082	0.078	0.370
Mn/Fe	0.92	1.53	0.80	0.98	28.8	0.81	0.97
Depth (m)	1872	945	2870	1678	3547	1694	4460

* Data from CRONAN (1977)

TABLE 6.3

Principal γ-ray energies and lowest limit of detection of the principal elemental constituents of Manganese nodules and associated sediments

Element	Thermal neutron absorption cross-section σ (barns)	Principal γ-Ray energy (MeV)	Intensity I(%) photons/ 100 neutrons	Lowest limit of detection (Wt.%)*
Manganese (Mn)	13.3	7.244 7.058	12.05 11.35	0.3
Iron (Fe)	2.62	7.646 7.632	22.14 27.19	0.3
Copper (Cu)	3.9	7.915 7.637	28.40 14.47	0.3
Nickel (Ni)	4.6	8.999 8.533	41.65 18.74	0.1
Cobalt (Co)	38	6.877 6.706	7.77 7.22	0.2
Silicon (Si)	0.16	3.539 4.934	79.58 70.55	2.0
Calcium (Ca)	0.430	6.420 4.419	28.09 10.79	3.0
Alluminium (Al)	0.235	7.724	20.10	2.5

* The limit of detection is quoted only for the most intense γ-ray.

TABLE 6.4

Average composition and grade of Manganese nodules from different regions of the Indian Ocean. (From CRONAN, 1983)

REGION	Mn %	Fe %	Mn/Fe	Ni %	Cu %	Co %	Grade*
CENTRAL INDIAN BASIN (Average)	20.4	9.6	2.1	0.86	0.74	0.14	1.7
- terrigeneous sediment	14.2	16.6	0.86	0.34	0.22	0.17	0.73
- carbonate ooze	16.6	13.4	1.2	0.57	0.23	0.17	0.97
- pelagic clay	15.4	12.2	1.3	0.61	0.35	0.17	1.1
- siliceous ooze	21.8	8.2	2.7	0.91	0.96	0.13	2.0
WHARTON BASIN (Average)	17.5	11.9	1.5	0.55	0.41	0.18	1.1
- terrigeneous sediment	16.2	14.2	1.1	0.43	0.20	0.15	0.78
- carbonate ooze	15.7	15.7	1.0	0.30	0.19	0.12	0.61
- pelagic clay	16.1	11.4	1.4	0.49	0.26	0.15	0.90
- siliceous ooze	20.3	11.4	1.8	0.70	0.56	0.17	1.4
SOUTH AUSTRALIAN BASIN (Average)	19.0	13.4	1.4	0.69	0.34	0.18	1.2
- Manganese pavement area	23.3	12.0	1.9	0.96	0.37	0.12	1.5
MADAGASCAR BASIN	12.3	16.4	0.75	0.21	0.12	0.27	0.60 (0.79)
CROZET BASIN (Average)	12.4	15.6	0.79	0.33	0.15	0.21	0.60 (0.80)
- siliceous ooze	14.2	9.4	1.5	0.69	0.23	0.11	1.0
AGULHAS PLATEAU (Average)	15.5	13.9	1.1	0.69	0.11	0.28	1.1 (1.3)
- 2,500m - 3,500m	18.0	12.9	1.4	0.89	0.17	0.35	1.4 (1.6)
MOSAMBIQUE RIDGE	16.1	13.3	1.2	0.41	0.13	0.34	0.88 (1.1)
MOSAMBIQUE CHANNEL	15.0	14.7	1.0	0.67	0.18	0.13	0.98
N.W. INDIAN OCEAN	16.6	17.8	0.93	0.35	0.07	0.61	1.03 (1.6)

* Nodule grade = Ni + Cu + Co; Ni equivalent grade = Ni + Cu/3 + 2 Co, and is (in brackets) where it is significantly higher that the grade.

TABLE 6.5

Average composition and grade of Manganese nodules from different regions of the Pacific Ocean. (From CRONAN, 1983)

REGION	Mn %	Fe %	Mn/Fe	Ni %	Cu %	Co %	Grade*
EQUITORIAL N.E. PACIFIC - Siliceous ooze	22.4	8.2	2.7	1.2	1.0	0.25	2.4
S.W. PACIFIC BASIN	17.1	20.7	0.80	0.42	0.24	0.40	1.1 (1.3)
SAMOA BASIN	17.3	19.6	0.88	0.23	0.17	0.23	0.63 (0.75)
PHOENIX ISLAND BASIN	18.1	17.2	1.05	0.40	0.29	0.34	1.0 (1.2)
SOUTH PENRYN BASIN	15.2	15.4	0.99	0.41	0.22	0.36	0.99 (1.2)
NORTH PENRYN BASIN	21.2	10.5	2.02	0.76	0.56	0.29	1.6 (1.5)

* Figures in brackets are Ni equivalent grade.

TABLE 6.6

Maximum, minimum and average contents of elements in Manganese nodules from the Pacific and Indian Oceans - 139 nodules. (from CRONAN 1983)

Element	Maximum	Minimum	Mean
Mn	30.28	5.41	16.63
Fe	26.32	4.36	13.11
Ni	1.68	0.136	0.545
Co	2.57	0.045	0.311
Cu	1.64	0.028	0.293

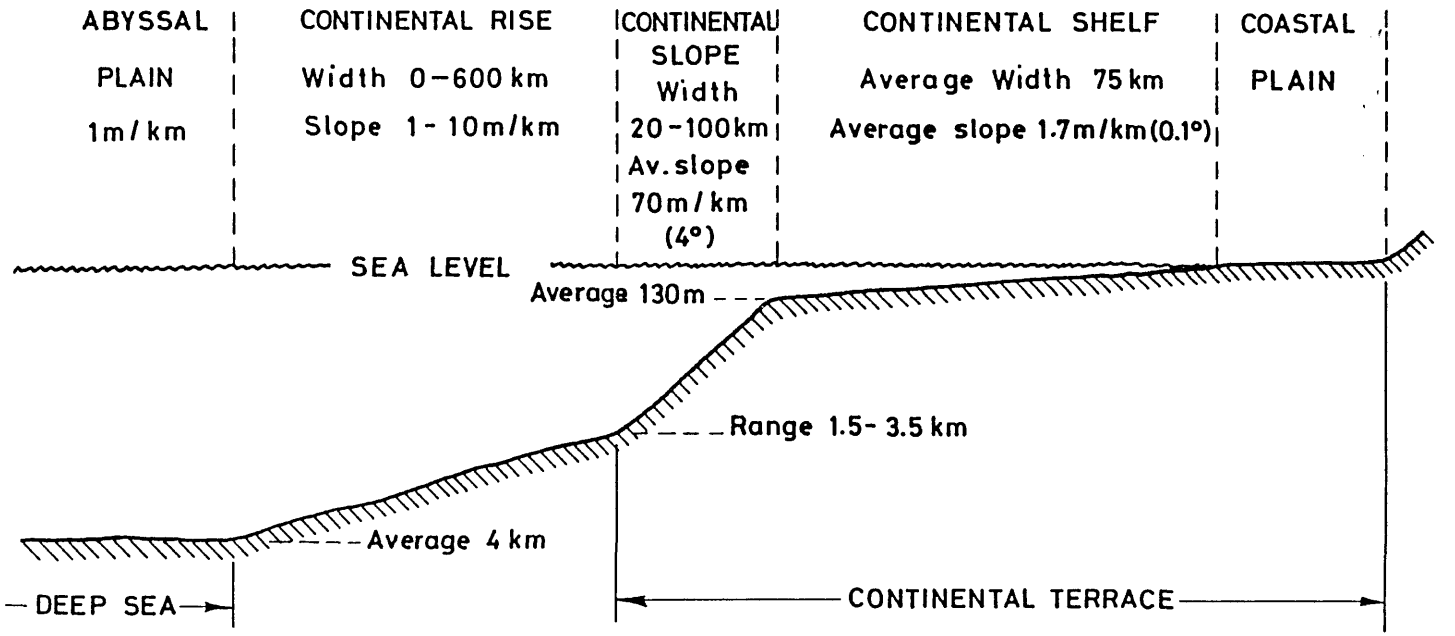

Figure 1.1 Diagrammatic profile of one type of off-shore region, showing average or range of depth, width, and slope of continental shelf, continental slope, continental rise and abyssal plain. (Vertical exaggeration 20x)

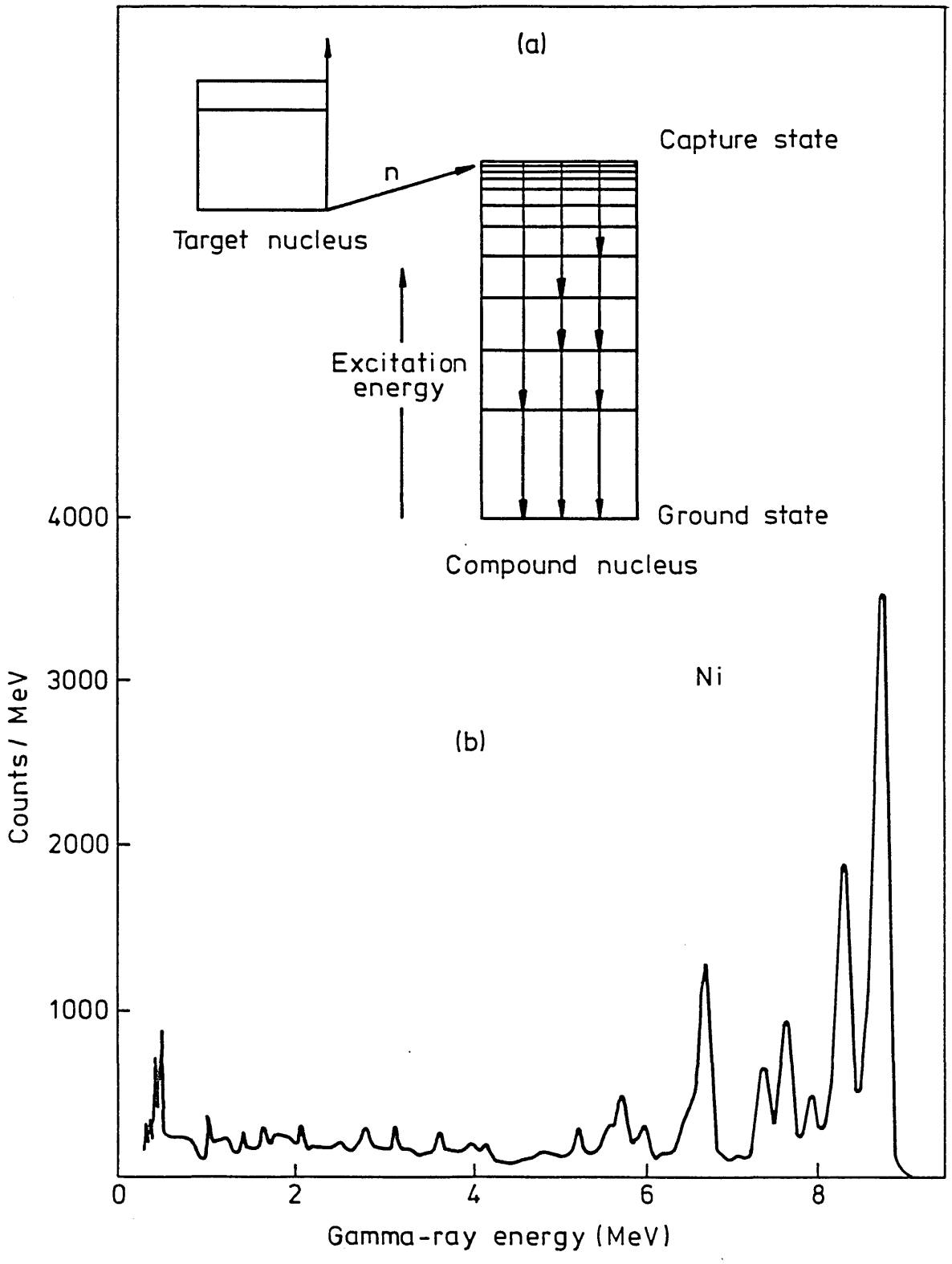

Figure 2.1 (a) Schematic diagram of neutron radiative capture reaction, showing possible modes of de-excitation.
(b) Energy distribution of gamma-rays resulting from neutron radiative capture (n,γ) by nickel.

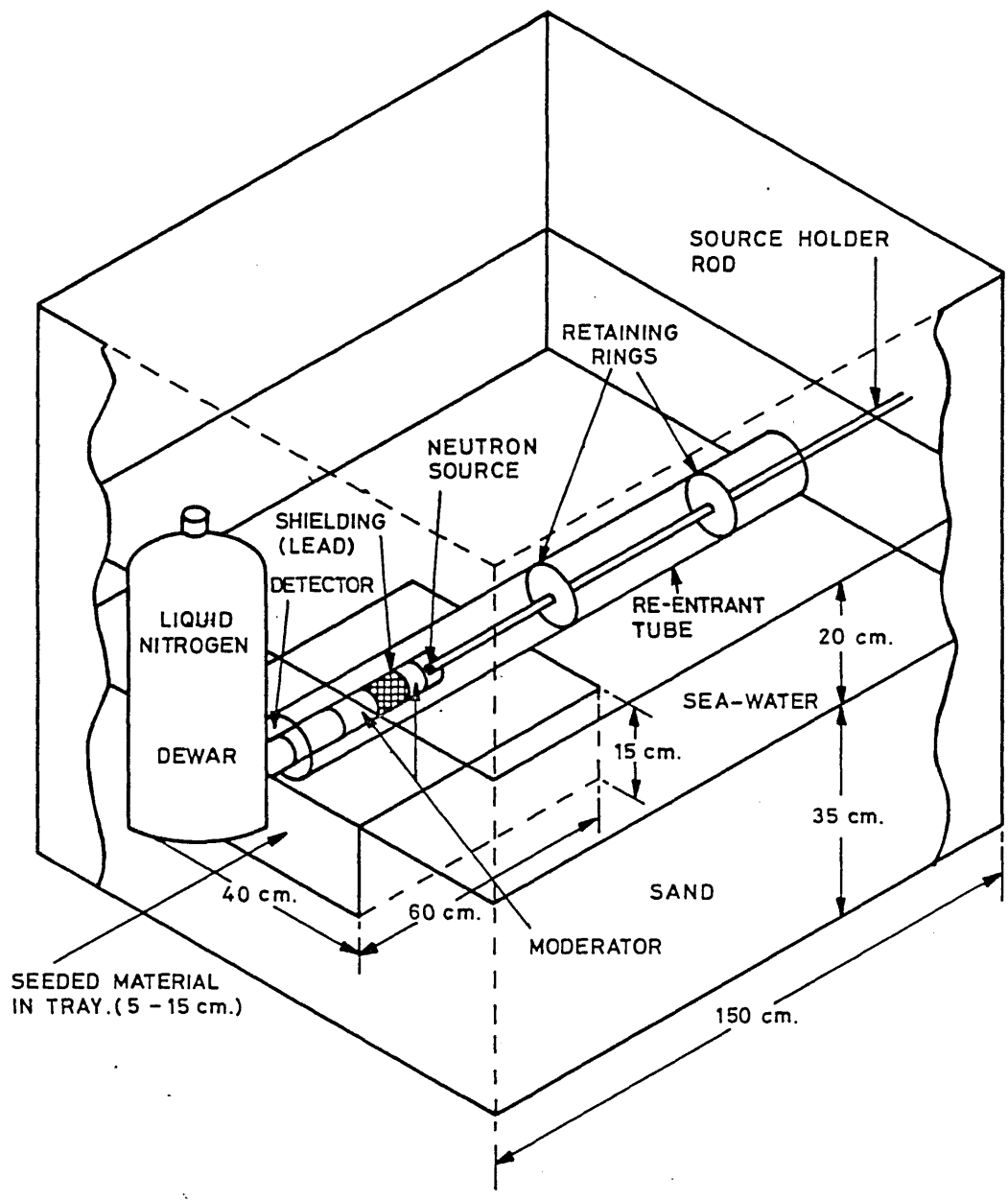

Figure 3.1 A perspective view of constructional features and essential components of the experimental tank.

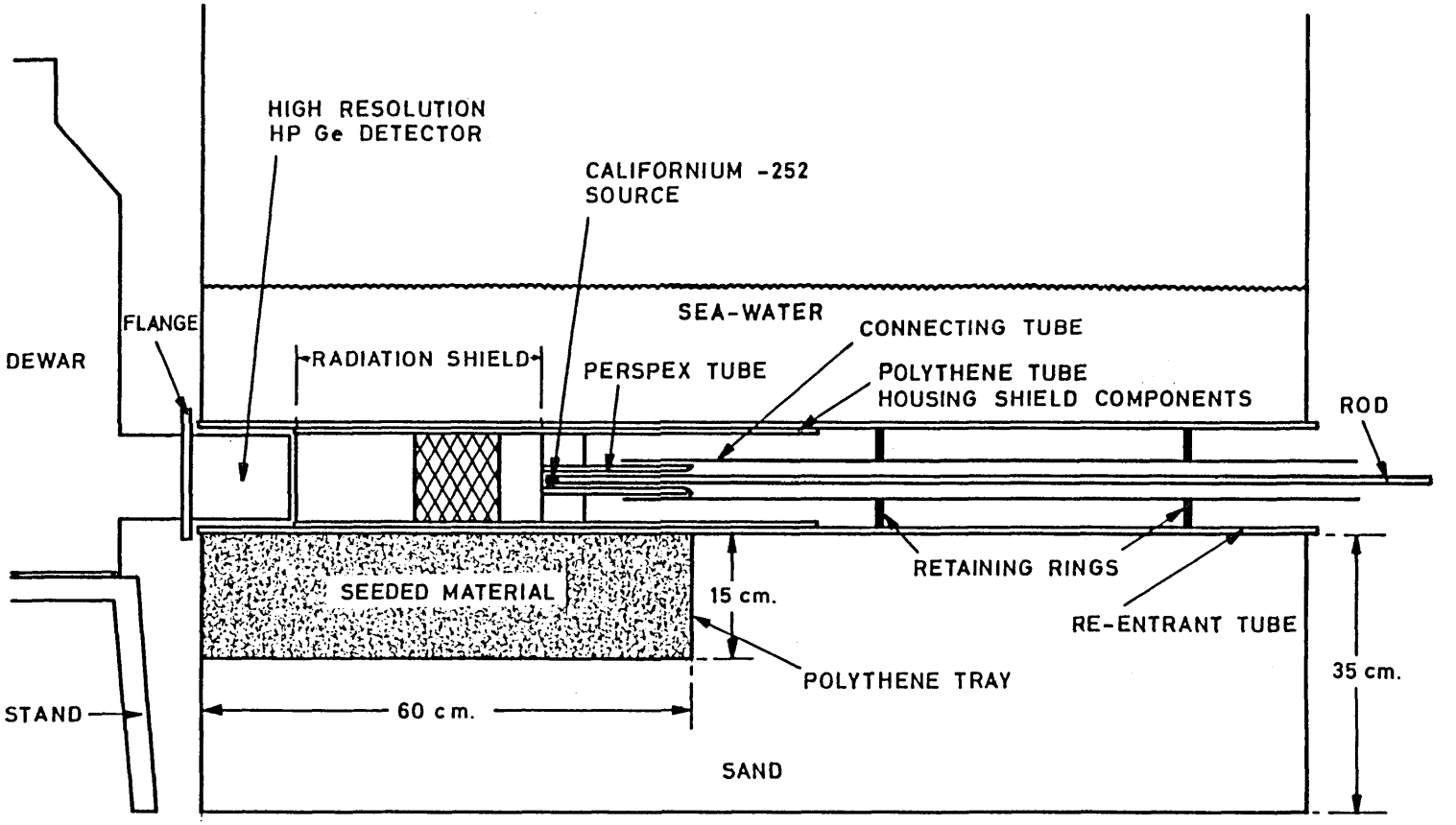

Figure 3.2 A sectional view of the arrangement of the various components of the probe in relation to the 'seeded' material in the simulated seabed.

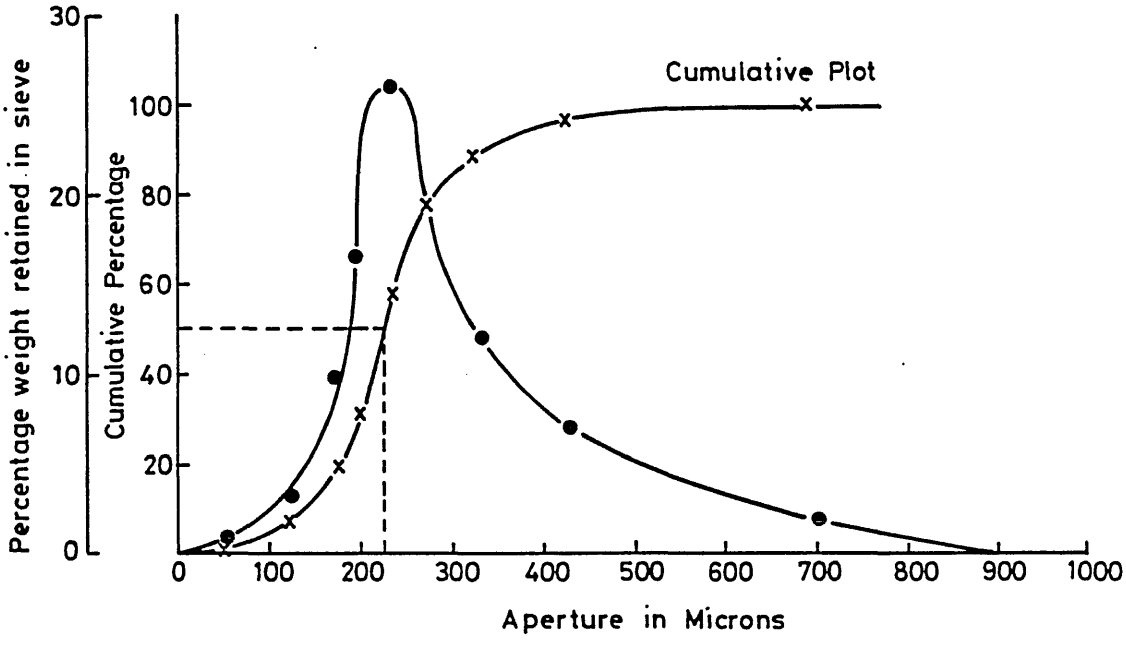

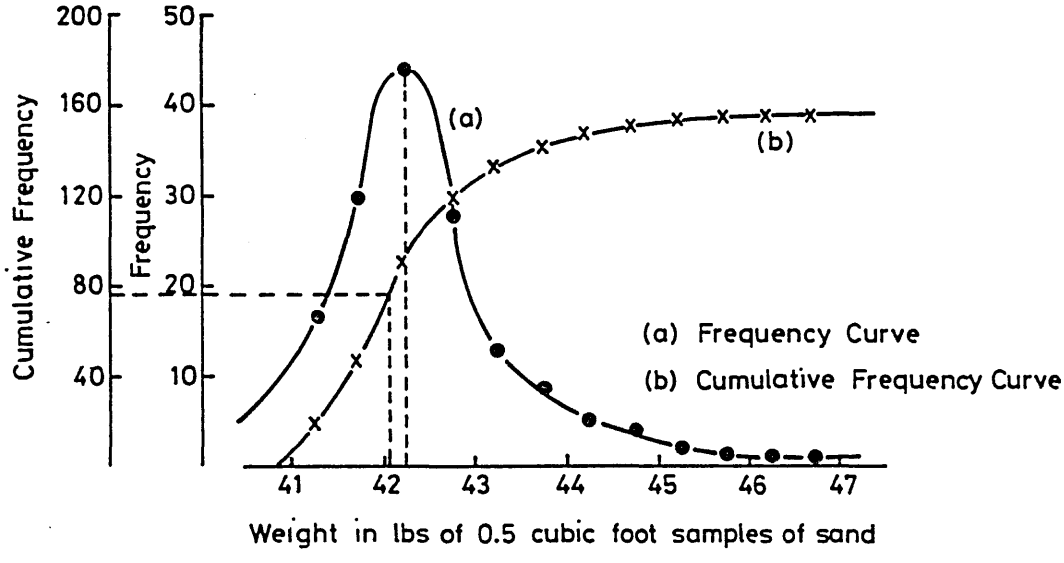

Figure 3.3 Frequency distribution curves for average grain-size and bulk density measurements of silica sand for the experimental seabed.

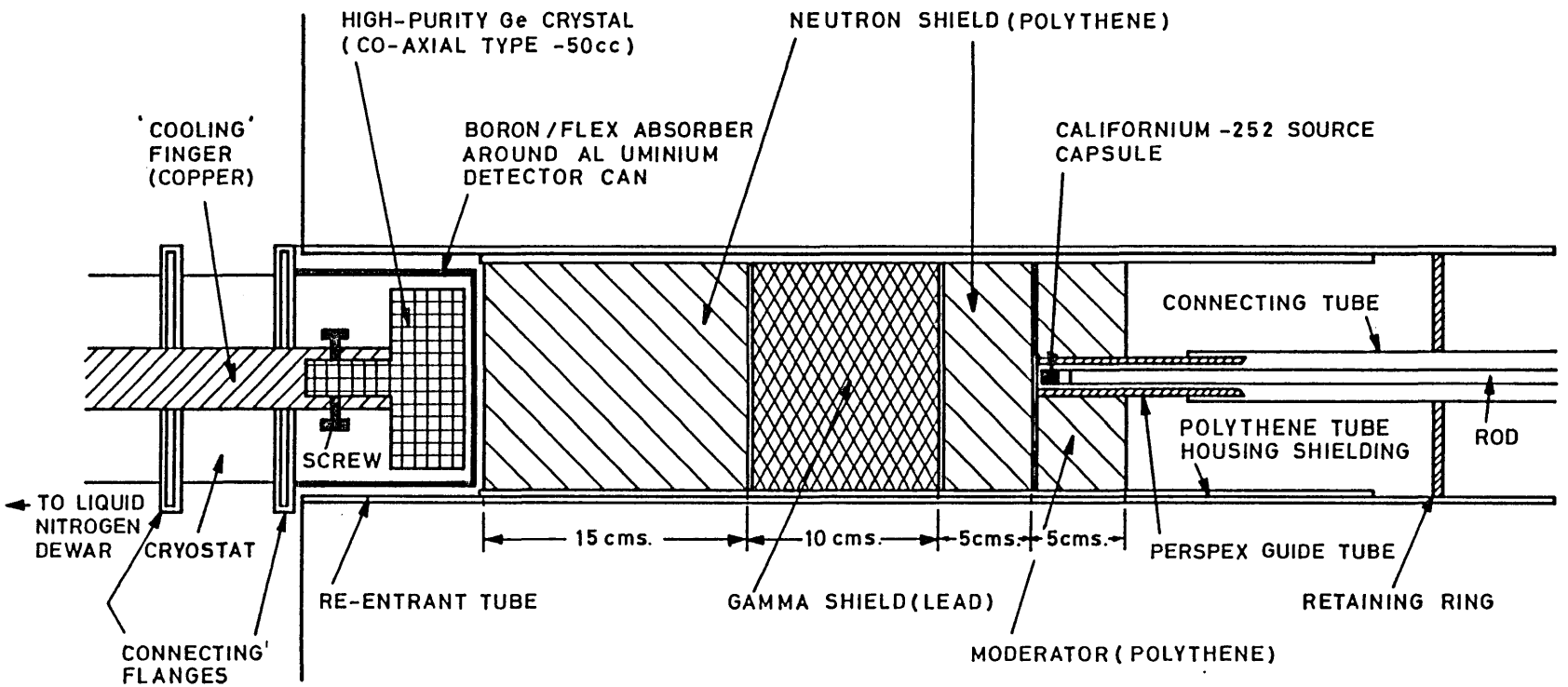

Figure 3.4 Enlarged sectional view of the probe assembly showing the internal configuration of the neutron source, radiation shield and essential components of the gamma-ray detector.

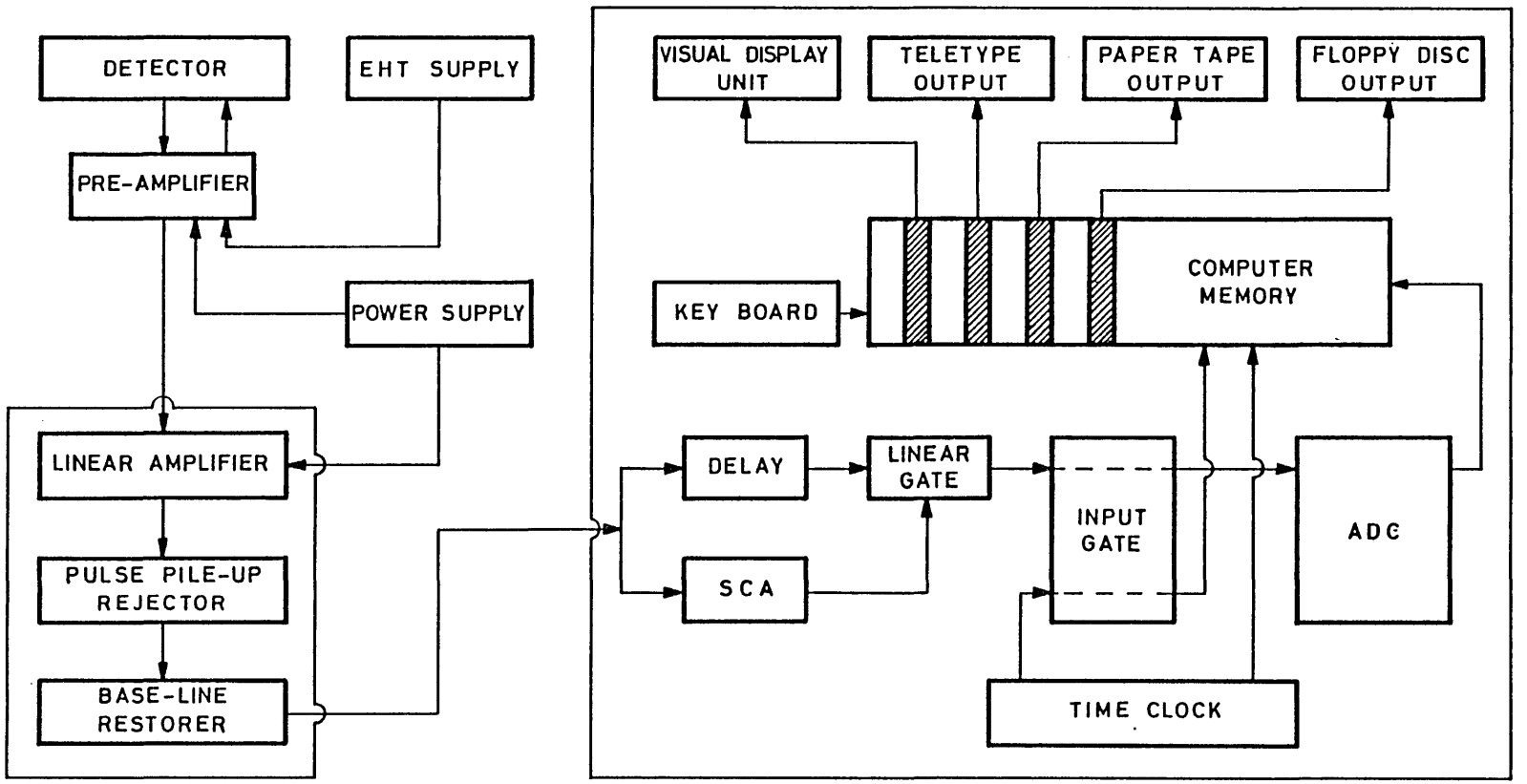

Figure 3.5 Functional block diagram of the detector, multi-channel pulse-height analyser, associated electronics, data acquisition and storage systems.

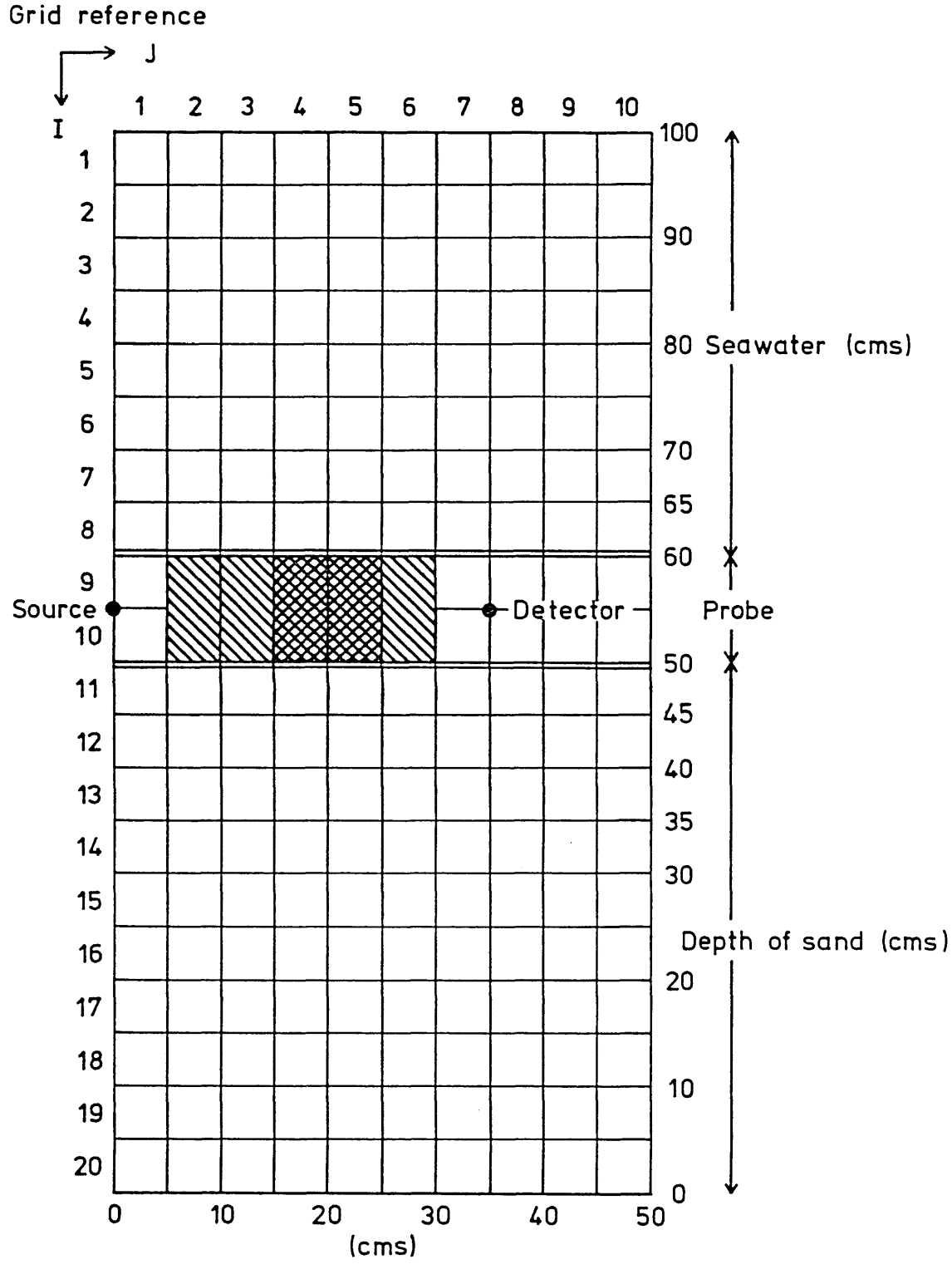

Figure 4.1 Grid representation of the experimental system for computer model. Each mesh area generates an annular region when rotated about the vertical axis through source.

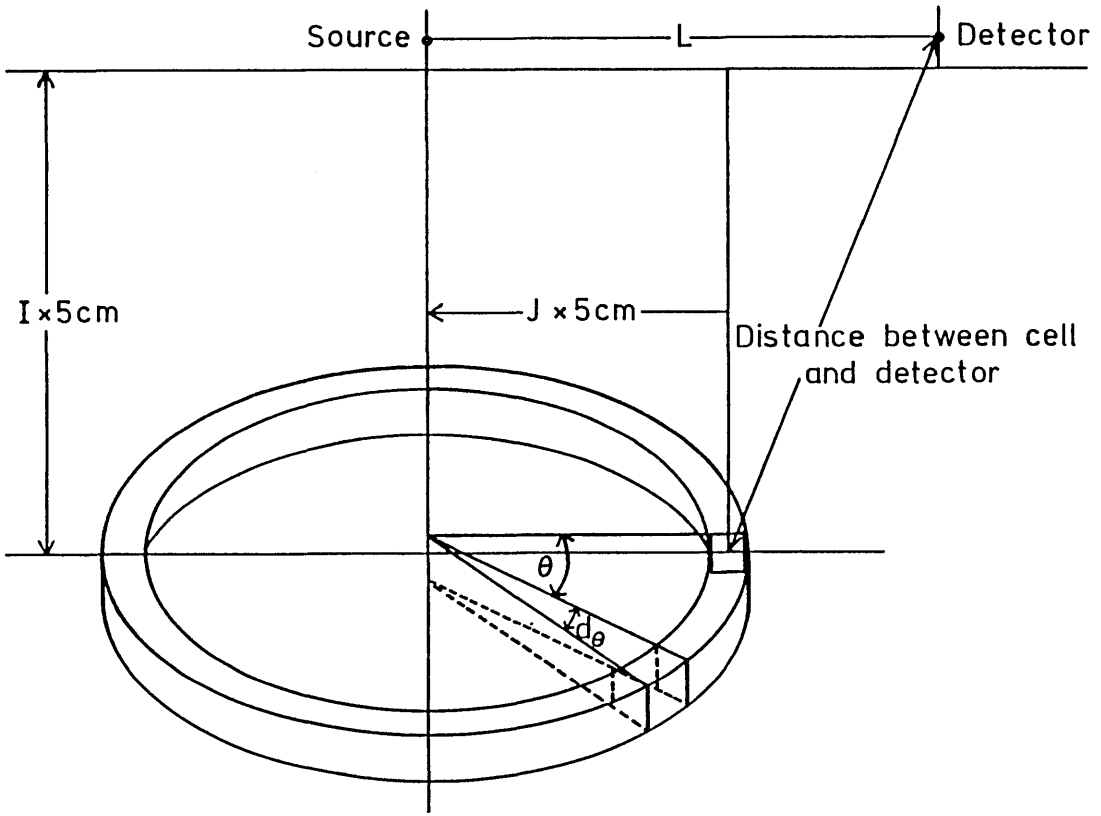

Figure 4.2 Diagrammatic representation of a typical annular region corresponding to a grid area showing the important parameters used in the computer calculations. Distance between cell and detector is re-calculated for each increment $d\theta$. Gamma count from each cell is then integrated over an angle 2π and procedure repeated for each grid area.

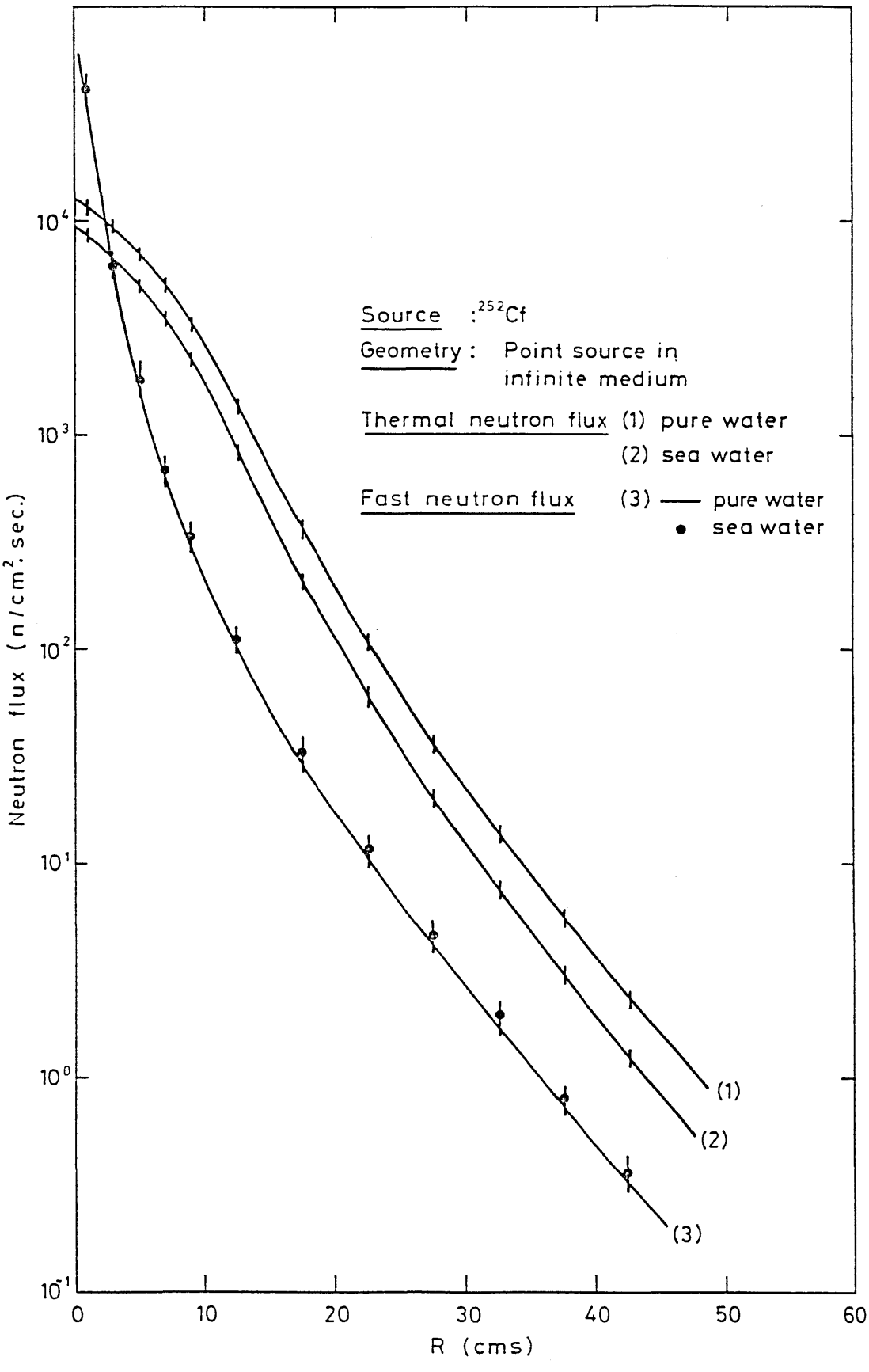

Figure 4.3 Calculated neutron flux in infinite media of pure water and seawater as a function of radial distance R, for a point isotopic 1 μg ^{252}Cf neutron source.

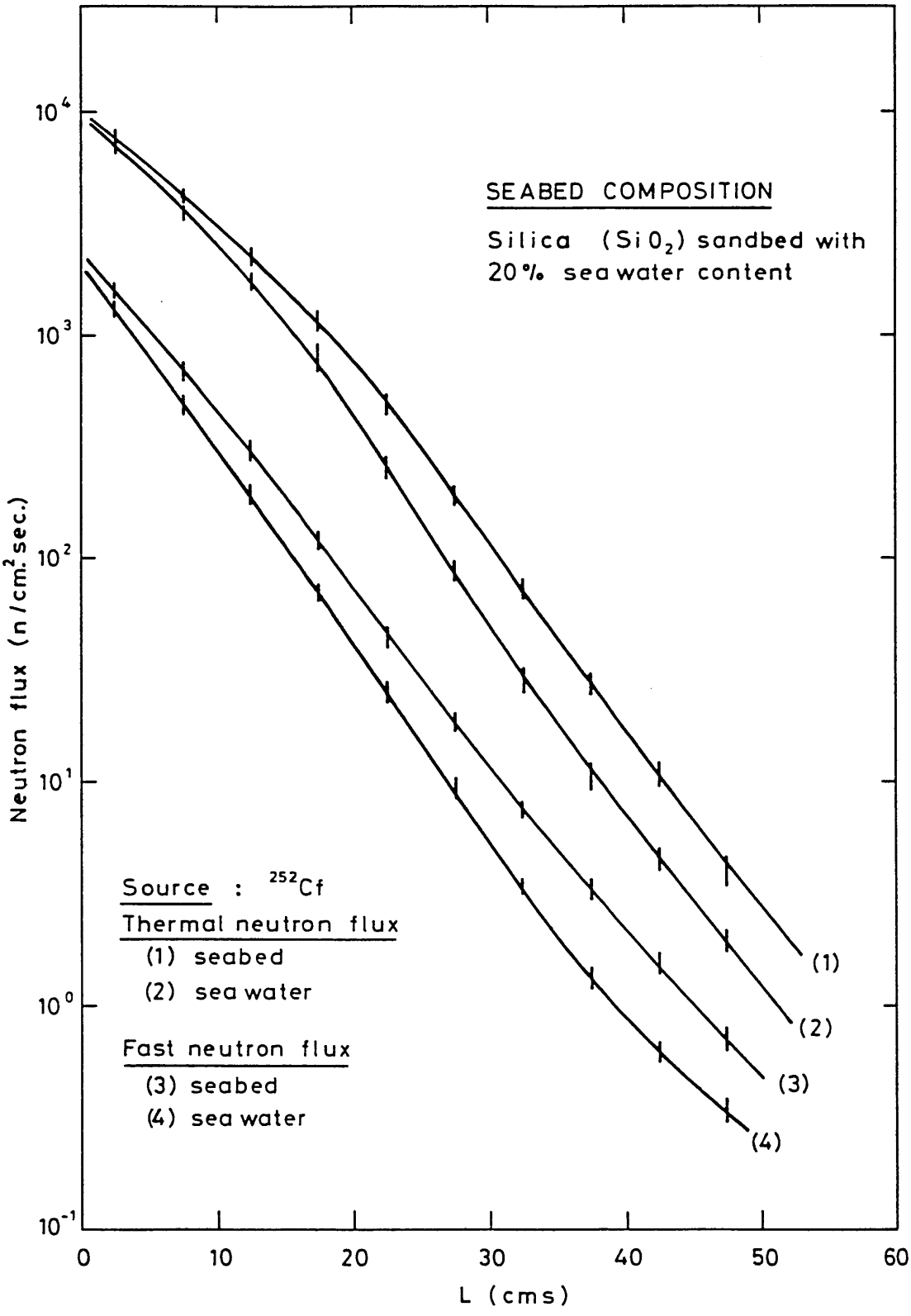

Figure 4.4 Calculated neutron flux in the simulated seabed as a function of distance L, for a 1 μg ^{252}Cf neutron source in the experimental probe.

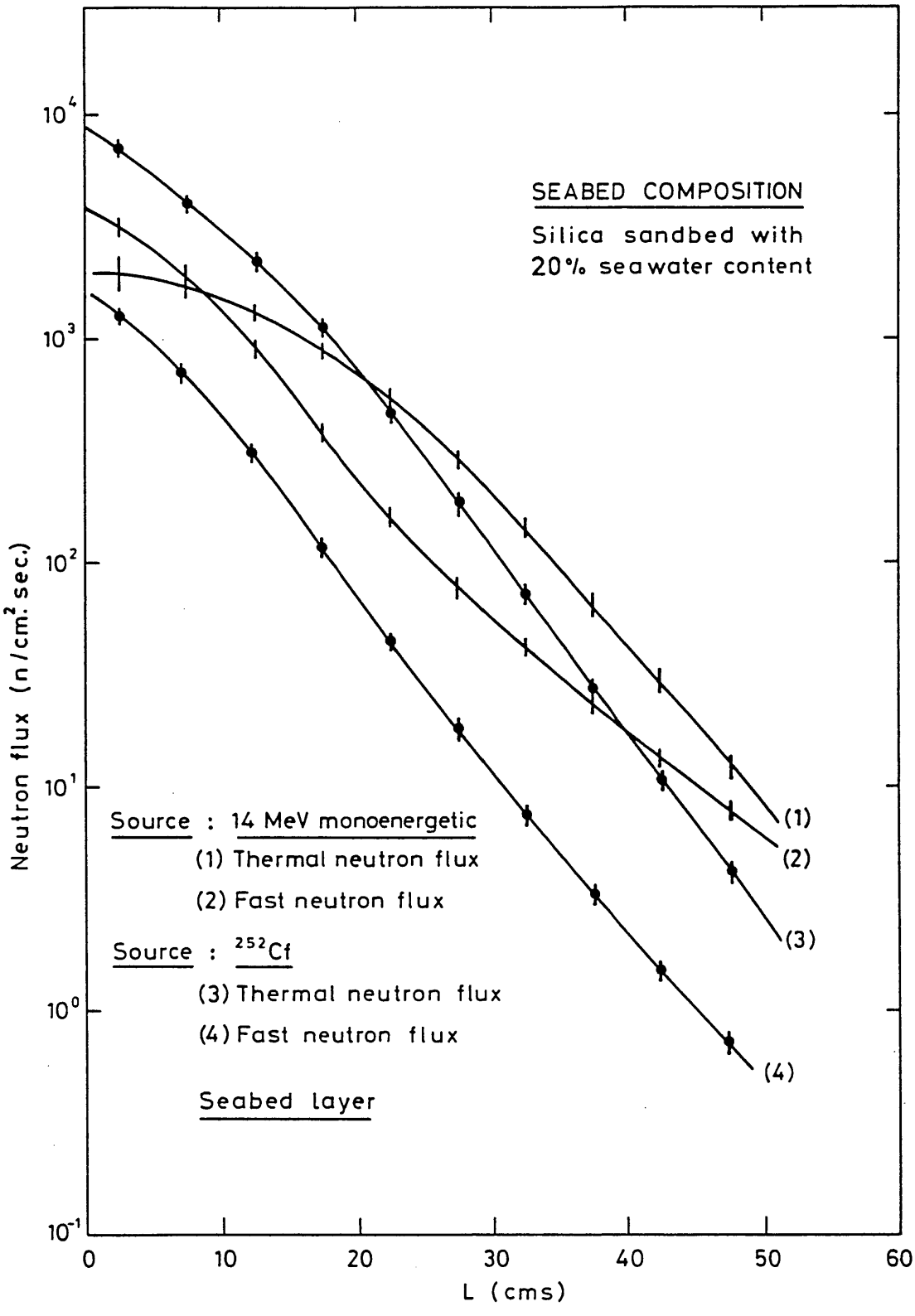

Figure 4.5 Calculated neutron flux in the seabed layer as a function of distance L, for (a) 14 MeV monoenergetic neutron source (b) ^{252}Cf neutron source in the experimental probe. Source strength in each case is assumed to be equivalent to 1 μg ^{252}Cf.

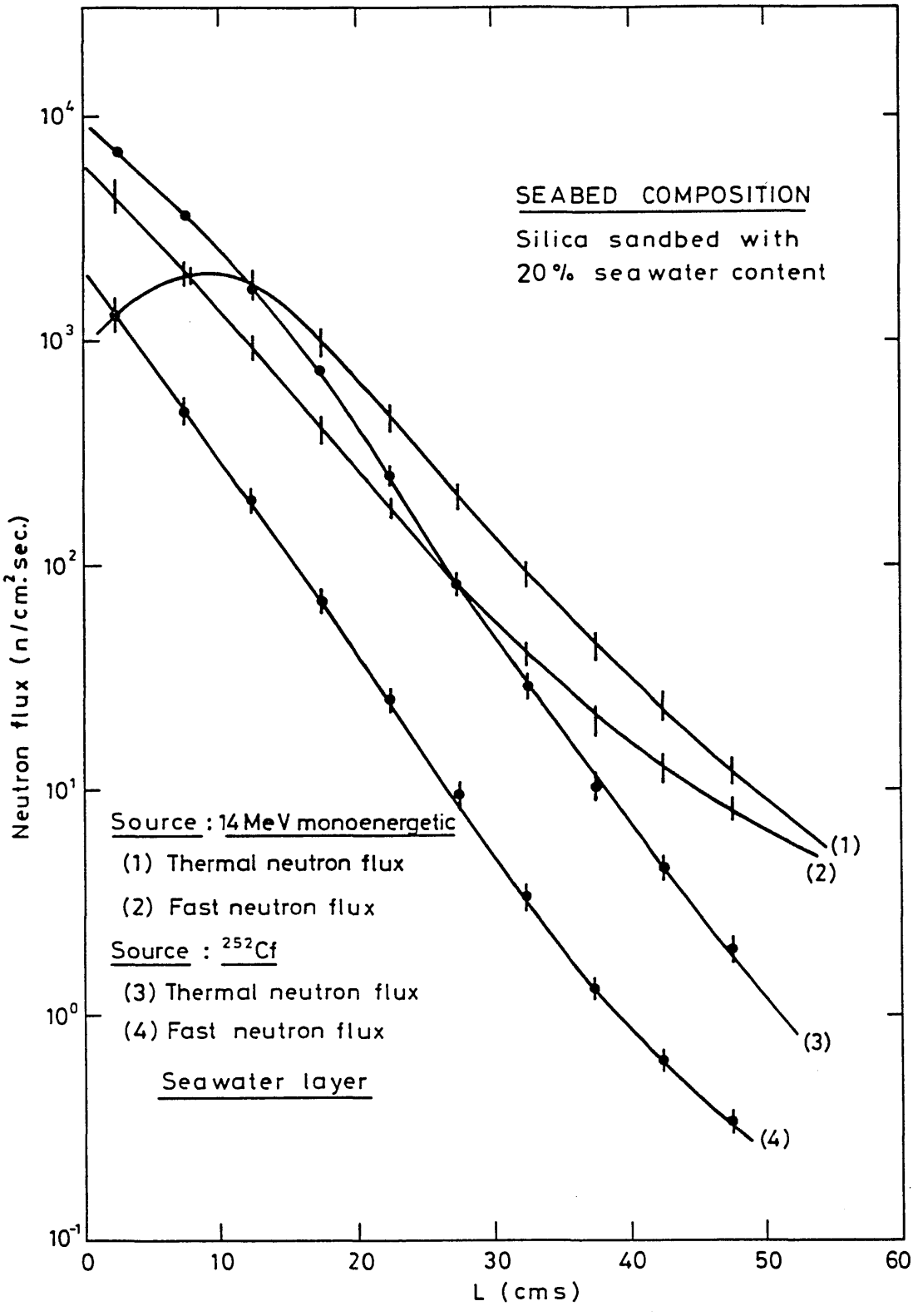

Figure 4.6 Calculated neutron flux in the overlying seawater layer as a function of distance L, for (a) 14 MeV monoenergetic neutron source (b) ^{252}Cf neutron source in the experimental probe. Source strength in each case is assumed to be equivalent to 1 μg ^{252}Cf.

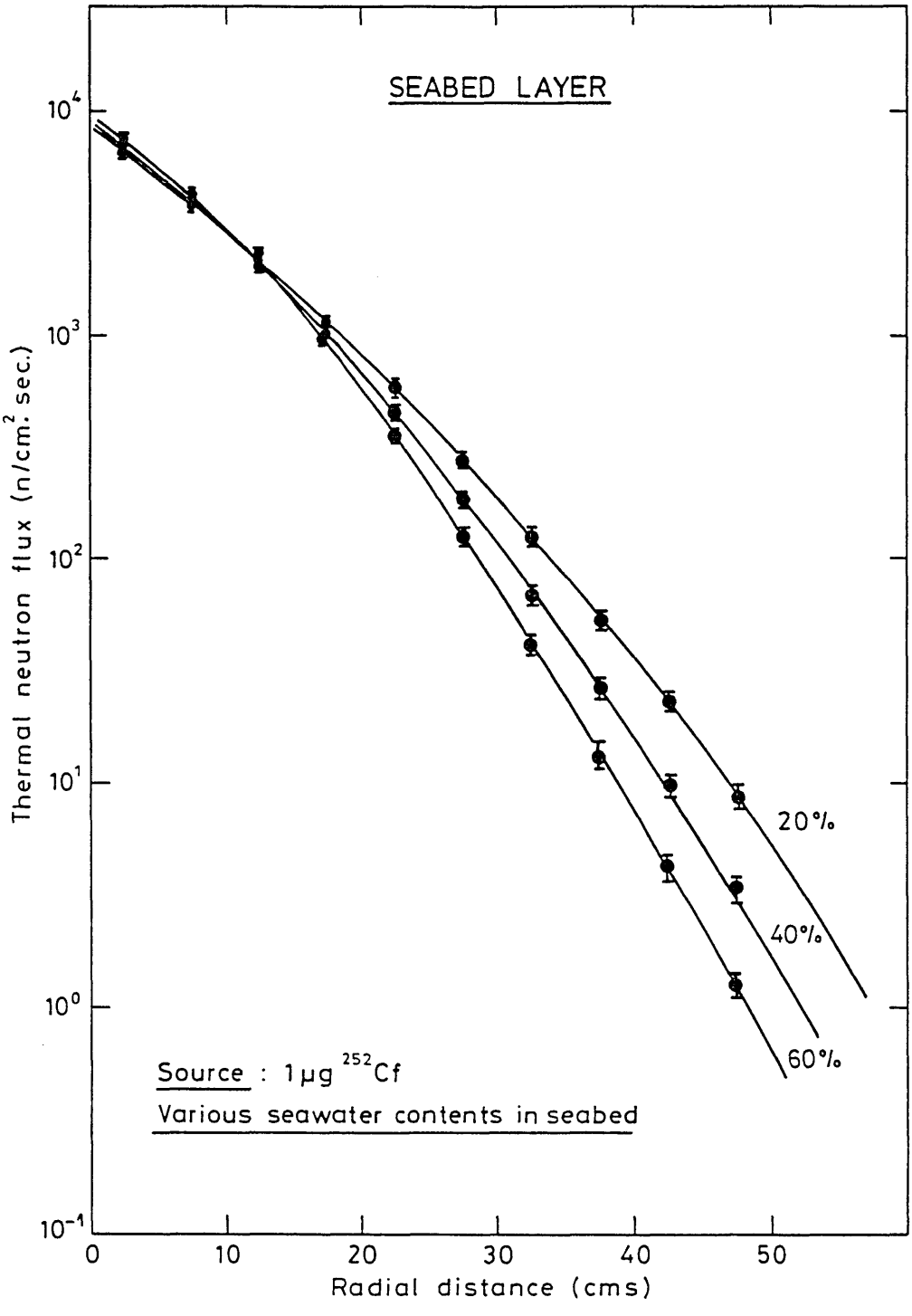

Figure 4.7 Calculated thermal neutron flux in the simulated seabed as a function of radial distance R, for a 1 μg ^{252}Cf neutron source for assumed seawater contents of 20%, 40% and 60% by weight.

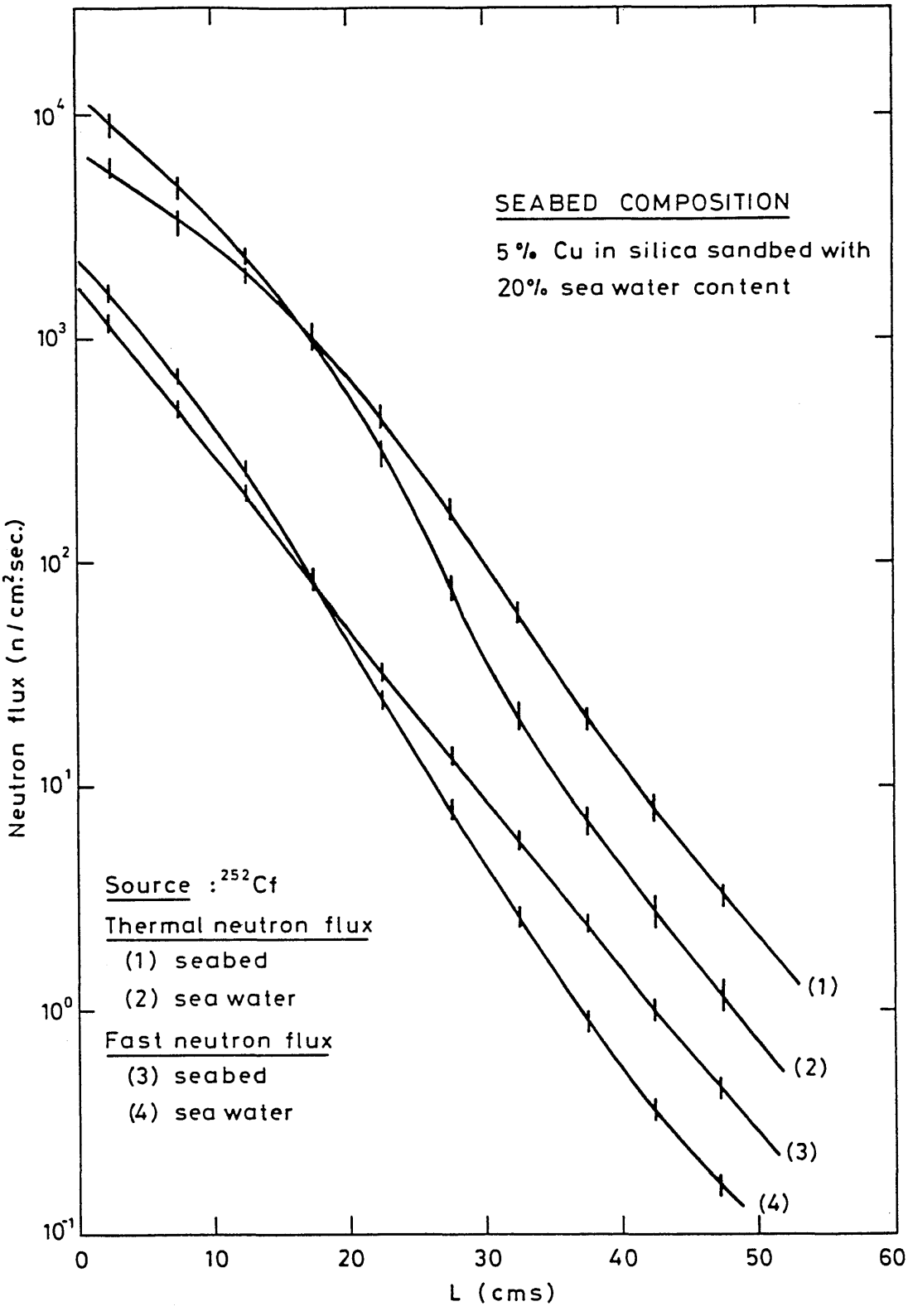

Figure 4.8 Calculated spatial neutron flux distributions in the simulated seabed and overlying seawater with 5% copper uniformly distributed in the seabed. Neutron source: 1 μg^{252}Cf.

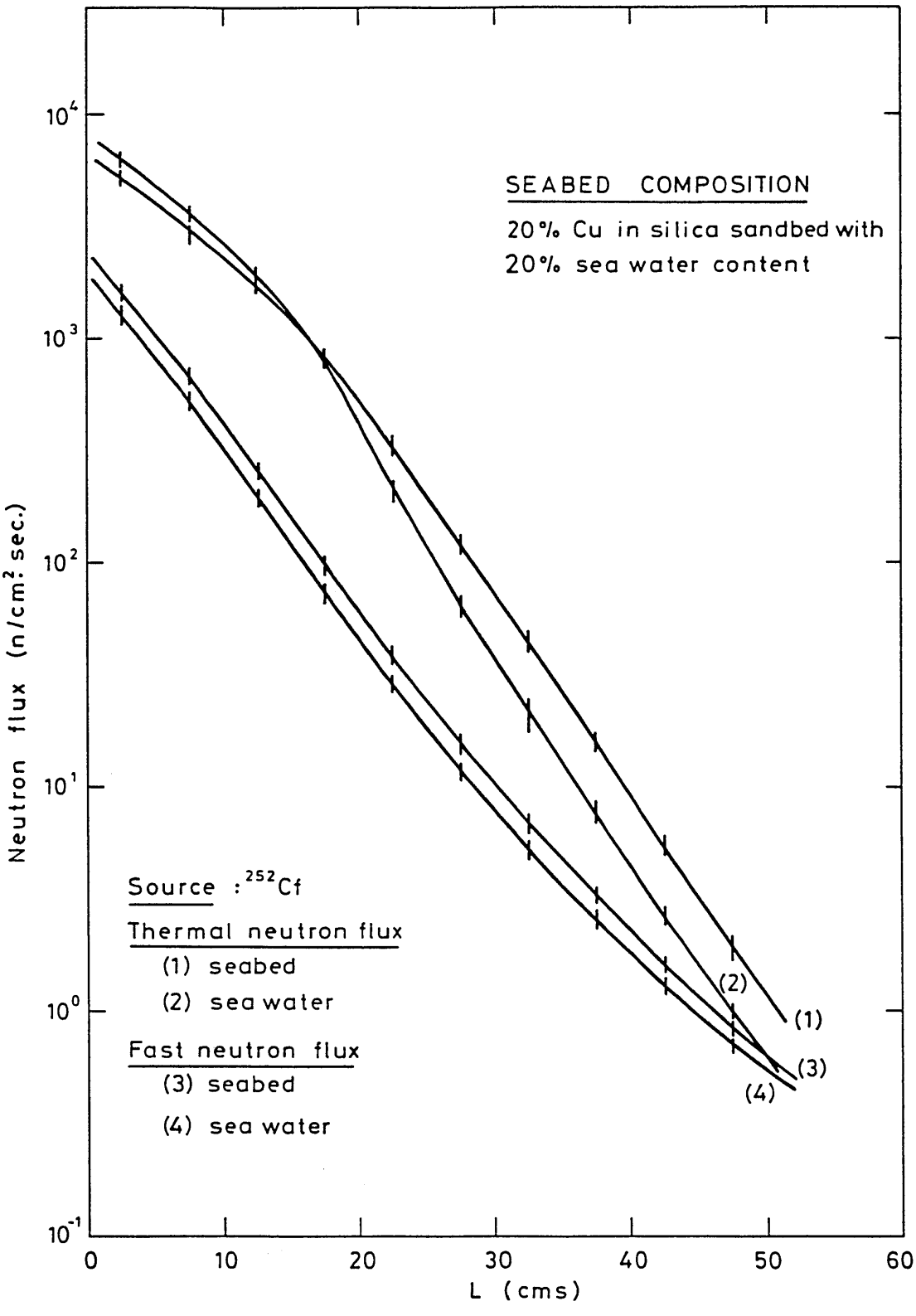

Figure 4.9 Calculated spatial neutron flux distributions in the simulated seabed and overlying seawater with 20% copper uniformly distributed in the seabed. Neutron source: 1 μg ^{252}Cf.

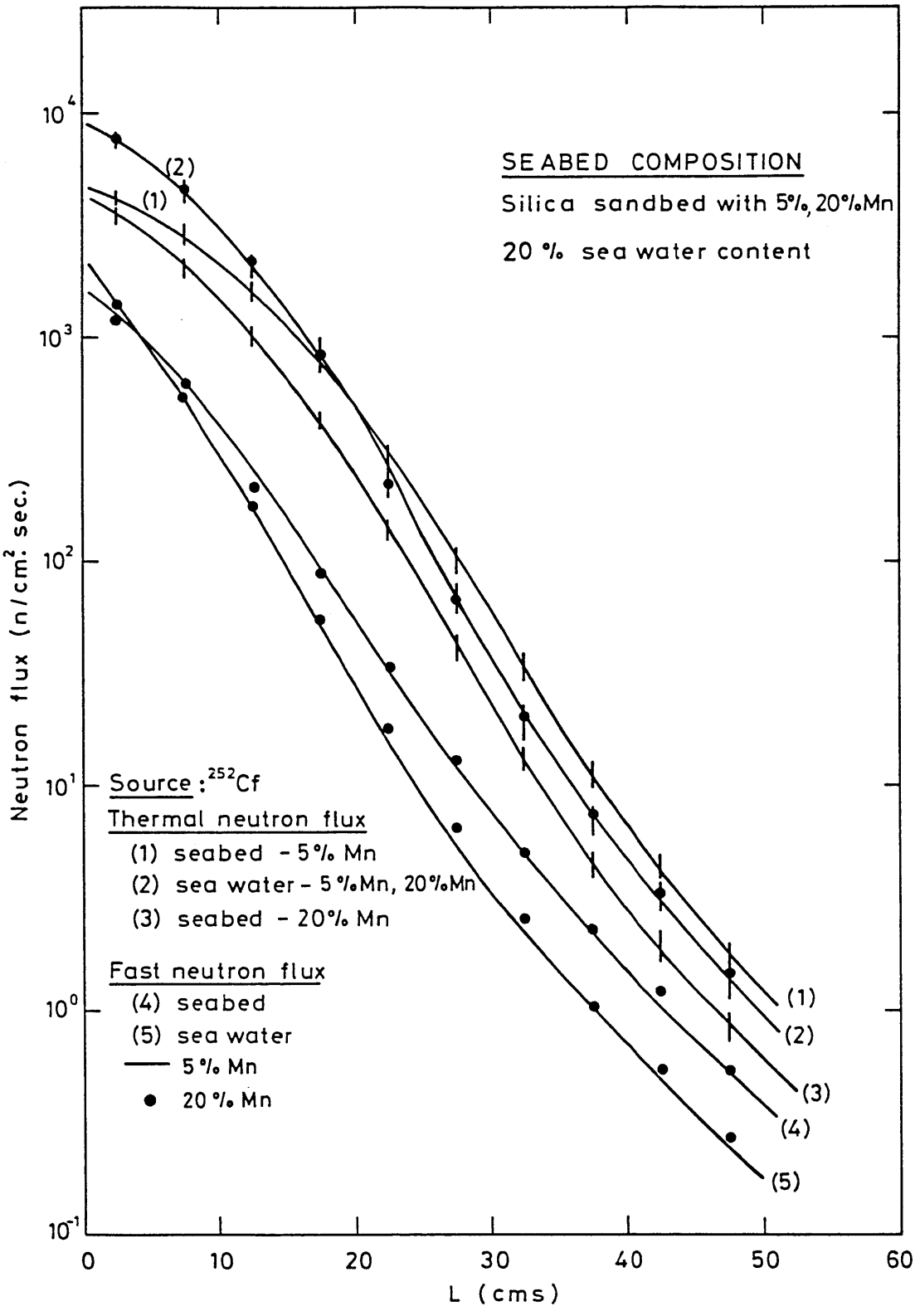

Figure 4.10 Calculated spatial neutron flux distributions in the simulated seabed and overlying seawater with (a) 5% manganese (b) 20% manganese distributed uniformly in the seabed. Neutron source: 1µg ^{252}Cf.

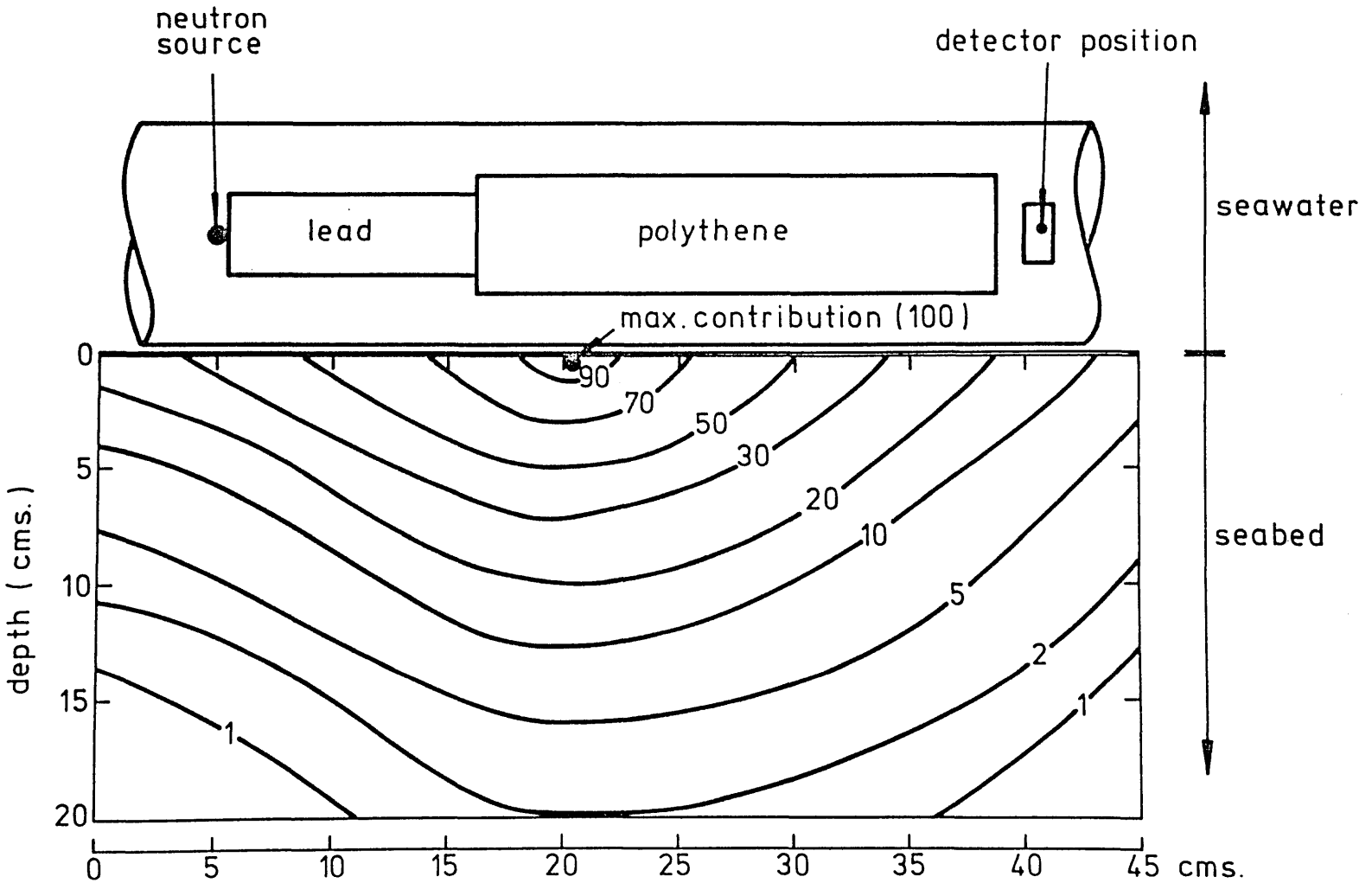

Figure 4.11 Sectional contour diagram showing seabed contributions to detector countrate (from unit volume) as percentages of the maximum value close to the surface.

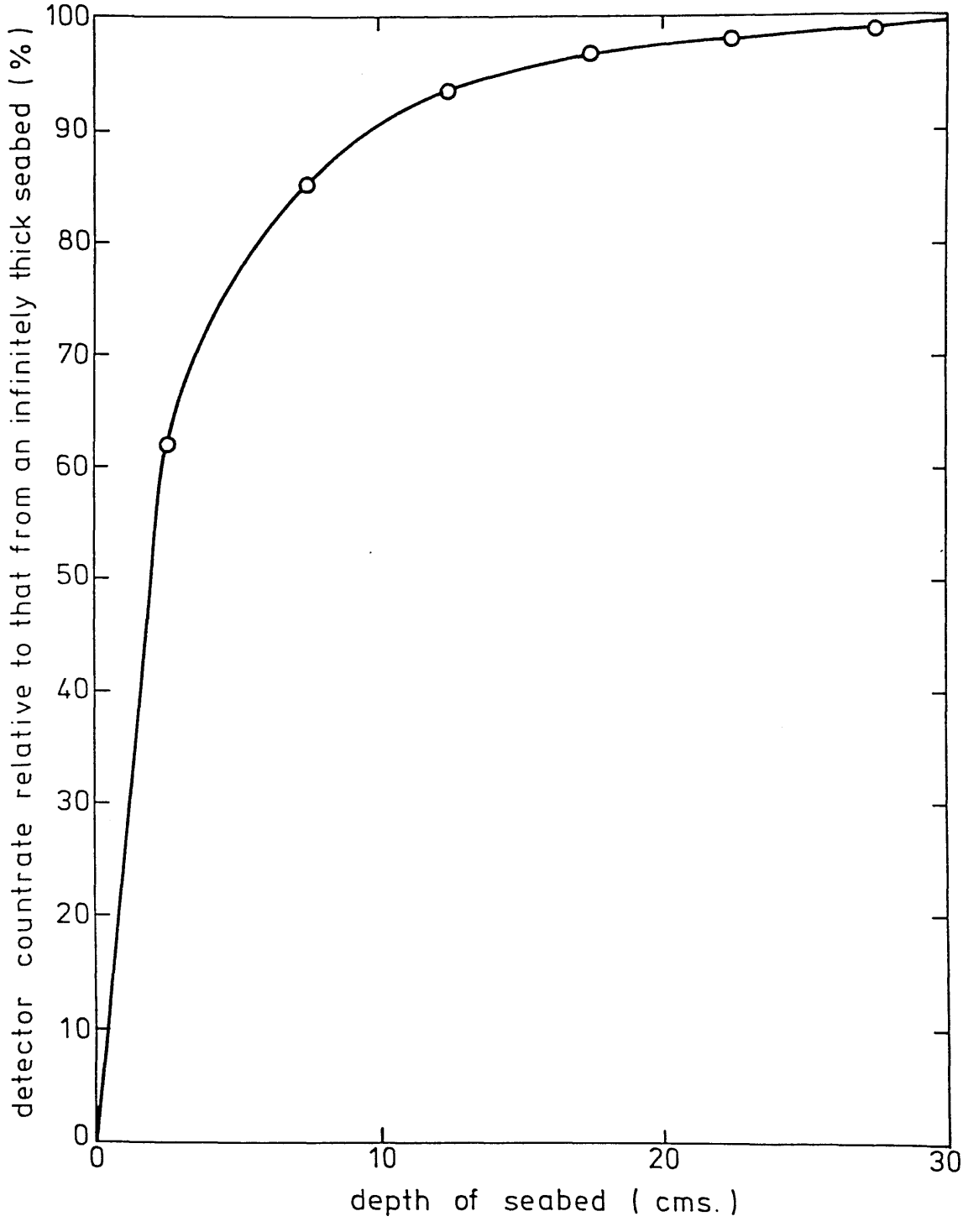

Figure 4.12 Calculation of the detector response to neutron capture gamma-rays as a function of seabed depth.

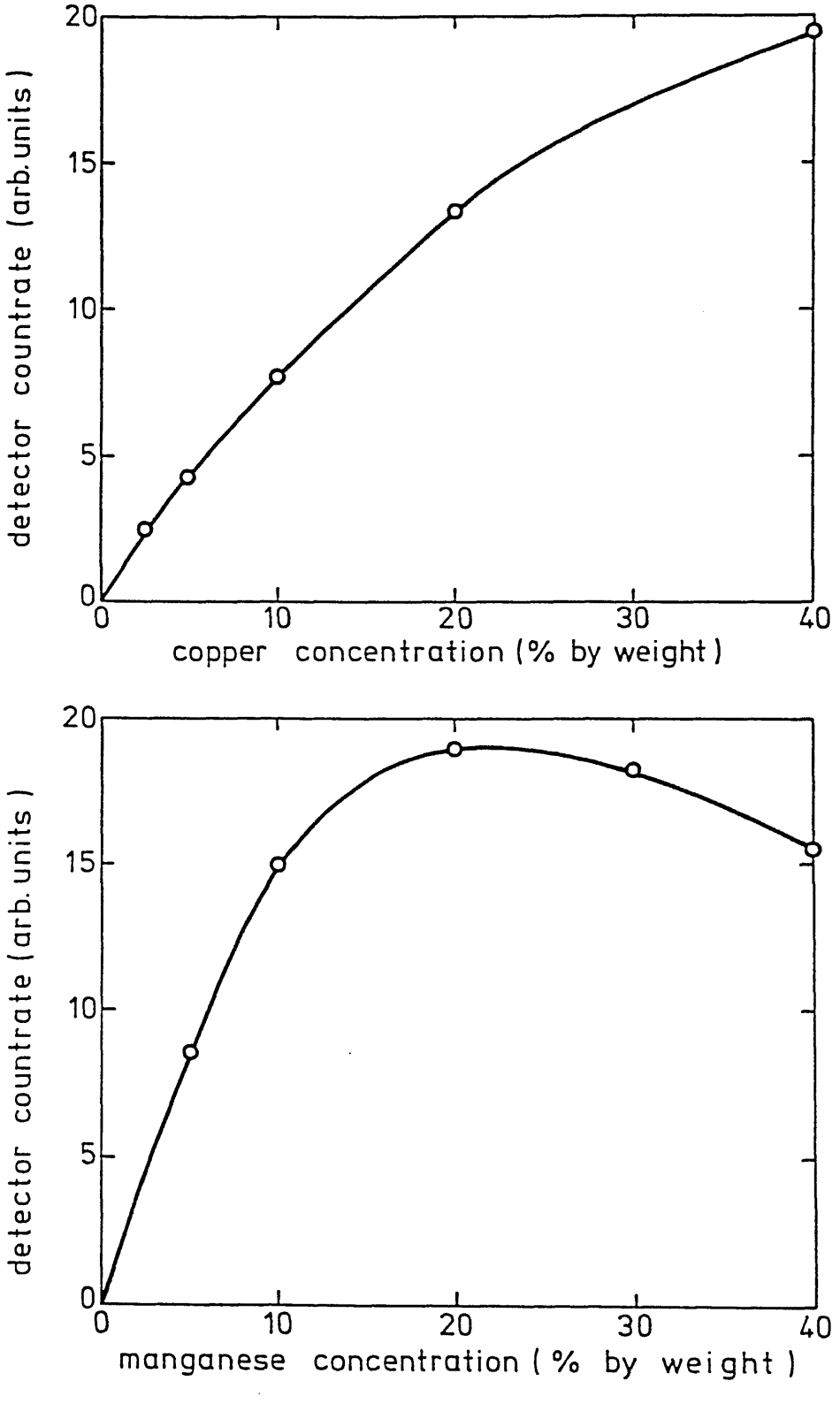

Figure 4.13 Calculations of detector countrate as a function of elemental concentration for seabeds seeded with copper or manganese nodule material.

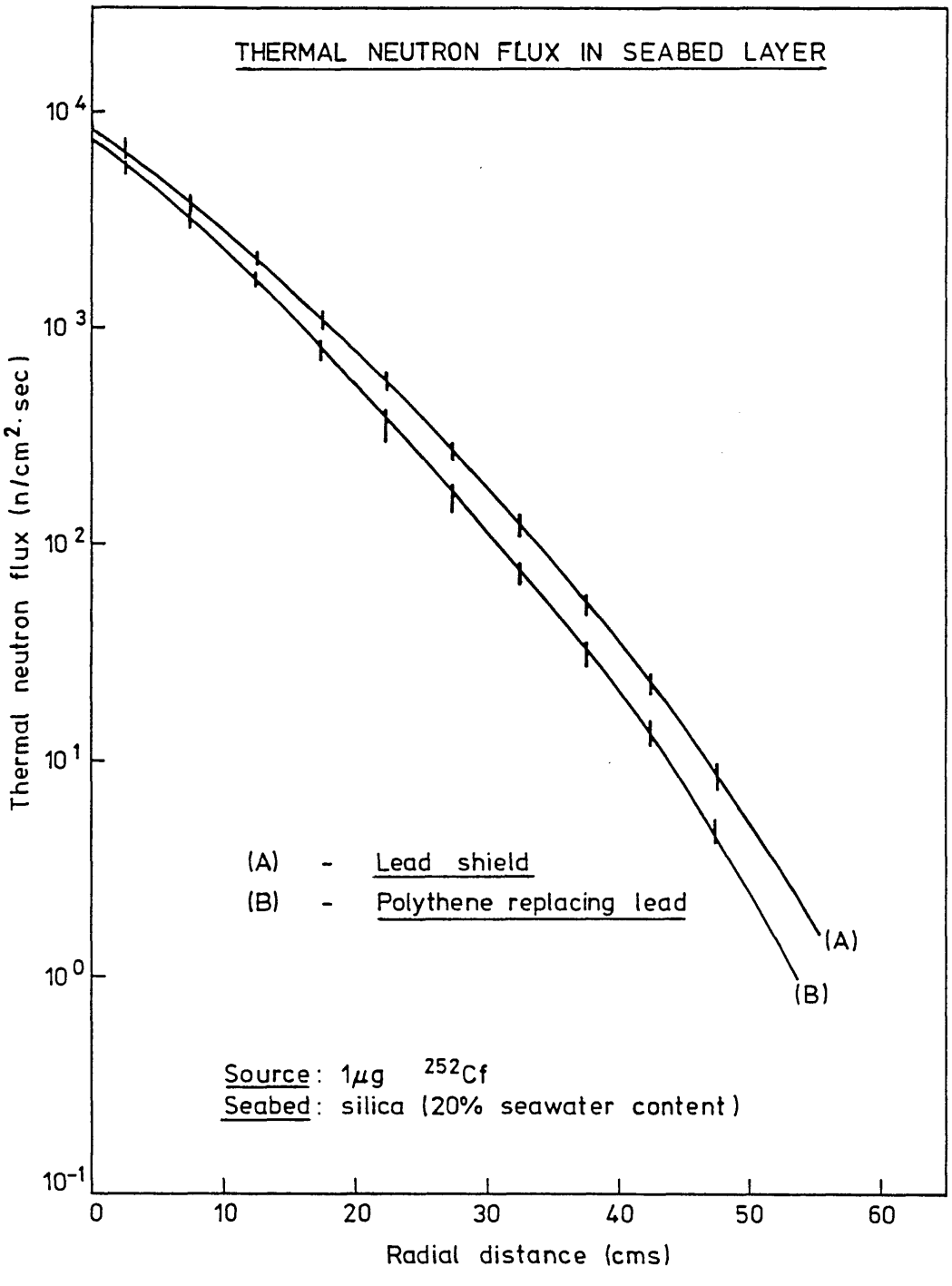

Figure 4.14 Calculated thermal neutron flux in the seabed as a function of radial distance R for a 1 μg ^{252}Cf neutron source in the probe with (a) 10 cm lead shield (b) lead replaced by polythene.

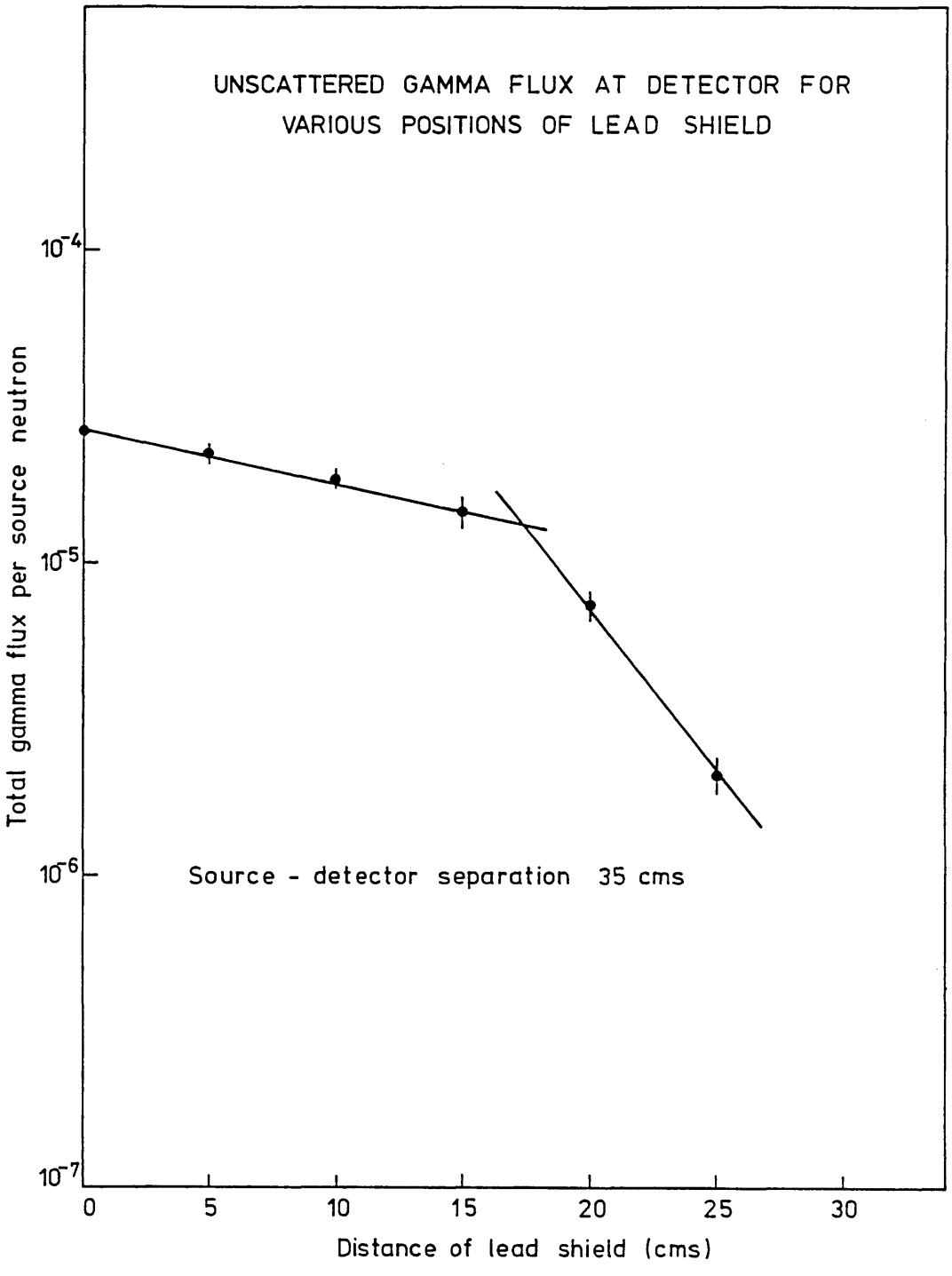

Figure 4.15 Calculated total unscattered γ-ray flux at detector for various positions of lead shield from neutron source for a fixed source-detector separation of 35 cm. Thickness of lead shield is 10 cm.

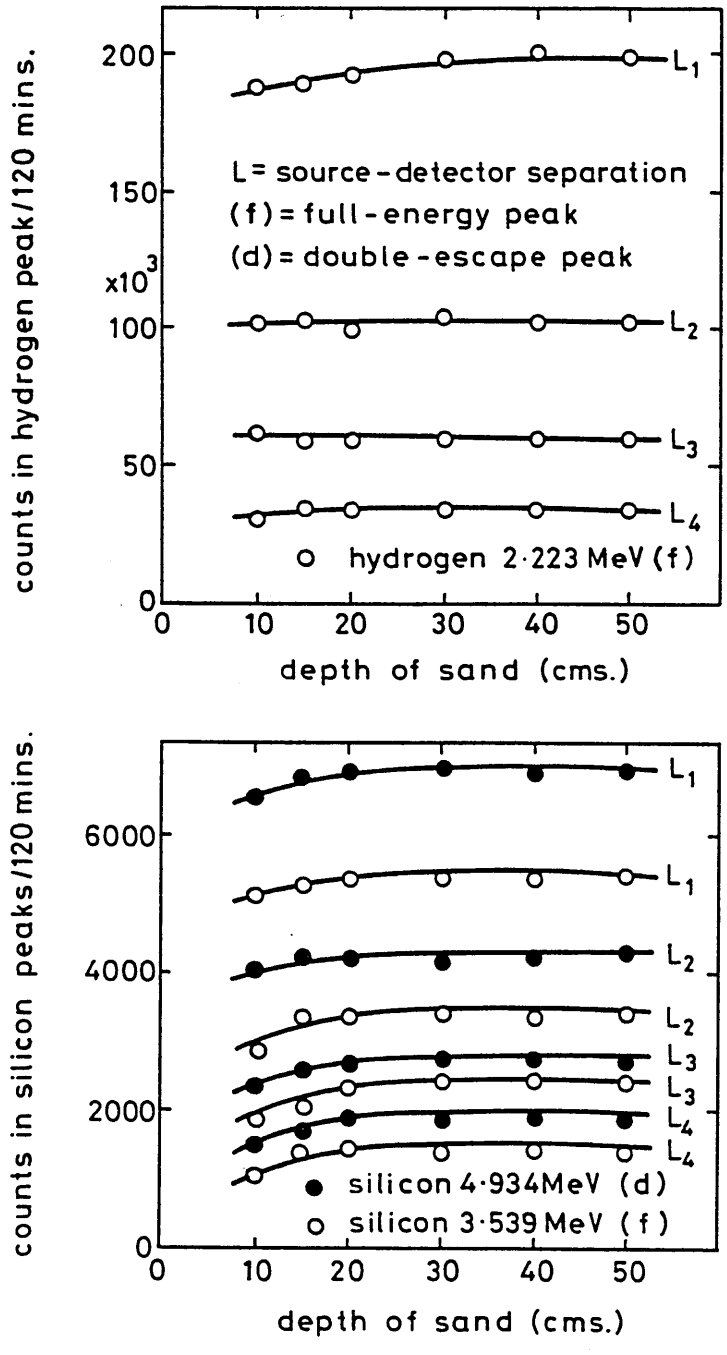

Figure 5.1 Variation of detector countrate in the hydrogen and silicon γ-ray energy peaks with depth of seabed for different source-detector separations; L_1 = 16.3 cm, L_2 = 26.3 cm, L_3 = 36.3 cm and L_4 = 46.3 cm.

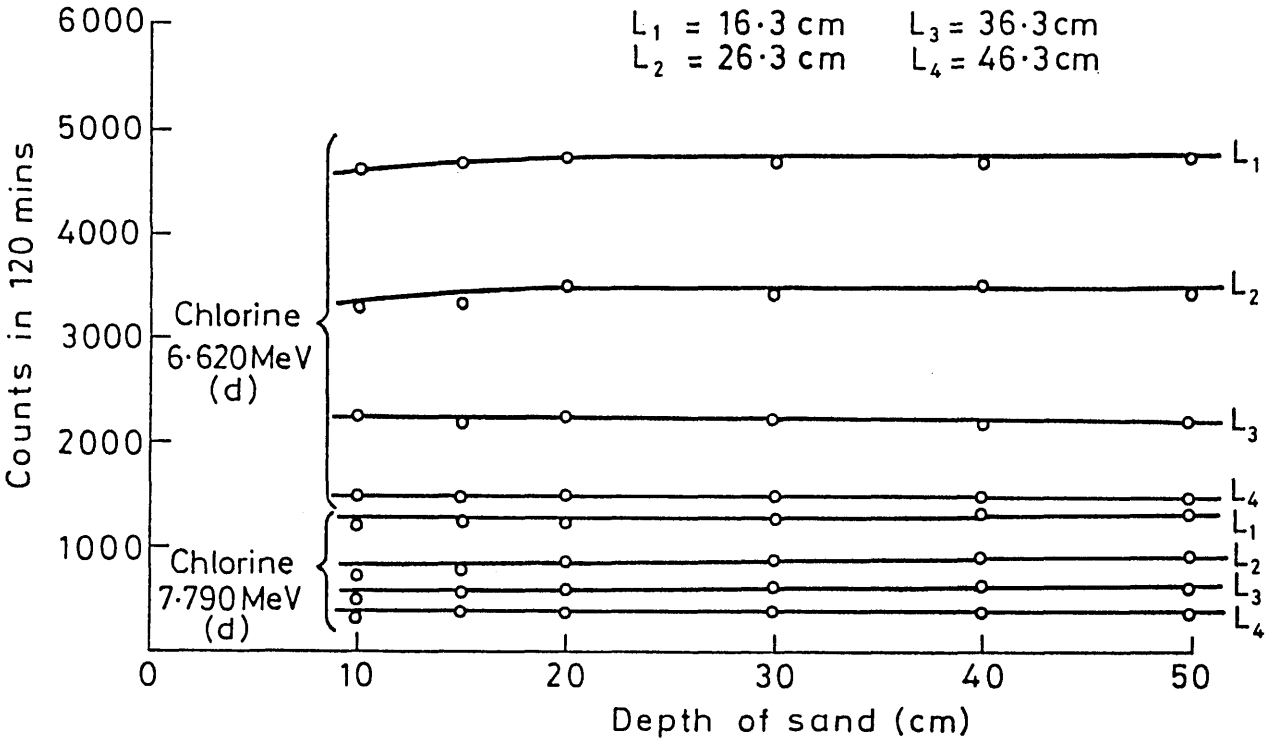

Figure 5.2 Variation of detector countrate in the chlorine 6.620 MeV and 7.790 MeV γ-ray energy peaks with depth of seabed for different source-detector separations L.

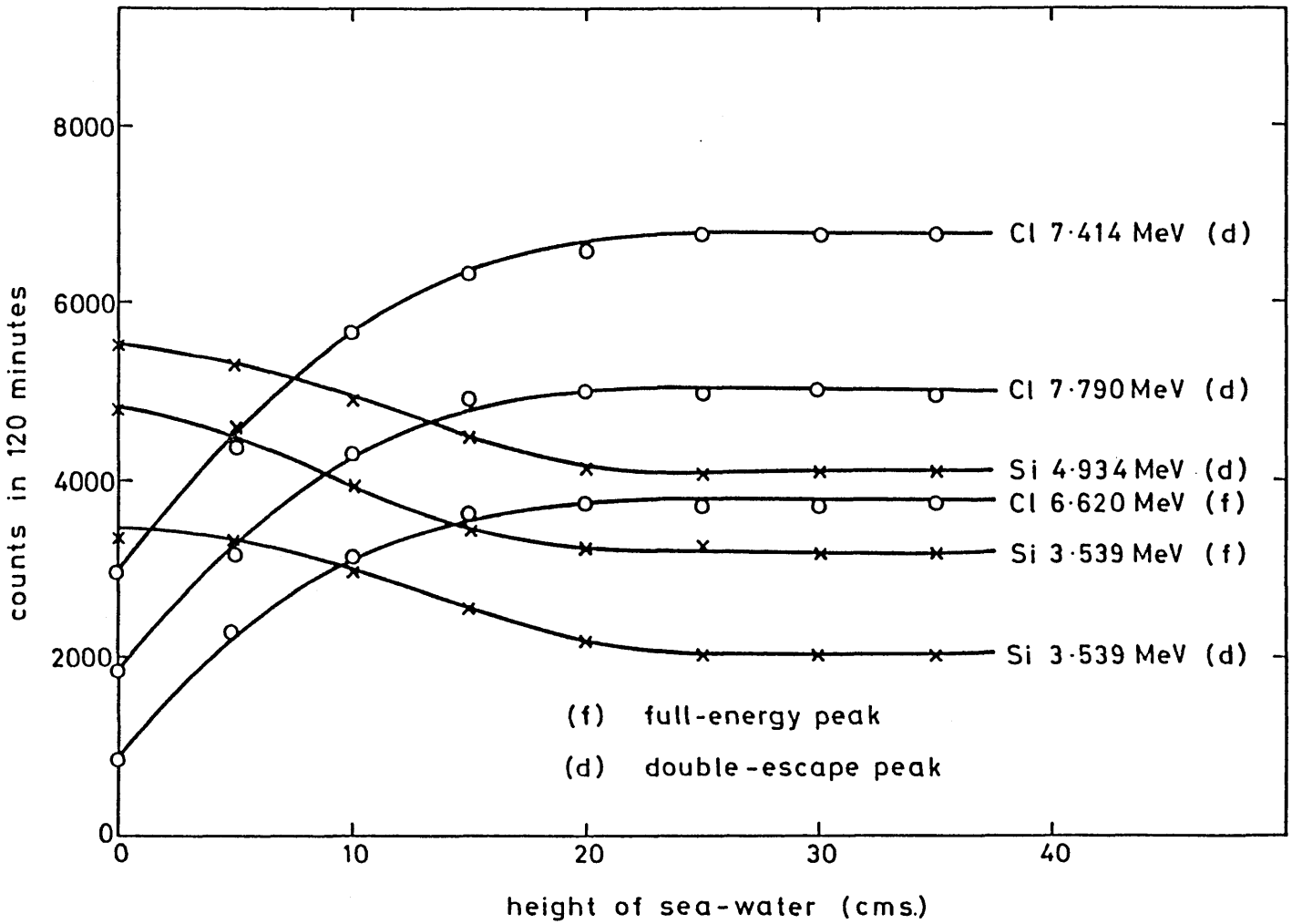

Figure 5.3 Variation of detector countrate in the principal chlorine and silicon γ-ray energy peaks with height of seawater in the simulated seabed. Source-detector separation 29.7 cm; depth of seabed 35 cm.

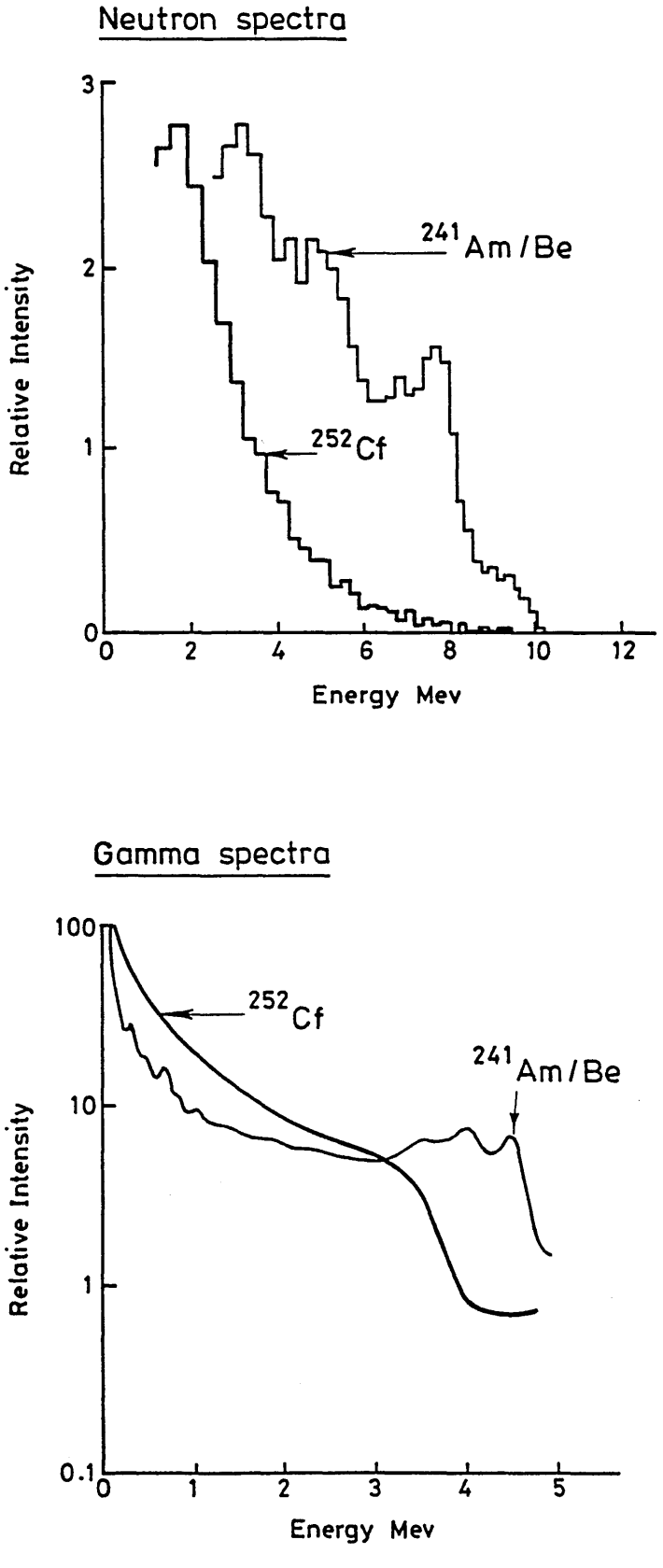

Figure 5.4 Neutron and gamma energy spectra of ^{252}Cf and $^{241}Am/Be$ neutron sources. (Data from STODDARD, 1965)

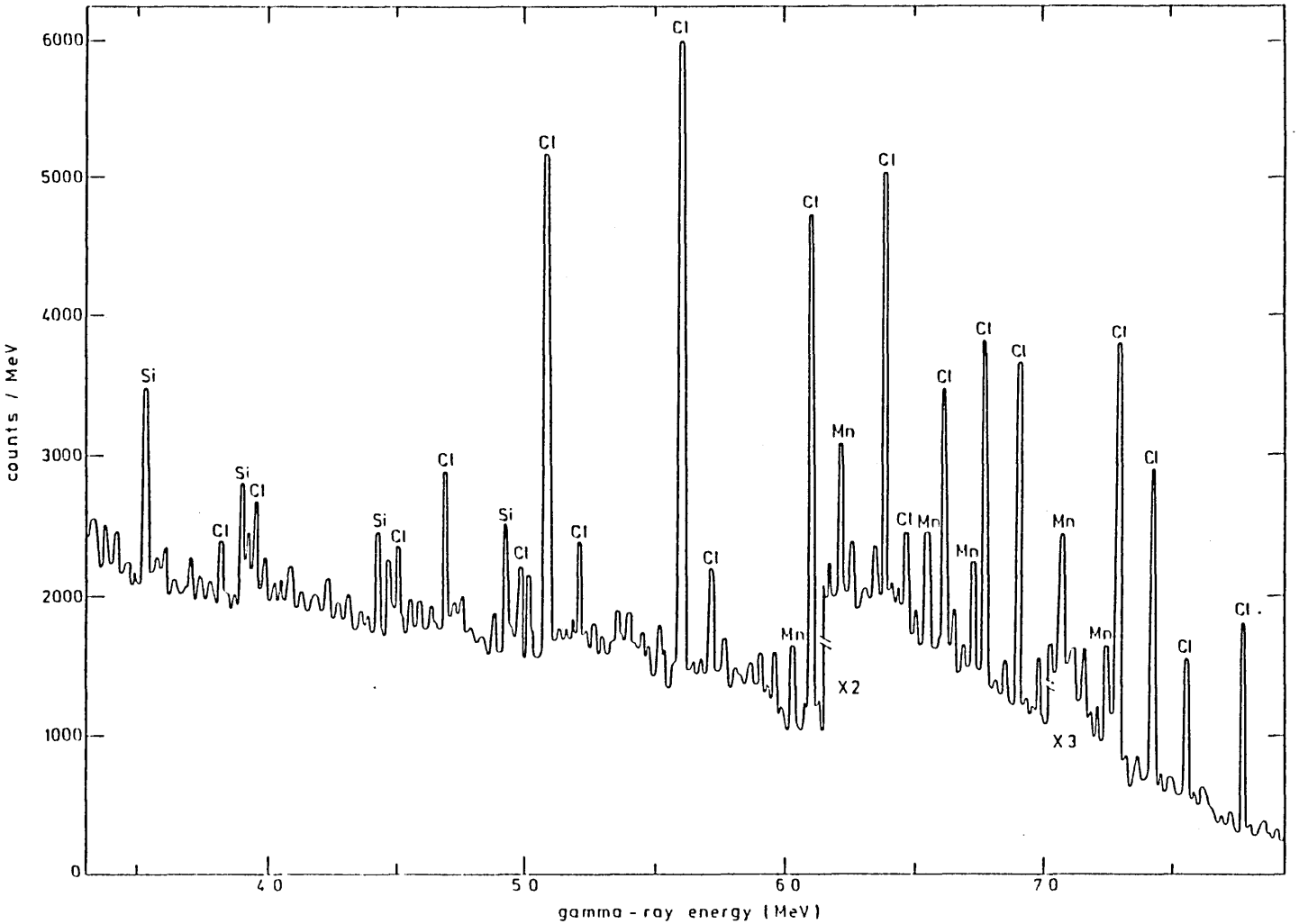

Figure 5.5 High energy γ-ray spectrum measured for a simulated seabed containing 4.3% manganese when irradiated by a ^{252}Cf neutron source. (Neutron emission rate of source: 4.26×10^6 n.sec^{-1})

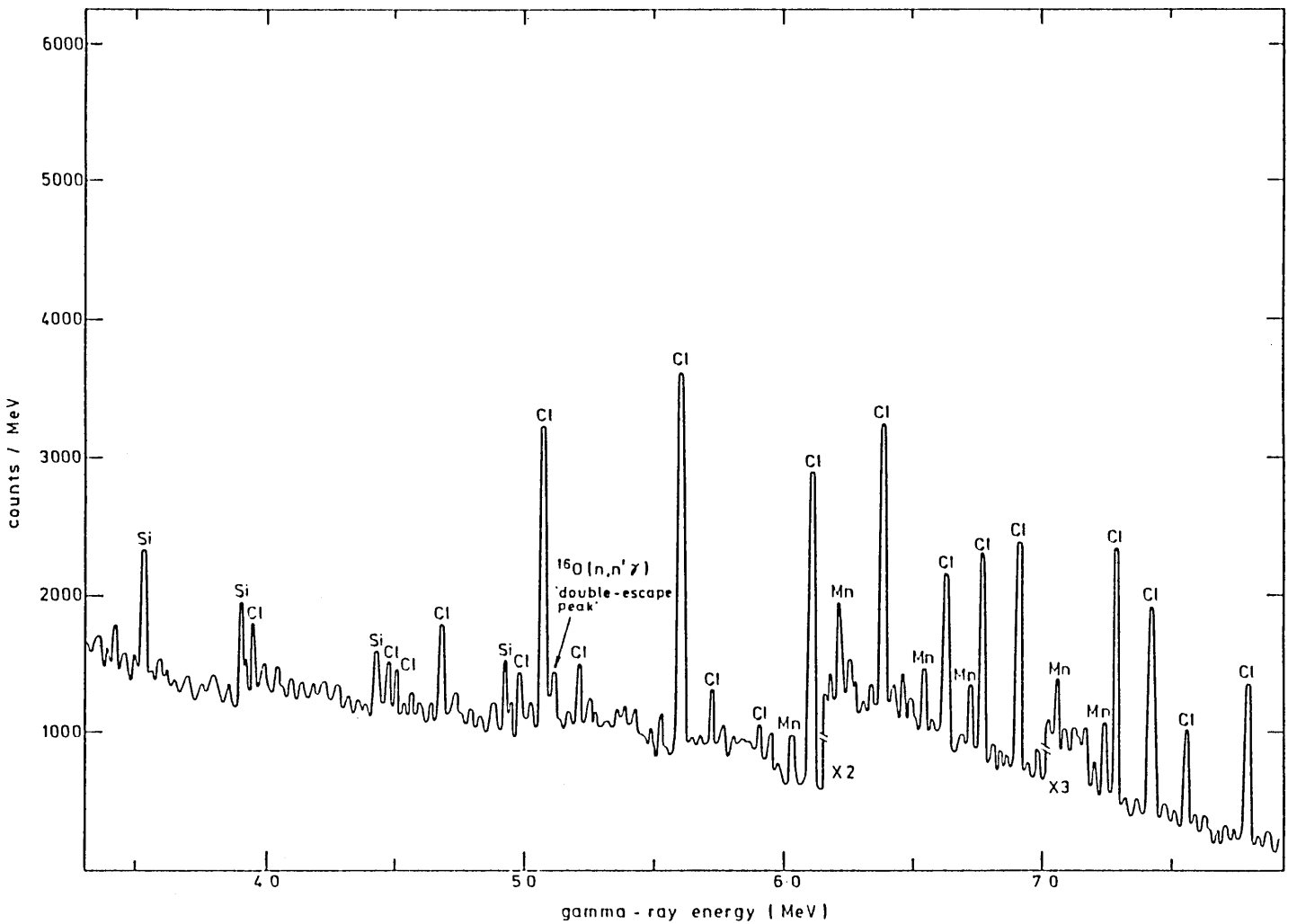

Figure 5.6 High energy γ-ray spectrum measured for a simulated seabed containing 4.3% manganese when irradiated by a $^{241}Am/Be$ neutron source. (Neutron emission rate of source: 2.5×10^6 n.sec^{-1})

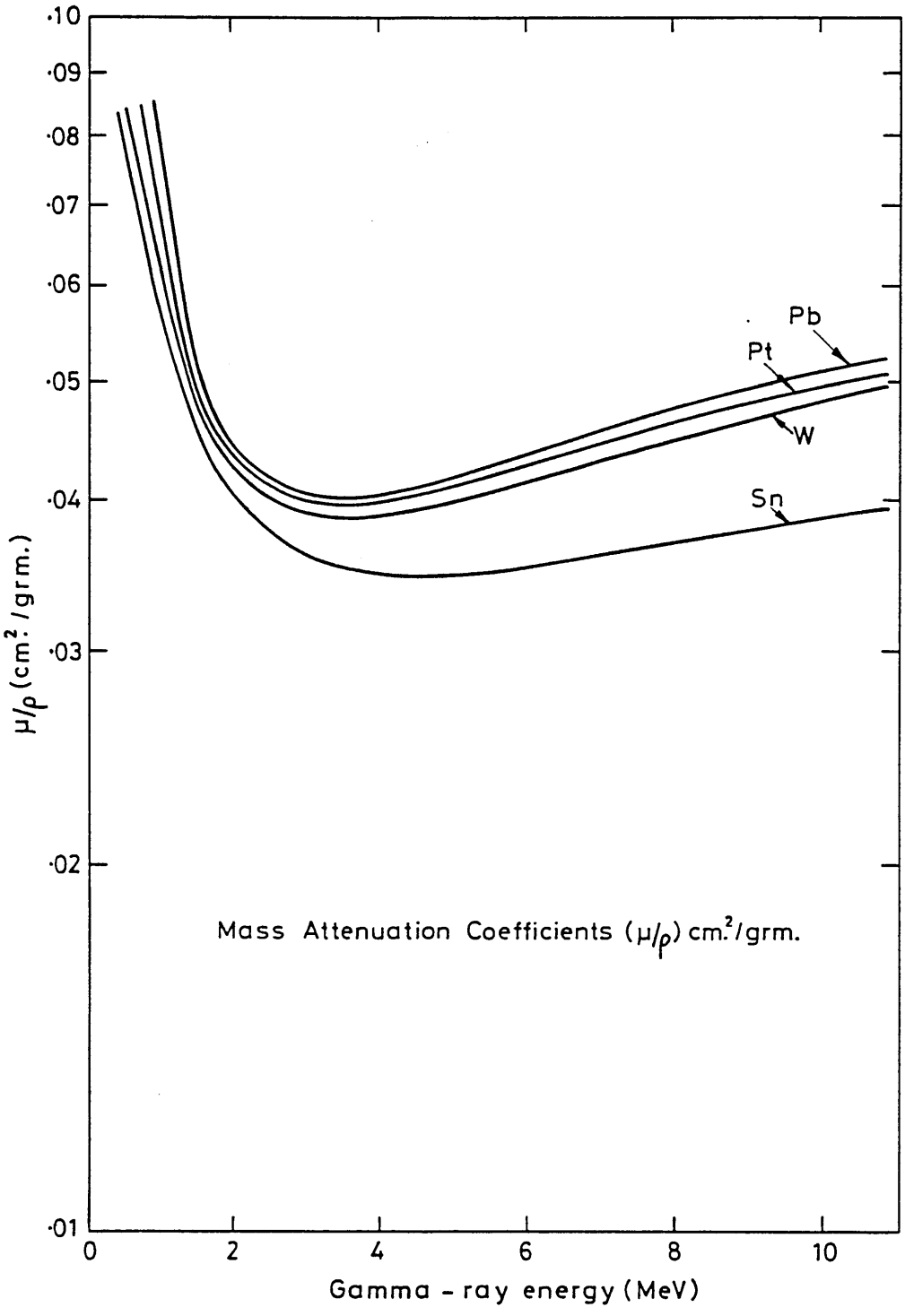

Figure 5.7 Mass gamma attenuation coefficients of some common shielding materials as a function of γ-ray energy

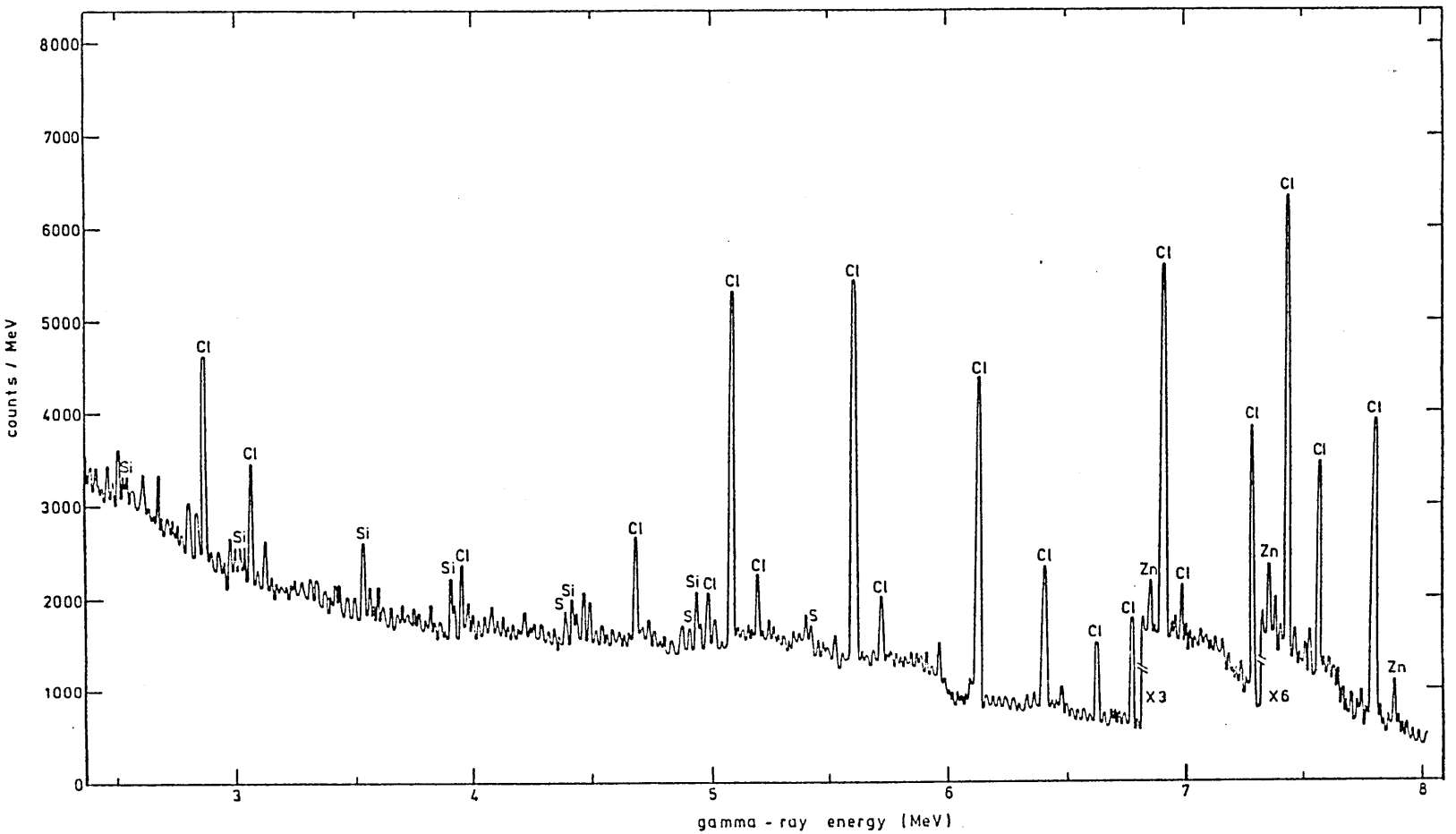

Figure 5.8 Measured high energy γ-ray spectrum for a silica seabed containing zinc (24%) and sulphur (6%) when irradiated by a 2.5 μg ^{252}Cf neutron source with a 10 cm lead shield adjacent to source.

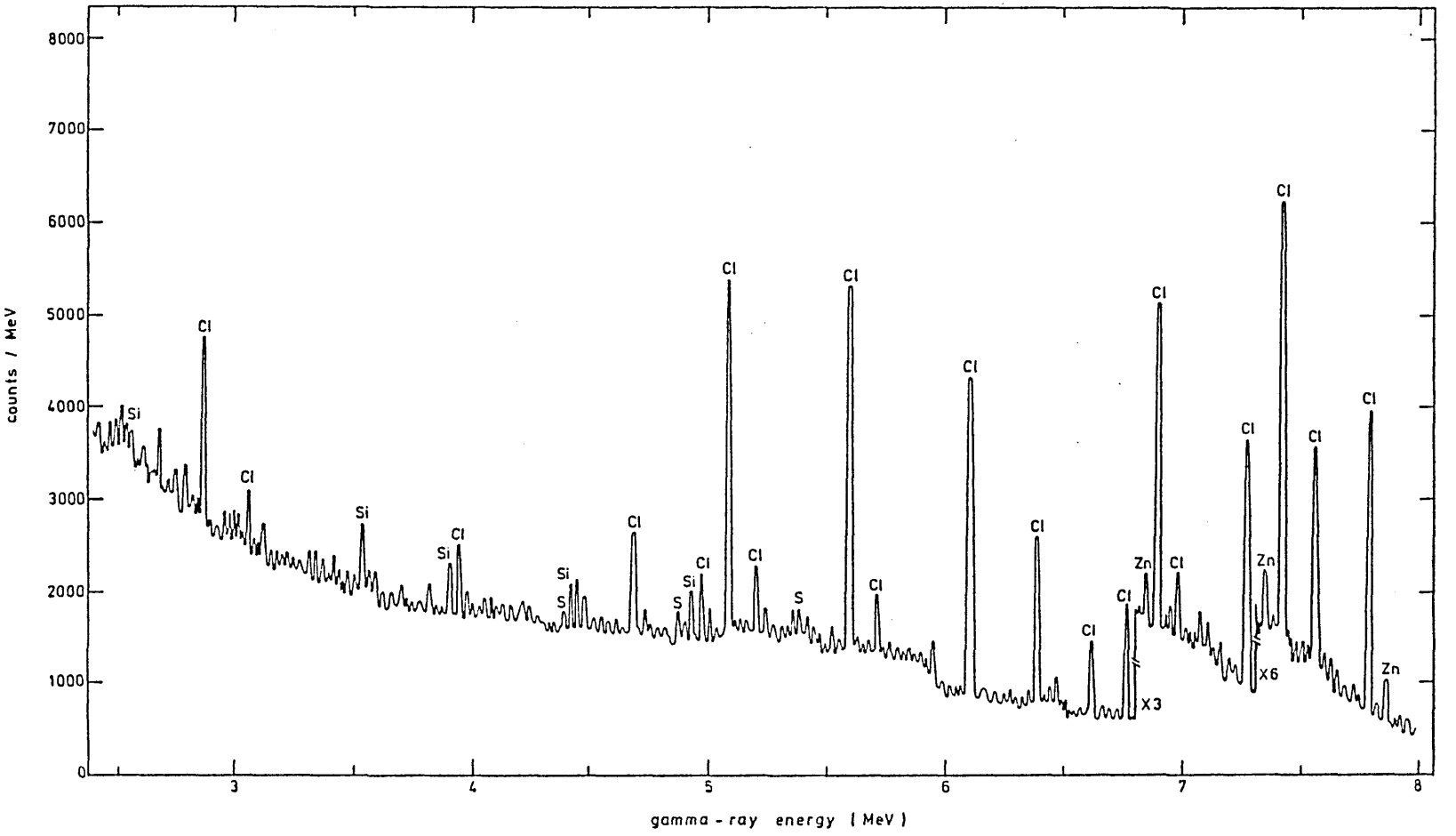

Figure 5.9 Measured high energy γ-ray spectrum for a silica seabed containing zinc (24%) and sulphur (6%) when irradiated by a 2.5 µg ^{252}Cf neutron source with a 10 cm tin shield adjacent to source

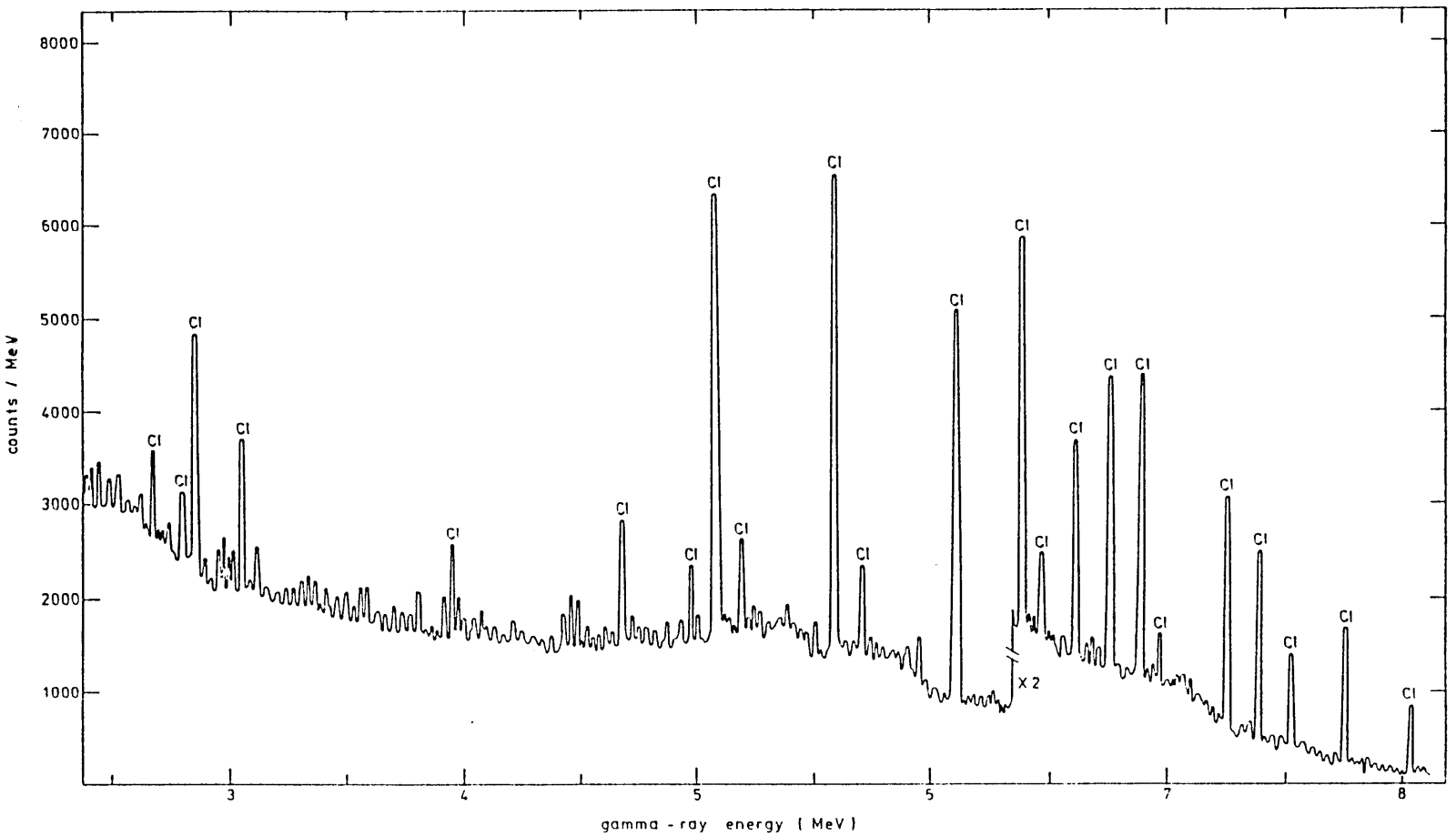

Figure 5.10 High energy γ-ray spectrum measured for seawater when irradiated by a ^{252}Cf neutron source

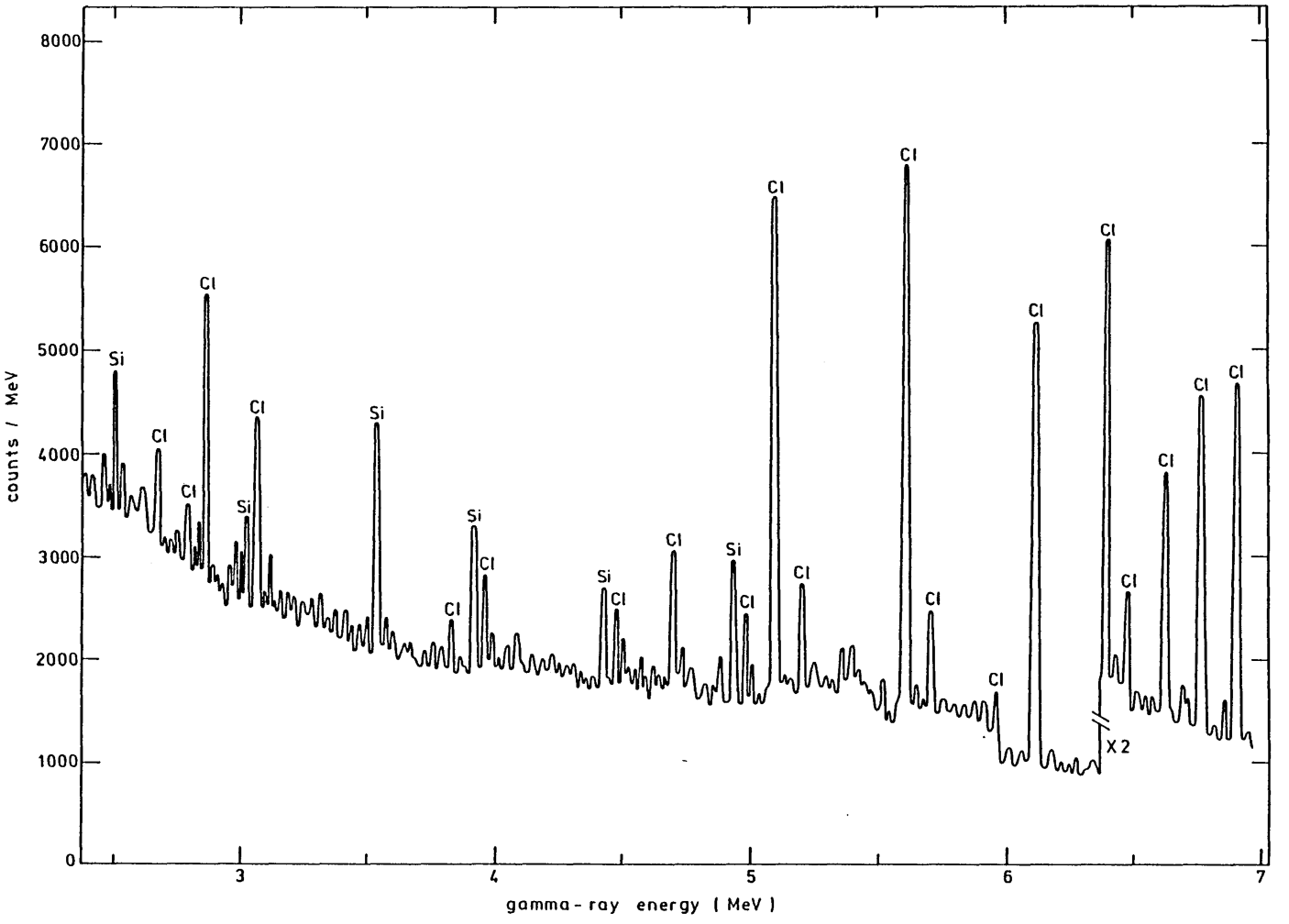

Figure 5.11 High energy γ-ray spectrum measured for a silica seabed when irradiated by a ^{252}Cf neutron source

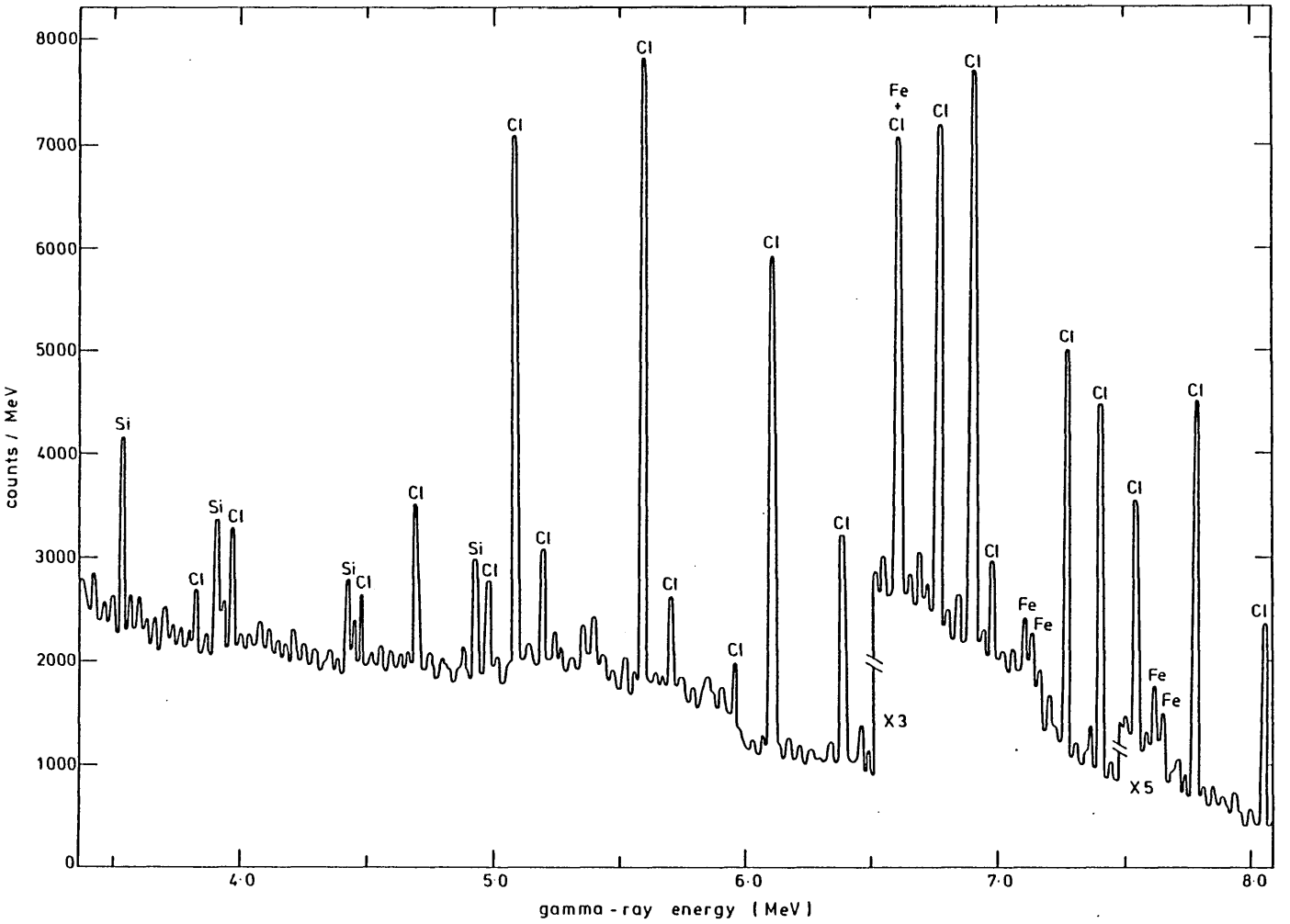

Figure 5.12 Measured γ-ray spectrum for a simulated seabed containing iron (3%) in a silica matrix when irradiated by a ^{252}Cf neutron source

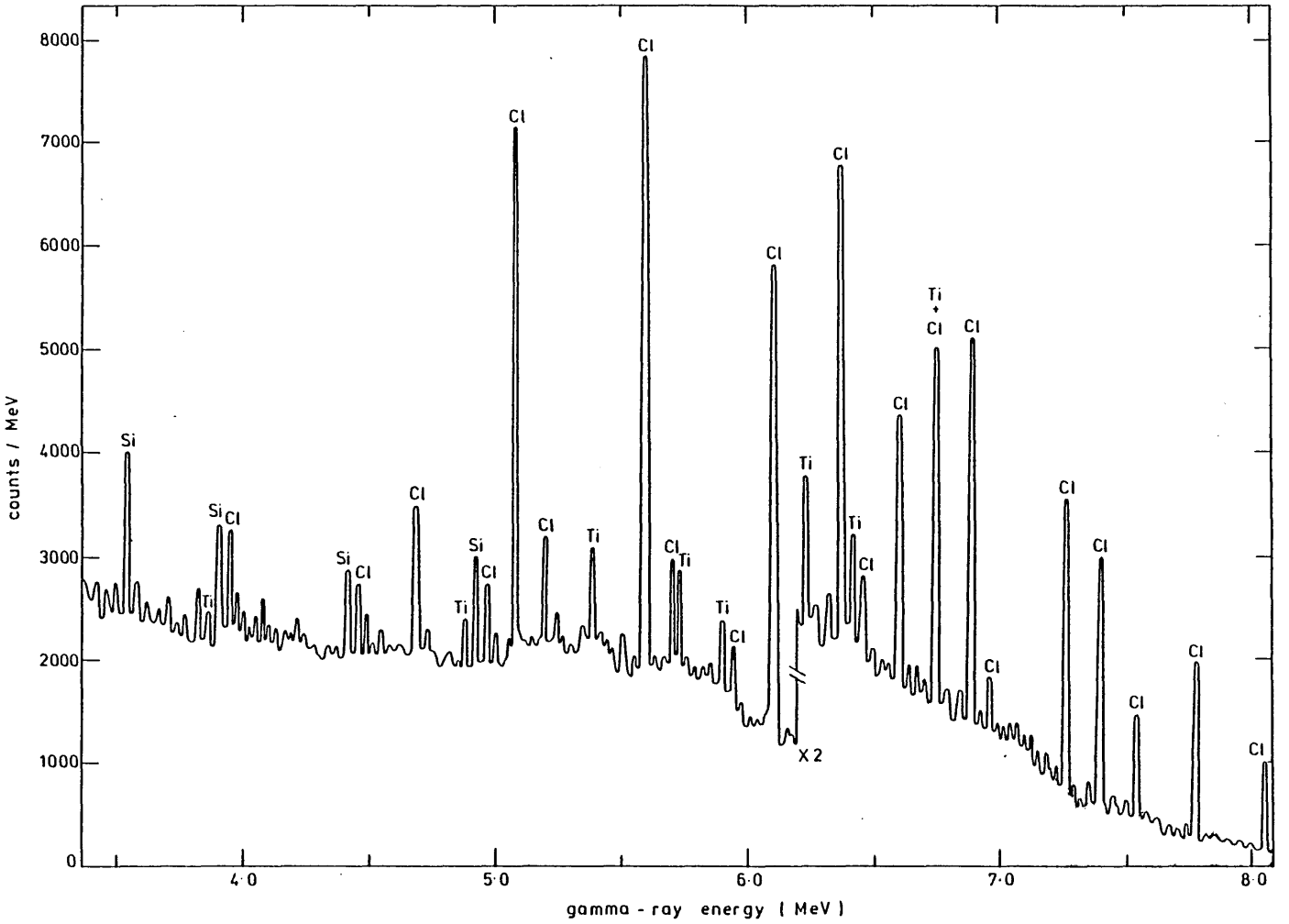

Figure 5.13 Measured γ-ray spectrum for a simulated seabed containing titanium (3%) in a silica matrix when irradiated by a ^{252}Cf neutron source

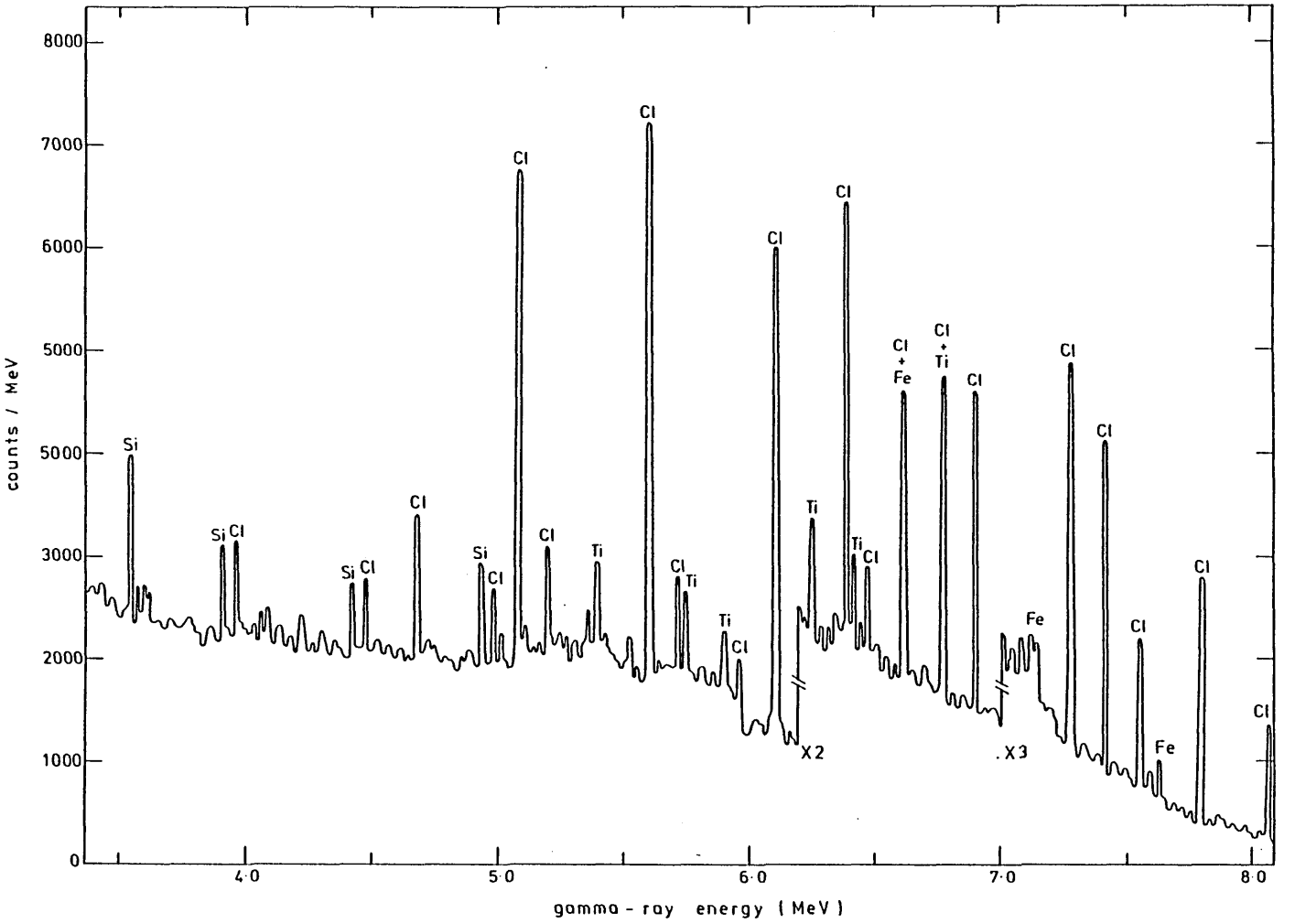

Figure 5.14 Measured γ-ray spectrum for a simulated seabed containing iron (2.9%) and titanium (2.5%) in a silica matrix when irradiated by a ^{252}Cf neutron source

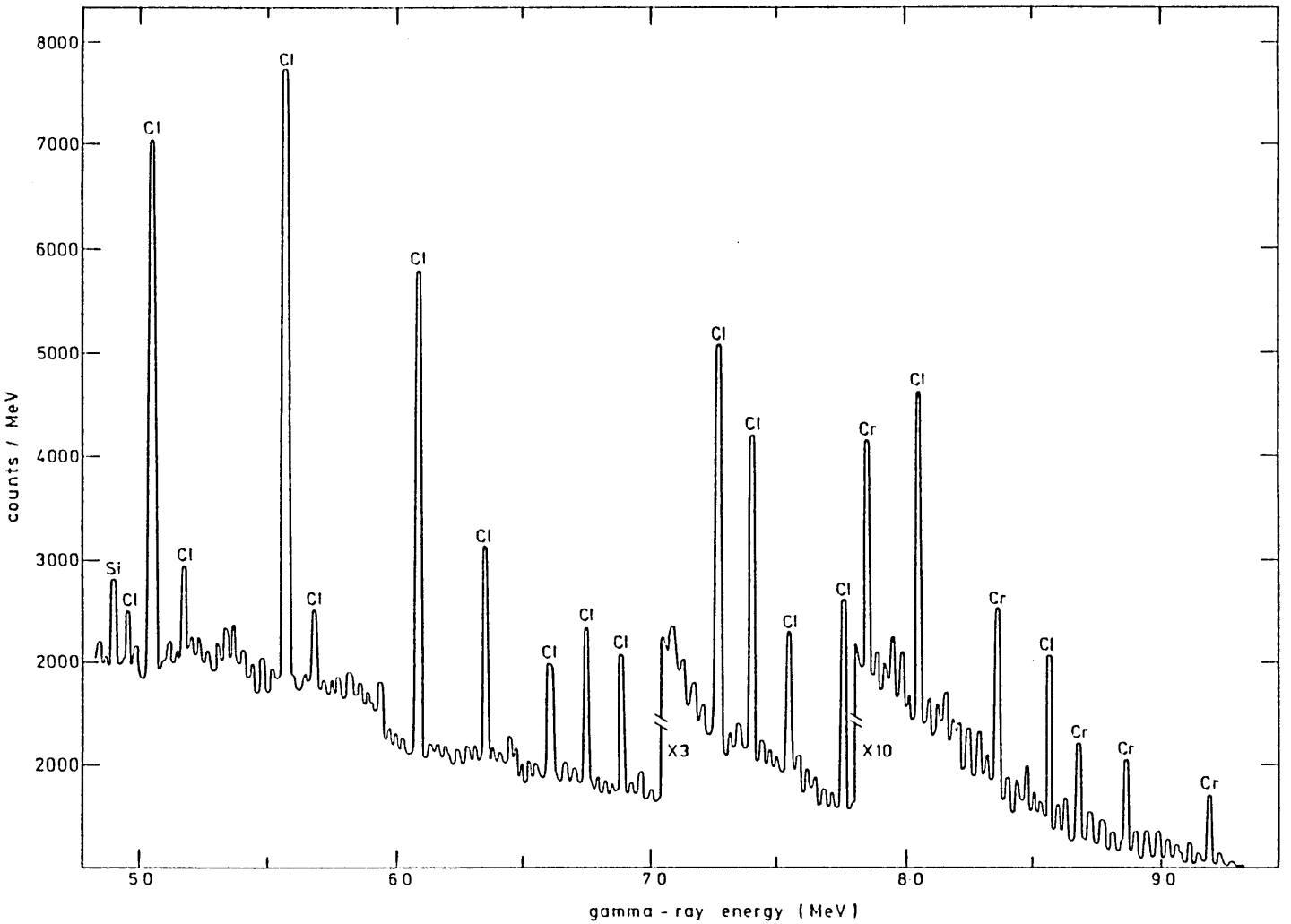

Figure 5.15 Measured γ-ray spectrum for a simulated seabed containing chromium (3.8%) in a silica matrix when irradiated by a ^{252}Cf neutron source.

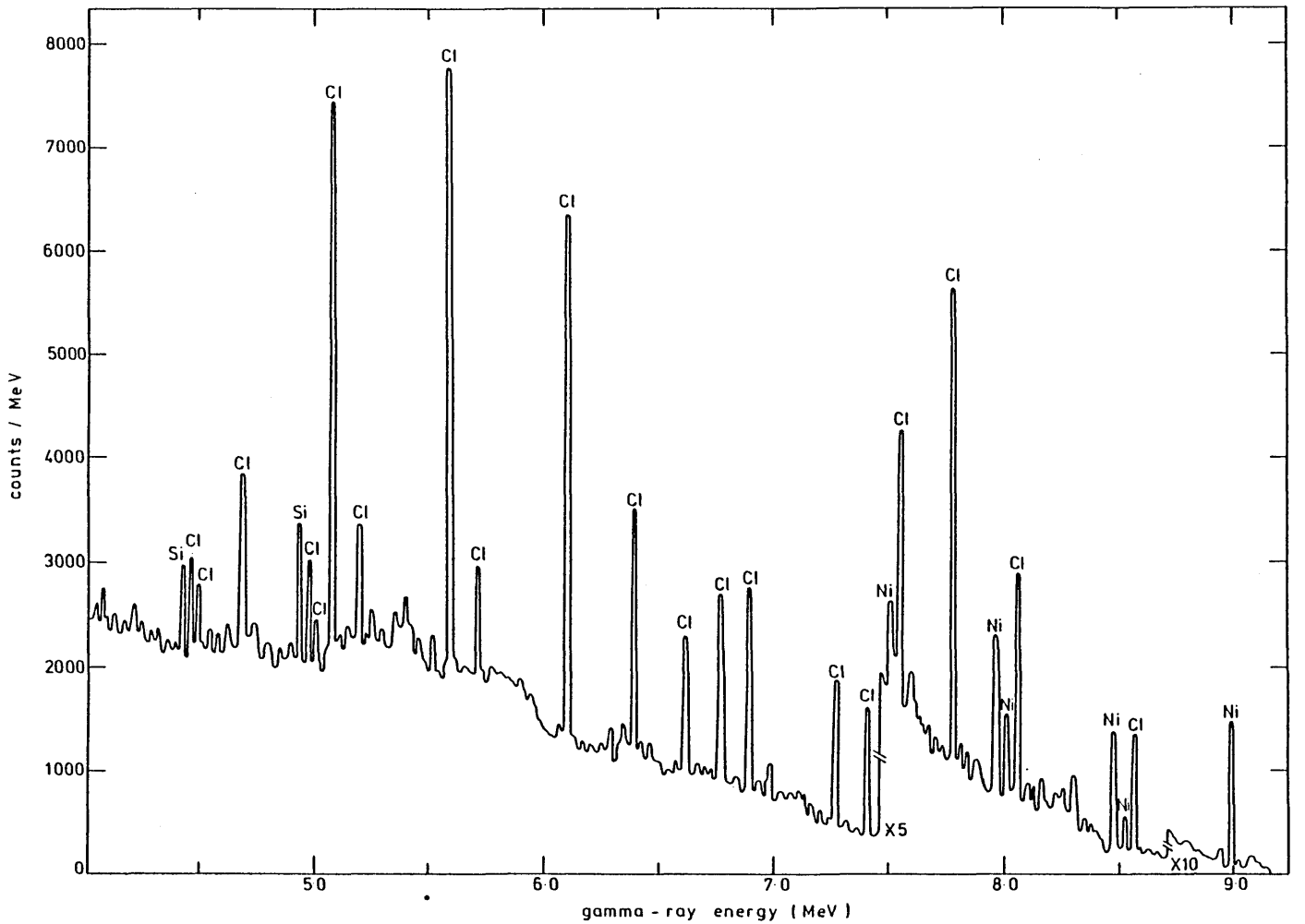

Figure 5.16 Measured γ-ray spectrum for a simulated seabed containing nickel (3%) in a silica matrix when irradiated by a ^{252}Cf neutron source

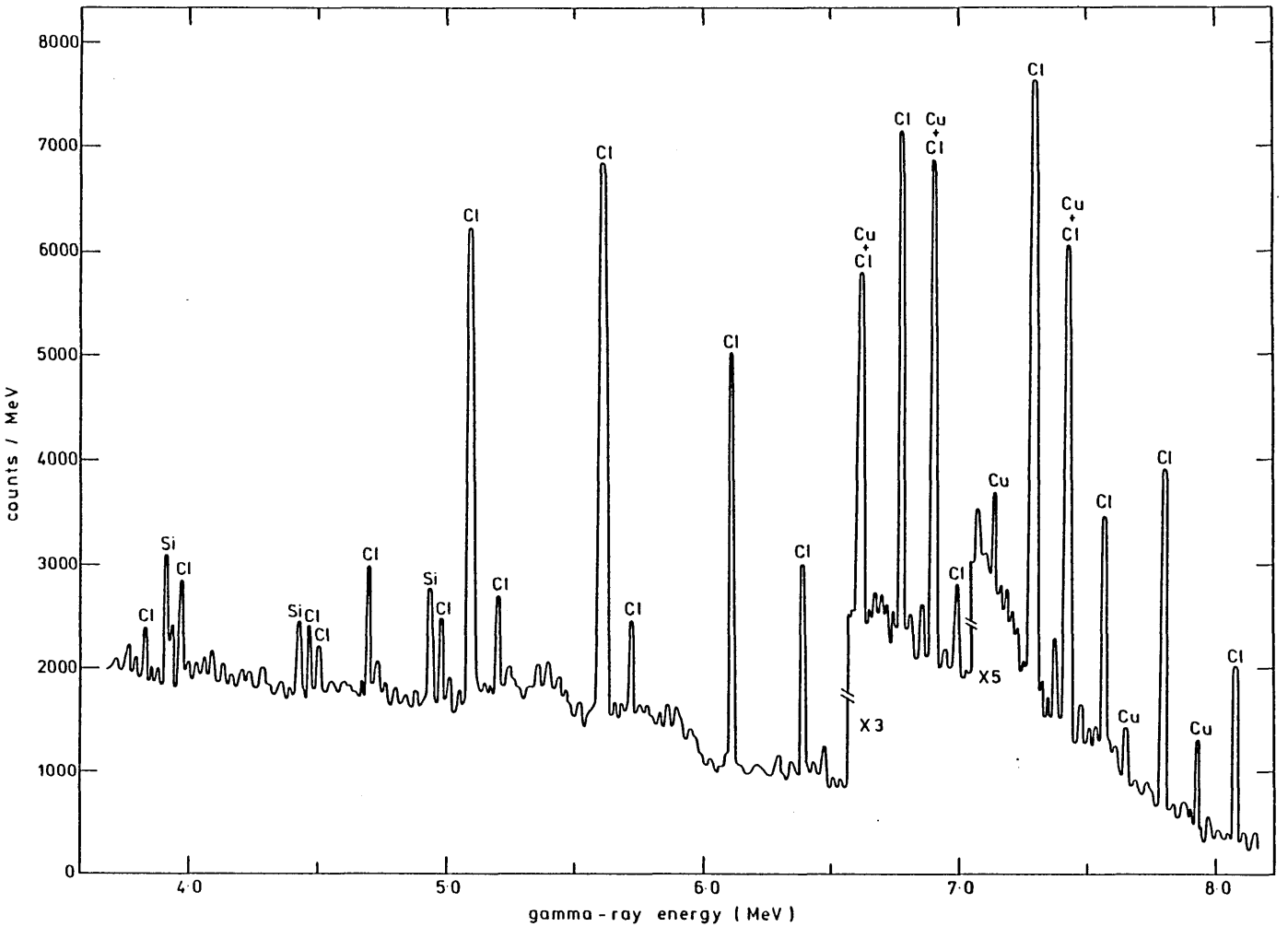

Figure 5.17 Measured γ-ray spectrum for a simulated seabed containing copper (5%) in a silica matrix when irradiated by a ^{252}Cf neutron source

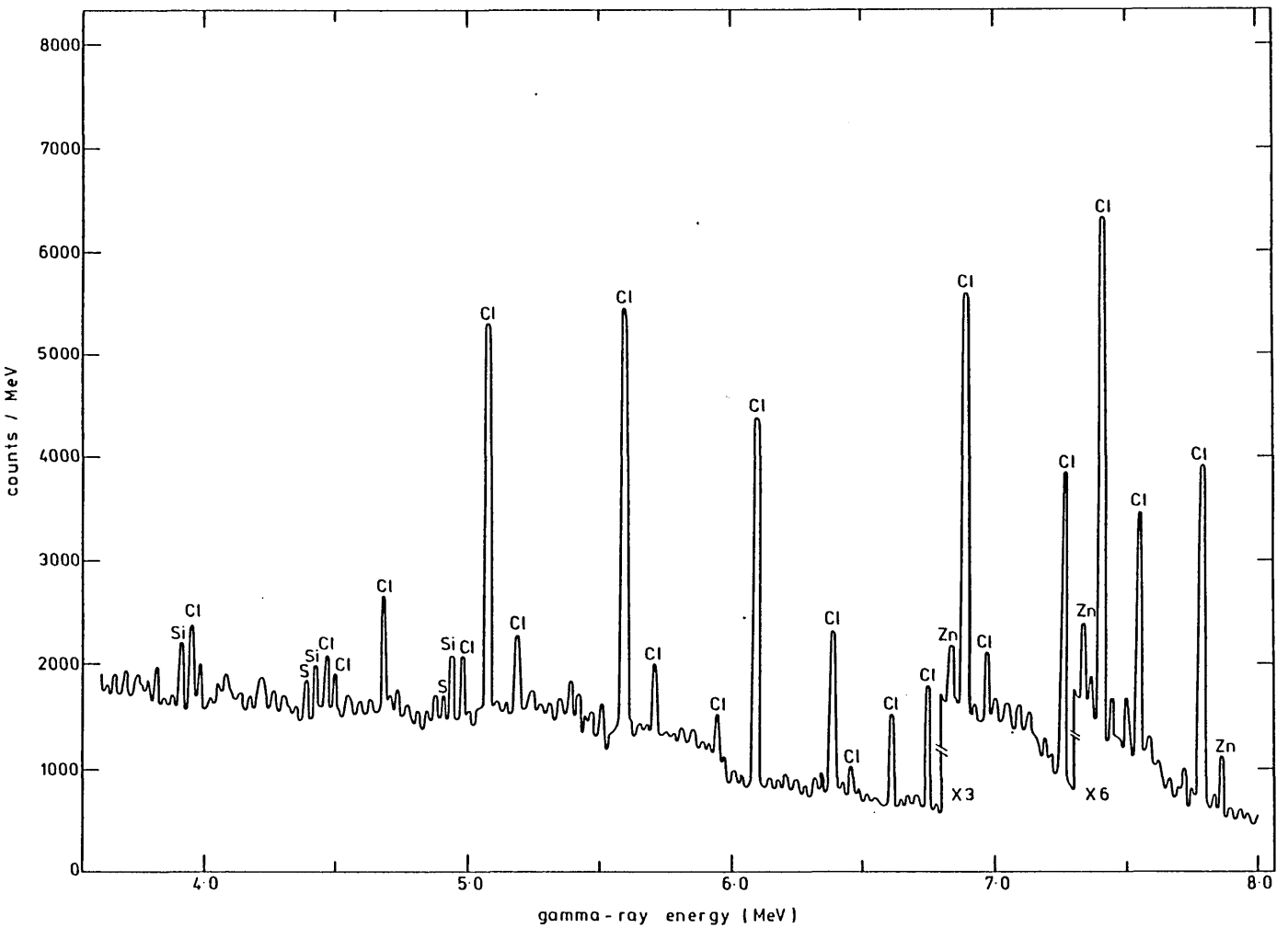

Figure 5.18 Measured γ-ray spectrum for a simulated seabed containing zinc (24%) and sulphur (6%) in a silica matrix when irradiated by a ^{252}Cf neutron source

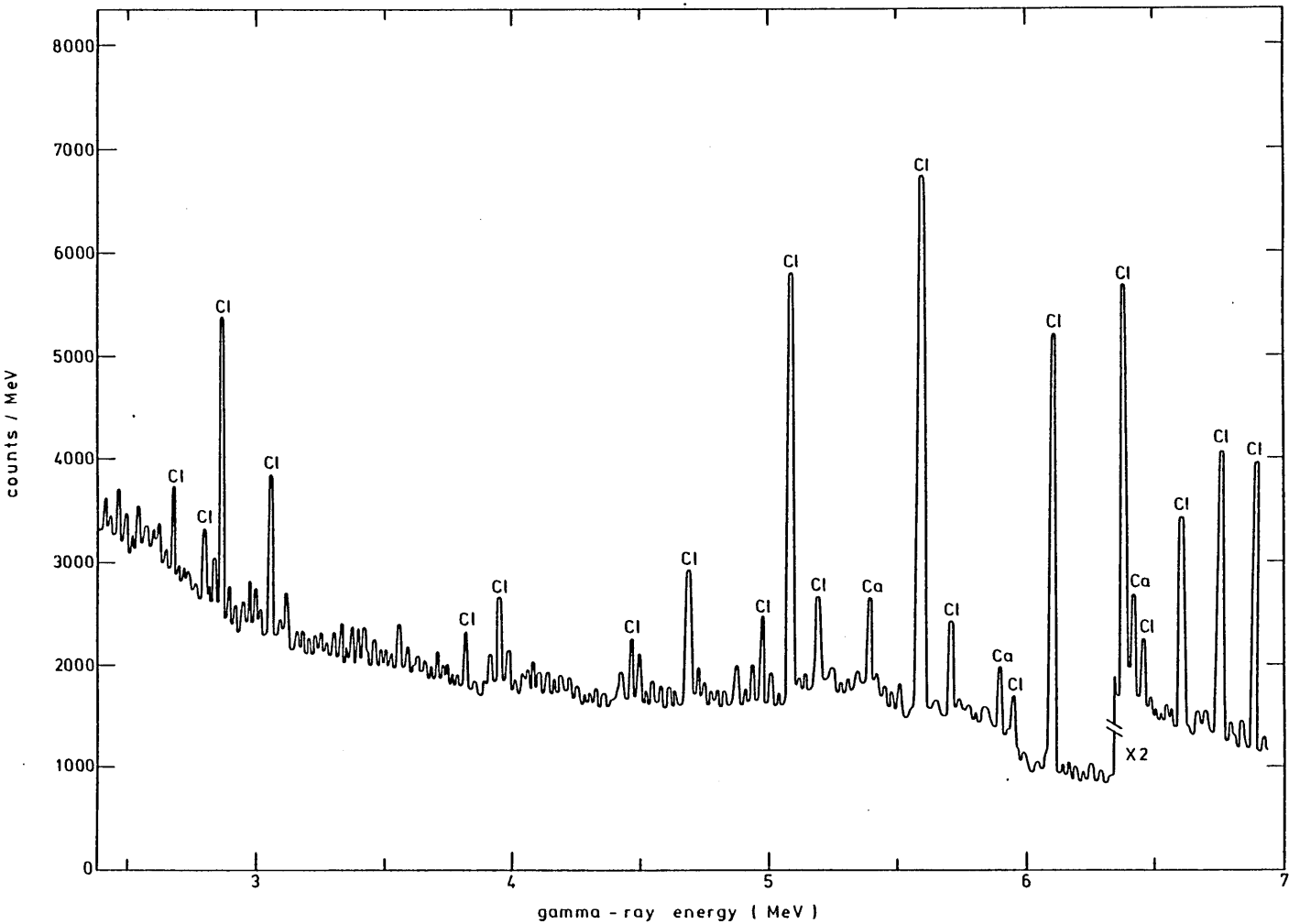

Figure 5.19 Measured γ-ray spectrum for a simulated seabed containing pure calcium carbonate (40% elemental calcium) when irradiated by a ^{252}Cf neutron source

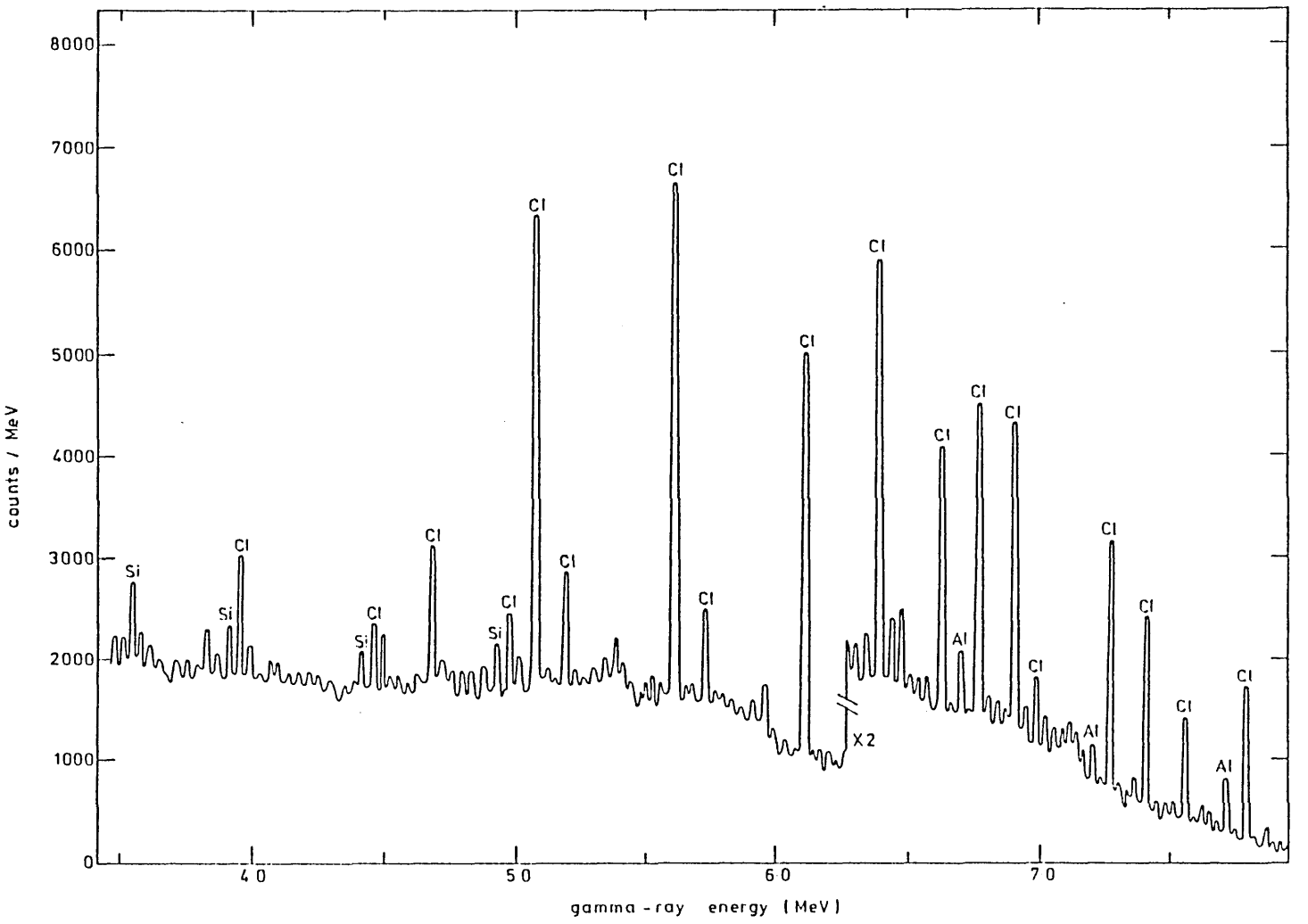

Figure 5.20 Measured γ-ray spectrum for a simulated seabed containing clay (21% aluminium and 22% silicon) when irradiated by a ^{252}Cf neutron source

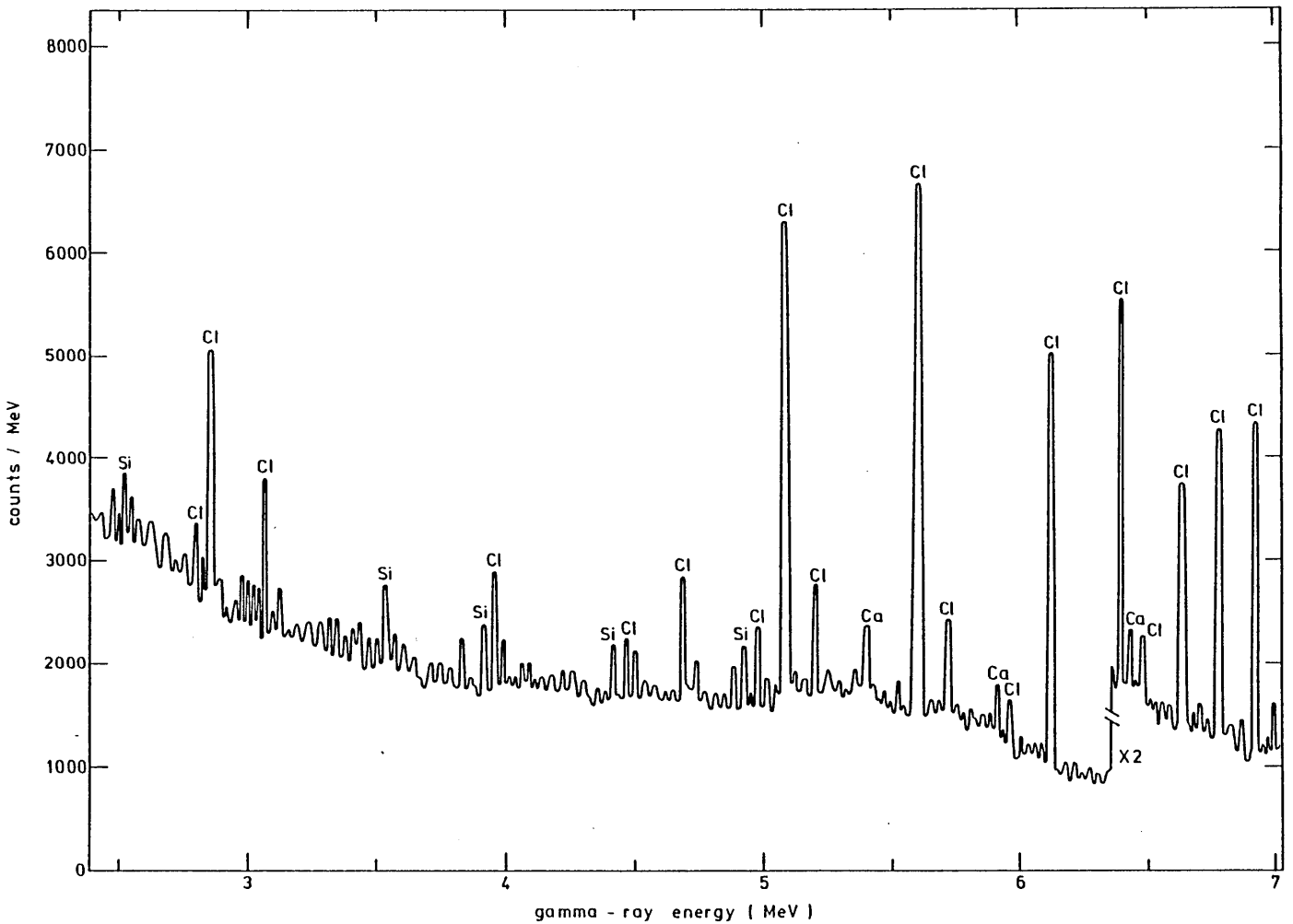

Figure 5.21 Measured γ-ray spectrum for a simulated seabed containing calcium (20%) and silicon (23%) when irradiated by a ^{252}Cf neutron source.

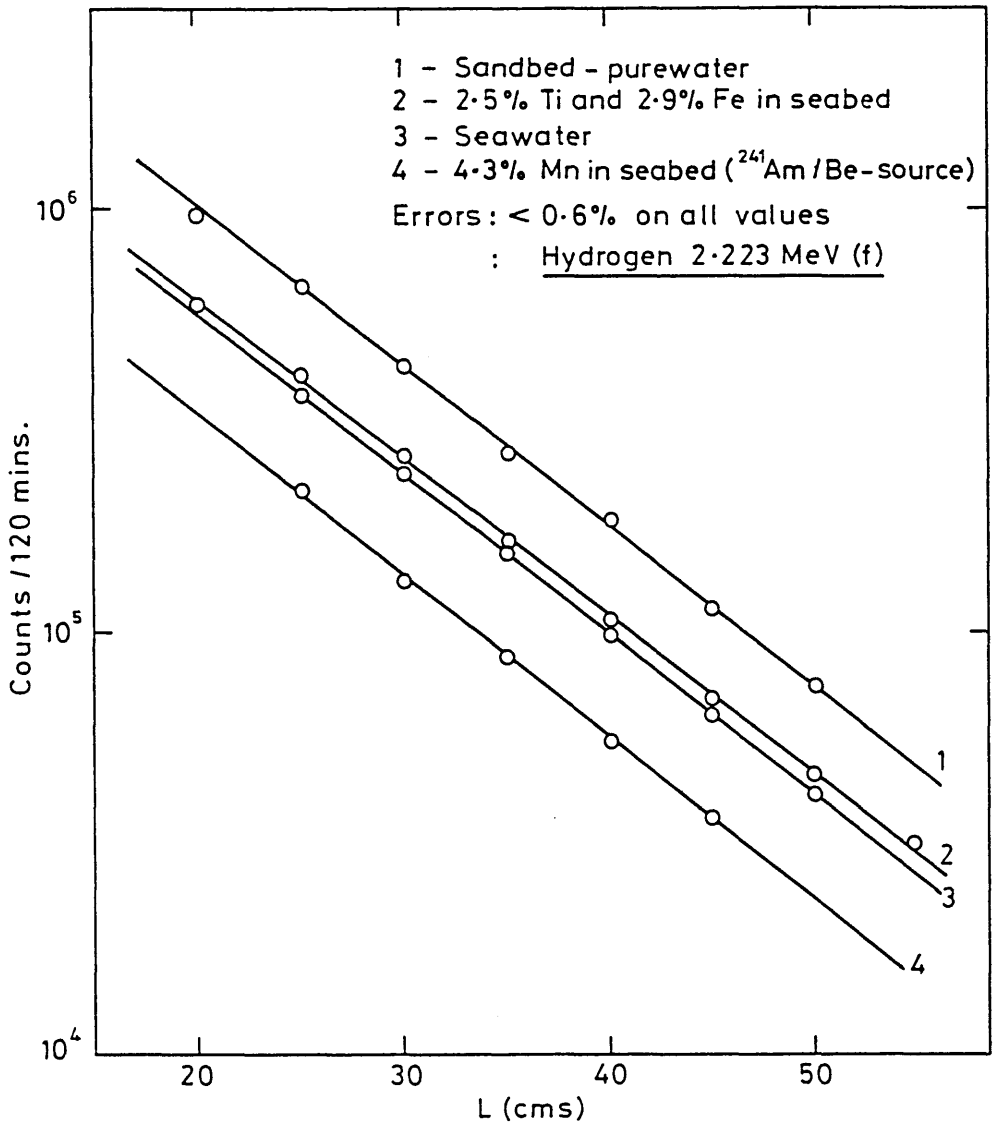

Figure 5.22 Detector countrate measured in the hydrogen 2.223 MeV γ-ray energy peak as a function of source-detector separation L, for different seabed conditions and neutron sources

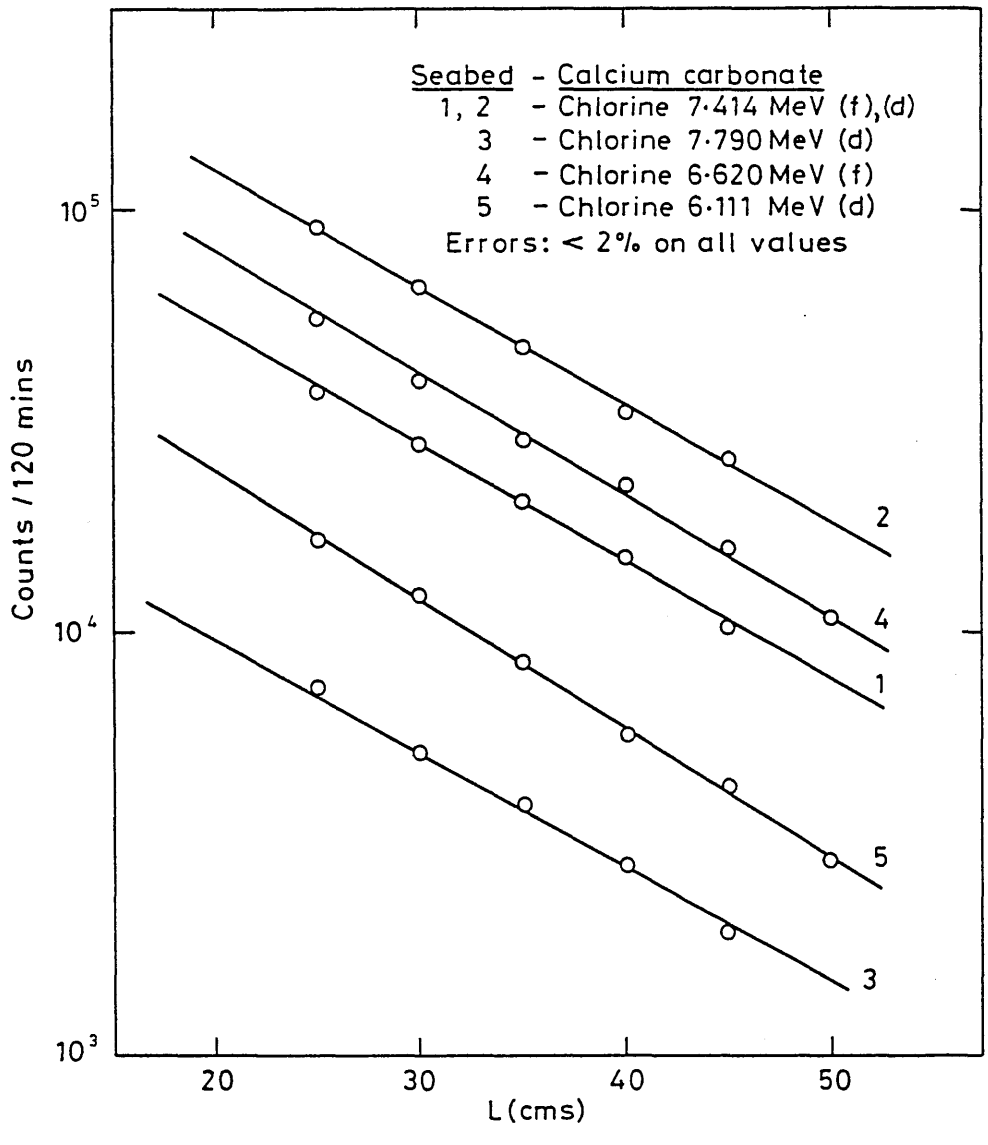

Figure 5.23 Detector countrate measured in the principal γ-ray energy peaks of chlorine for a pure calcium carbonate seabed as a function of source-detector distance L.

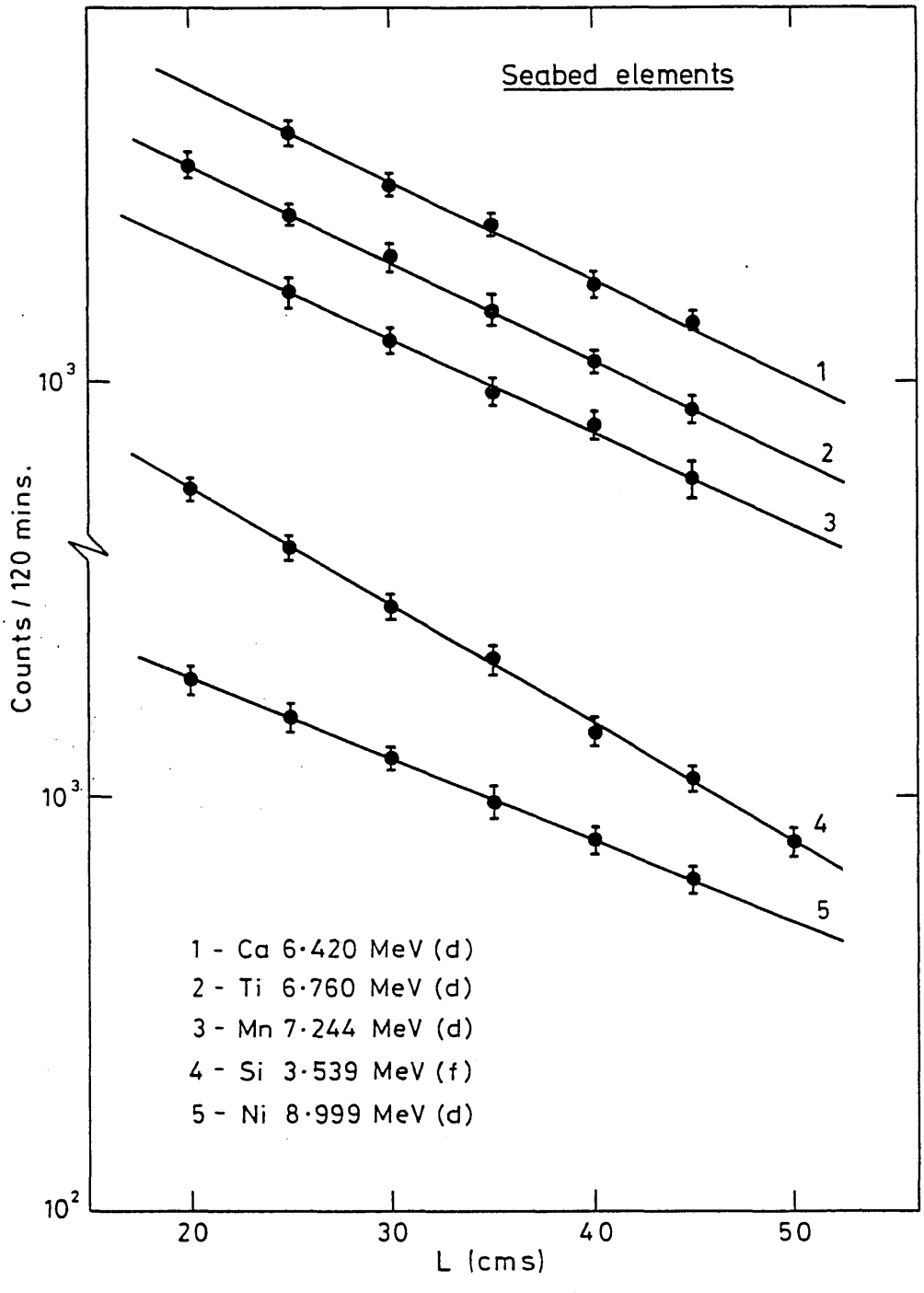

Figure 5.24 Detector countrate measured in the γ-ray energy peaks of some elements in a simulated seabed as a function of source-detector separation L.

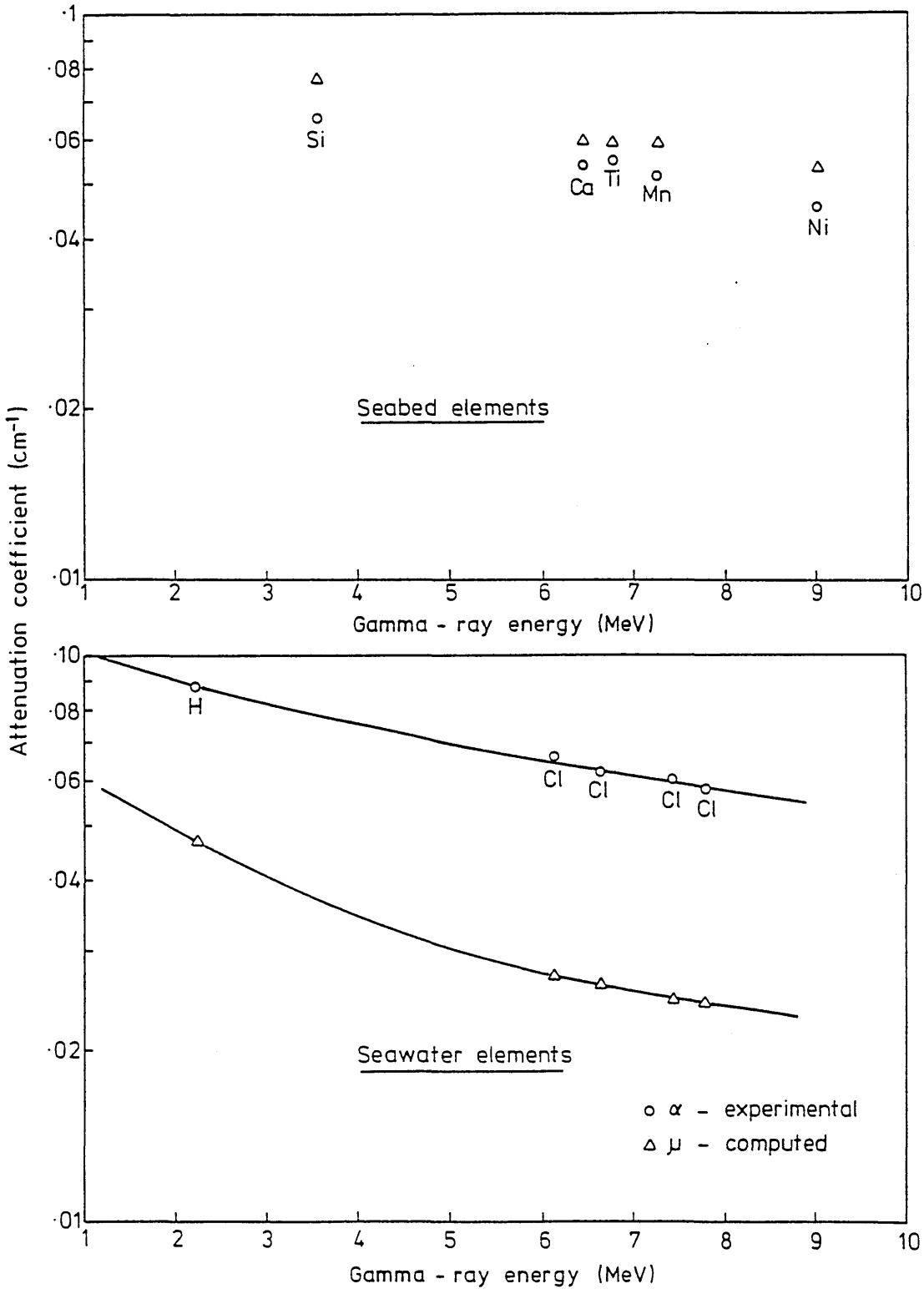

Figure 5.25 Measured and calculated attenuation for seawater and some seabed elements in a simulated seabed as a function of γ-ray energy

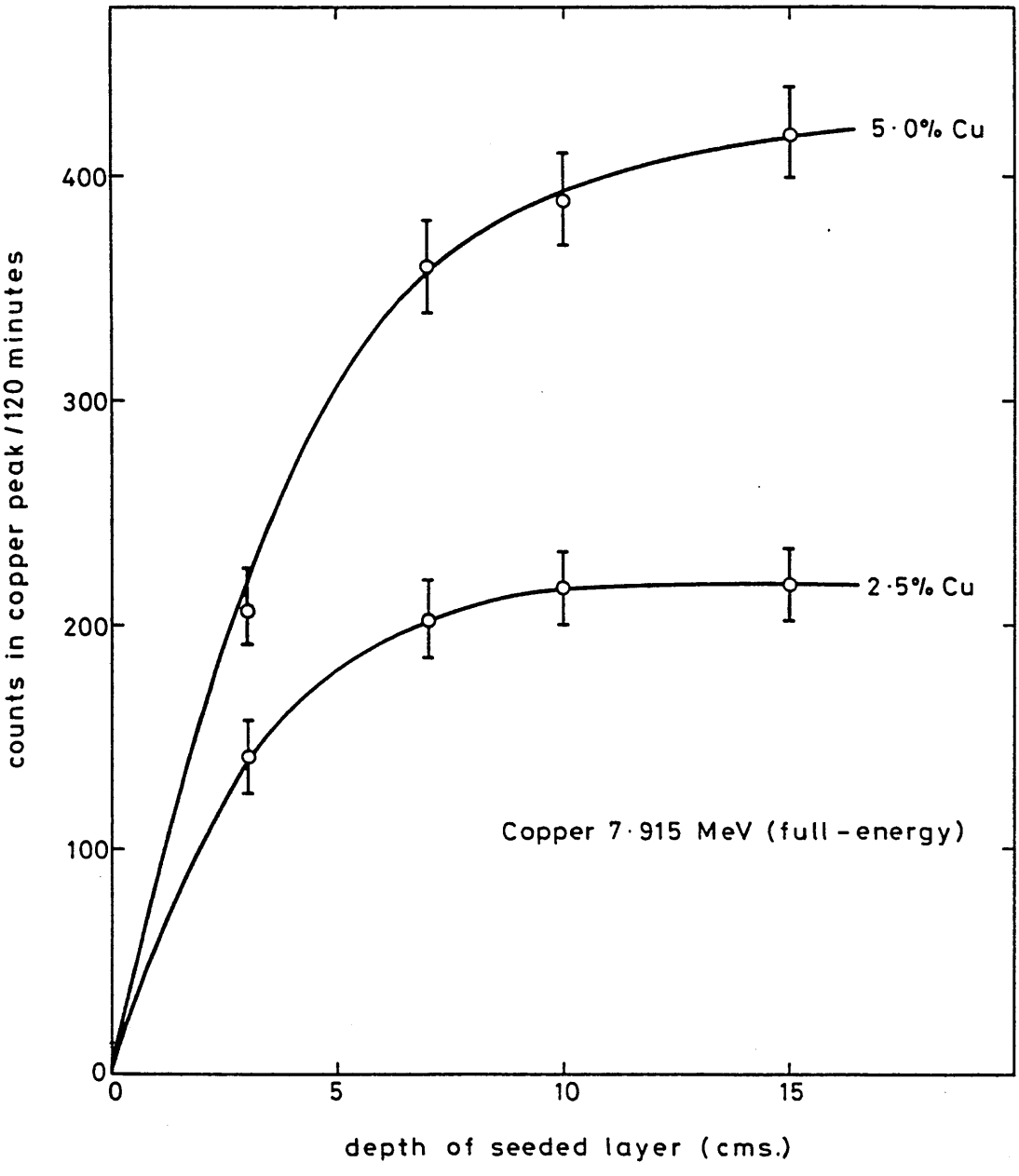

Figure 5.26 Detector response to 7.915 MeV capture γ-rays from copper in a simulated seabed for varying depths at concentrations of 2.5% and 5.0%

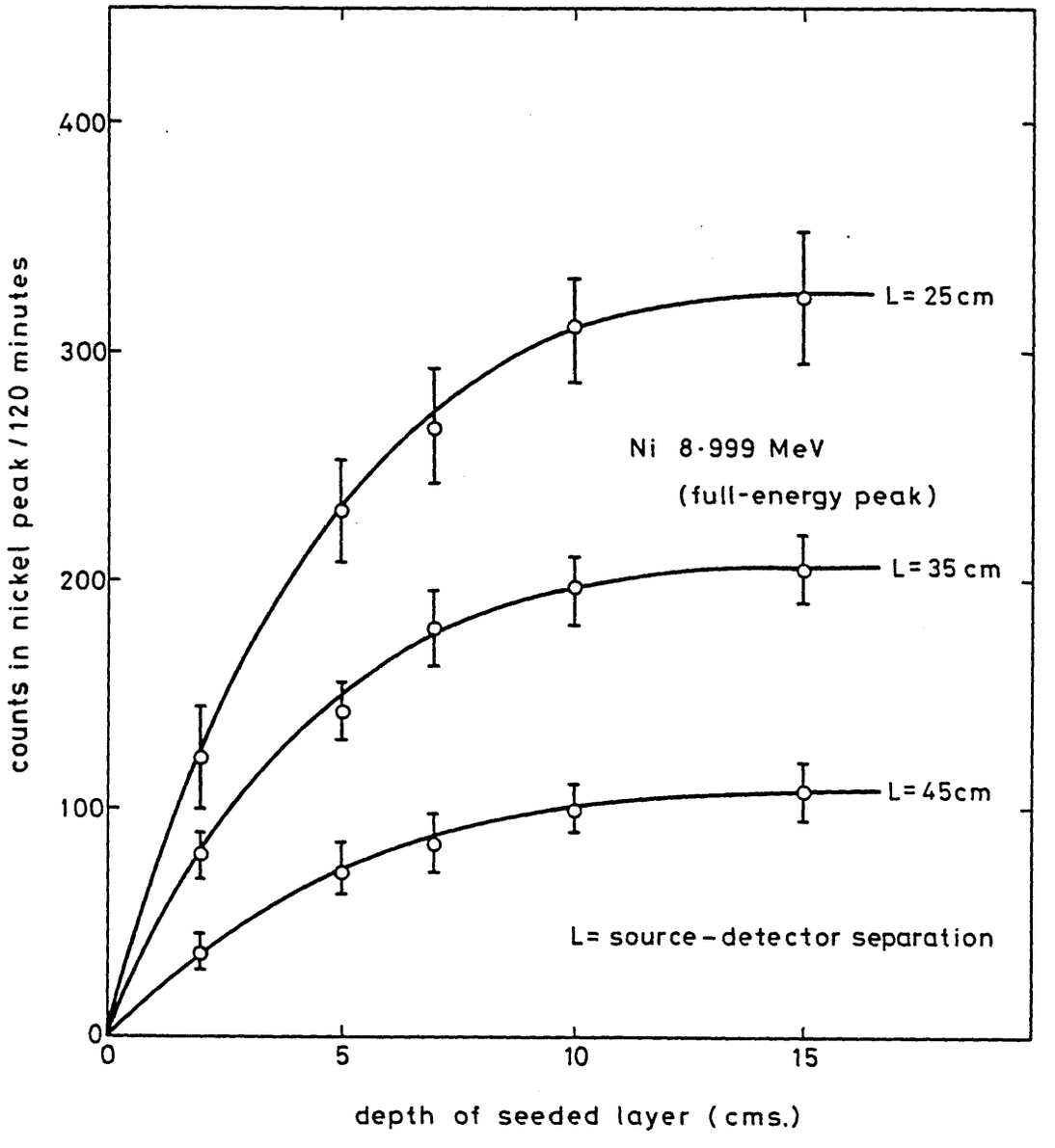

Figure 5.27 Detector response to 8.999 MeV capture γ-rays from nickel (3%) in a simulated seabed for varying depths with different source-detector separations L.

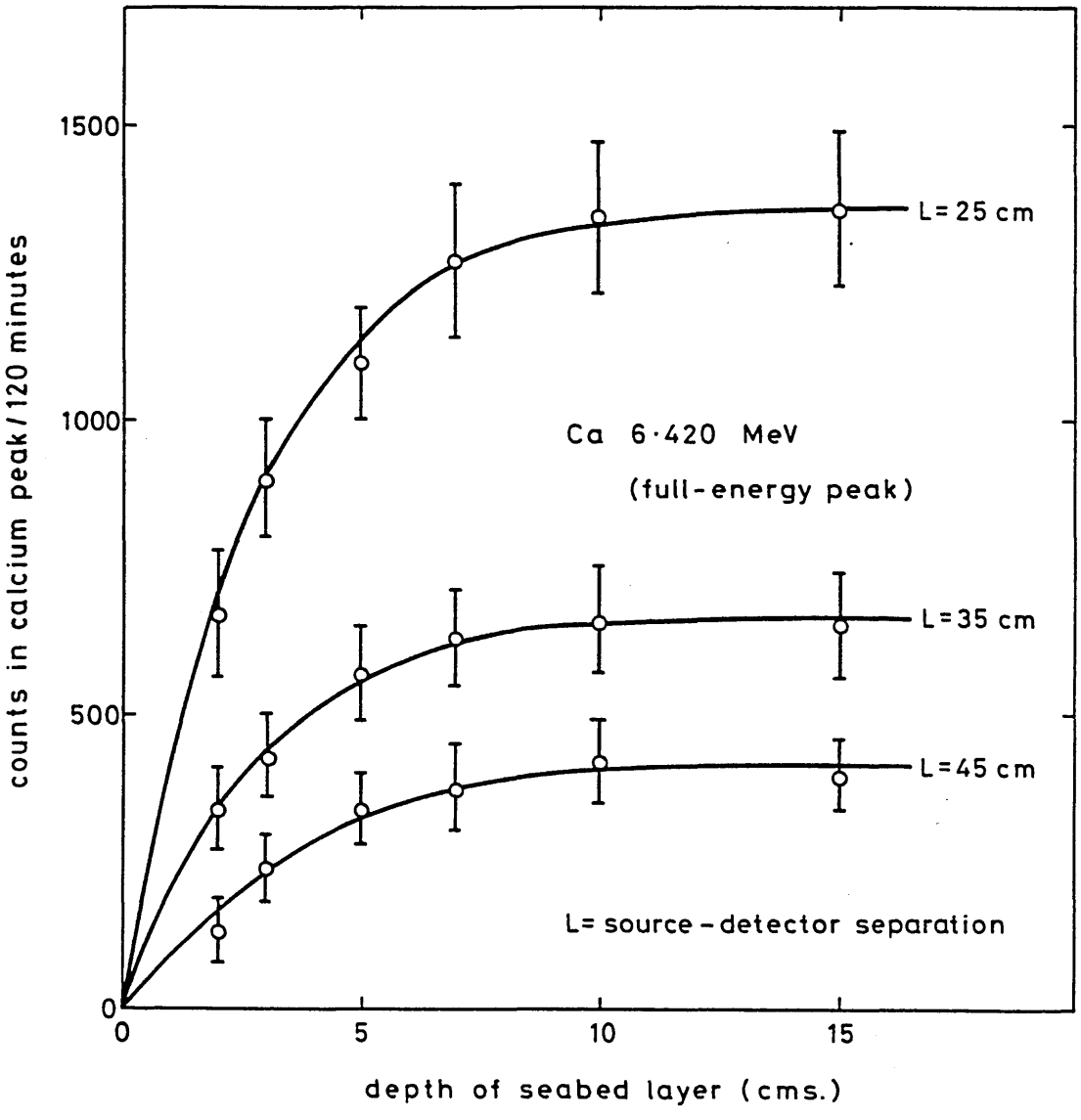

Figure 5.28 Detector response to 6.420 MeV capture γ-rays in the full-energy peak of calcium (40%) in a simulated seabed for varying depths with different source-detector separations L.

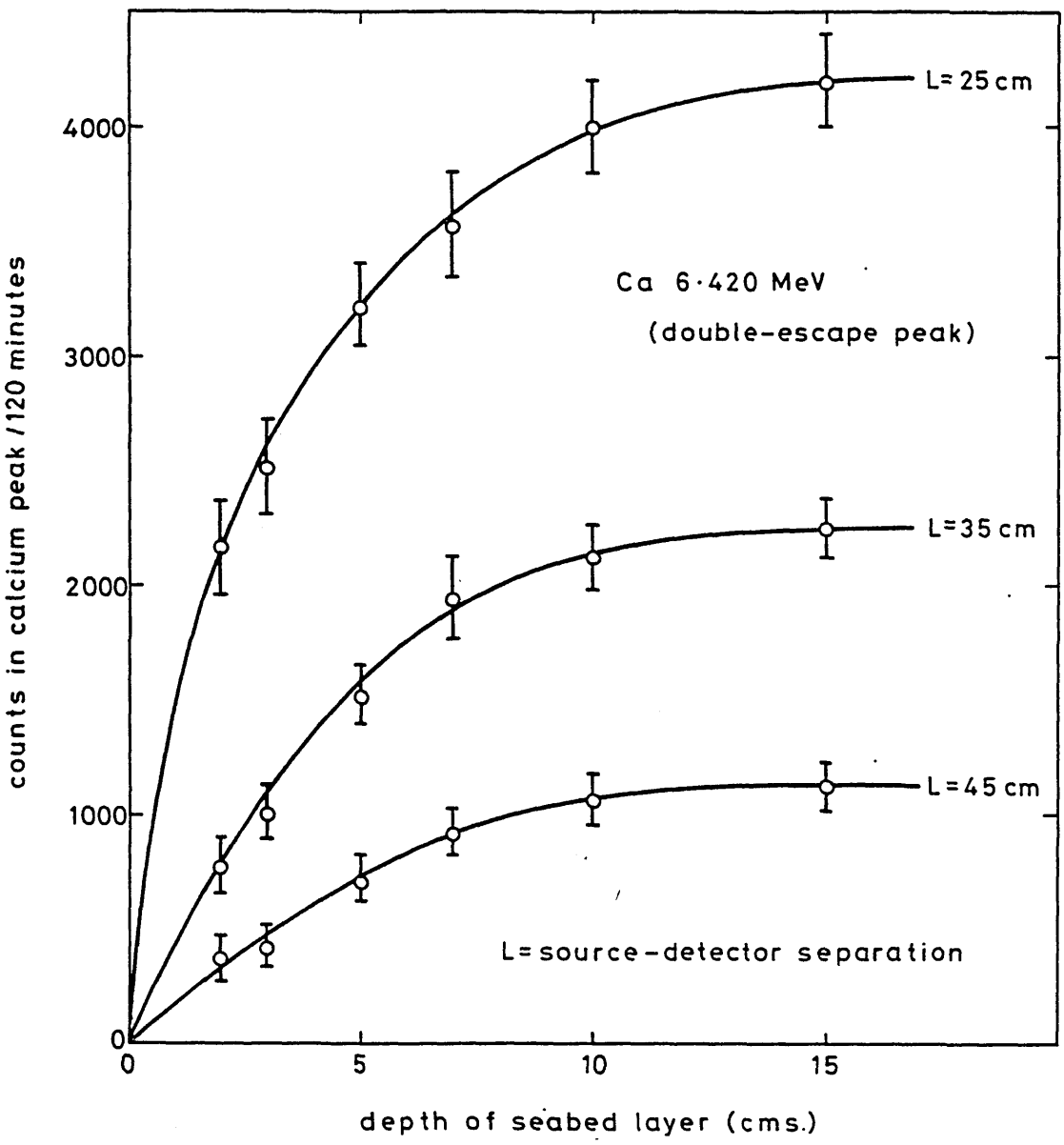

Figure 5.29 Detector response to 6.420 MeV capture γ-rays in the double-escape peak of calcium (40%) in a simulated seabed for varying depths with different source-detector separations L.

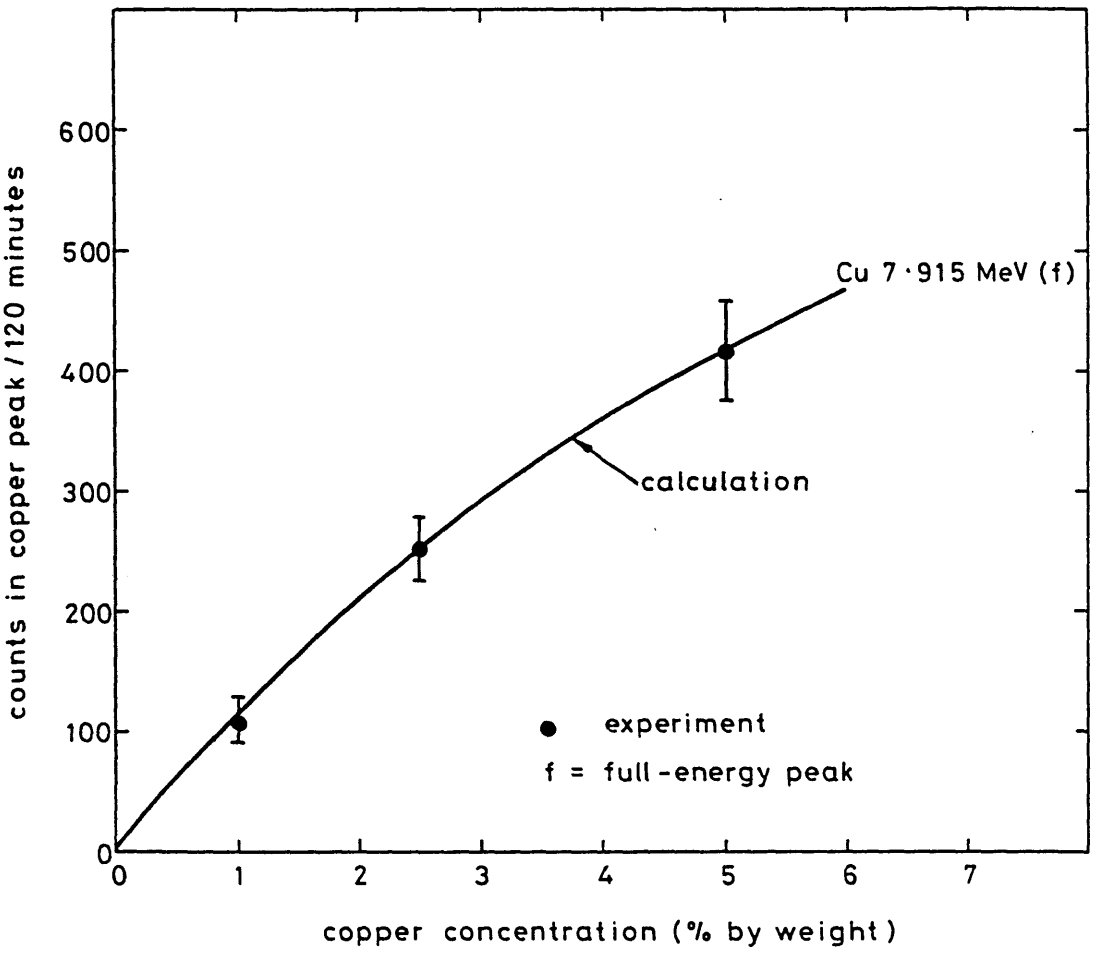

Figure 5.30 Comparison of the calculated and measured detector response to 7.915 MeV capture γ-rays from a simulated seabed containing various concentrations of copper

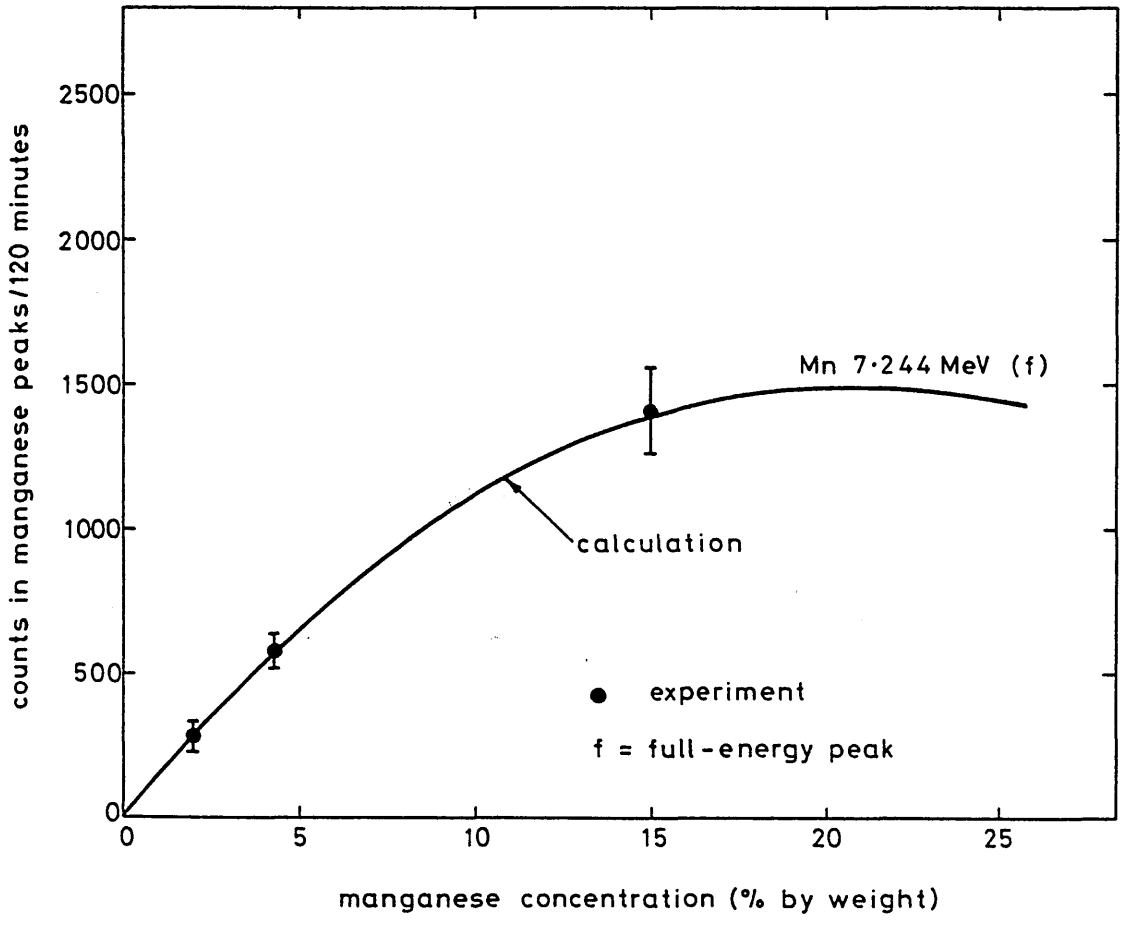

Figure 5.31 Comparison of the calculated and measured detector response to 7.244 MeV capture γ-rays from a simulated seabed containing various concentrations of manganese

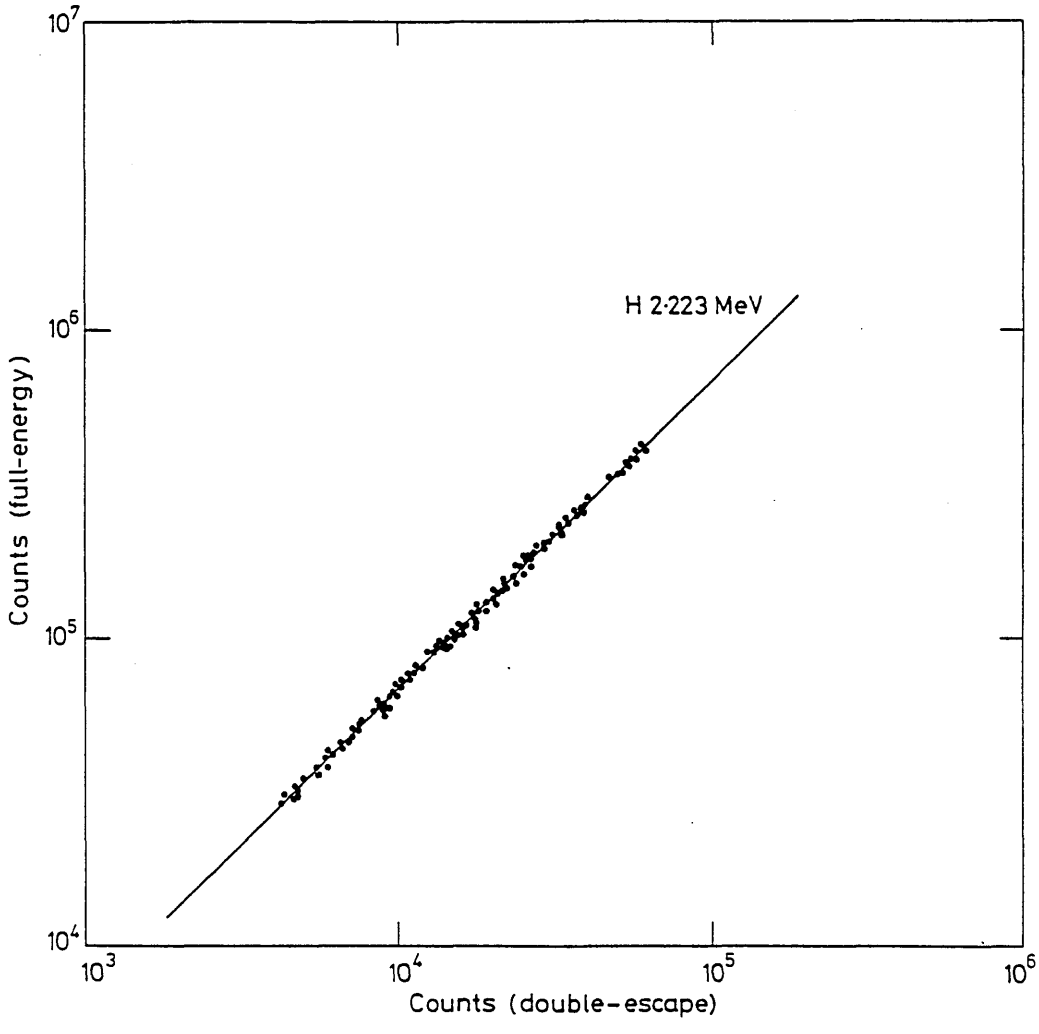

Figure 5.32 Correlation between countrates in the full and double-escape peaks from 2.223 MeV capture γ-rays of hydrogen from various seabeds and for different source-detector separations

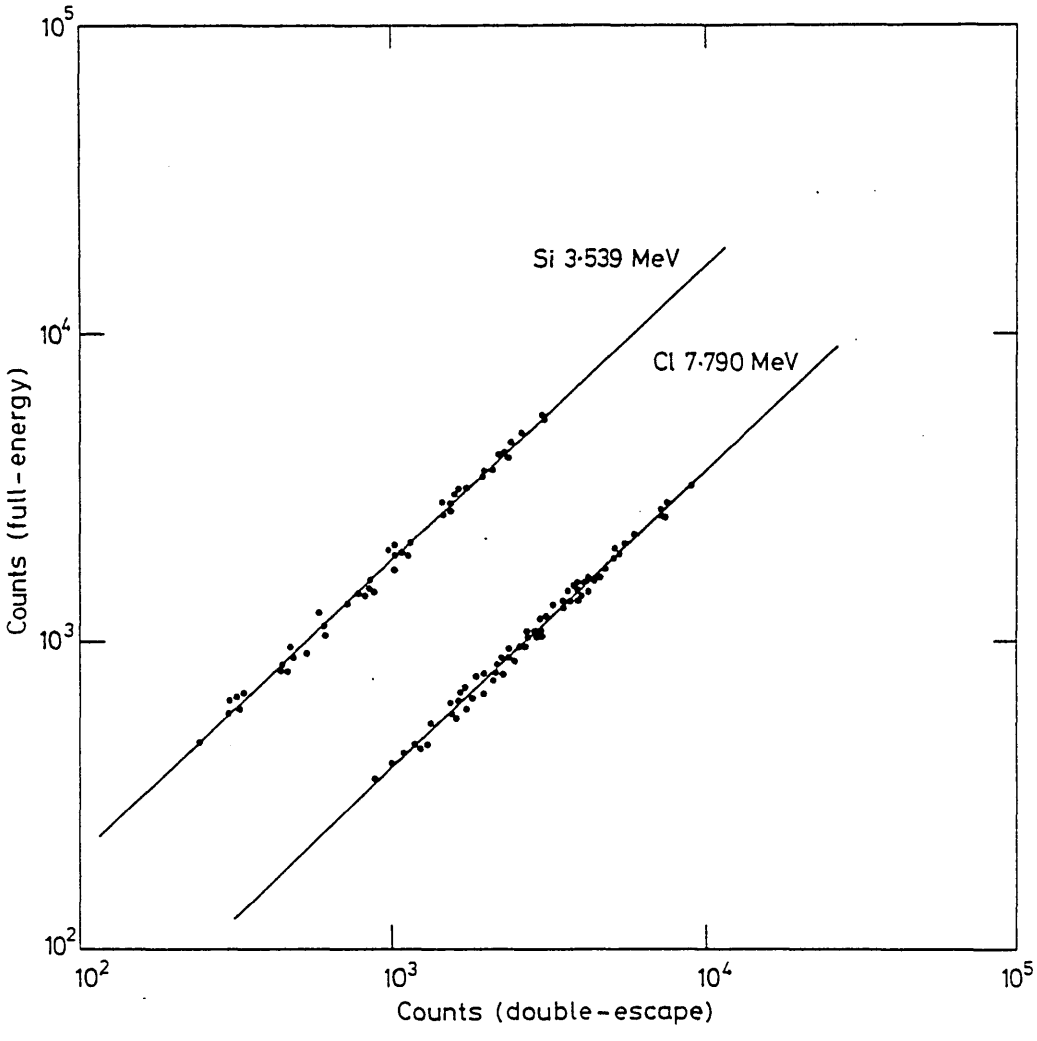

Figure 5.33 Correlation between countrates in the full and double-escape peaks from silicon 3.539 MeV and chlorine 7.790 MeV capture γ-rays from various seabeds and for different source-detector separations

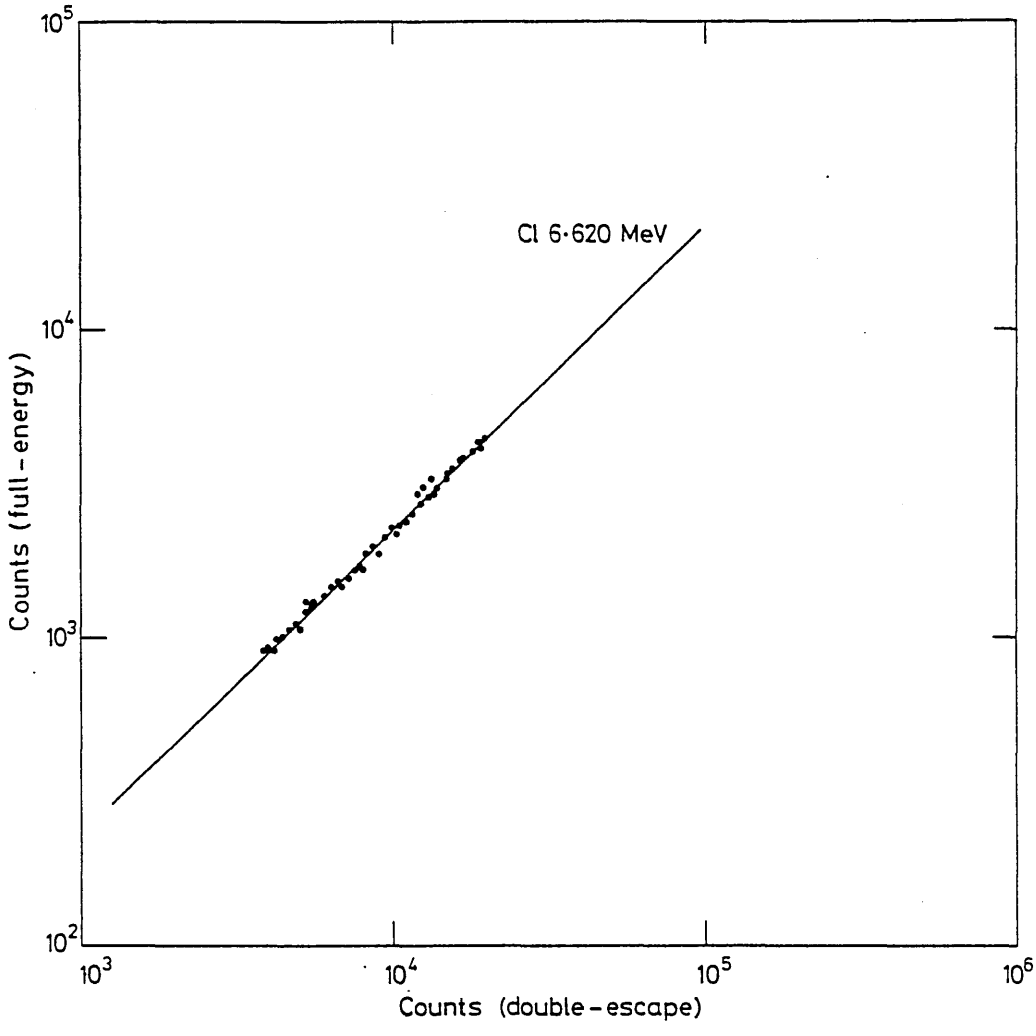

Figure 5.34 Correlation between countrates in the full and double-escape peaks from 6.620 MeV capture γ-rays of chlorine from various seabeds and for different source-detector separations

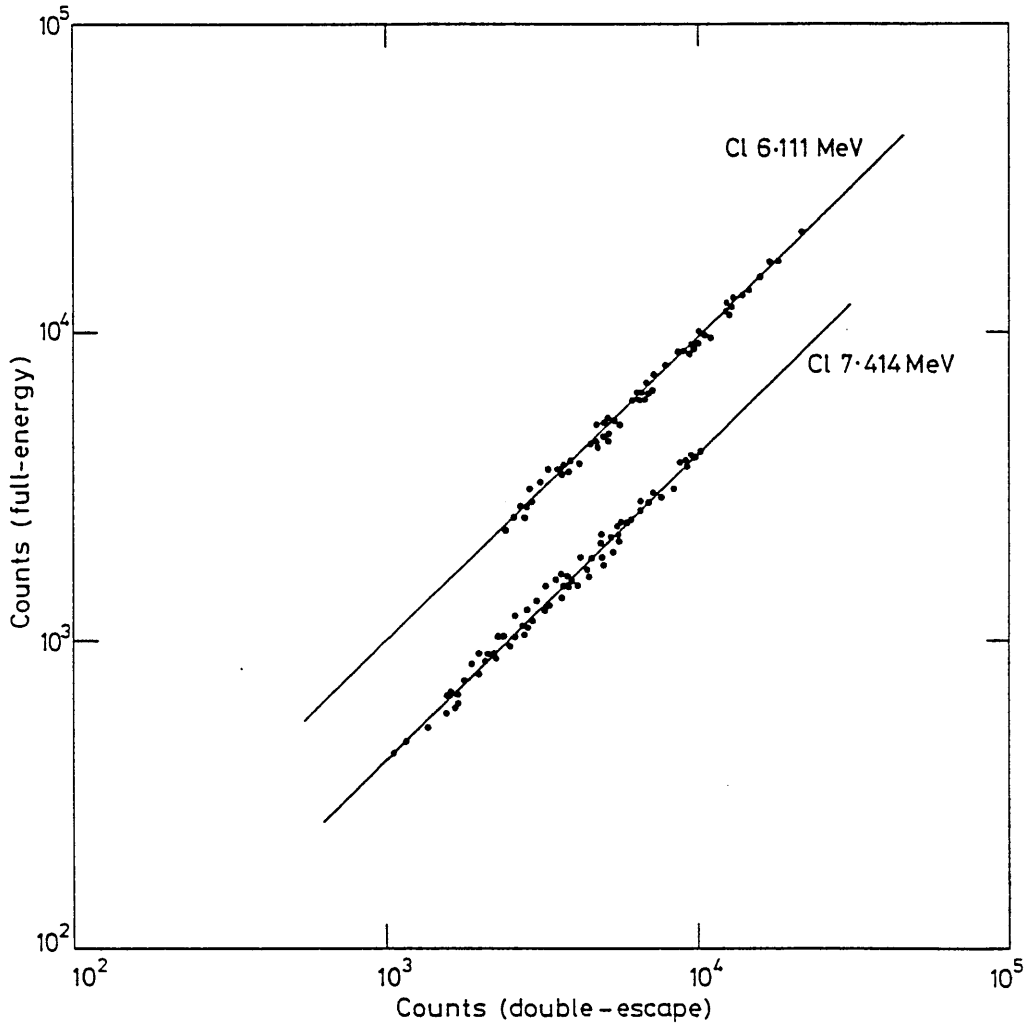

Figure 5.35 Correlation between countrates in the full and double-escape peaks from 6.111 MeV and 7.414 MeV capture γ-rays of chlorine from various seabeds and for different source-detector separations

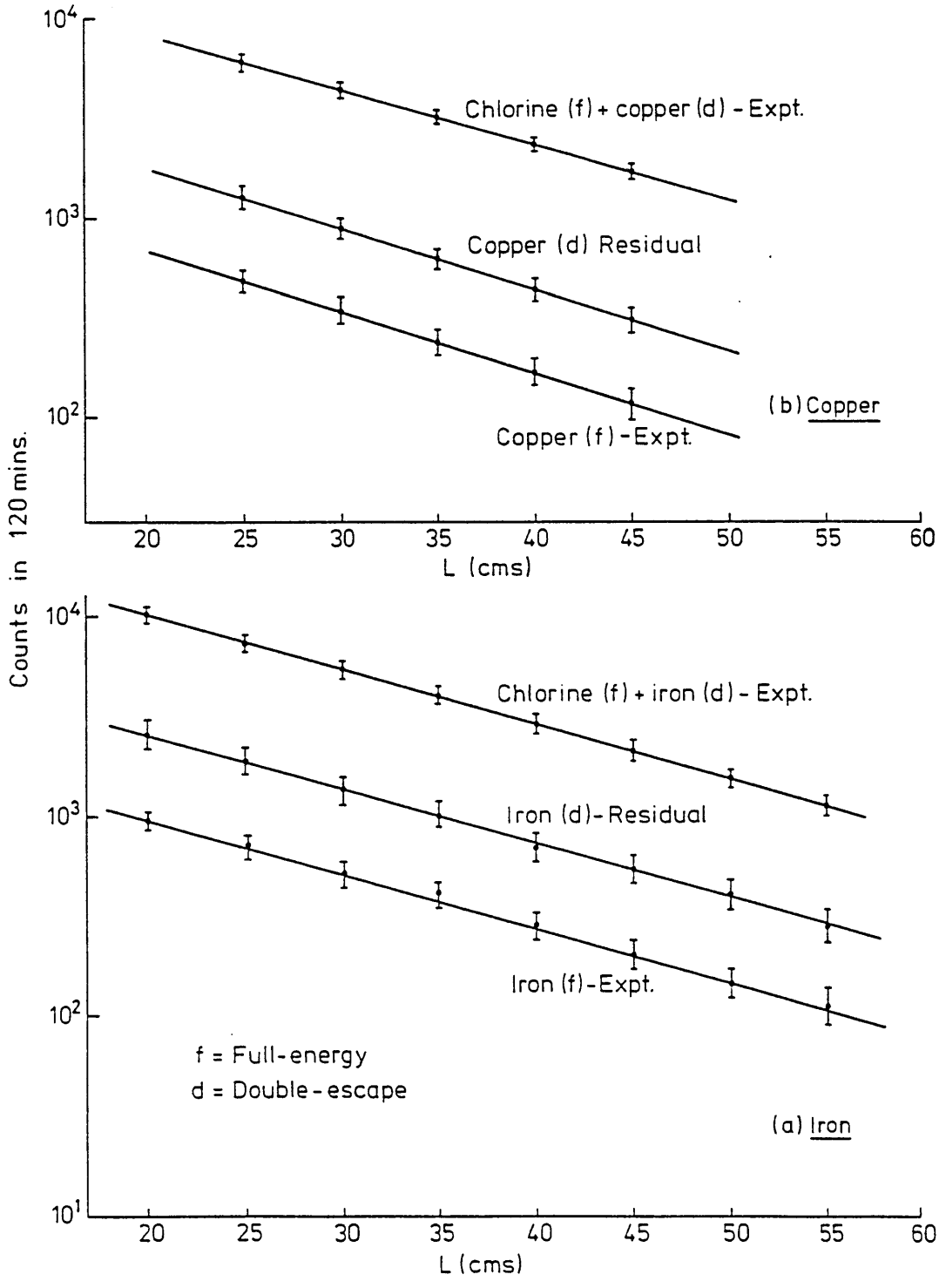

Figure 5.36 Determination of countrates from (a) iron and (b) copper capture γ-rays in a simulated seabed from energy peaks contaminated with chlorine

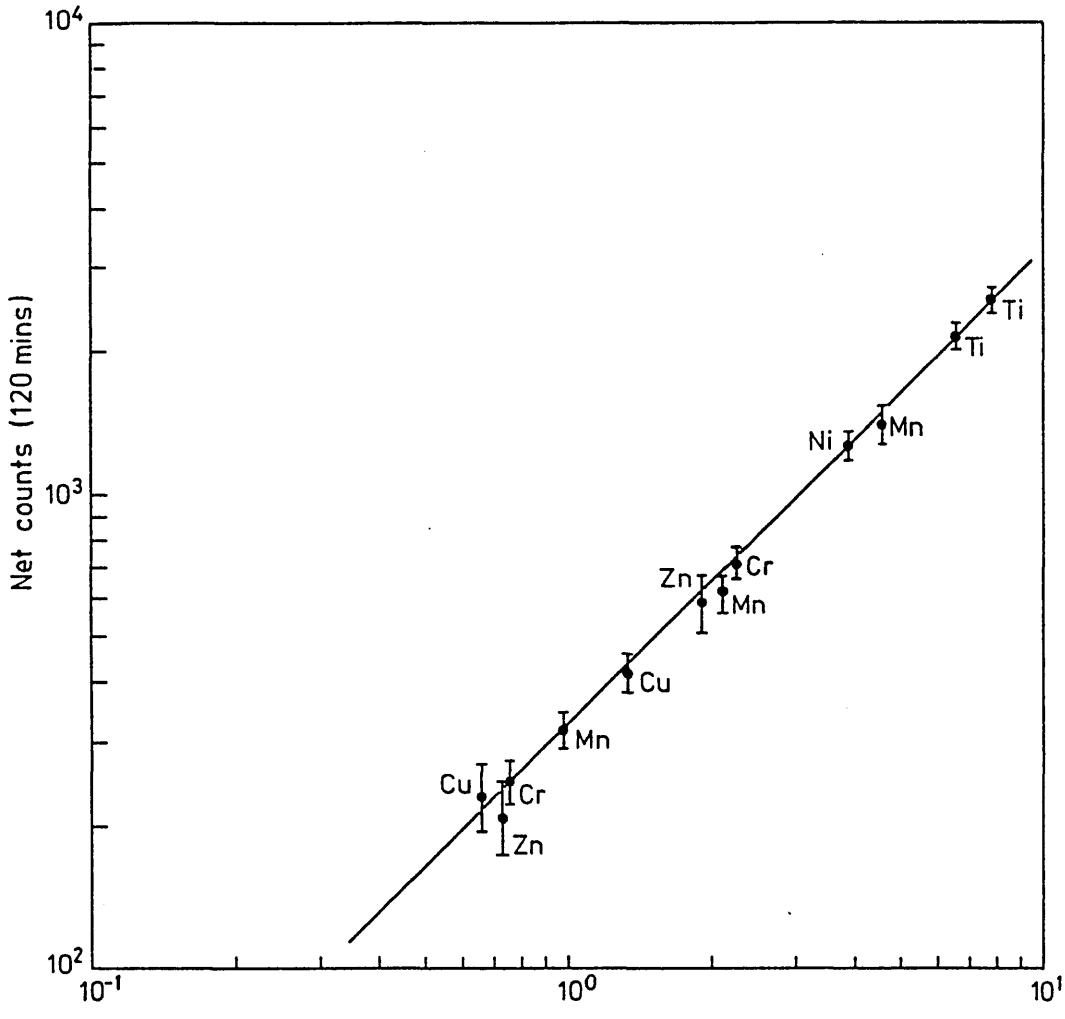

$$\lambda = \left(\frac{I\sigma_a}{A}\right)_{E_\gamma} \cdot \zeta(E_\gamma) \cdot \omega$$

Figure 5.37 Measured countrates from capture γ-rays of various seabed elements as a function of response parameter λ

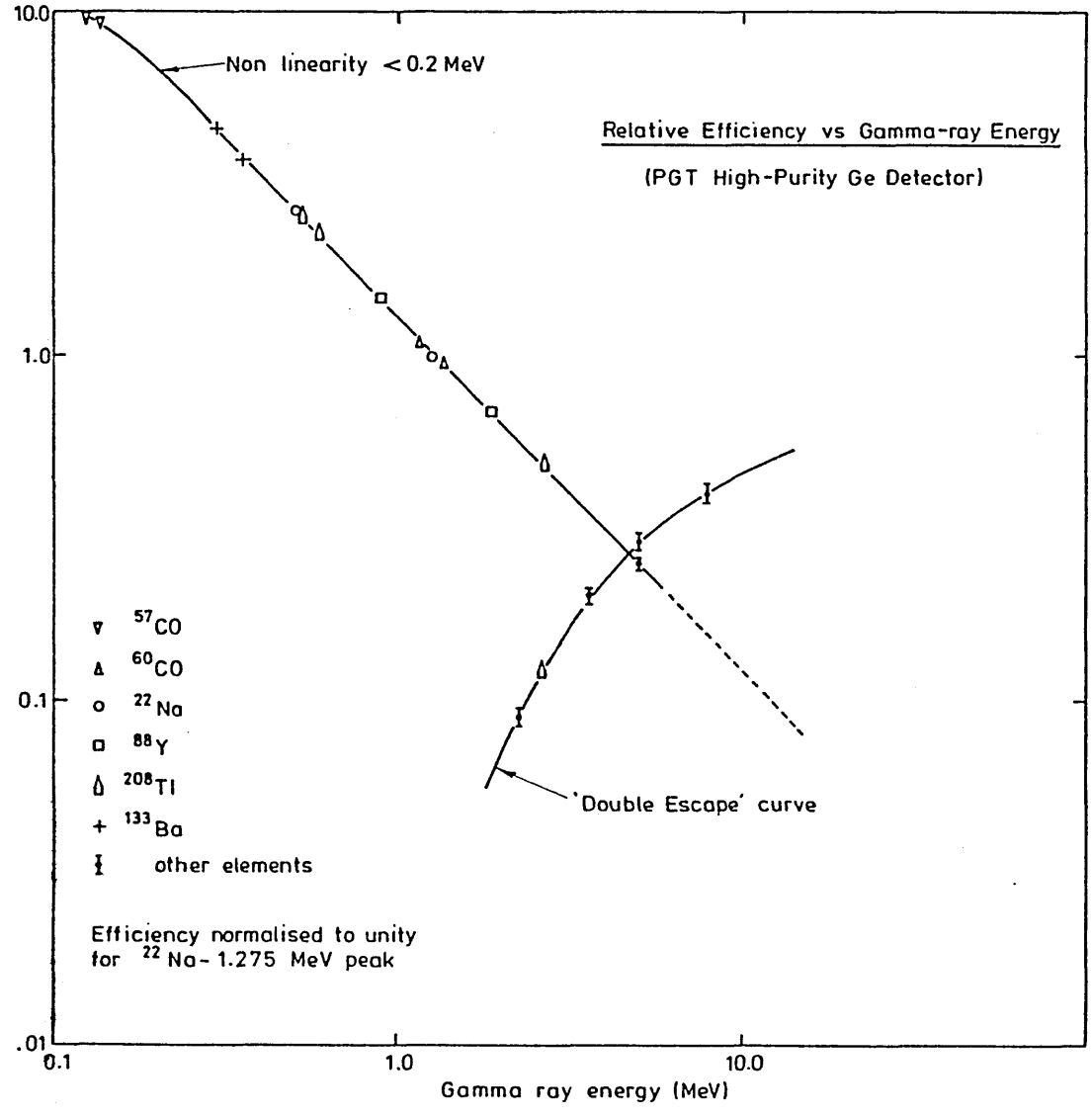

Figure 5.38 Measured full and 'double-escape' relative peak efficiency of the high-purity Ge detector of 50 cc active volume for various γ-ray energy

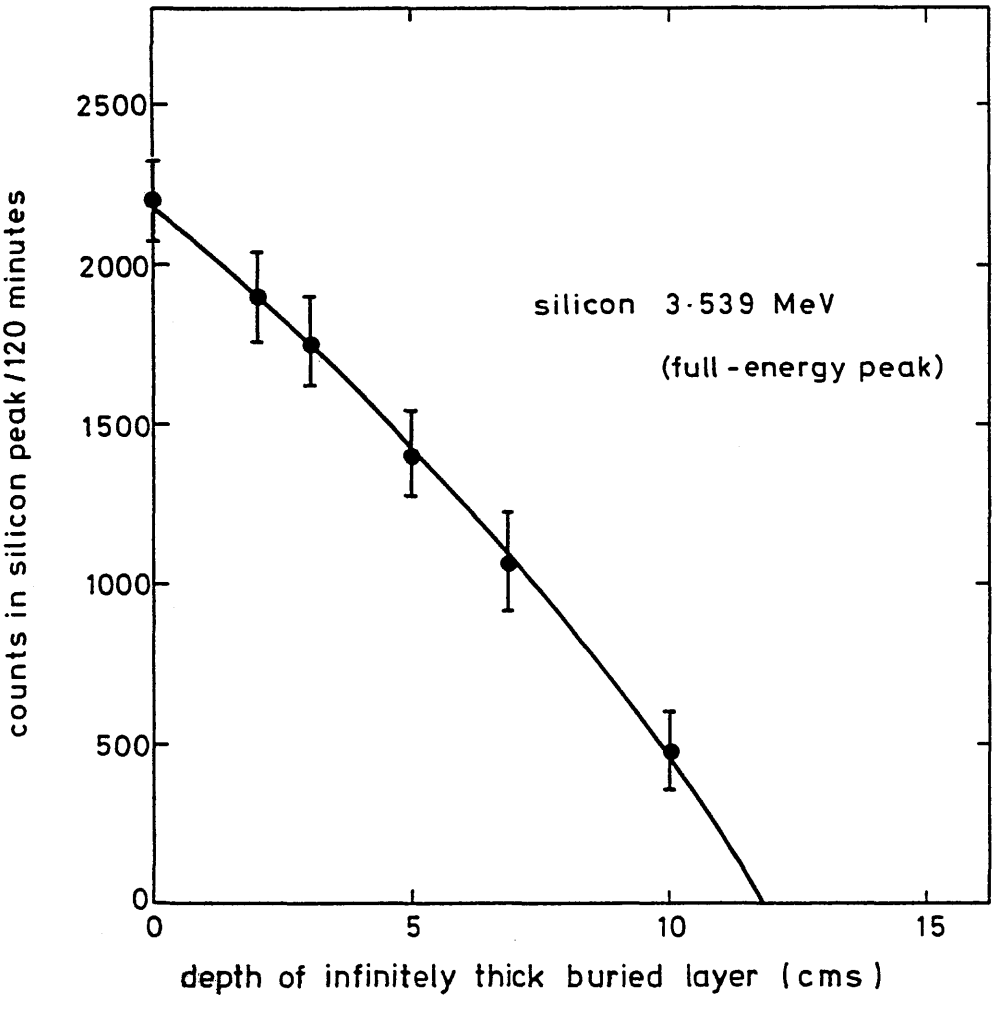

Figure 5.39 Measured detector response to 3.539 MeV capture γ-rays from silicon in an infinitely thick buried layer for varying depths

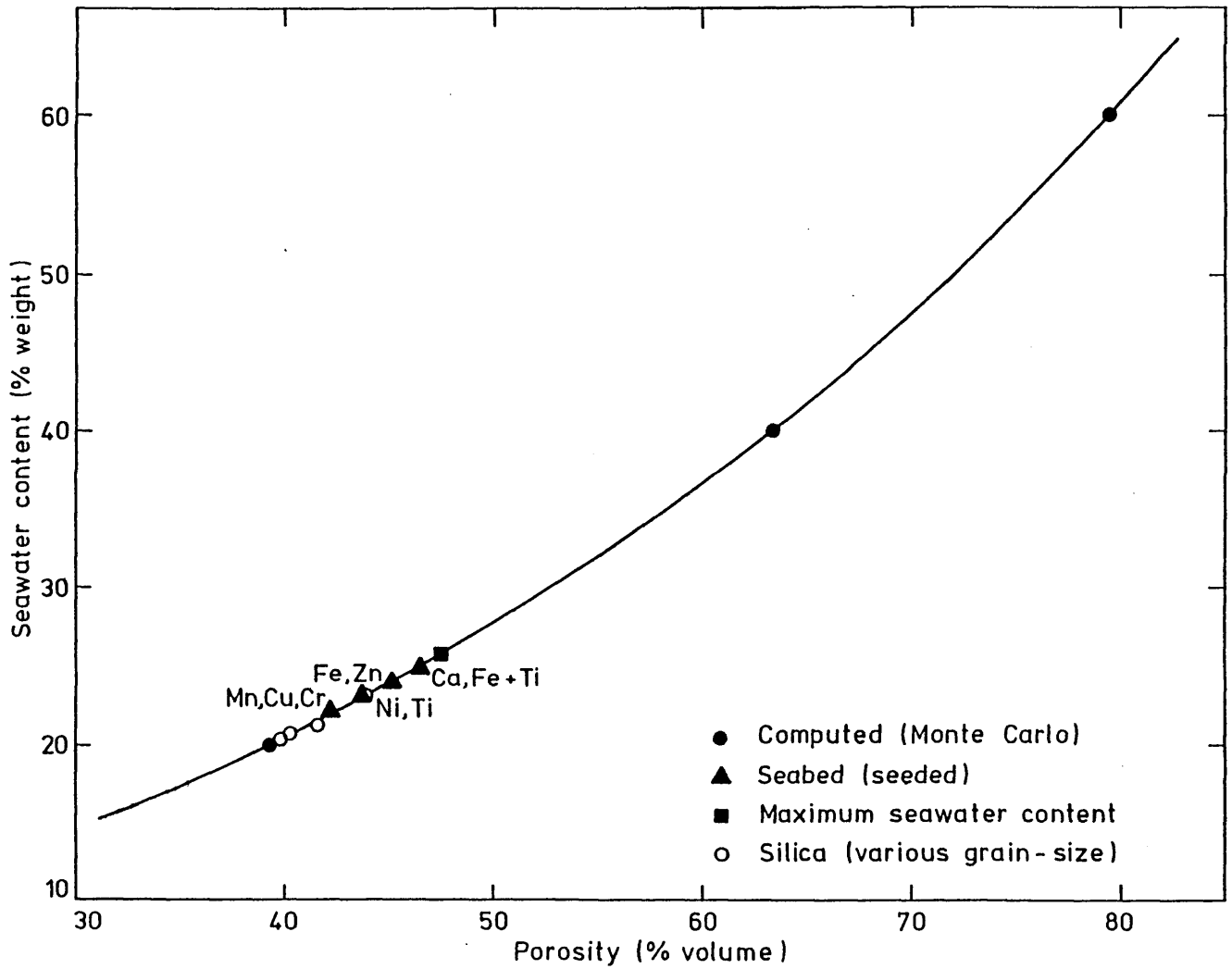

Figure 5.40 Measured and calculated seawater content of various unconsolidated sediments in relation to porosity

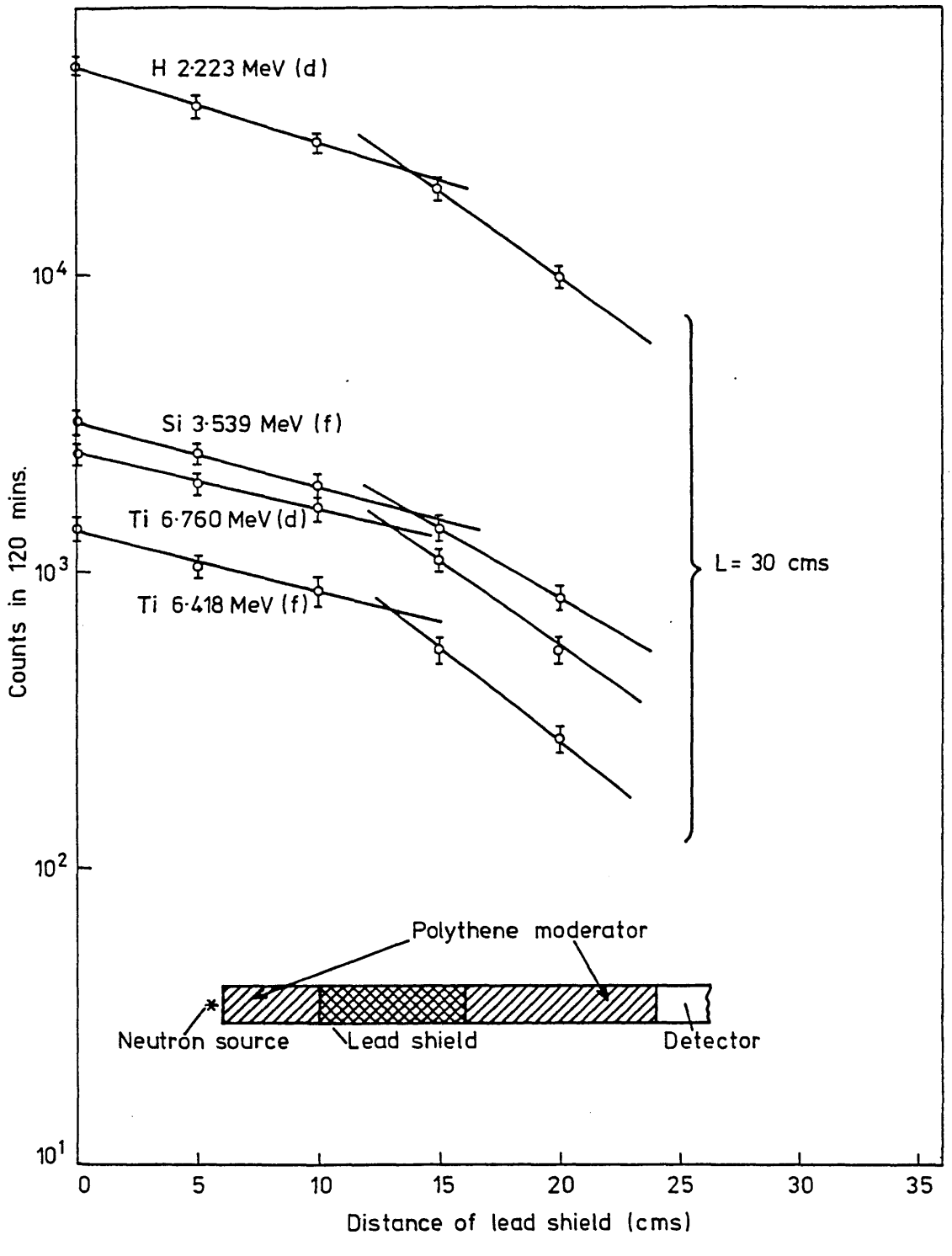

Figure 5.41 Measured detector response to capture γ-rays from elements in a simulated seabed for a fixed source-detector separation of 30 cm and for various distances of the γ-ray shield from the neutron source

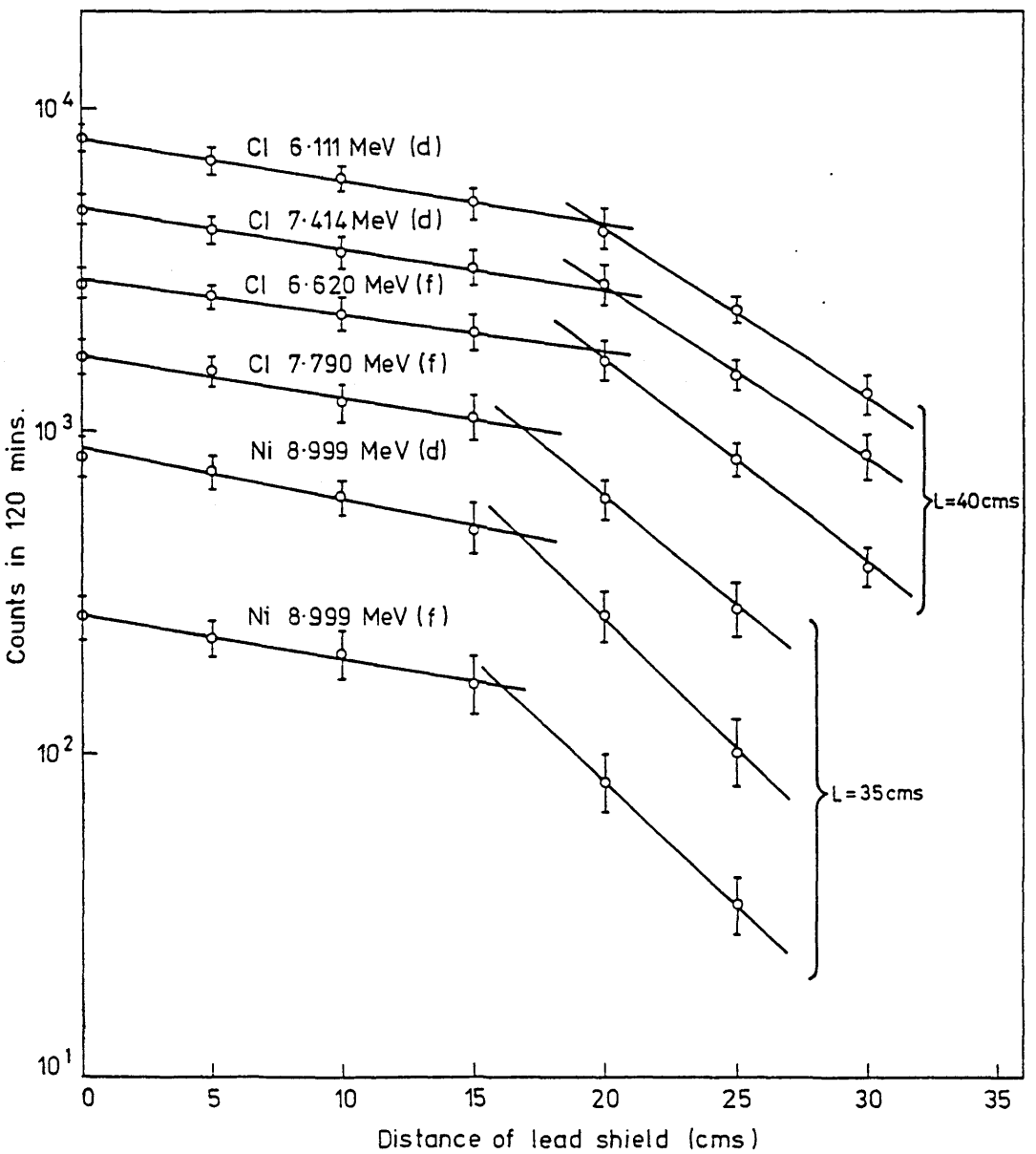

Figure 5.42 Measured detector response to capture γ-rays from nickel and chlorine in a simulated seabed for fixed source-detector separations 35 cm and 40 cm and for various distances of the γ-ray shield from the neutron source